THE UNIVERSITY OF OKLAHOMA

GRADUATE COLLEGE

STRUCTURAL, PROTONATION, AND COMPLEXATION STUDIES OF IONOPHORES A23187, 4-ClA23187, AND 23,24-Br_2A23187

A Dissertation

SUBMITTED TO THE GRADUATE FACULTY

in partial fulfillment of the requirements for the

degree of

DOCTOR OF PHILOSOPHY

By

KENDRA L. COX

Norman, Oklahoma

2006

UMI Number: 3207534

UMI Microform 3207534

ProQuest Information and Learning Company
300 North Zeeb Road
P.O. Box 1346
Ann Arbor, MI 48106-1346

STRUCTURAL, PROTONATION, AND COMPLEXATION STUDIES OF IONOPHORES A23187, 4-ClA23187, AND 23,24-Br_2A23187

A DISSERTATION APPROVED FOR THE
DEPARTMENT OF CHEMISTRY AND BIOCHEMISTRY

_____
Dr. Richard W. Taylor, chair

_____
Dr. Paul F. Cook

_____
Dr. Ann H. West

_____
Dr. Helen I. Zgurskaya

_____
Dr. Mark A. Nanny

ACKNOWLEDGMENTS

I owe many people thanks for their help. In particular, I am appreciative for all of the time and patience that Dr. Taylor put into teaching me both chemical concepts and experimental methods. I am also grateful for my advisory committee: Drs. Cook, West, and Zgurskaya have all been helpful and knowledgeable throughout my graduate studies, and I am very grateful to Dr. Nanny, whose assistance at short notice is greatly appreciated.

I am very thankful to have had Bo Tan and Gary Smith as labmates. They have both taught me a great deal, and I will miss discussing chemistry and non-chemistry related topics with them both.

The chemistry department is full of departmental personnel that have helped me tremendously. Arlene Crawford was always very helpful. I am also grateful to Carl Van Buskirk for his assistance with lab equipment. Drs. Russon, Alguindigue, Khan, and Powell were helpful in teaching me about ESI-MS, NMR, and X-ray crystallography, respectively.

I would also like to thank my family, who supported my goals no matter how much they changed as I grew up. I would also like to thank my husband Mike for his help.

Also, I am grateful to the University of Oklahoma and to the organizations OCAST and NIH for funding of my graduate research.

TABLE OF CONTENTS

CHAPTER VI. DISCUSSION

LIST OF TABLES

LIST OF FIGURES

ABSTRACT

A23187 is a carboxylic acid polyether ionophore best known for transporting calcium through membranes. However, it has been shown that it transports Zn^{2+}, Cd^{2+}, and Mn^{2+} more selectively than Ca^{2+}. Derivatives of A23187 may increase this selectivity by disrupting the hydrogen bonding network of MA_2 complexes and selectively transporting metal ions by alternate transport complexes. The goal of this project is to characterize binding properties of two derivatives, 4-ClA23187 and 23,24-Br_2A23187, which may exhibit an increase in selectivity (relative to A23187) for metal ions Zn^{2+}, Mn^{2+}, and Cd^{2+} relative to Ca^{2+}.

Protonation properties have been studied for A23187, and one new protonation constant, pK_{a2} (representing the deprotonation of the pyrrole nitrogen), was measured to be 11.4. 4-ClA23187 and 23,24-Br_2A23187 also were found to have pK_{a2} values of 11.4.

The derivative 4-ClA23187 was determined to have lower binding constants for K_{HMA} than the parent compound, and increased transport selectivity of Zn^{2+}, Cd^{2+}, and Mn^{2+} over Ca^{2+}. The basis for this increase in selectivity may be due to the lower binding constants (K_{HMA} and K_{MA2}) than the parent compound, and a weakened hydrogen bond network due to the presence of the chlorine substituent on the benzoxazole moiety.

The derivative 23,24-Br_2A23187 was determined to have approximately equal K_{HMA} values as the parent compound, and increased selectivity for transport of Zn^{2+}, Cd^{2+}, and Mn^{2+} over Ca^{2+}. The basis for the increase in selectivity may be due to the higher values for K_{MA} for Zn^{2+} and Cd^{2+} than for Ca^{2+}. The MA complex has four donor atoms from one ligand and a neutral charge, which may be sufficient to transport some divalent metal ions with no additional ions binding to the complex.

CHAPTER I

INTRODUCTION

A. Ionophores

Many metals are present in biological systems. The cations Ca^{2+}, Mg^{2+}, Fe^{2+}, Cu^{2+}, Zn^{2+}, Mn^{2+}, Na^{+}, and K^{+} play important roles in the proper functioning of many organisms. For example, metalloenzymes containing metals such as Zn^{2+}, Cu^{2+}, and Fe^{2+} are involved in the fixation of nitrogen, oxygen transport, and many other functions. Mg^{2+} is a co-factor for many enzymes and the central ion found in chlorophyll. Transmission of Na^{+} and K^{+} across a neuronal cell results in transmission of an impulse along the cell membrane. Ca^{2+} acts as a second messenger, inducing many types of cells to carry out their particular function (e.g. muscle contraction, vesicle release, etc.).

Several of these cations (Ca^{2+}, Mg^{2+}, Na^{+}, and K^{+}) have well-known regulatory pathways that involve transport across a cell membrane. For example, a Na^{+}/K^{+} pump restores the potential gradient across the membrane after a signal is transmitted, calcium activity is regulated by proteins such as troponin-C and calmodulin, and the concentration of free Zn^{2+} within *E. coli* cells is highly controlled by regulatory proteins.[1]

Ionophores are molecules that facilitate the transport of metal ions across biological membranes.[2] Unassisted transport is made very difficult by the repulsion between the hydrophilic, charged metal ion and the hydrophobic, phospholipid rich cell membrane interior. The metal ion may also have water molecules surrounding it that further reduce the possibility of transport.

There are several methods by which ionophores are thought to transport metal ions across membranes. All ionophores possess both hydrophobic and hydrophilic regions to achieve compatibility with both the membrane interior and the metal ion.[3] Metal ions can be transported by the formation of a channel that stretches across the membrane with a hydrophobic exterior interacting with the membrane and a hydrophilic interior which metal ions can pass through. Alternatively, metal ions can be complexed by a molecule with properties that allow it to shield the metal from the hydrophobic interior of the membrane. These carrier-metal ion complexes passively diffuse through the membrane, and the metal ion is released on the opposite side. The ionophore is then free to diffuse back across the membrane and assist in further metal ion transport. Channel-forming and carrier-type transport methods are illustrated in Figure I.1.

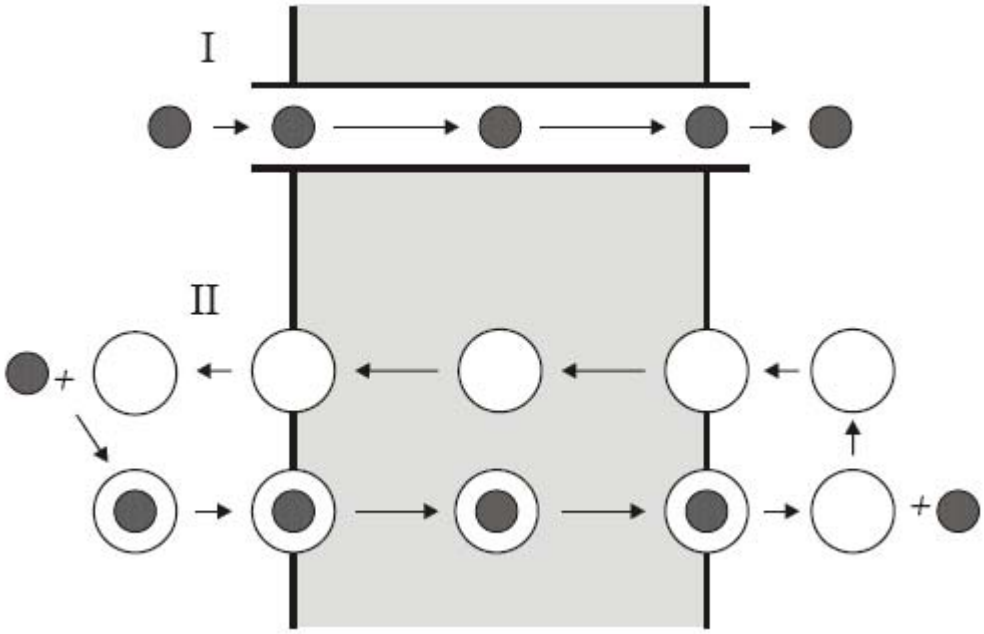

Figure I.1. Channel (I) and carrier (II) transport through a membrane

Carrier-type ionophores use two main modes of transport: electrogenic and electroneutral. Electrogenic transport, shown in Figure I.2, occurs when ionophore-mediated transport results in a change in electric potential across a membrane.

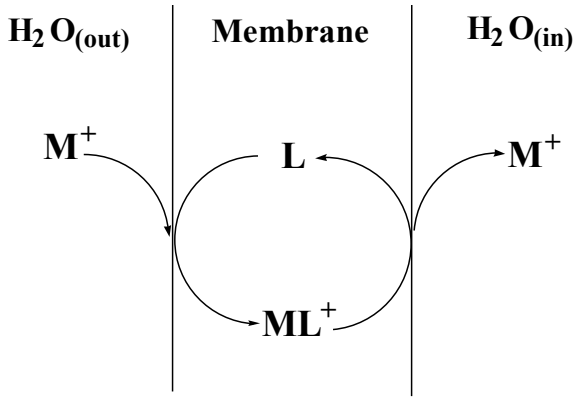

L = valinomycin, enniatin, nonactin

Figure I.2. Electrogenic transport scheme

For this to occur, at some point in the transport a charged species must diffuse through the membrane. This can occur by either the ionophore transporting a charged metal ion complex and diffusing back as a neutral molecule, or by the ionophore transporting as a neutral complex and diffusing back in charged form.

The second form of transport is electroneutral transport, shown in Figure I.3. In this model, the net charge on both sides of the membranes remains constant. For this to occur, both diffusing species (into and out of the cell) must possess the same charge. Due to the hydrophobicity of the membrane interior, this charge is most often zero. Since the metals transported are cations, the ionophore must acquire a negative charge to neutralize the cation, which is commonly achieved through deprotonation of the molecule.

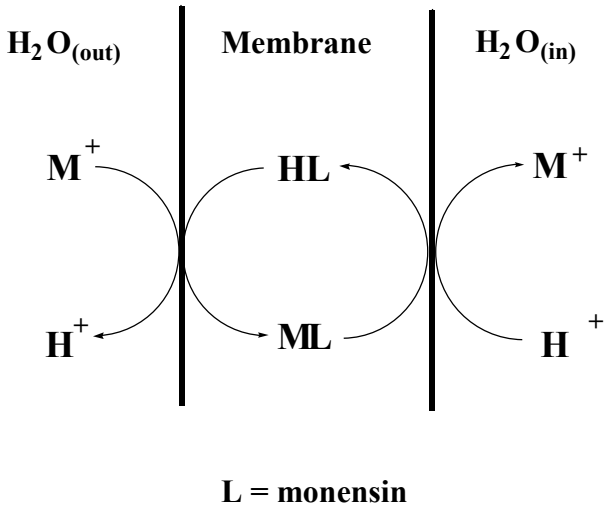

Figure I.3. Electroneutral transport scheme

A neutral metal-ionophore complex is formed either in the exterior solution or on the membrane exterior, and then diffuses through the membrane to the opposite side. The cation is released, the ionophore picks up a different cation to become a neutral species, and diffuses back through the membrane. On the opposite side, the ionophore can release the cation and then transport further metal species. In cases where the one of the cations is a proton, the transport cycle results in a change in pH across the membrane. Accumulation of hydrogen ions on one side of the membrane, in the absence of other forms of transport, will ultimately result in a pH gradient that halts further transport. Ionophores may transport metals by electrogenic, electroneutral, or both forms of transport. The type of transport observed may also vary depending on the environmental conditions such as pH, concentration of metal, gradient of any cation or anion in the system, etc.

B. Uses of Selective Ionophores

Many ionophores show selectivity of transport for certain metal ions; that is, they transport some cations preferentially over others. For example, the polyether carboxylic acid ionophores nigericin, monensin, and salinomycin are highly selective transporters of Pb^{2+} compared to other divalent cations.[4-6] Their structures are shown in Figure I.4.[7]

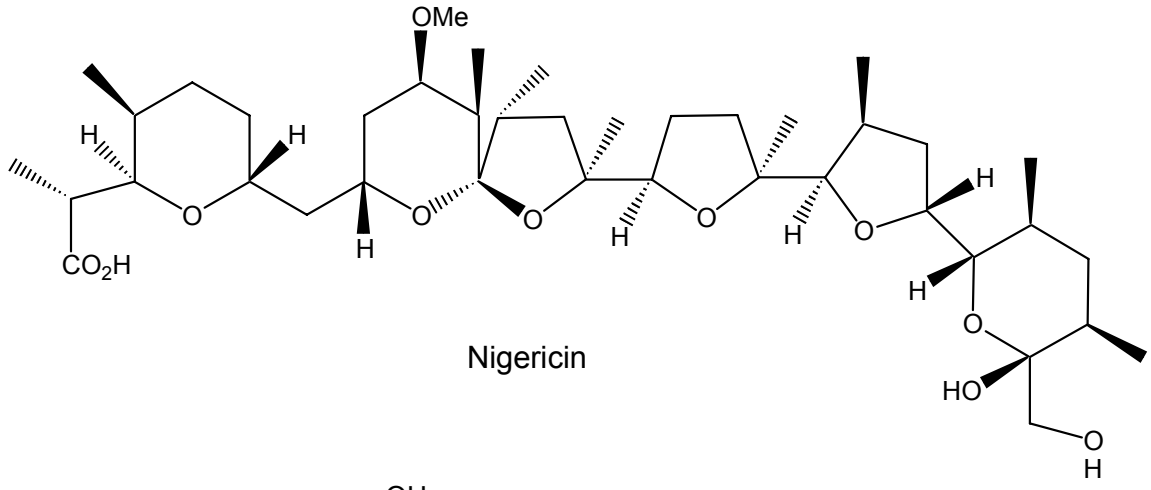

Nigericin

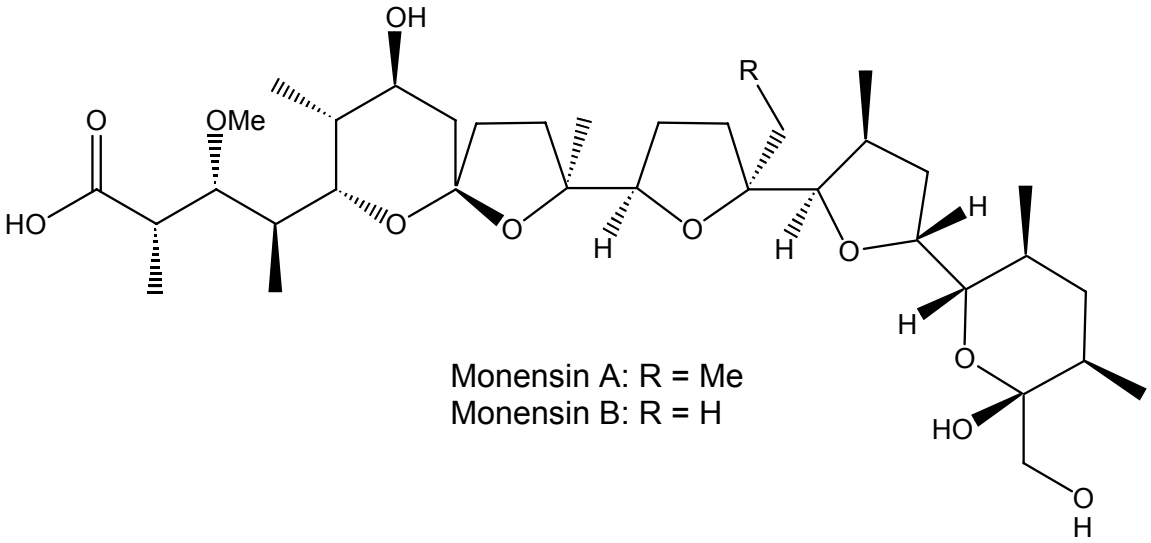

Monensin A: R = Me
Monensin B: R = H

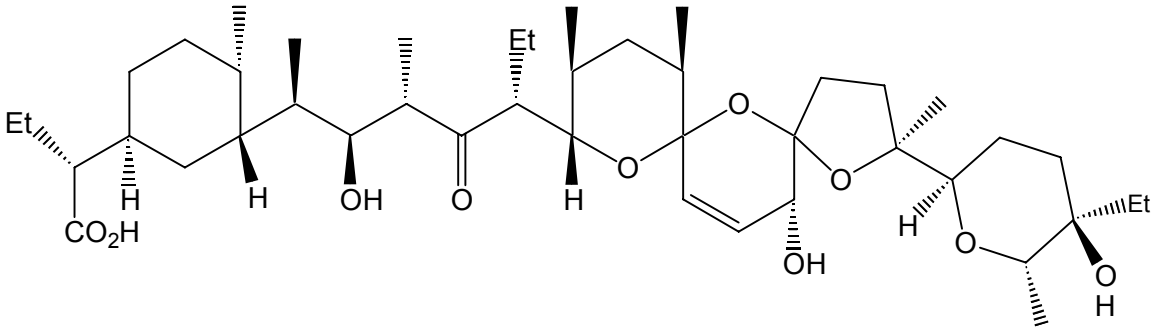

Salinomycin

Figure I.4. Structures of ionophores nigericin, monensin, and salinomycin

C. A23187

A23187 is a carboxylic acid polyether ionophore. It is known to transport several divalent cations across membranes, however it is best known as a calcium ionophore. It is also called calcimycin. It is produced by the bacteria *Streptomyces chartreusis*, presumably as a mechanism to reduce environmental competition for food by interfering with other organisms' essential metal gradients.[8] It is unknown how *S. chartreusis* itself remains unaffected by the ionophore. The structure of the ionophore, shown in Figure I.5, has been elucidated by ^{1}H NMR, ^{13}C NMR, and X-ray crystallography.[8-11]

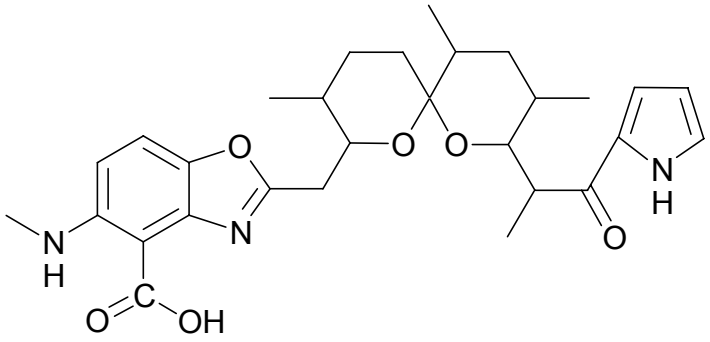

Figure I.5. Structure of A23187

It has a hydrophilic interior, composed of a carboxylic acid, two ether groups, a carbonyl group, and a pyrrole group. The opposite side, or exterior, of the molecule consists of hydrophobic areas composed mainly of carbon and hydrogen.

The solid state structures of the MA_2 complex for A23187 and Ca^{2+}, Fe^{2+}, and Mg^{2+} have been solved by X-ray crystallography.[12-14] In each complex, the metal is bound by three donor sites per ligand (carboxylate oxygen, benzoxazole nitrogen, and ketopyrrole oxygen). Each ligand is oriented head-to-tail with respect to the other ligand, and interligand hydrogen bonding is observed on both ends between a carboxylate oxygen (the oxygen bound to the metal) and the hydrogen attached to the pyrrole nitrogen of the opposite ligand. Intraligand hydrogen bonding is also observed between the carboxylate oxygen not bound to metal and the hydrogen attached to the methylamino nitrogen of the same ligand. The general structure of the MA_2 complex is shown in Figure I.6.

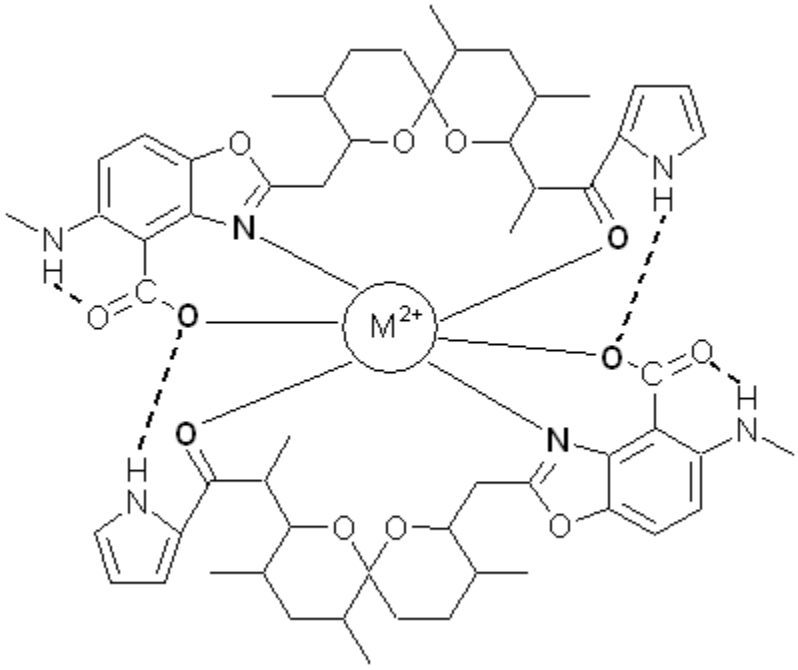

Figure I.6. Solid state structure of MA_2[12-14]

The benzoxazole and ketopyrrole moieties of A23187 give the molecule spectral features suitable for studying protonation and metal complexation properties. In CH_3CH_2OH[15-16], CH_3OH[17-18], 80% CH_3OH/H_2O[19-21], and aqueous suspensions of POPC or DMPC vesicles[22-23] it is possible to differentiate between the anionic, protonated, and metal-bound forms of A23187 by observing the UV-vis absorbance spectra in the 250 to 450 nm wavelength range. The peaks present in either metal titrations with A23187 at fixed pH^* or pH^* titrations of A23187 and a fixed ratio of metal result in a spectrum whose features differ depending on the pH and metal involved in the titration. In general, three wavelength areas in which observable changes in absorbance occur are at ~ 280 nm, 330 nm, and 370 nm. The absorbance observed at 370 has been attributed to the

benzoxazole moiety,[16] while the absorbance at 330 nm is presumably due to a combination of the ketopyrrole and benzoxazole moieties.

Titrations of A23187 with metal illustrate the change in speciation and can be used to determine binding constants, as well as stoichiometry of metal/A23187 complexes at fixed pH^*. The benzoxazole moiety of A23187 is responsible for the fluorescent properties of A23187. In CH_3CH_2OH, the excitation spectrum of A23187 has three peaks, the largest of which is centered at 380 nm.[16] Two smaller peaks are centered at 294 nm and 280 nm. The emission spectrum consists of a single peak centered at 437 nm. Fluorescence has been used to determine metal binding constants at very low concentrations (~ 30 nM).[16, 20] With a very low concentration of ionophore, addition of metal results in formation of the MA^+ complex with little interference caused by formation of MA_2 complex. This set of conditions allows for the stability constant for formation of the MA^+ complex to be measured.

D. Transporting species

A23187 can potentially transport metals across membranes in several ways. For a molecule of A23187 that has a deprotonated carboxylate and a protonated pyrrole nitrogen (the generally accepted state of protonation for A23187 when bound to metal ions), the addition of a divalent cation results in a 1:1 complex with a +1 charge. This complex can either transport across the membrane in electrogenic transport mode, or bind a second ion of -1 charge to become a neutral complex. Ions thought to bind this way include Cl^- and OH^-. Additional methods for achieving a neutral charge are to add a second molecule of $A23187^-$ or to deprotonate the pyrrole nitrogen.

Stability constants for several equilibria involved in the formation of transportable complexes of A23187/M^{2+} have been measured spectroscopically and potentiometrically. For divalent cations, the overall exchange reaction for formation of MA_2 is described in equation I.1 as follows:

$$2HA + M^{2+} \leftrightarrows MA_2 + 2H^+ \qquad \text{Eq. I.1}$$

This overall reaction consists of the acid dissociation reaction, the stepwise formation of a 1:1 A23187:metal complex, and subsequent addition of a second molecule of A23187, as shown in equations I.2- I.6.

$$HA \leftrightarrows H^+ + A^- \qquad \text{Eq. I.2}$$

$$K_a = \frac{[H^+][A^-]}{[HA]} \qquad \text{Eq. I.3}$$

$$A^- + M^{2+} \leftrightarrows MA^+ \qquad \text{Eq. I.4}$$

$$K_{MA} = \frac{[MA^+]}{[M^{2+}][A^-]} \qquad \text{Eq. I.5}$$

$$MA^+ + A^- \leftrightarrows MA_2 \qquad \text{Eq. I.6}$$

In the presence of excess metal past the point of completion of equation I.4 (formation of MA_2 from MA^+), the 2:1 complex breaks down into 1:1 complex, as shown in equation I.7.

$$MA_2 + M^{2+} \leftrightarrows 2MA^+ \qquad \text{Eq. I.7}$$

Stability constants that are pH^*-dependent for formation of the MA^+ complex from HA are found by metal titrations at fixed pH^*. The pH^* at which the titrations are performed is low enough that essentially all of the uncomplexed ionophore exists as the protonated form, or $[HA] \approx [A]_{free,tot}$. Stability constants are extracted from the titration data by plotting changes in absorbance from the first observed equilibrium in UV-vis spectra of the titration as a function of titrant (in this case, M^{2+}). The ratio of $[MA^+]$ to [HA] at each titration point is found by equation I.8[20]:

$$[MA^+]/[HA] = \frac{\Delta S_{obsd}/\Delta S_{max}}{1 - \Delta S_{obsd}/\Delta S_{max}} \qquad \text{Eq. I.8}$$

where ΔS_{obsd} and ΔS_{max} are represented in Figure I.7.

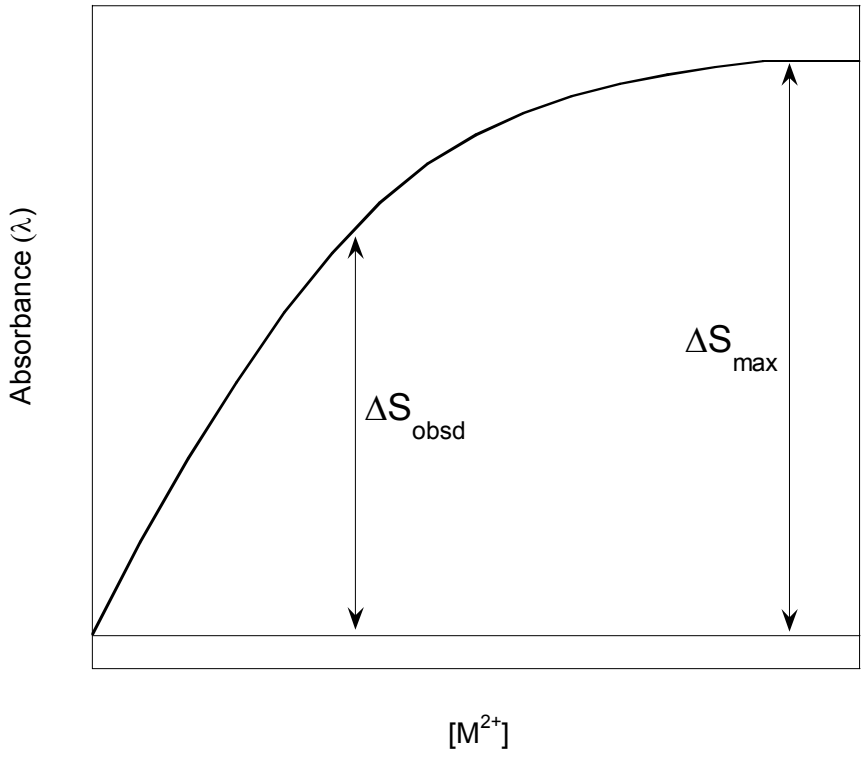

Figure I.7. ΔS_{obsd} and ΔS_{max} in spectrophotometric titrations

ΔS_{obsd} is the difference between the given absorbance at a particular wavelength and ΔS_{max} is the maximum difference in absorbance at the same wavelength. The log of $[MA^+]/[HA]$ is plotted as a function of pM, and the value of the x-intercept is the log K_{MA}', or the apparent stability constant described in equation I.9. The pH^* dependent

K_{MA}' is converted to a pH^*-independent K_{MA} using equations I.9-I.10. The relationship between K_{MA}' and K_{MA} is

$$K_{MA} = K_{MA}' - \log \alpha_A \qquad \text{Eq. I.9}$$

where

$$\alpha_A = [A^-]/([A^-] + [HA]) = K_a/(K_a + a_H^*) \qquad \text{Eq. I.10}$$

and a_H^* is the activity of H^+ in 80% CH_3OH/H_2O.

In cases where $pH^* \leq pK_a - 2$, α_A can be simplified to $\alpha_A \approx K_a/a_H^*$, which simplifies equation I.9 to the equation described in equation I.11.

$$\log K_{MA} = \log K_{MA}' + pK_a - pH^* \qquad \text{Eq. I.11}$$

K_{MA} values determined this way are listed in Table I.1[20]:

cation	log K_{MA}
H^+	7.85 ± 0.05
Ni^{2+}	7.54 ± 0.06
Co^{2+}	7.07 ± 0.06
Zn^{2+}	6.79 ± 0.07
Mn^{2+}	6.08 ± 0.06
Mg^{2+}	4.55 ± 0.05
Ca^{2+}	4.50 ± 0.05
Sr^{2+}	3.86 ± 0.06
Ba^{2+}	3.60 ± 0.06

Table I.1. Stability constants for 1:1 complexes between A23187 and cations in 80% CH_3OH/H_2O[20]

A two phase extraction technique was used by Pfeiffer and Lardy[15] to determine the stability constants of 2:1 A23187:metal complexes. A solution of A23187 in 70% toluene-30% butanol was extracted with an aqueous solution of metal of varying pH, forming MA_2 complex through the reaction described by equation I.12.

$$2HA_{org} + M^{2+}{}_{aq} \leftrightarrows MA_{2org} + 2H^{+}{}_{aq} \qquad \text{Eq. I.12}$$

The amount of metal ion in the organic phase after extraction, found by either $^{45}Ca^{2+}$ scintillation counting or atomic absorption, determined the amount of metal extracted into the organic phase by the ionophore. The stability constant for MA_2 formation (K_{ex}) in equation I.9, was defined by equation I.13.[15].

$$K_{ex} = \frac{[(MA_2)_{org}]\,[(H^+)_{(aq)}]^2}{[(HA)_{(org)}]^2[(M^{2+})_{(aq)}]} \qquad \text{Eq. I.13}$$

The stability constants measured by two-phase extraction are listed in Table I.2.[15]

Divalent Cation	- log $K_{extraction}$
Mg^{2+}	6.9
Ca^{2+}	6.5
Sr^{2+}	9.0
Ba^{2+}	11.8
Mn^{2+}	3.9
Co^{2+}	3.5
Ni^{2+}	4.2
Zn^{2+}	2.9

Table I.2. MA_2 stability constants measured by two-phase extraction for A23187 with divalent cations[15]

The stepwise stability constants for formation of MA^+ (K_1) and MA_2 (K_2) complexes in methanol have been measured by potentiometric titration and are listed in Table I.3.[17,18]

Metal ion	log K_1	log K_2	log K_1 – log K_2
Mn^{2+}	8.9	8.8	-0.1
Fe^{2+}	9.8	9.6	-0.2
Co^{2+}	9.7	9.4	-0.3
Ni^{2+}	10.0	9.2	-0.8
Cu^{2+}	12.5	10.7	-1.8
Zn^{2+}	9.3	9.1	-0.2
Cd^{2+}	9.1	8.6	-0.5
Hg^{2+}	13.6	9.9	-3.7
Pb^{2+}	9.2	- - - -	- - - -
Ca^{2+}	7.8	8.2	+0.4
Mg^{2+}	7.4	8.1	+0.7

Table I.3. Stability constants K_1 and K_2 for the formation of MA^+ and MA_2 in methanol at 25 °C, I = 0.1[17,18]

For each metal ion studied, except for Cu^{2+} and Hg^{2+}, the stepwise stability constant for formation of the MA_2 complex is approximately equal to, and in some cases greater than, the stability constant for formation of the MA^+ complex. This is an unusual relationship between the first and second binding constants. Normally, successive binding constants (K_n, K_{n+1}) decrease as a function of n.[26] For example, the stability constants K_1 and K_2 for several divalent cations binding to the tridentate ligand diethylenetriamine show that K_2 is generally smaller than K_1 by several orders of magnitude, as listed in Table I.4.[27]

Metal ion	log K_1	log K_2	log K_1 – log K_2
Mn^{2+}	4.0	2.9	1.1
Fe^{2+}	6.2	4.3	1.9
Co^{2+}	8.6	6.2	2.4
Ni^{2+}	11.0	8.3	2.7
Cu^{2+}	15.0	5.0	10.0
Zn^{2+}	8.8	5.5	3.3
Cd^{2+}	8.0	5.8	2.2
Pb^{2+}	8.5	1.9	6.6

Table I.4. Stability constants K_1 and K_2 for diethylenetriamine and divalent cations[27]

There are several factors that contribute to successively smaller stability constants associated with ligand molecules binding consecutively to a metal ion. The entropy associated with binding of ligand to metal decreases with each additional ligand bound, which makes the binding of additional ligand molecules increasingly unfavorable.[26] Steric constraints impose restrictions on the possible locations each additional ligand may bind, which reduces the chance that the incoming ligand will be in a location available for complexation.[26] A third consideration is that with each additional ligand bound (in place of a solvent molecule) the chances increase that a solvent molecule will replace a ligand on the metal ion.[26] Additionally, in the case of a negatively charged ligand (such as deprotonated A23187) binding to a positively charged metal ion, the first ligand binding is likely to be most favorable due to the difference of charge between the ligand and metal ion. However, upon binding, the complex becomes less positive and thus less attractive to an second negatively charged ligand molecule. Each of these factors can contribute to the trend observed for many ligands to have successively smaller stability constants for stepwise complexation with a metal ion.

The observation that the stability constants for A23187 and divalent cations do not exhibit this trend indicates that there is cooperativity observed in binding of the second ligand to the metal, which is likely due to the interligand hydrogen bonds that serve to stabilize the 2:1 complex.[24,25]

Chapman et al.[20] found a third equilibria present in spectrophotometric titrations of A23187 at fixed pH* with the transition metals Zn^{2+}, Co^{2+}, and Ni^{2+} in 80% methanol. At suitably high pH*, the 1:1 or 2:1 A23187/M^{2+} complex forms a third species postulated to be species MAOH, formed through equations I.14 or I.15.

$$MA^{+} + OH^{-} \leftrightarrows MAOH \qquad \text{Eq. I.14}$$

$$MA_2 + OH^{-} \leftrightarrows MAOH + A^{-} \qquad \text{Eq. I.15}$$

The equilibrium between ZnAOH and ZnA^{+} was determined by saturating a solution of A23187 with Zn^{2+} (to ensure that all A23187 was complexed in a 1:1 ratio with Zn^{2+}) and then titrating the solution with OH^{-}. This produced spectra with a single isosbestic point, and a plot of the data shows a linear relationship between log [ZnAOH]/[ZnA^{+}] and - log [OH^{-}], with a slope of -1.0. The stability constant for formation of ZnAOH from ZnA^{+} is found by determining the value of –log [OH^{-}] when log [ZnAOH]/[ZnA^{+}] = 0. This value is 7.65 for formation of ZnAOH.[20]

Other metals studied in this manner either did not appear to form the MAOH complex, or conditions required by the studies did not permit observation of the hydroxide complex. These metals include Mn^{2+}, Ca^{2+}, Mg^{2+}, and Sr^{2+}.[20]

E. Solvents

The binding properties of A23187 have been studied in many solvents, including methanol, ethanol, toluene-butanol (70%-30%) various ratios of methanol/water, and in suspensions of unilamellar vesicles composed of palmitoyloleoylphosphatidylcholine (POPC). The vesicle solutions serve as a simplified model for cell membranes. Like cell membranes, they form a bilayer with a hydrophilic "head" pointed outward from the bilayer and a hydrophobic "tail" comprising the interior of the bilayer. The structure of POPC is shown below in Figure I.8, along with its role in the membrane bilayer.

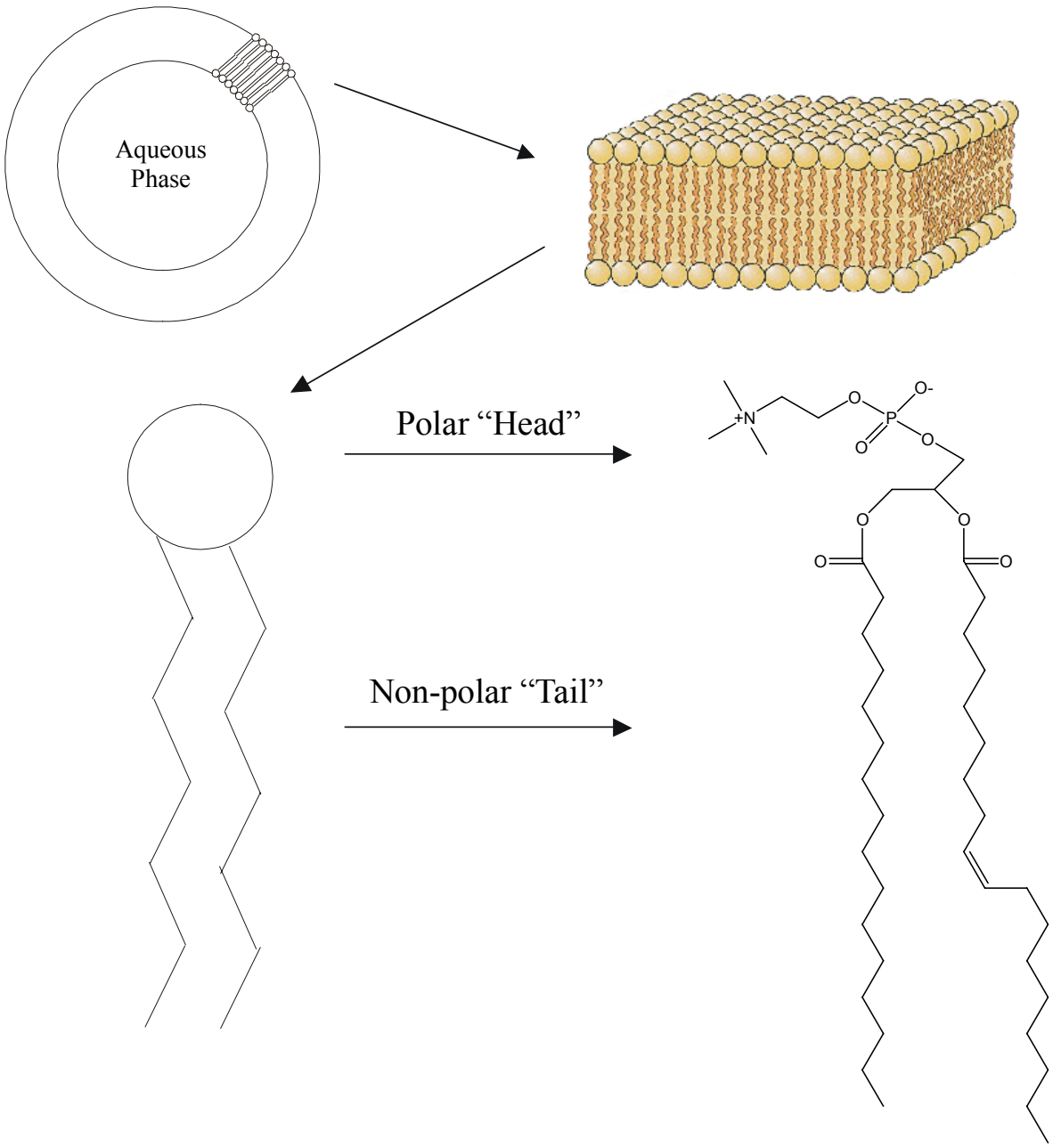

Figure I.8. Structure of POPC and vesicle modeling of cell membranes

A thorough study of POPC vesicles proved them to be a suitable model for cell membranes.[23] A freeze-thaw extrusion method was developed to produce unilamellar vesicles of uniform size. These vesicles were used in transport studies in which a chelating reporter dye trapped inside the vesicles was monitored by UV-vis absorbance to track the transport of metal from the exterior to the interior of the vesicles by A23187.

Several solvent systems were investigated to find an appropriate homogenous solution in which to carry out stability studies of the metal/A23187 complexes. Appropriate solvents must possess properties of both the polar and non-polar regions of the ionophore. Most model solvent systems investigated were various ratios of methanol and water, however, other studies incorporated acetonitrile, ethanol, or toluene-butanol (70%-30%). The ratio of 80% methanol:20% water (prepared gravimetrically) proved a suitable model due to the similarity of binding constants found in the solvent and those found in POPC suspensions.[24] Thomas et al. also found that circular dichroism spectra of NiA_2 and MgA_2 in POPC suspensions were very similar to those in 80% methanol.[25]

F. Derivatives of A23187

There are several main classes of derivatives of A23187. The benzoxazole ring may contain additional substituents,[28,29] the methylamino group at the 3 position of the benzoxazole ring[29] may either be altered or replaced, or the pyrrole moiety may contain substituents.[28] The first class, the benzoxazole substituent derivatives, contains the commercially available 4-BrA23187, shown in Figure I.9.

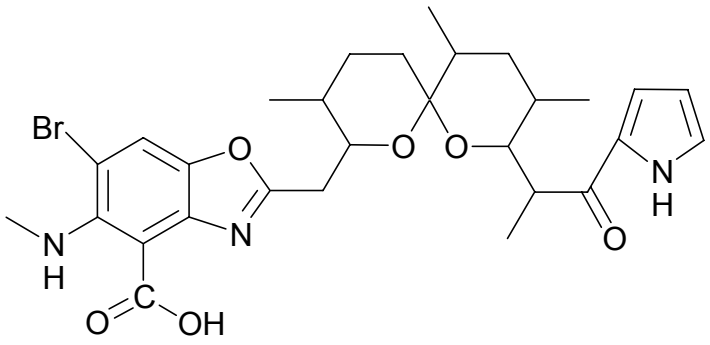

Figure I.9. Structure of 4-BrA23187

Like A23187, this ionophore is used primarily as a calcium ionophore. However, the presence of a bromine atom on the benzoxazole ring quenches the fluorescence observed in the parent compound.[30] This feature allows 4-BrA23187 to be used in studies that employ other fluorophores for detection purposes without interference. Binding properties of this derivative for H^+ and Mg^{2+} in CH_3OH are listed in Table I.5.[31]

Equilibrium	log K A23187	log K 4-BrA23187
$H^+ + A^- \leftrightarrows HA$	11.16	9.04
$Mg^{2+} + A^- \leftrightarrows MgA^+$	7.50	6.0
$Ca^{2+} + A^- \leftrightarrows CaA^+$	8.20	6.08
$Mn^{2+} + A^- \leftrightarrows MnA^+$	6.38	5.03
$Zn^{2+} + A^- \leftrightarrows ZnA^+$	8.24	6.72

Table I.5. Equilibrium constants for A23187 and 4-BrA23187 in methanol at 25 °C, I = 0.1[31]

From the data above it is evident that the presence of the bromine at the 4 position of A23187 lowers binding constants for all cations considered. The halogen may affect binding by either imposing steric effects, inductive effects, or both upon the molecule.

Pfeiffer et al. published the results of a 4-BrA23187 transport study in 1996.[30] By assembling unilamilar 1-palmitoyl-2-oleoyl-*sn*-glycerophosphatidylcholine (POPC) vesicles loaded with fluorescent indicator Quin-2, they were able to monitor transport of divalent cations from aqueous solution outside the vesicle to the interior by the ionophore. Once inside the vesicle, Quin-2 chelated the metal, an event monitored by change in absorbance properties of the indicator. The change in absorbance at 264 nm, as compared to a wavelength of constant absorbance, was monitored with respect to time,

and a kinetic plot of μM cation transported as a function of time is produced. The results of these studies for A23187 and 4-BrA23187 are shown in Figure I.10.

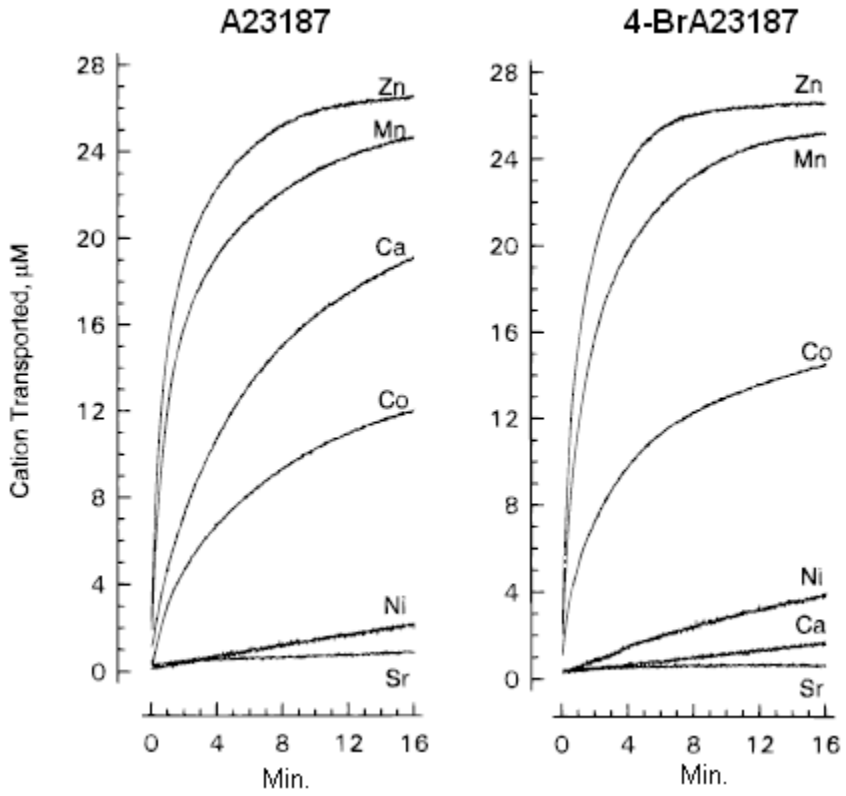

Figure I.10. Transport studies of 0.1 μM A23187 and 0.1 μM 4-BrA23187 for Zn^{2+}, Mn^{2+}, Ca^{2+}, Co^{2+}, Ni^{2+}, and Sr^{2+} into POPC vesicles at pH 7.0.[30]

The transport selectivity among the cations studied is apparent from the graphs. A23187 transports Zn^{2+} and Mn^{2+} with highest selectivity, but it also transports Ca^{2+} and Co^{2+} at significant rates as well. The transport data for 4-BrA23187 indicates that the derivative is much more selective for the metals Zn^{2+} and Mn^{2+} over Ca^{2+} than the parent compound. The rates of transport of Zn^{2+}, Mn^{2+}, and Co^{2+} are approximately equal for both ionophores, but the transport rate of Ca^{2+} is much lower for 4-BrA23187 than for A23187. The basis for the difference in selectivity observed is investigated through further transport studies. The effect of ionophore concentration on the rate of transport of metal into POPC vesicle is measured. The data is plotted as log initial rate (μM/sec) as a function of log [ionophore] (μM). As shown in equation I.16, The slope of the resulting line suggests the stoichiometry of the transporting species.

$$\text{rate} = k[\text{ionophore}]^x[\text{metal}]^y \qquad \text{Eq. I.16}$$

Since [metal] is constant, equation I.16 can be re-written as equation I.17:

$$\text{rate} = k' [\text{ionophore}]^x \qquad \text{Eq. I.17}$$

where $k' = k [\text{metal}]$.

The log function of both sides results in equation I.18.

$$\log \text{rate} = \log k' + x \log [\text{ionophore}] \qquad \text{Eq. I.18}$$

If the log rate is graphed as a function of log [ionophore], the slope x gives the order of the transport reaction with respect to the ionophore. The stoichiometries of A23187 and 4-BrA23187 with respect to transport of Zn^{2+}, Mn^{2+}, and Ca^{2+} at pH 6.0, 7.0 and 8.0 are listed in Table I.6.[30]

Ionophore	Slope at pH 6.00	Slope at pH 7.00	Slope at pH 8.00
A23187			
Zn^{2+}	1.42	1.46	1.31
Mn^{2+}	1.52	1.56	1.54
Ca^{2+}	1.96	1.98	1.80
4-BrA23187			
Zn^{2+}	1.37	1.40	1.12
Mn^{2+}	1.42	1.46	1.25
Ca^{2+}	1.65	1.85	1.71

Table I.6. Stoichiometries of A23187 and 4-BrA23187 as measured by transport data[30]

For a species that transports metal solely as the 2:1 ligand:metal complex, the stoichiometry observed would be 2. A species that transports solely as a 1:1 ligand:metal complex would have a slope of 1. A species that transported as a mix of the 2:1 complex and 1:1 complex would have a slope between 1 and 2. This data indicates that the Ca/A23187 transport complex is predominantly 2:1 for pH values 6.0 and 7.0, but may be

somewhat more mixed (2:1 and 1:1) at pH 8. Zn/A23187 transport is a mixture of 2:1 and 1:1 for pH values 6.0 and 7.0; however, at pH 8 the fraction transported by the 1:1 complex is increased. The ratio of 1:1 and 2:1 transport complexes for Mn/A23187 are unaffected by pH.

4-BrA23187/Ca transport also uses mainly the 2:1 complex at all pH values; however, each slope is smaller than the corresponding slope for Ca/A23187. Additionally, the slope at pH 7.0 is greater than the slope at either 6.0 or 8.0. The Zn/4-BrA23187 transport data indicates that at pH 6.0 and 7.0 there is slightly more 1:1 transporting species than 2:1, however, at pH 8.0, transport is primarily 1:1. The same trend is observed for Mn/4-BrA23187 transport, however, slopes are slightly higher for all pH values than for the Zn/4-BrA23187 system.

Overall, the transport data indicates that there are significant differences in the stoichiometry of the transporting species of A23187 and 4-BrA23187, and that pH alters the ratio of 2:1 and 1:1 complexes involved for each metal ion.

The 4-ClA23187 derivative, discussed in this work, differs from the 4-BrA23187 only by the size and electronegativity of the halogen substituent. This work aims to investigate the effect of altering the size and electronegativity of the substituent at the 4 position.

Another class of derivatives of A23187, shown in Figure I.11, consists of compounds with different substituents at position 3 (R1) of the benzoxazole moiety.

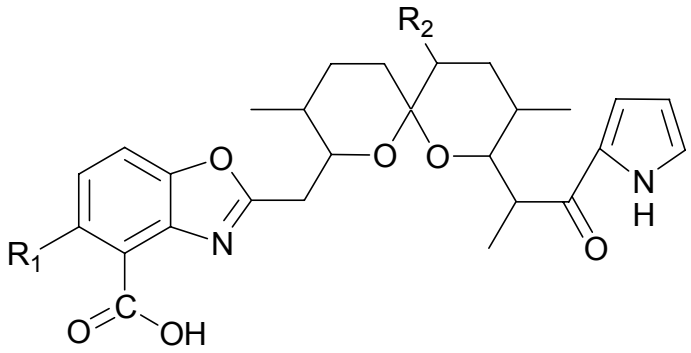

	R_1	R_2
A23187	$NH(CH_3)$	CH_3
cezomycin	H	CH_3
X-14885A	OH	H
3-OH A23187	NH_2	CH_3
3-CH_3 A23187	CH_3	CH_3
3-$N(CH_3)_2$- A23187	$N(CH_3)_2$	CH_3
3-$NHCOCH_3$- A23187	$NHCOCH_3$	CH_3

Figure I.11. Derivatives of A23187

The naturally occurring antibiotic cezomycin belongs to this class.[29] In this molecule, the entire methylamino substituent is replaced with a hydrogen atom. This prevents some of the intra-molecular hydrogen bonding observed in the parent compound from occurring. Another member of this group is X-14885A, which is also a naturally occurring molecule. This molecule has a hydroxyl group in place of the methylamino

group, and does not have a methyl group attached to carbon in the 15 position (in the spiroketal region). There are many synthetic members of this group as well that replace the methylamino group with various substituents: OH, CH_3, $N(CH_3)_2$, and $NHCOCH_3$.[29]

A common feature of these natural and synthetic derivatives of A23187 is the inability to form inter- and intra-molecular hydrogen bonds. These substituents also potentially affect the electronegativity of the carboxylate oxygen atoms. In 1983, Prudhomme et al. determined binding properties for many of these derivatives that include the pK_a's of the compounds in 70% CH_3OH/H_2O and metal extraction constants in a two phase system consisting of H_2O-toluene-butanol.[29] The pK_a measured refers to the deprotonation reaction of the carboxylic acid functionality of A23187, described in equations I.19 and I.20.

$$HA \leftrightarrows H^+ + A^- \qquad \text{Eq. I.19}$$

$$K_a = \frac{[H^+][A^-]}{[HA]} \qquad \text{Eq. I.20}$$

To determine the extraction constants, the pH of the aqueous solution is varied and the ratio of $[M^{2+}]$/[[ionophore] is plotted as a function of aqueous pH using the same procedure as Pfeiffer and Lardy.[x] The data yields a sigmoid curve in which the inflection point represents the pH value at which half-saturation ($[M^{2+}]$:[ionophore] = 0.25) of the reaction described in equations I.21 and I.22 occurs. Data at this point are used to determine the overall extraction constants summarized in Table I.7.[29]

$$2HA_{org} + M^{2+}_{aq} \leftrightarrows MA_{2org} + 2H^{+}_{aq} \qquad \text{Eq. I.21}$$

$$\beta_{extraction} = \frac{[H^+]^2[(A_2M)_{org}]}{[(AH)_{org}]_2[M^{2+}]} \qquad \text{Eq. I.22}$$

Compound	pK_a in 70% CH_3OH	-log $\beta_{extraction}$ Ca^{2+}	-log $\beta_{extraction}$ Mg^{2+}
A23187	7.30	6.4	6.9
cezomycin	6.02	5.1	5.9
3-CH_3 A23187	5.19	7.7	8.1
3-OH A23187	4.40	1.7	2.3
3-$N(CH_3)_2$-A23187	7.10	9.4	10.3
3-$N(CH_3)COCH_3$-A23187	4.95	5.5	6.9
X-14885A	4.48	1.7	2.3

Table I.7. pK_a's in 70% CH_3OH/H_2O and overall extraction constants (-log β) in a water-toluene-butanol (70:30) two phase system[29]

All derivatives have lower pK_a values for the carboxylic acid relative to A23187, although some substituents affect the pK_a more than others. Each ionophore has extraction properties that are similar for Ca^{2+} and Mg^{2+}, and their ability to extract these metal ions are varied relative to the parent compound A23187. The derivatives with the most improved extraction ability over A23187 (3-OH A23187 and X-14885A) have lower pK_a's than the parent compound and the ability to form an intraligand hydrogen

bond with a carboxylate oxygen atom. The ionophore with the poorest ability to transport these metal ions (3-N$(CH_3)_2$-A23187) has a bulkier amine group at R_1 than A23187, a carboxylic acid group that is only slightly more acidic than that of A23187, and an inability to form an intraligand hydrogen bond with a carboxylate oxygen atom.

A third class of derivatives of A23187 involves the pyrrole end of the molecule. 23,24-Br_2A23187, a subject of study in this work, belongs to this class, as do several other derivatives shown in Figure I.12.

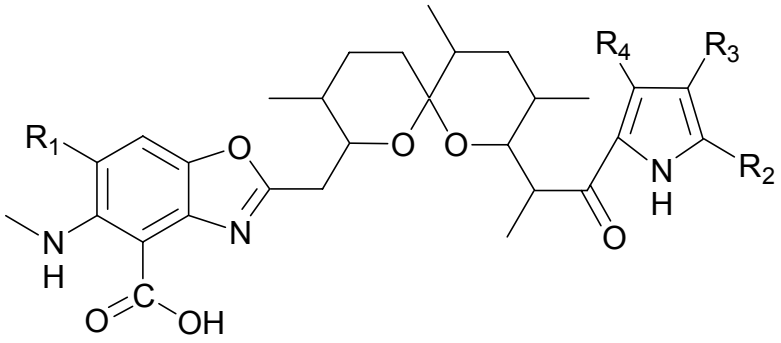

Ionophore	R_1	R_2	R_3	R_4
23-BrA23187	H	H	Br	H
23,24-Br_2A23187	H	Br	Br	H
4,23-Br_2A23187	Br	H	Br	H
4,22,23,24-Br_4A23187	Br	Br	Br	Br
23-IA23187	Br	H	I	H
23,24-I_2A23187	H	I	I	H

Figure I.12. Pyrrole substituent derivatives of A23187[28]

These derivatives also affect the ability of the molecule to form interligand hydrogen bonds by interfering with the steric, electronic, or a combination of these properties of the pyrrole group. These derivatives include bromination or iodination of various carbons on the pyrrole moiety, or a combination of bromination of the benzoxazole ring (position 4) and the pyrrole ring.[28] While all of these derivatives have been synthesized,[28] their metal binding properties have not been previously studied.

G. Summary of Studies

Selective ionophores have potential in research applications, such as in isolated destruction of a single metal ion gradient, metal ion detection by spectroscopic methods, and toxic metal ion removal from biological systems without disruption of essential metal ion concentrations. A23187 was generally thought to be such an ionophore for the transport of Ca^{2+} until studies showed that A23187 transports Zn^{2+}, Mn^{2+}, and Cd^{2+} at greater rates than it transports Ca^{2+}.

The unique properties of the 2:1 metal ion complex of A23187, generally thought to be the transporting species for this ionophore, focus on the stabilization of the complex by inter-molecular hydrogen bonding between the two ionophores of the complex. The ability of a derivative to destabilize the hydrogen bond network is thought to result in altered transport selectivity that would transport metal ions that could more easily form neutral 1:1 complexes with the derivatized ionophore. One derivative in particular,

4-BrA23187, has greatly increased selectivity for transport of Zn^{2+} and Mn^{2+} over Ca^{2+}. It is not clear if the difference is due to inductive or steric effects, or a combination of the two.

This work focuses on the study of two derivatives of A23187. Both are thought to disrupt the hydrogen bond network of the 2:1 metal ion complex by addition of halogen atoms to either end of the molecule, near the location of the hydrogen bond donors and acceptors. The first derivative, 4-ClA23187, is expected to have transport properties similar to that of 4-BrA23187. However, since the chlorine atom is both smaller, and more electronegative, than the bromine atom, an increase in transport selectivity would indicate a larger role of the electronegativity, rather than size, of the substituent at the 4 position of the benzoxazole ring.

This project is divided into three parts. The first focuses on structural studies of A23187. The structures of free A23187 and several metal ion complexes are studied in solid state by X-ray crystallography and in solution (polar and non-polar) by circular dichroism (CD) and UV-vis spectroscopy. Theses studies provide information about the coordination and stereochemistry of the metal ion complexes, as well as the effect of solvent on the complex, and the ability of the complex to form inter-molecular hydrogen bonds under various conditions. Additionally, the protonation equilibria of A23187 were studied at a higher pH^* range than previous studies by pH^* titration followed by UV-vis spectroscopy.

The second component of the project includes the synthesis and characterization of binding and transport properties of 4-ClA23187. The synthesis protocol, from Debono et al.,[32] consists of a one-pot reaction, purification by extraction and crystallization, and

characterization by TLC, +ESI-MS, ^{1}H NMR, and X-ray crystallography. Binding and properties are characterized by titrations of the ionophore with metal ion (at fixed pH*) and as a function of pH* (at fixed metal ion concentration). The titrations are followed by UV-vis spectroscopy. Titrations as a function of pH* are also performed without metal ion present to determine the protonation equilbria for the ionophore.

Transport selectivity of 4-ClA23187 for several metal ions of interest is determined through the use of vesicles loaded with a chelating reporter dye. The vesicles, present as a suspension in aqueous media, are intended to mimic the environment of a cell membrane.

The third part of this study is the synthesis and characterization of 23,24-Br_2A23187. Like 4-ClA23187, 23,24-Br_2A23187 is synthesized and purified according to protocol described in a paper by Debono et al.[32] After a one-pot synthesis the product is purified by extraction and chromatography and characterized by TLC, +ESI-MS, ^{1}H NMR, and X-ray crystallography. The binding properties of 23,24-Br_2A23187 are studied by titrations of the ionophore with metal ion (at fixed pH*) and titrations of the ionophore with base (at a fixed metal ion concentration), both of which are followed by UV-vis spectroscopy. Protonation equilibria are determined by titration of the ionophore as a function of pH* with no metal present, followed by UV-vis spectroscopy.

The transport selectivity of 23,24-Br_2A23187 is determined by following the rate of metal ion transport in a vesicle suspension in aqueous medium. A chelating reporter dye within the vesicle monitors the rate at which each metal ion is transported.

REFERENCES

1. Outten, C. E. and O'Halloran, T. V. *Science* **2001**, *292*, 2488-2491.

2. Westley, J. W. in *Polyether Antibiotics: Naturally Occurring Acid Ionophores*; Westley, J. W., Ed.; Marcel Dekker: New York **1982**; Vol 1.

3. Painter, G. R. and Pressman, B. C. in *Metal Ions in Biological Systems*; Sigel, H., Ed; Marcel Dekker: New York **1973**; Vol. 19.

4. Hamidinia, S. A., Tan, B., Erdahl, W. L., Chapman, C. J., Taylor, R. W., and Pfeiffer, D. R. *J. Biol. Chem*. **2002**, *277*, 38111-38120.

5. Hamidinia, S. A., Shimelis, O. I., Tan, B., Erdahl, W. L., Chapman, C. J., Taylor, R. W., and Pfeiffer, D. R. *Biochemistry* **2004**, *43*, 15956-15965.

6. Erdahl, W. L., Chapman, C. J., Taylor, R. W., and Pfeiffer, D. R. *J. Biol. Chem*. **2000**, *275*, 7071-7079.

7. Dutton, C. J., Banks, B. J., and Cooper, C. B., In *Natural Product Reports* **1995**, *12*, 165-181.

8. Chaney, M. O., Demarco, P. V., Jones, N. D., and Occolowitz, J. L. *J. Am. Chem. Soc*. **1974**, *96*, 1932-1933

9. Pfeiffer, D. R., Taylor, R. W., and Lardy, H. A. *Ann. N. Y. Acad. Sci*. **1978**, *307*, 402-423.

10. Deber, C. M., and Pfeiffer, D. R. *Biochemistry* **1976**, *15*, 132-141.

11. Faure, R., Chauvet-Monges, A. M, and Crevat, A. *Spectrosc. Lett*. **1989**, *22*, 945-954.

12. Smith, G. D. and Duax, W. L. *J. Am. Chem. Soc*. **1976**, *98*, 1578-1580.

13. Baker, E., Maslen, E. N., Watson, K. J., and White, A. H. *J. Am. Chem. Soc*. **1984**, *106*, 2860-2864.

14. Alleaume, M., and Barrans, Y. *Can. J. Chem.* **1985**, *63*, 3482-3485.

15. Pfeiffer, D. R., and Lardy, H. A. *Biochemistry* **1976**, *15*, 935-943.

16. Pfeiffer, D. R., Reed, P. W., and Lardy, H. A. *Biochemistry* **1974**, *13*, 4007-4014.

17. Ouahabi, A., Tissier, M., Pointud, Y., Jeminet, G., and Juillard, J. *J. Chem. Phys*. **1997**, *94*, 782-798.

18. Tissier, C. Julliard, J., Boyd, D. W., and Albrecht-Gary, A. M. *J. Chim. Phys*., **1985**, *82*, 899-906.

19. Tissier, M. Ouahabi, A., Jeminet, G., and Julliard, J. *J. Chim. Phys*., **1993**, *90*, 595-608.

20. Chapman, C. J., Puri, A. K., Taylor, R. W., and Pfeiffer, D. R. *Biochemistry* **1987**, *26*, 5009-5018.

21. Taylor, R. W., Pfeiffer, R. W., Chapman, C. J., Craig, M. E., and Thomas, T. P. *Pure and Appl. Chem.* **1993**, *65*, 579-584.

22.Chapman, C. J., Puri, A. K., Taylor, R. W., and Pfeiffer, D. R., *Arch. Biochem. Biophys*. **1990**, *281*, 44-57.

23. Kauffman, R. F., Taylor, R. W., and Pfeiffer, D. R. *Biochemistry* **1982**, *21*, 2426-2435.

24. Kauffman, R. F., Chapman, C. J., and Pfeiffer, D. R. *Biochemistry* **1983**, *83*, 3985-3992.

25. Thomas, T. P. *Ph.D Dissertation* **1991**, University of Oklahoma, Norman, OK.

26. Basolo, F. and Johnson, R. *Coordination Chemistry: The Chemistry of Metal Complexes*; Johnsen, R., Ed.; W. A. Benjamin, Inc.: New York **1964**.

27. Smith, R. M. and Martell, A. E. **1976** *Critical Stability Constants*, Plenum, New York.

28. Debono, M., Molloy, R. M., Dorman, D. E., Paschal, J. W., Babcock, D.F., Deber, C. M., and Pfeiffer, D. R. *Biochem*., **1981**, *20*, 6865-6872.

29. Prudhomme, M., Dauphin, G., and Jeminet, G. *J. Antibiot*. **1986**, *39*, 922-933.

30. Erdahl, W. L., Chapman, C. J., Wang, E., Taylor. R. W., and Pfeiffer, D. R. *Biochemistry* **1996**, *35*, 13817-13825.

31. Schmid, N. *Rapport du Stage,* **1988**, Laboratoire de Chimie Physique et d'Electroanalyse, Strasbourg, France.

Chapter II

EXPERIMENTAL

A. Reagents

Solvents:

1. Deionized-distilled water (ddH_2O): Deionized water from the tap was distilled using a Corning Megapure MP-3A distillation apparatus.

2. Methanol (CH_3OH): Methanol was purchased from Fisher (reagent grade) and distilled.

3. Chloroform ($CHCl_3$): Chloroform was purchased from Fisher (reagent grade) and distilled.

4. Carbon tetrachloride (CCl_4): Carbon tetrachloride was purchased from Fisher (reagent grade, anhydrous) and used as is.

5. 80% Methanol/water: 80% CH_3OH/H_2O was prepared by weight using distilled CH_3OH and dd H_2O.

6. Deuterated chloroform ($CDCl_3$): Deuterated chloroform (99.8% D) was purchased from Cambridge Isotope Laboratories and used as is.

7. Glacial acetic acid: Glacial acetic acid (99.7%) was purchased from Fisher and used as is.

8. 95% Ethanol: 95% CH_3CH_2OH/H_2O (w/w) was prepared by weight with

absolute CH_3CH_2OH (purchased from Fisher) and dd H_2O.

9. 70% Perchloric acid: 70% $HClO_4/H_2O$ (w/v) was purchased from Fisher and used as is.

Metal Solutions: Standardization of all metal solutions were carried out by EDTA titrations using procedures described by Vogel.[1]

1. Zinc Perchlorate ($Zn(ClO_4)_2$): Solutions were made by weighing a desired amount of ZnO (Alfa Aesar, 99.99%) to a small amount of ddH_2O and stirring to form a paste. 70% $HClO_4$ was added dropwise until a stoichiometric amount of acid was added to the paste. This converted ZnO into $Zn(ClO_4)_2$ which was transferred to a volumetric flask and diluted to the desired concentration. Zn^{2+} solutions were standardized by titration with EDTA at pH 10 (achieved by addition of NH_3/NH_4^+ buffer) in the presence of indicator eriochrome black T (EBT).

2. Calcium perchlorate ($Ca(ClO_4)_2$): Solutions were made by adding a small amount of water to $CaCO_3$ (Aldrich, 99.99%) to form a paste, and then adding a stoichiometric amount of concentrated $HClO_4$ to the paste, resulting in the following reaction:

$$CaCO_3 + 2HClO_4 \rightarrow Ca^{2+} + H_2CO_3 + 2ClO_4^- \qquad \text{Eq. II.1}$$

The carbonate species further reacted to ultimately form CO_2 that is released as a gas to near completion upon heating the solution:

$$H_2CO_3 \rightarrow H_2O + CO_2\uparrow \qquad \text{Eq. II.2}$$

The Ca^{2+} solution was standardized by EDTA at pH 10 (achieved by addition of NH_3/NH_4^+ buffer) using the indicator methylthymol blue (MTB).

3. Copper chloride ($CuCl_2$): 99.995% copper chloride was purchased from Aldrich and used as is. Solutions were standardized by EDTA using hexamine buffer (pH 6) and fast sulphon black (FSB) indicator.

4. Bismuth nitrate ($Bi(NO_3)_3 \cdot 5H_2O$): 99.99% bismuth nitrate was purchased from Aldrich and used as is. Solutions were standardized using a back titration of EDTA, involving addition of a known amount of Cu^{2+} at pH 6 (achieved through addition of hexamine buffer) and using the indicator napthylazoxine S (NAS).

5. Zinc perchlorate ($Zn(ClO_4)_2 \cdot 6H_2O$): 99.999% Zinc perchlorate was purchased from Alfa Aesar and used as is. Solutions were standardized in the same way as described for ZnO.

6. Indium perchlorate ($In(ClO_4)_3 \cdot xH_2O$): 99.995% indium perchlorate from Aldrich and used as is. The solution was standardized by back titration of EDTA (to prevent precipitation of the indium as $In(OH)_3$ at the pH desired to perform the titration). As the

In-EDTA complex, the pH could be raised to 6 through incremental additions of NH_3/NH_4^+ buffer, and titrated with a standardized Cu^{2+} solution using the indicator NAS.

7. Gallium nitrate ($Ga(NO_3)_3 \cdot xH_2O$): 99.9% gallium nitrate was purchased from Aldrich and used as is. The solution was standardized with EDTA at pH 6 (hexamine buffer) and indicator xylenol orange (XO) or MTB.

8. Yttrium nitrate ($Y_2(NO_3)_3$): Yttrium oxide (Aldrich, 99.999%) was mixed with a small amount of ddH_2O to form a paste, then treated with a stoichiometric amount of HNO_3 and heat to dissolve. The solution was standardized by back titration using EDTA and standardized Cu^{2+} at pH 6 using hexamine buffer and the indicator XO or MTB.

9. Cadmium perchlorate ($Cd(ClO_4)_2$): 99.995% pure cadmium nitrate was purchased from Aldrich and used as is. The solution was standardized by titration with EDTA using NH_3/NH_4 buffer at pH 10 and the indicator EBT.

10. Gadolinium nitrate ($Gd_2(NO_3)_3$): Gadolinium oxide (Aldrich, 99.99%) was mixed with a small amount of ddH_2O to form a paste. The paste was dissolved by addition of a stoichiometric amount of concentrated HNO_3 followed by heating. The concentration of Gd^{3+} in the solution was calculated by weight.

11. Cobalt chloride ($CoCl_2$): 99.99% cobalt chloride was purchased from Aldrich and used as is. The stock solution was standardized by direct titration with EDTA using the buffer hexamine (pH 6) and indicator MTB.

12. Magnesium chloride ($MgCl_2$): 99.99% magnesium chloride was purchased from Aldrich and used as is. The stock solution was standardized by direct titration with EDTA at pH 10 (using NH_3/NH_4^+ buffer) and the indicator EBT.

13. Magnesium perchlorate ($Mg(ClO_4)_2$): $Mg(OH)_2MgCO_3 \cdot 3H_2O$ (Aldrich, 99.99%) was mixed with a small amount of ddH_2O to form a paste. The paste was dissolved by treatment with a slight excess of perchloric acid. The solution was standardized by direct titration with EDTA using pH 10 buffer NH_3/NH_4 and indicator EBT.

14. Manganese (II) chloride tetrahydrate ($MnCl_2 \cdot 4H_2O$): 99.99% manganese chloride tetrahydrate was purchased from Aldrich as used as is. The stock solution was standardized by direct titration with EDTA at pH 6 (using hexamine buffer) and the indicator MTB.

15. Silver perchlorate ($AgClO_4 \cdot H_2O$): 99.999% silver perchlorate was purchased from Aldrich and used as is.

16. Lanthanum perchlorate ($La(ClO_4)_3$): La_2O_3 (99.99%, Aldrich) was mixed with a small amount of ddH_2O to form a paste. The paste was dissolved by treatment with a slight excess of perchloric acid.

17. Lutetium chloride hexahydrate ($LuCl_3 \cdot 6H_2O$): lutetium chloride was purchased from Aldrich and used as is.

18. Lead perchlorate hydrate ($PbClO_4 \cdot H_2O$): 99.995% lead perchlorate was purchased from Aldrich and used as is.

Acid washed glassware: All glassware used in experiments involving A23187 or metals were washed, soaked overnight in an acid bath of composition 3:1 v/v sulfuric acid: nitric acid, rinsed five times with distilled water, and dried prior to use.

EDTA: The disodium salt of ethylenediaminetetraacetic acid (Na_2H_2EDTA) was purchased from Aldrich and standardized by titration with a solution prepared from a primary standard solution made from oven-dried $CaCO_3$.

Tetramethylammonium hydroxide: Solutions of approximately 0.01 M were prepared by dissolving $(CH_3)_4NOH$ purchased from Fisher in 80% CH_3OH/H_2O, along with 0.04 Et_4NClO_4 to maintain the total ionic strength of the solution at 0.05 M. The base was standardized by titration with oven-dried, primary standard grade potassium hydrogen phthalate (KHP). Freshly distilled CH_3OH and CO_2-free ddH_2O (prepared by boiling ddH_2O for at least 10 minutes) were used in all base solutions. Base solutions were stored under Ar or N_2 at all times to minimize contamination by CO_2.

Tetraethylammonium perchlorate (TEAP): $(CH_3CH_2)_4NClO_4$ was prepared by stoichiometric addition of 70% $HClO_4$ to a solution of 20% $(CH_3CH_2)_4NOH$ (Aldrich). The resulting product was recrystallized from hot water four times, dried under vacuum, and stored in a desiccator.

Buffers:

1. MES: 2-(*N*-Morpholino)ethanesulfonic acid was purchased from Sigma Chemical Co. and used without further purification.
2. MOPS: 3-(*N*-Morpholino)propanesulfonic acid was purchase from Sigma Chemical Co. and used without further purification.

3. DESPEN: *N-N'*-diethyl-*N-N'*-bis(sulfopropyl)ethylendiamine was purchased from GFS Chemicals and used without further purification.

4. PIPPS: *N,N'*-bis(3-Propanesulfonic acid) was purchased from GFS Chemicals and used without further purification.

5. DEPP: *N,N'*-Diethylpiperazine was purchased from GFS Chemicals and without further purification. As a liquid, DEPP was measured by volume rather than by weight. The purity of DEPP was confirmed by ^{1}H NMR, and the density measured by weighing 1 mL aliquots. The average density of neat DEPP was determined to be 0.85 g/mL. This density was used in calculations to determine the correct volume of DEPP required to prepare buffer solutions at the desired concentration.

A23187: [6,*S* - 6α (2*S**, 3*S**), 8β (*R**), 9β, 11α]-5-(methylamino)-2-[[3,9,11-trimethyl-8-[1-methyl-2-oxo-2(1*H*-pyrrol-2-yl) ethyl]-1,7-dioxaspiro [5,5] undec-2-yl] methyl]-4-benzoxazole carboxylic acid. The structure of A23187, also known as calcimycin, is shown in Figure II.1. A23187 was obtained from Fermentek as the free acid (HA). Purity was confirmed by positive and negative electrospray ionozation mass spectrometry (ESI-MS). The positive ion mass spectrum showed two peaks: one at 524 m/z and one at 546 m/z, due to, respectively, the H^+ and Na^+ adducts of A23187 (M = 523). The negative ion mass spectrum showed one peak at 522 m/z, due to the anionic form of A23187. Thin layer chromatography (TLC) also indicated that sources of HA arrived pure. Silica gel plates were spotted with HA dissolved in $CHCl_3$ and eluted with the same solvent. These results indicated that A23187 was obtained in relatively pure form and did not require additional purification.

Stock solutions of A23187 were prepared in $CHCl_3$ and stored at 4° C. Solutions of A23187 in 80% CH_3OH/H_2O were prepared by evaporating the appropriate volume of the stock solution to near dryness under a stream of N_2 and then dissolving the residue in a solution of 80% CH_3OH/H_2O containing 0.05 M $(C_2H_5)_4NClO_4$. A23187 was standardized by potentiometric titration with $(CH_3)_4NOH$. All solutions of A23187 were kept wrapped in aluminum foil to prevent photo-degradation of the molecule.[2]

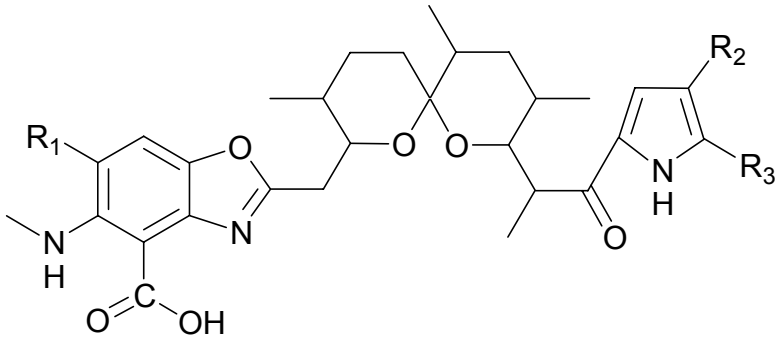

A23187: R_1, R_2, R_3 = H

4-ClA23187: R_1 = Cl, R_2, R_3 = H

23,24-Br_2A23187: R_1 = H, R_2, R_3 = Br

Figure II.1. Structure of A23187 and Derivatives of A23187

4-ClA23187: The 4-chloro derivative of A23187 was prepared using the method described by Debono et al[3]. A23187 was first converted to the magnesium complex (MgA_2) by extracting approximately 50 mg of the acid form of A23187 (HA) in $CHCl_3$ with an aqueous solution containing 10 mM Mg^{2+} at pH 10. The complexation reaction is illustrated by Equation II.3. UV-vis spectra of the $CHCl_3$ solution were recorded after

each extraction. The extraction was repeated until the spectra ceased to change from that of the preceding extraction.

$$2HA_{(org)} + Mg^{2+}_{(aq)} \longrightarrow MgA_{2\,(org)} + 2H^{+}_{(aq)} \qquad \text{Eq. II.3}$$

After removing $CHCl_3$, $Mg(A23187)_2$ was reacted with a stoichiometric amount of the chlorinating agent *N,N*-1,3,-dichlorodimethyl hydantoin in anhydrous $CHCl_4$ in the presence of pyridine, as illustrated by Equation II.4.

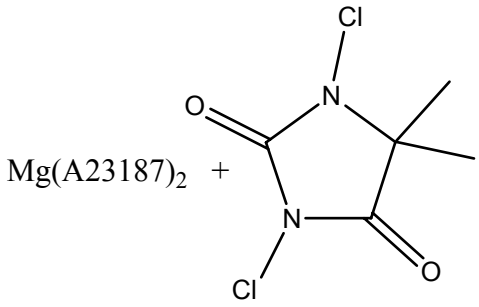

$Mg(A23187)_2$ + → $Mg(4\text{-}ClA23187)_2$ Eq. II.4

1 eq. pyridine, 60° C
4 hours, dark

The reaction was conducted in the dark (using aluminum foil) at 60° C, maintained by immersion of the reaction flask in an oil bath whose temperature was monitored by thermometer. The reaction took place with constant stirring, under N_2, and with a condenser to prevent loss of solvent. After four hours, the reaction flask was cooled to room temperature, solvent was removed by rotary evaporation and the product dissolved in $CHCl_3$. This solution was extracted twice with 2% Na_2SO_3, once with ddH_2O, and dried overnight over Na_2SO_4. The solution was then filtered to remove Na_2SO_4 and dried under vacuum. The product was purified by crystallization from CH_3OH. Crystals were washed with CH_3OH, dried under vacuum, and stored in aluminum foil-wrapped vials inside a dessicator. The product was characterized by positive and negative electrospray

mass spectrometry (ESI-MS), shown in Figure II.2. The assignments of peaks observed in the positive ESI-MS are summarized in Table II.1.

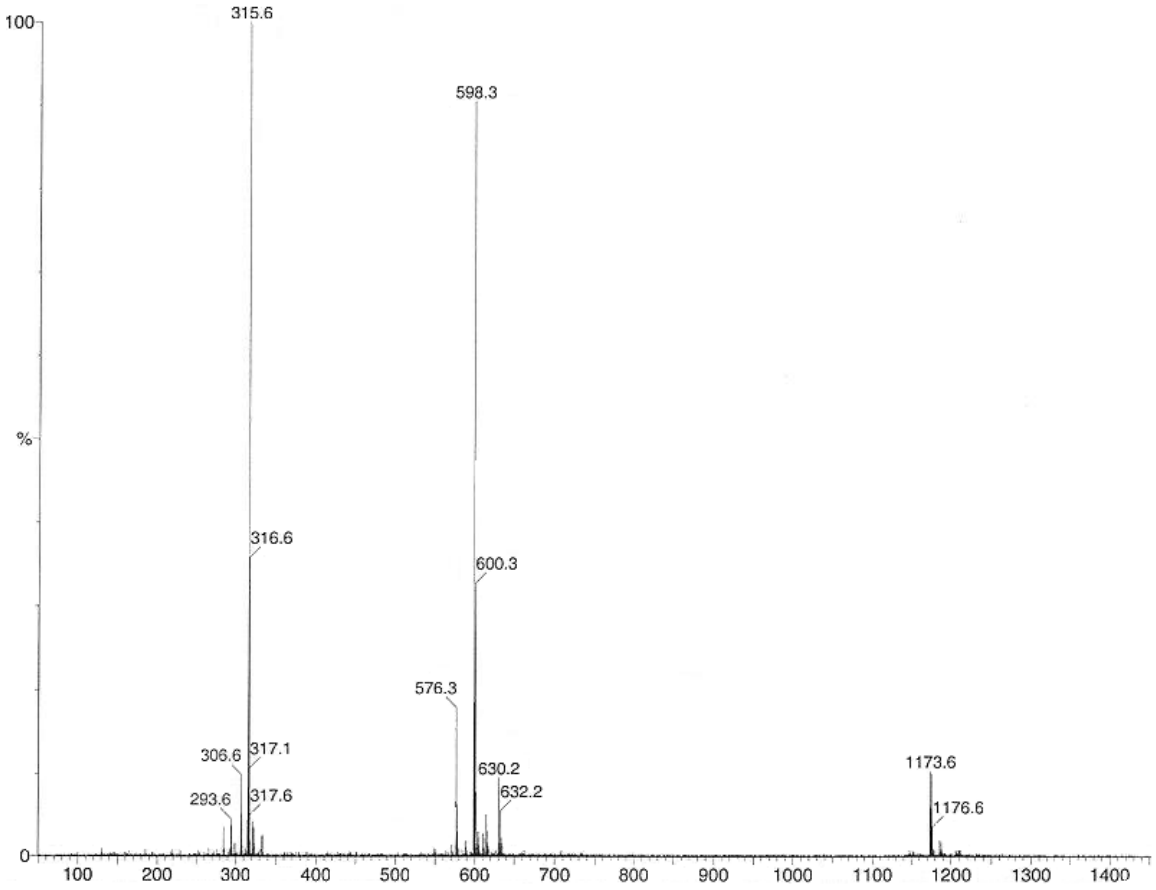

Figure II.2. + ESI-MS of $Mg(4\text{-ClA23187})_2$ in CH_3OH

m/z	
315.6	4-ClA + CH_3OH + H_2O + Mg^{2+}
576	4-ClA + H_2O + H^+
598	4-ClA + K^+
630	4-ClA + CH_3OH + H_2O + Na^+
1173.6	$(4\text{-ClA})_2$ + H_2O + K^+

Table II.1: Peak assignments for positive ESI-MS of $Mg(4\text{-ClA23187})_2$ in CH_3OH

All peaks in the mass spectrum of $Mg(A23187)_2$ (m = 1138) correspond to the m/z ratio of a single molecule of 4-ClA23187 (m = 558) with various adducts, with the exception of a small peak at 1173.6 that corresponds to the m/z ratio of a 2:1 complex of 4-ClA23187, potassium, and H_2O. An isotopic peak indicative of a mono-chlorinated molecule accompanies all molecular ion peaks in table II.1. This peak is present at (m + 2) for all peaks in table II.1, with an intensity that is approximately 1/3 that of the main peak as expected based on the natural abundance of isotopes ^{35}Cl (76%) and ^{37}Cl (24%). The molecular ion peak at 315.6, however, has an isotope peak at (m + 1) because the charge on the complex is +2. The molecular ion peak at 1173.6 has a unique set of isotope peaks due to the presence of two chlorine molecules in the complex. These isotope peaks are observed at (m + 2) at 65% intensity relative to m, and (m + 4) at 11% intensity relative to m.

The negative ESI mass spectrum consists of a single molecular ion peak at 574, corresponding to the anionic form of 4-ClA23187 plus the weight of a single molecule of water. A small (m + 2) peak was also observed.

The position of the chlorine added to A23187 was confirmed by ^1H NMR of the product in $CDCl_3$, which is shown in Figure II.3. Several features of the ^1H NMR spectrum of the reaction product differentiate it from the ^1H NMR spectrum of starting material $Mg(A23187)_2$. In the reaction product spectrum, the doublet (δ 6.6 ppm) corresponding to the hydrogen in the 4 position is absent, and the doublet corresponding to the hydrogen in the 5 position becomes a singlet because there is no longer an adjacent hydrogen to split the peak. All other peaks remain unchanged, notably the pyrrole

hydrogens, which serves as confirmation that no chlorination of the pyrrole moiety occurred.

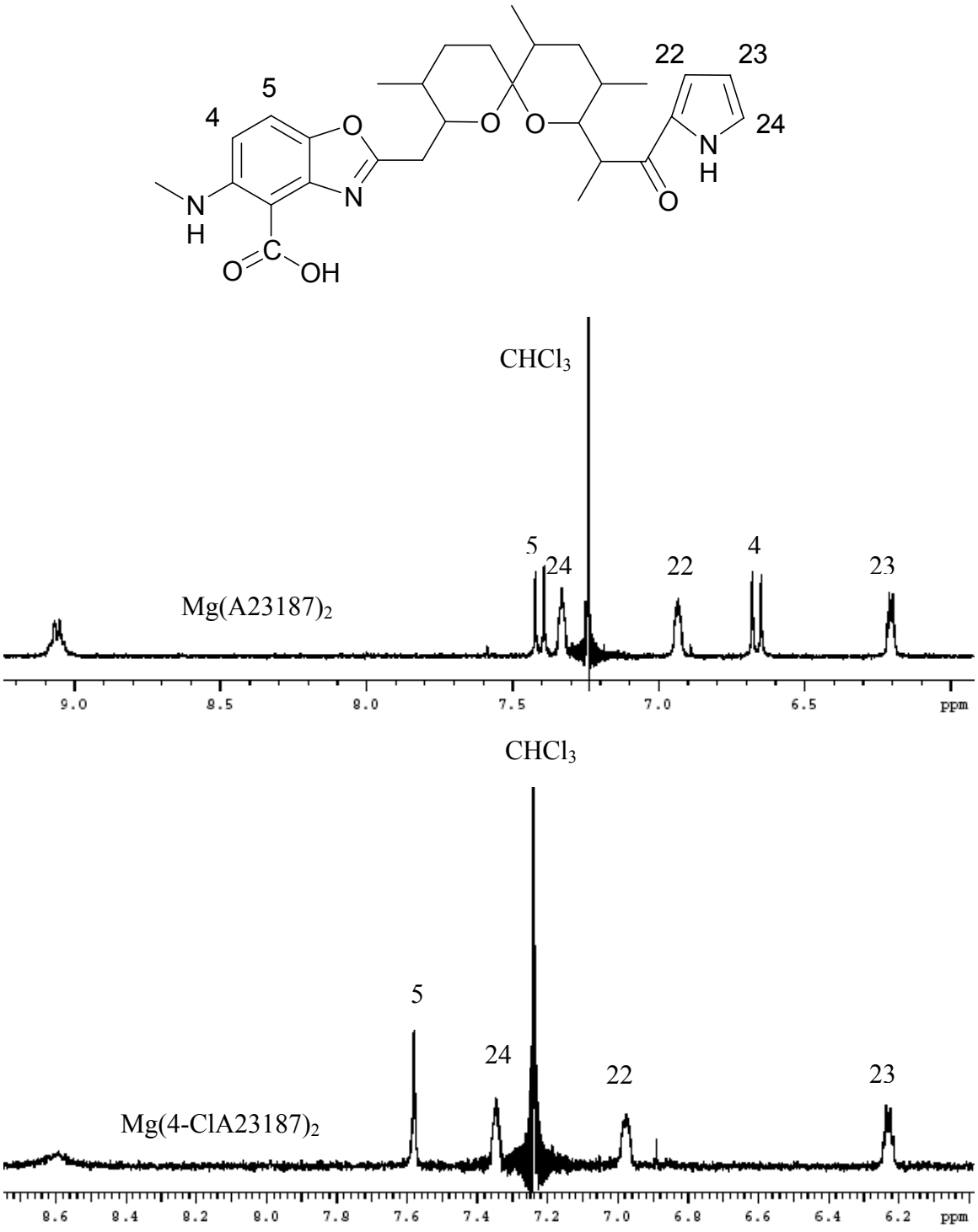

Figure II.3. ^{1}H NMR spectra of $Mg(A23187)_2$ (top) and $Mg(4\text{-}ClA23187)_2$ (bottom) from ppm ~ 6 to ppm ~ 9 in $CDCl_3$

4-ClA23187 was stored as the crystalline form of the magnesium complex. To convert the magnesium complex into the free acid form (4-ClA23187), crystals of Mg(4-ClA23187)$_2$ were dissolved in approximately 50 mL $CHCl_3$ and extracted three times with equal volumes of 0.1 N HCl. To remove the excess acid, the $CHCl_3$ solution was washed three times with equal volumes of ddH_2O. After removal of $CHCl_3$, 4-ClA23187 was dissolved in 80% CH_3OH/H_2O containing 0.05 M $(C_2H_5)_4NClO_4$. Solutions of 4-ClA23187 were standardized by potentiometric titration with $(CH_3)_4NOH$ in 80% CH_3OH/H_2O.

23,24-Br_2A23187: The pyrrole-substituted dibromo derivative of A23187 was obtained using the method described by Debono et al.[3] The reaction is illustrated by Equation II.5.

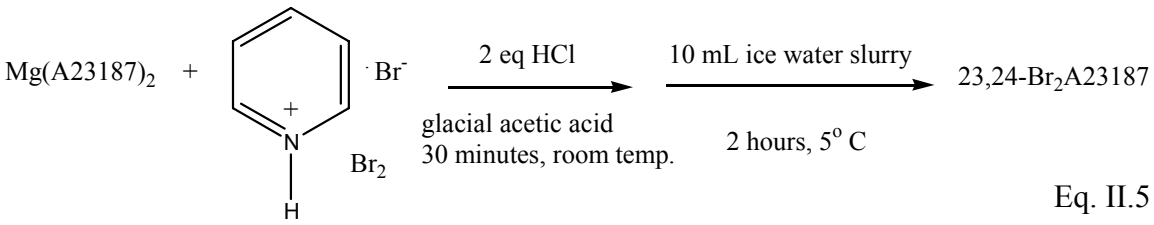

Eq. II.5

The magnesium complex of A23187 (0.05 mmole) was dissolved in 3 mL glacial acetic acid and 100 μL 1 N HCl in a 5 mL conical vial protected from light with aluminum foil. Four equivalents of pyridinium bromide perbromide ($C_5H_5NH^+ \cdot Br_3^-$) were added and the reaction mixture was stirred for 30 minutes at room temperature. The

product was precipitated by addition of the reaction mixture to 10 mL of an ice-water slurry which was then allowed to stand for 2 hours at 5° C. The solid product was collected by filtration, washed with ddH_2O, and dissolved in $CHCl_3$. The $CHCl_3$ solution was washed twice with 5% Na_2SO_3 and three times with ddH_2O. The product was then applied to a citric acid infused silica gel column (~ 20 g) and eluted with $CHCl_3$. The citric acid was present to prevent streaking due to metal ion contaminants. The silica gel was treated with citric acid by soaking the gel in CH_3CH_2OH containing 0.16 M citric acid, decanting the excess solution, and drying the gel by rotary evaporation. The eluted fractions were observed under a UV lamp to detect the presence of product. Fractions that were fluorescent were tested for purity by TLC using $CHCl_3$ as the mobile phase. TLC silica gel plates were treated with citric acid to prevent streaking caused by metal ion contaminants. Treatment consisted of soaking all plates in C_2H_5OH containing 0.16 M citric acid until they appeared saturated and then allowing them to dry overnight. A single fluorescent spot on the TLC plate was observed under UV light for all fractions containing product. Fractions containing product were combined and solvent was removed by vacuum.

After solvent removal, the product was characterized by ESI-MS and ^1H NMR. The positive ESI mass spectrum shown in Figure II.4 shows sets of triplets centered at 682 and 704 m/z, corresponding to the H^+ and Na^+ adducts of Br_2A23187 (m = 681). Each set of triplets displays a 1:2:1 intensity pattern that corresponds to the three possible isotope combinations of the two isotopes of bromine: ^{79}Br (relative abundance 51%) and ^{81}Br (relative abundance 49%).

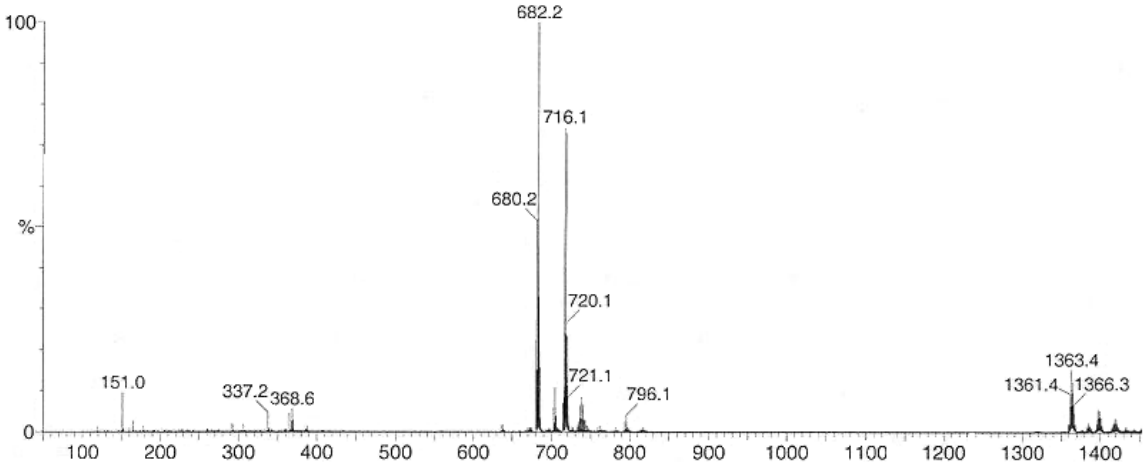

Figure II.4. Positive ion ESI-MS of 23, 24-Br_2A23187

A quartet centered at 717 m/z indicates the presence of a tri-brominated molecule that corresponds to the weight of a Br_3A moiety that has lost a carboxylic acid group. The species represented by the quartet is likely an artifact of the MS instrument and not a true representation of the composition of the sample because no extraneous peaks are observed in the ^{1}H NMR. The ^{1}H NMR of the product in $CDCl_3$, as shown in Figure II.5, indicates that the bromine atoms are located in the desired positions. Comparison of the product ^{1}H NMR with the ^{1}H NMR spectrum of the parent compound Mg(A23187)$_2$ shown in Figure II.3 shows that signals for the protons at positions 23 and 24 are absent and the remaining pyrrole proton signal is coupled only to the pyrrole nitrogen proton. In addition, the presence of two doublets assigned to protons 4 and 5 indicate that the benzoxazole region has not been brominated.

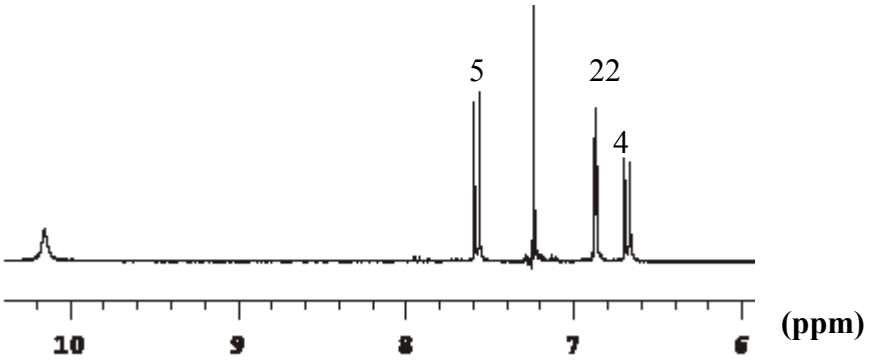

Figure II.5. ^{1}H NMR spectrum of 23,24-Br_2A23187 from ppm ~6 to ~10 in $CDCl_3$

23,24-Br_2A23187 was stored in free acid form in aluminum foil-wrapped vials inside a dessicator. To prepare solutions of Br_2A23187 in 80% CH_3OH/H_2O, a known amount of Br_2A23187 was dissolved in $CHCl_3$ and an appropriate volume was transferred to a new vial and the solvent evaporated under a N_2 stream. The residue was then dissolved in 80% CH_3OH/H_2O containing 0.05 M $(C_2H_5)_4NClO_4$ and standardized by potentiometric titration with $(CH_3)_4NOH$.

B. Measurements and Data Analysis

Potentiometric Titrations:

pH measurements: pH measurements were made with either an Orion 8103 combination glass electrode or a Ross pH glass double junction electrode. The internal filling solution for electrodes was 3 M KCl. Potentiometric titrations were performed with a Fisher Accumet pH meter model 825 MP. Both meters were standardized prior to use using commercial buffers (Fisher, Gram-pac) of pH 9.18, 6.86, and 4.01. Contamination of the 9.18 buffer with CO_2 was kept to a minimum by using CO_2-free water to prepare the buffer and storing it under either N_2 or Ar. For pH measurements in 80% CH_3OH/H_2O solutions, the electrode was soaked in 80% CH_3OH/H_2O after standardization for two hours prior to measurements.

Determination of %CO_2 in $(CH_3)_4NOH$ solutions: The amount of CO_2 was checked by a Gran plot[4] of a titration of the base with a dilute solution of $HClO_4$. Six points before and after the endpoint were used in the equation

$$\phi = (V_0 + V_{base}) \times 10^{\pm R} \qquad \text{Eq. II.6}$$

where V_0 = the initial volume, V_{base} = the volume of base added, R = the reading on the pH meter, and "-" is used in the acidic region, while "+" is used in the basic region. The value of ϕ is plotted as a function of volume (mL) base added, which creates two straight

lines corresponding to the acidic and basic regions. The x-intercept of each line (intercepts 1 and 2, respectively) yields a value (mL base) that is used in the following equation:

$$\% CO_2 = \frac{|\text{intercept}_2 - \text{intercept}_1|}{(2 \times \text{intercept}_2) \times 100} \qquad \text{Eq. II.7}$$

These calculations generally yielded values around 0.4% CO_2 for freshly made base. A solution found to contain over 2% CO_2 would be discarded, although no actual base solution prepared was found to have such a high CO_2 concentration.

pH*: pH is the measure of hydrogen ion activity in water, while pH^* is the measure of hydrogen ion activity in a solvent other than water, which in these studies is 80% CH_3OH/H_2O. pH^* is determined potentiometrically the same way as pH, but an additional correction step is required to correct for solvent effects. The pH observed by the electrode is converted to pH^* using Equation II.8:

$$pH^* = pH_{obsd} - \delta \qquad \text{Eq. II.8}$$

The correction term δ is found by titrating an acid of known pK_a in the desired non-aqueous solvent. For all studies, the acid used is acetic acid, with a pK_a of 6.4 in 80% CH_3OH/H_2O.[5] The difference between the observed pK_a and the literature pK_a comprises the correction factor δ, as shown in Equation II.9:

$$\delta = pK_{a\ lit} - pK_{a\ obsd} \qquad \text{Eq. II.9}$$

The correction term used in potentiometric titrations was measured prior to each titration. The values for δ varied from 0.02 to 0.36.

Determination of Protonation Constants: Protonation constants for 4-ClA23187 and 23,24-Br_2A23187 were determined by titration of the ionophore with the strong base $(CH_3)_4NOH$. Ionic strength of both solutions was maintained at 0.05 M by addition of $(CH_3CH_2)_4NClO_4$. Titrations were conducted in 80% CH_3OH/H_2O mainly because comparison of previous studies conducted in this solvent show that the binding properties of A23187 with metals and protons are similar in 80% CH_3OH/H_2O to those obtained in aqueous suspensions of POPC vesicles. Another factor is the solubility properties of A23187. A23187 is soluble in millimolar concentrations in 80% CH_3OH/H_2O, but not in H_2O.

An autotitrator system composed of a Zenith 158-42 computer attached to a Fisher Accumet pH meter and an Orion Ross 8103 combination electrode was used to collect potentiometric data. The autotitrator delivered a known volume of titrant to the solution in which the electrode was immersed, and the electrode measured the resulting pH. The titrations were conducted under Ar to prevent CO_2 absorption during titration. The Ar was sent through a trap containing Drierite and Ascarite to absorb moisture and CO_2, respectively, and then bubbled through consecutive flasks of CH_3OH/H_2O and H_2O to saturate the gas and prevent loss of solvent in the titrated solution.

pH data fitting: Potentiometric data was fit with either data fitting program PKAS or BEST.[4] PKAS is used to determine protonation constants, while BEST can be used for protonation and metal binding constants. Input data consists of millimoles ligand, molarity of base, initial volume, and volume base added versus pH. If metal is present, then the millimoles of metal are required input as well. The data is fit using a non-linear least squares program. The fit of the data is measured by the sigma (σ) value. An additional titration is required to correct for the electrode measuring pH in solvent other than water. A solution of approximately 0.02 M acetic acid in the solvent used for titration of ligand was titrated by the base. The data was fit by BEST or PKAS and the protonation constant was compared to a literature value of acetic acid protonation in the desired solvent. The difference in experimental and literature values served as a correction factor in all titrations of ligand in the solvent. A new acetic acid titration was required every time the electrode was standardized. The correction factor was an additional input value into the PKAS or BEST program.

Spectrophotometric Titrations: Metal complexation titrations were conducted using a HP-8452A Diode Array Spectrophotometer for UV-Vis titrations, and an Aviv 202-01 Circular Dichroism Spectropolarimeter for CD titrations. Both UV-Vis and CD titrations were conducted using 1 cm pathlength quartz cuvettes from Starna Corp. UV-Vis spectra were collected from 190 to 820 nm at a constant temperature of 25 °C. A blank spectrum, consisting of solvent and an appropriate concentration of any buffers, was recorded and subtracted from subsequent recording of analyte spectra. CD spectra were recorded from

220 to 450 nm at a constant temperature of 25 °C. A blank spectrum was recorded and subtracted from all analyte spectra. An N_2 atmosphere was maintained inside the CD to prevent the formation of ozone.

Metal complexation titrations were performed by adding small aliquots (3 or 5 μL) of metal solution of known concentration and comparable pH to the ligand solution, inverting the cuvette 15 times to ensure thorough mixing, and waiting two minutes before recording the spectrum to ensure equilibrium. Titrations to determine protonation constants were performed by adding small aliquots of base to ligand, inverting the cuvette 15 times to ensure thorough mixing, and recording the pH measured by pH meter prior to recording the spectra. Titrations of buffers were conducted to check for changes in absorbance due to change in protonation state, and none were found. This meant the buffers could be considered unchanging at variable pH and thus one buffer spectra could be considered an appropriate blank for solutions ranging in pH from 2 to 10.

Transport Kinetic Studies: The rate of transport of divalent cations Zn^{2+}, Cd^{2+}, Mn^{2+}, Co^{2+}, Ni^{2+}, Pb^{2+}, Cu^{2+}, Ca^{2+}, and Sr^{2+} by A23187 and two derivatives through a model membrane were studied by collaborators at The Ohio State University. A suspension of vesicles was used as a model for the lipid bilayer of a cell membrane. Metal transport into the vesicles is monitored by a chelator trapped inside the vesicles with UV-vis absorbance properties that differ depending on the complexation state of the molecule, as shown in Figure II.6.

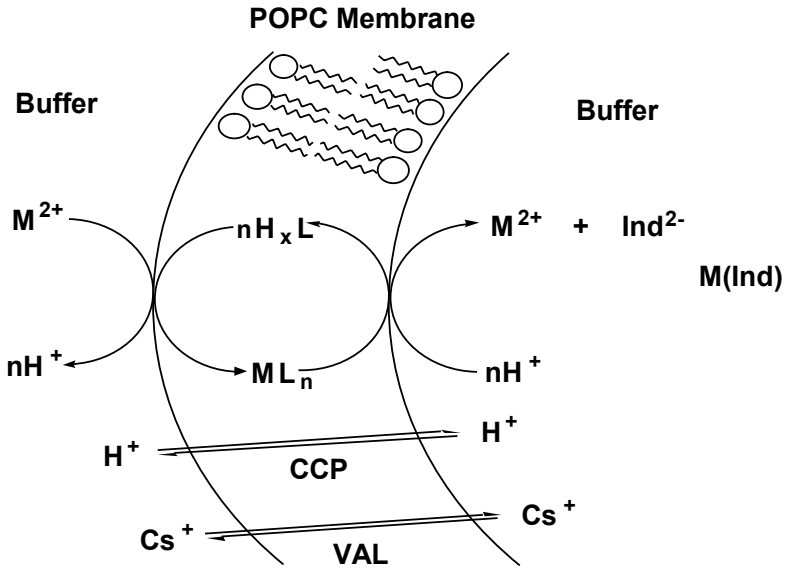

Figure II.6. Vesicle transport scheme

The absorbance is measured using an Aminco DW2a spectrophotometer in dual wavelength mode. An Oriel 59800 band-pass filter is used to prevent detection of the fluorescence emitted by A23187 and Quin-2. Absorbance at 264 nm is measured against a reference wavelength that differs depending on the metal being studied which is determined by the isosbestic point in a titration of Quin-2 with the metal in the vesicle suspension solution.[6]

Vesicles composed of a single bilayer of 1-palmitoyl-2-olelyl-*sn*-glycerophosphatidylcholine (POPC) obtained from Avanti Polar Lipids, Inc. were prepared by a method consisting of several cycles of freeze-thaw and extrusion described by Erdahl et al.[6] A solution of POPC in chloroform is transferred to a 25 x 150 mm tube and dried under N_2 to form a thin wall of POPC and then dried under vacuum for 4 hours.

The POPC is then suspended in a solution containing 5 mM Quin-2 (the reporter dye), 10 mM pH buffers (MES and HEPES), 50 mM ionic buffer ($CsNO_3$), 5.0 μM CCP and 0.50 μM valinomycin, whose functions are to prevent the formation of either a pH or ionic gradient, respectively, from forming as a result of metal transport. The mixture is then subjected to three cycles of vortexing and freezing in an acetone-dry ice bath. Then the mixture is extruded three times through two 100 nm polycarbonate membrane filters. This overall freeze-thaw/extrusion process is repeated six additional times. The solution containing the resulting vesicles is cleaned (to remove Quin-2 not trapped within vesicles) by elution through a G-50 minicolumn. The concentration of vesicles is determined by phosphorus analysis. The concentration of Quin-2 is found by spectrophotometric titration with standardized $CaCl_2$.

C. Crystallographic Studies

Solid-state structures of several metal ion-A23187 complexes were obtained by X-ray crystallography. Each complex was formed by dissolving the free acid form of A23187 in $CHCl_3$ and extracting with aqueous solutions containing the appropriate metal ion. The pH of the metal ion solution was adjusted using small aliquots of concentrated $(C_2H_5)_4NOH$ to as high a value as possible without formation of the metal hydroxide precipitate. UV-vis spectra were taken after each extraction to follow complexation progress, and complexation was considered complete when the spectra ceased to change from one extraction to the next. Solvent was removed and the complex was dissolved in a

small a volume of 95% (v/v) CH_3CH_2OH. The solution was kept at room temperature and was protected from UV light with aluminum foil. The evaporation of solvent was controlled by sealing the top of the vial with aluminum foil wrapped at the ends with parafilm, and forming a single, small hole in the foil for solvent evaporation. The crystals usually formed in 1-4 days, depending on the volume of solvent used. In the singular case of $Mn(A23187)_2$, Mn^{2+} had to be protected from spontaneous oxidation by air. This was accomplished by bubbling argon through all solutions involved in Mn^{2+}/A23187 extractions and maintaining all solutions of Mn^{2+} and $Mn(A23187)_2$ under an argon atmosphere before and during crystallization.

The general parameters for collecting diffractometer data are given below:

The data were collected at 100(2) K on a Bruker Apex diffractometer[7] using MoKα (λ = 0.71073 A) radiation. Intensity data, which approximately covered the full sphere of the reciprocal space, were measured as a series of ω oscillation frames each 0.3° for 21 sec / frame. The detector was operated in 512 x 512 mode and was positioned 6.12 cm from the crystal. Coverage of unique data was 99.7 % complete to 55°(2θ). Cell parameters were determined from a non-linear least squares fit.

The structure was solved by the direct method using SHELXTL system,[8] and refined by full-matrix least squares on F^2 using all reflections. All the non-hydrogen atoms were refined anisotropically. For structures of metal/A23187 complexes, all hydrogen atoms were included with idealized parameters.

REFERENCES

1. Vogel, A. I. *A Text-Book of Quantitative Inorganic Analysis Including Elementary Instrumental Analysis*; Wiley: New York, **1961**; 3rd. Ed. 415-443.

2. Thomas, T. P., Chapman, C. J., Puri, A. K., Taylor, R. W., and Pfeiffer, D. R. *Arch. Biochem. Biophys*. **1990**, *281*, 44-57.

3. Debono, M., Molloy, R. M., Dorman, D. E., Paschal, J. W., Babcock, D. F., Deber, C. M., and Pfeiffer, D. R. *Biochem*. **1981**, *20*, 6865-6872.

4. Martell, A. E. and Motekaitis, R. J. *Determination and Use of Stability Constants*, 2nd Ed., VCH Publishers, Inc.: New York, **1992**.

5. Rorabacher, D. B., MacKellar, W. J., Shu, F. R., and Bonavita, S. M. *Anal. Chem.* **1971**, *43*, 561-573.

6. Erdahl, W. L., Chapman, C. J., Wang, E., Taylor, R. W., and Pfeiffer, D. R. *Biochem*. **1996**, *35*, 13817-13825.

7. Bruker (2002) SMART (version 5.625), GEMINI (version 1.0) and SAINT-plus (version 6.29), Bruker **AXS** Inc., Madison, Wisconsin.

8. Bruker (1997) SHELXTL: Version 6.12, Bruker **AXS,** and Madison, Wisconsin.

CHAPTER III

A23187 RESULTS

Structural and binding properties of A23187 have been studied to better understand the basis for its observed transport selectivity of metal cations and also as a basis of comparison for structural, binding, and transport properties of derivatives of A23187. While many important properties of A23187 have already been elucidated, the determination of several metal ion/ligand complex structures in both solid and solution state, along with the identification and determination of the stability constant of the di-deprotonated ligand state. The structural studies stress the importance of the interligand bonding in the 2:1 complex to the cooperativity observed for K_{ML} and K_{ML2} for A23187 and divalent metal cations. Additional structural information is found in alteration of the solvent of the metal ion/A23187 complex that has implications for the composition of the transporting species of metal:ligand complex.

Additionally, a third protonation state, A^{2-}, has been identified by spectroscopic titration of A23187. If it is possible to lower the stability constant for formation of this species (by either metal binding or substituent effects), this deprotonation step will become an important part of the binding events that lead to metal ion transport.

A. Structural Properties of A23187

1. Circular Dichroism (CD) Studies of A23187 Titrated with Divalent and Trivalent Metal Ions in 80% CH_3OH/H_2O

CD titrations of A23187, at concentrations ranging from 40 to 80 μM, in 80% methanol with many di- and tri-valent metals result in spectra whose characteristics vary according to coordination number and stereochemistry of the metal/A23187 complex. The most common titration spectra are observed when A23187 is titrated with divalent metals that can easily form complexes with a coordination number of 6. These metals produce a set of spectral features that include a large positive peak at ~ 290 nm, due to a combination of the benzoxazole and ketopyrrole moieties, and a set of exciton-coupled peaks centered at ~ 340 nm that are due presumably to the benzoxazole moiety.[1] The order of the coupled peaks indicates the absolute stereochemistry about the metal center: a negative peak at higher wavelength and positive peak at lower wavelength indicate a negative absolute stereochemistry.[2] The CD spectra obtained for titration of A23187 with Zn^{2+}, Cd^{2+}, Co^{2+}, Ni^{2+}, Mn^{2+}, and Mg^{2+} are shown in Figures III.1-III.6, respectively.

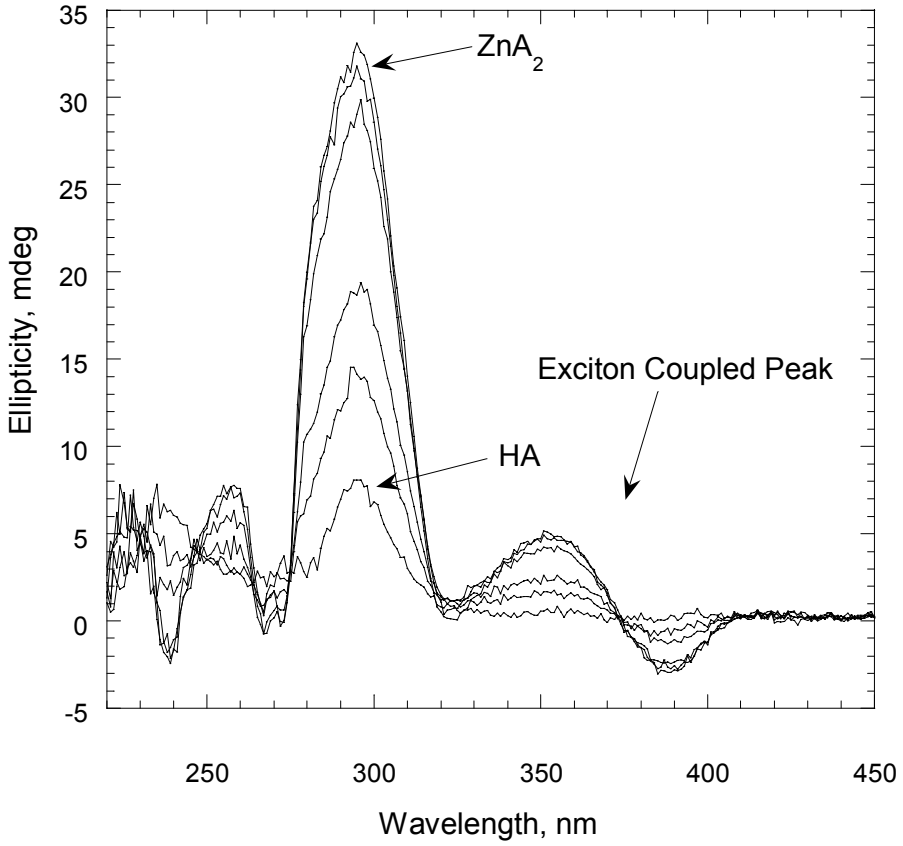

Figure III.1. CD Titration of ~50 μM A23187 with Zn^{2+} in 80% CH_3OH/H_2O at pH^* 6.0

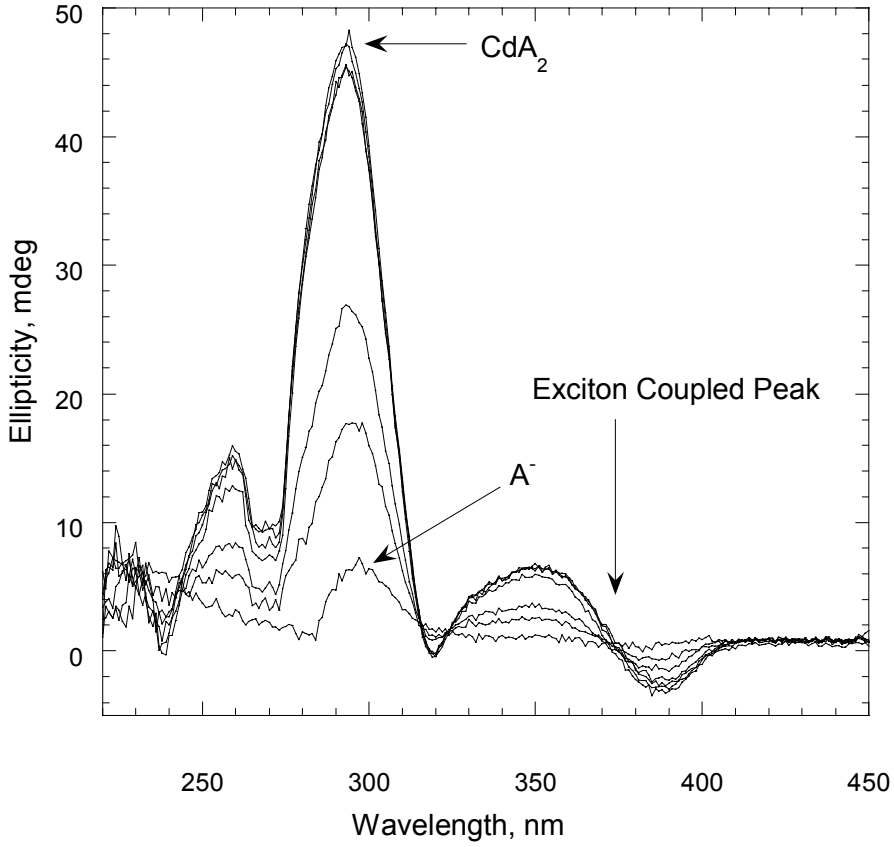

Figure III.2. CD titration of ~50 μM A23187 in 80% CH_3OH/H_2O with Cd^{2+} at pH^* 8.0

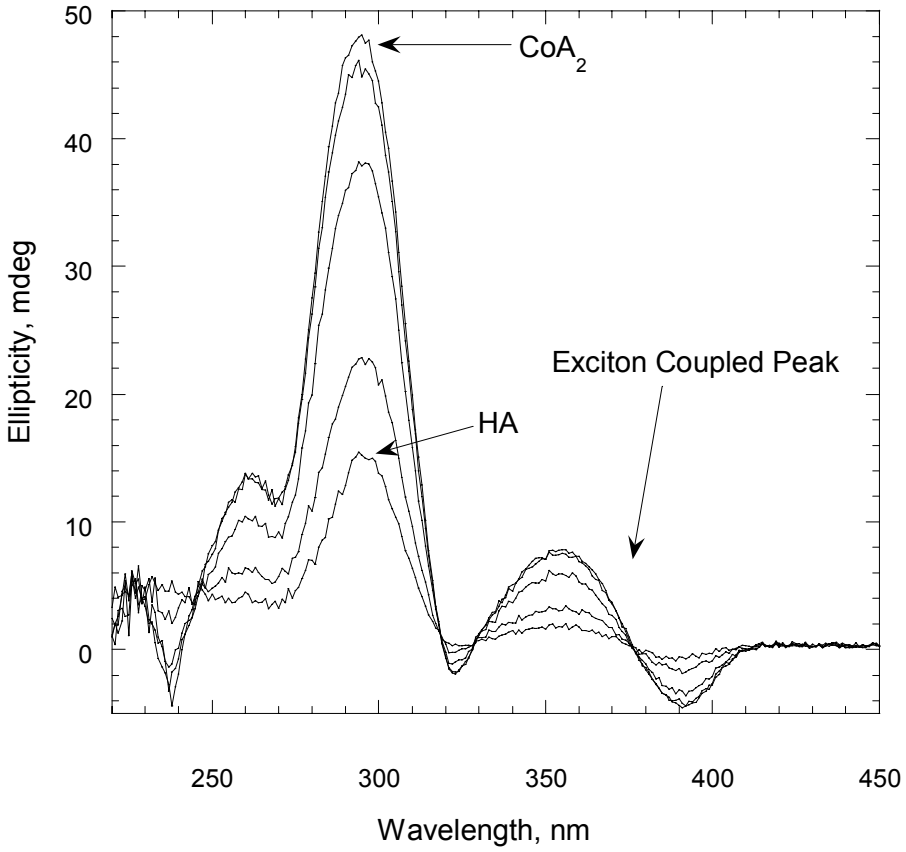

Figure III.3. CD titration of ~50 μM A23187 in 80% CH_3OH/H_2O with Co^{2+} at pH^* 6.0

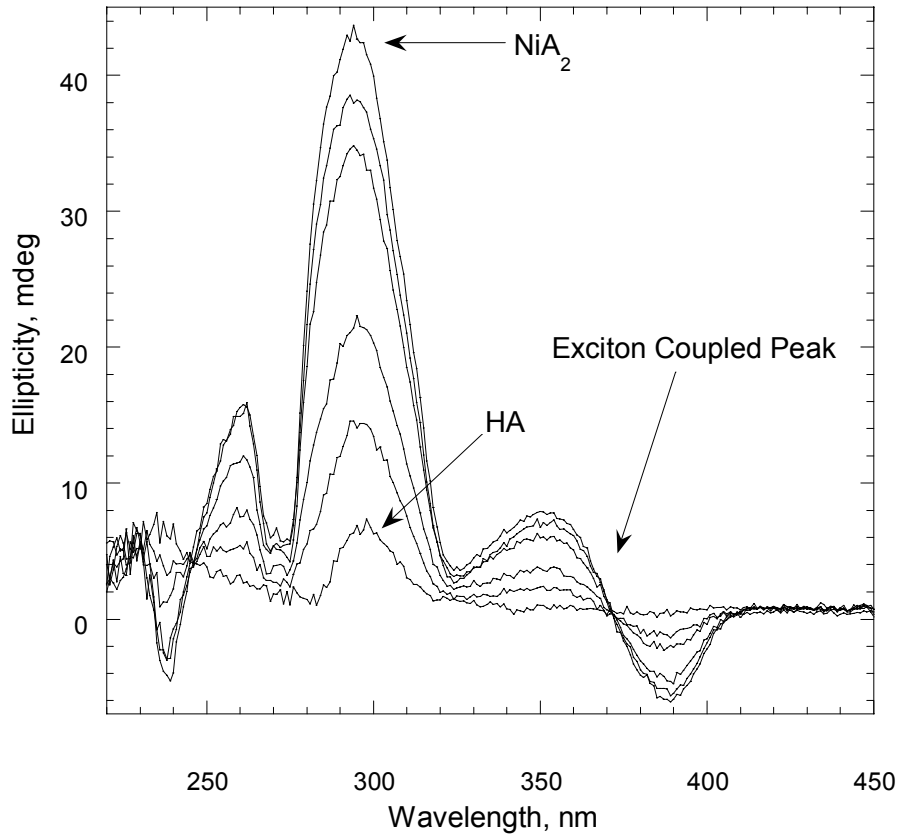

Figure III.4. CD titration of ~50 μM A23187 in 80% CH_3OH/H_2O with Ni^{2+} at pH^* 7.0

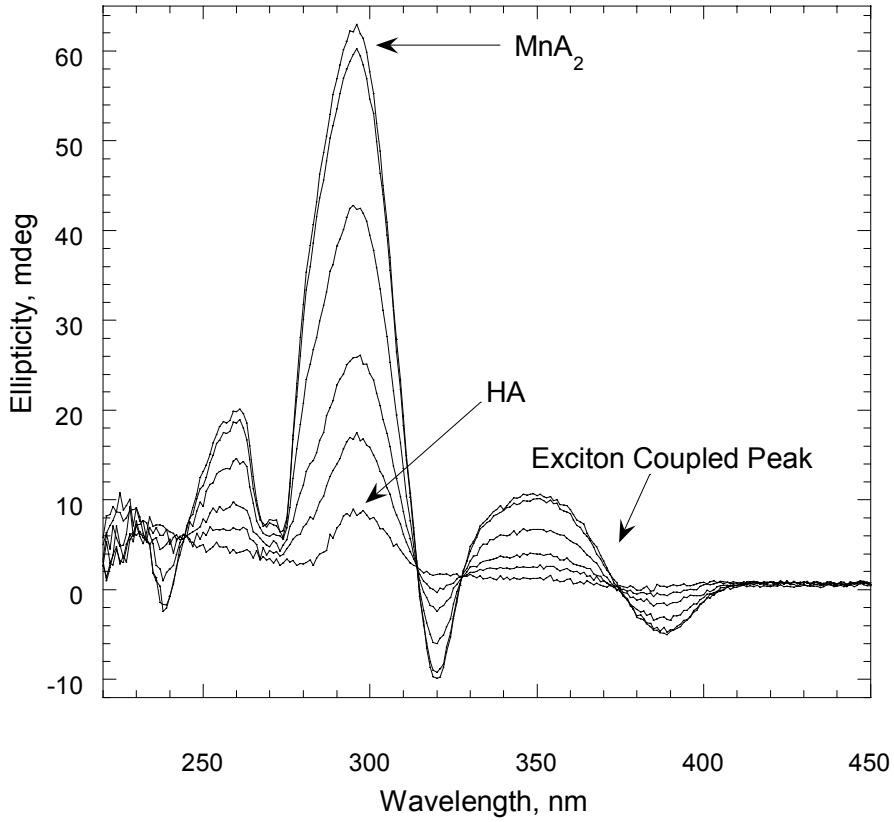

Figure III.5. CD titration of ~50 μM A23187 in 80% CH_3OH/H_2O with Mn^{2+} at pH^* 6.5

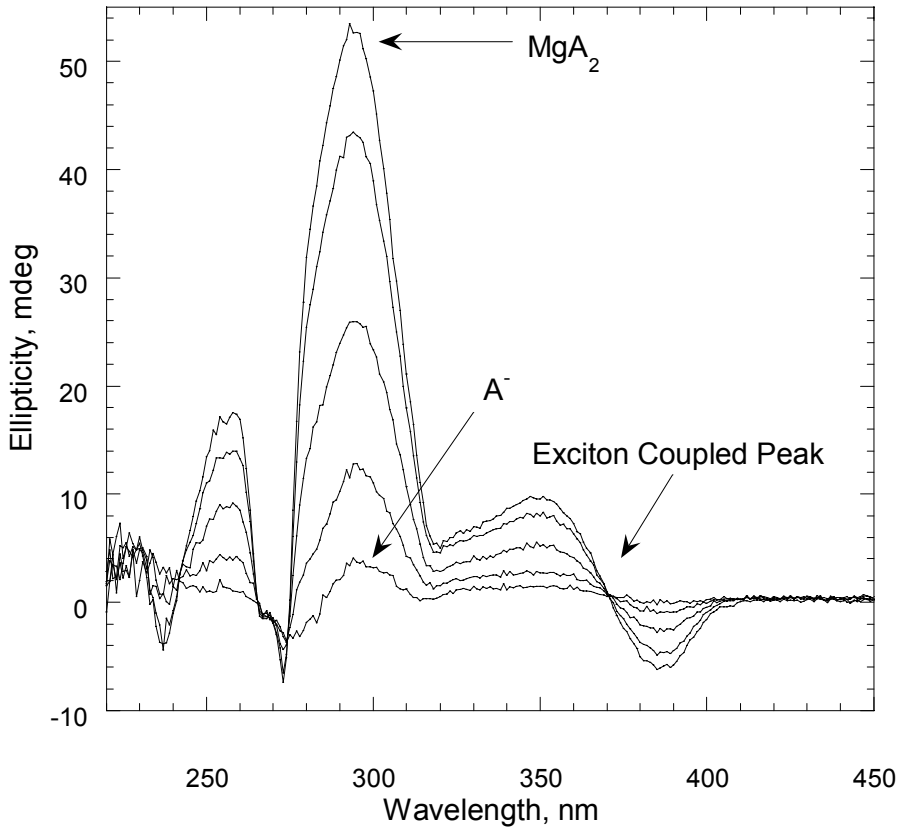

Figure III.6. CD titration of ~50 μM A23187 with Mg^{2+} in 80% CH_3OH/H_2O at pH^* 9.0

For titrations with Ca^{2+}, Sr^{2+}, and Ba^{2+}, several other types of spectral characteristics are observed that indicate a deviation from the typical 6-coordinate, octahedral geometry. Titrations with Ca^{2+} result in spectra that share the features described above, but also include two extra peaks at wavelengths lower than the large peak at ~290 nm. These spectral characteristics are also observed for the alkaline earth metals Sr^{2+} and Ba^{2+}, although a large excess of Ba^{2+} is required to produce the same spectral changes observed

using lower metal concentrations in titrations of Ca^{2+} and Sr^{2+}. The spectra of A23187 titrated with Ca^{2+}, Sr^{2+}, and Ba^{2+} are shown in Figures III.7-9.

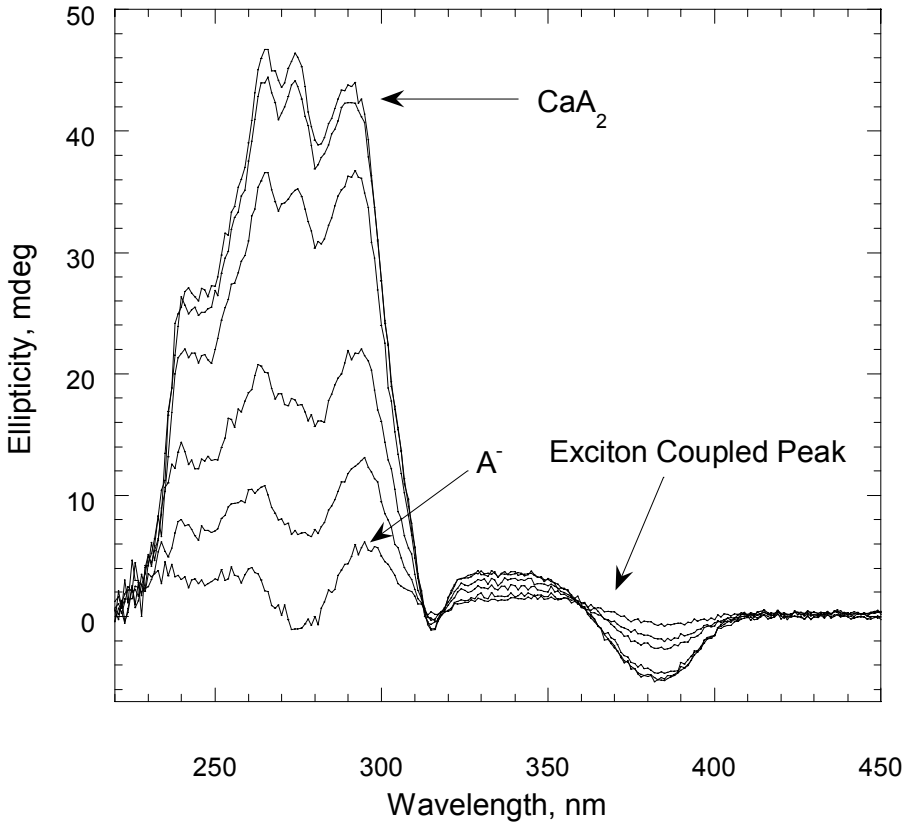

Figure III.7. CD titration of ~50 μM A23187 in 80% CH_3OH/H_2O with Ca^{2+} at pH^* 10.0

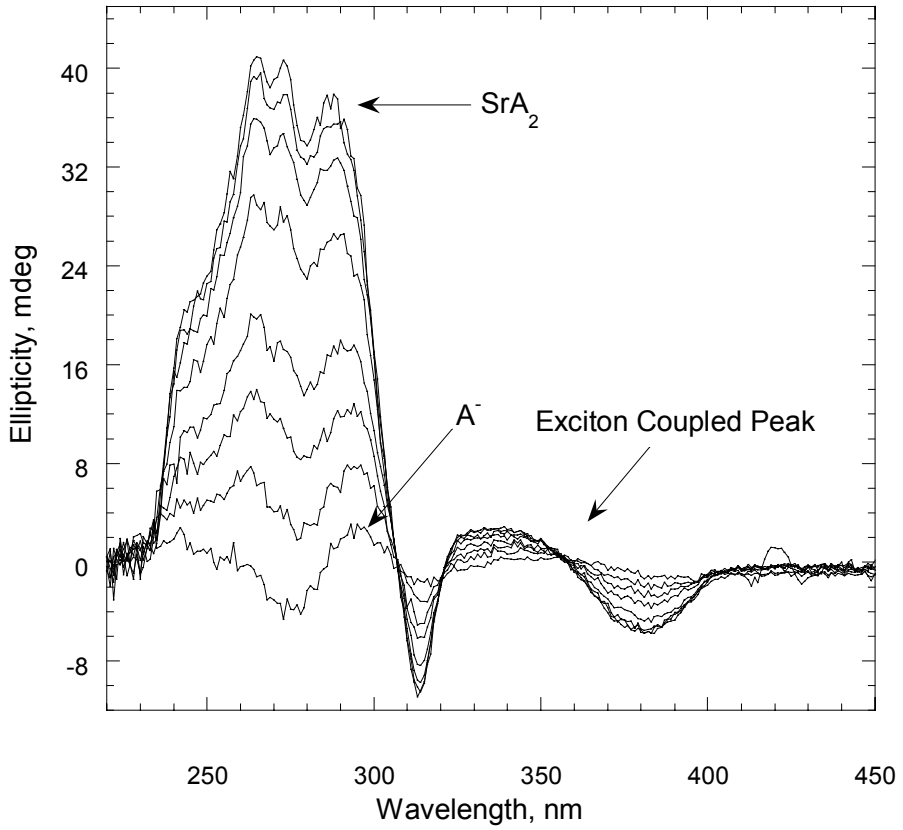

Figure III.8. CD titration of ~50 μM A23187 in 80% CH_3OH/H_2O with Sr^{2+} at pH^* 10.0

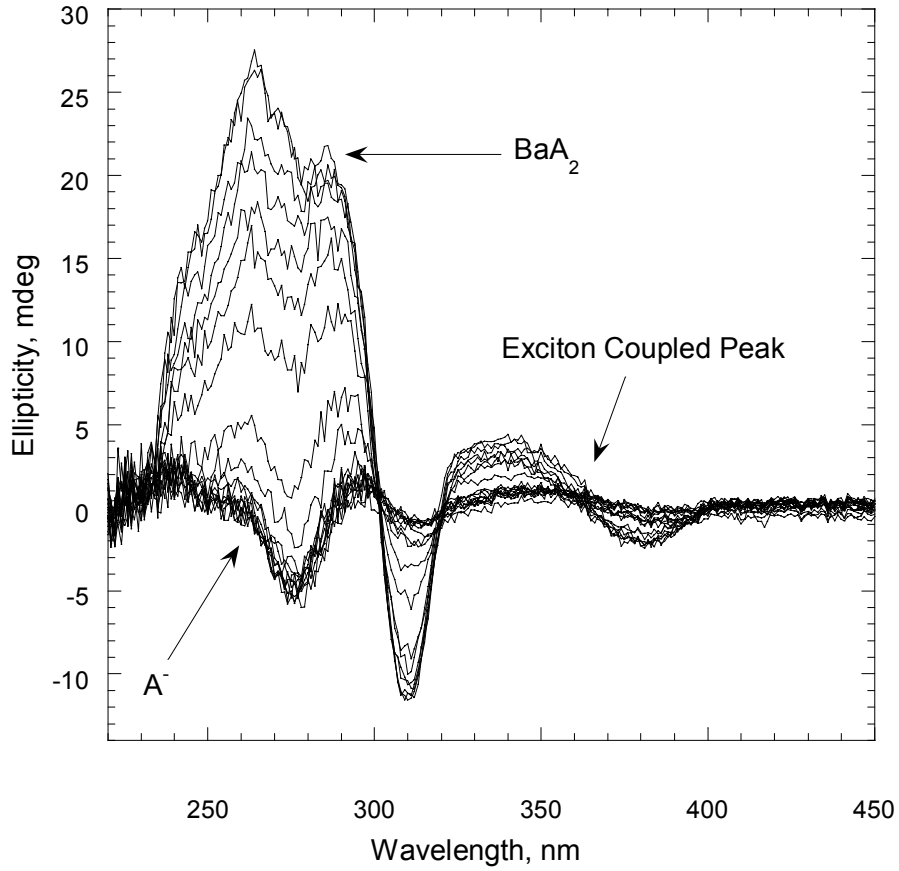

Figure III.9. CD titration of ~50 μM A23187 in 80% CH_3OH/H_2O with Ba^{2+} at pH^* 10.0

The additional peaks observed in titrations of A23187 with Ca^{2+}, Sr^{2+}, and Ba^{2+} are also observed in titrations with several trivalent metals. These metals are often seven-coordinate,[3] so it is reasonable to conclude that Ca^{2+}, which typically has coordination numbers ranging from seven to nine, would form a seven-coordinate complex with A23187 and thus resemble other seven-coordinate complexes in CD spectra. In the X-ray

crystal structure of $Ca(A23187)_2$, Ca^{2+} is 7-coordinate, with 6 sites occupied by two molecules of A23187, and the seventh site occupied by a solvent molecule.[4]

The CD spectra of A23187 titrated with trivalent metals Sc^{3+}, Y^{3+}, La^{3+}, Gd^{3+}, and Lu^{3+} are shown in Figures III.10-14.

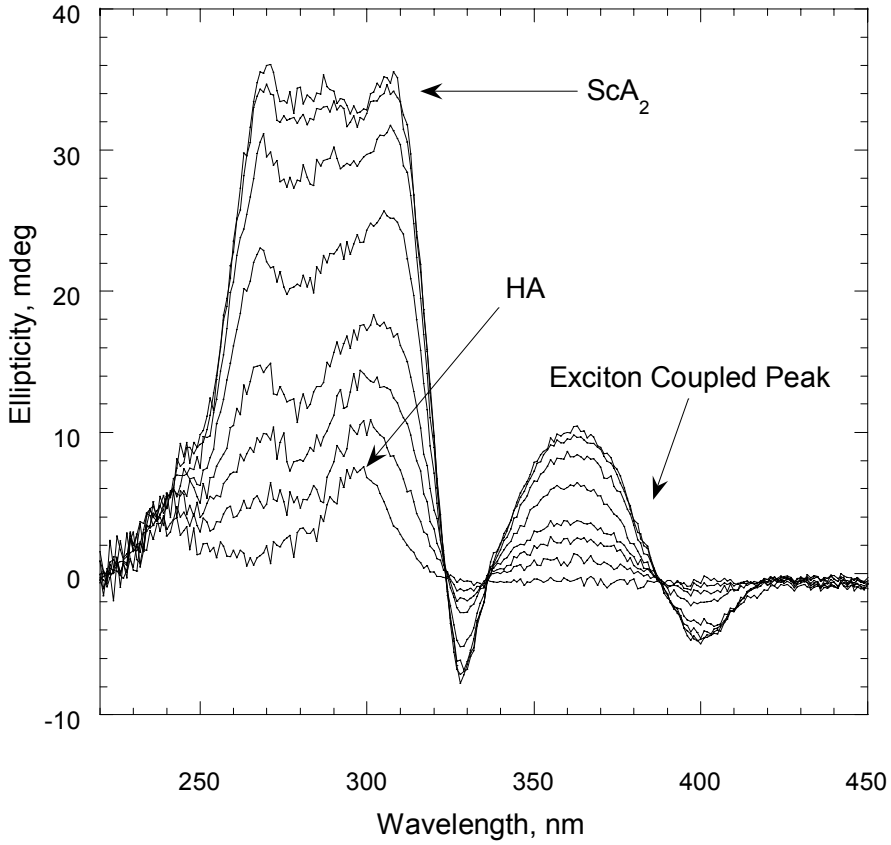

Figure III.10. CD titration of ~50 μM A23187 in 80% CH_3OH/H_2O with Sc^{3+} at pH^* 5.0

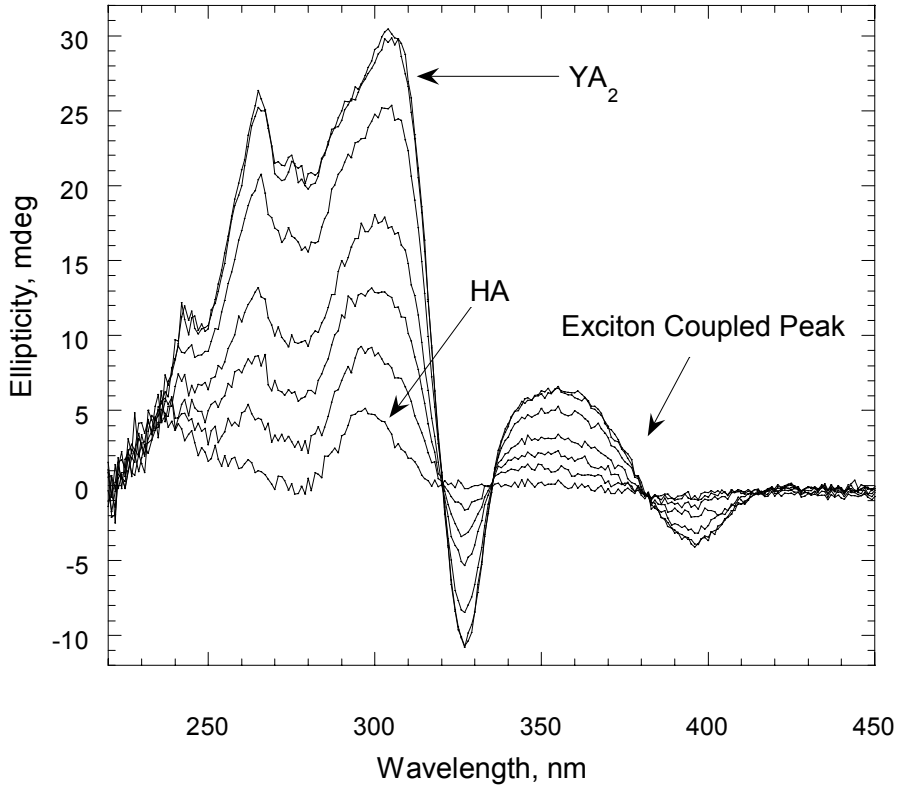

Figure III.11. CD titration of ~50 μM A23187 in 80% CH_3OH/H_2O with Y^{3+} at pH^* 7.0

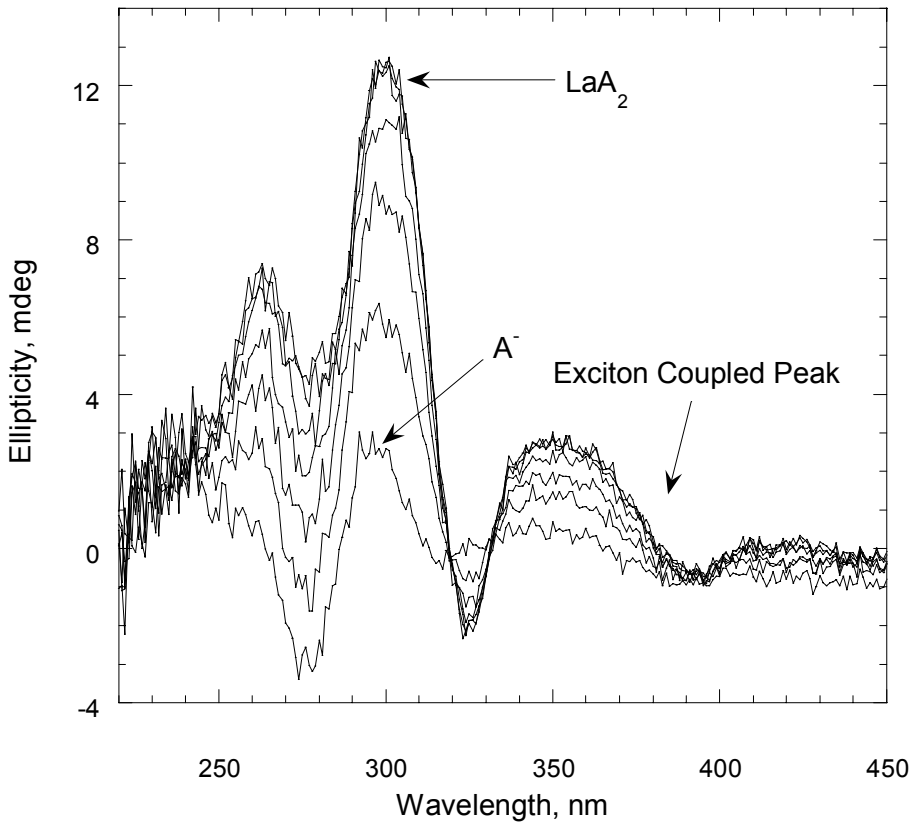

Figure III.12. CD titration of ~50 μM A23187 in 80% CH_3OH/H_2O with La^{3+} at pH^* 8.4

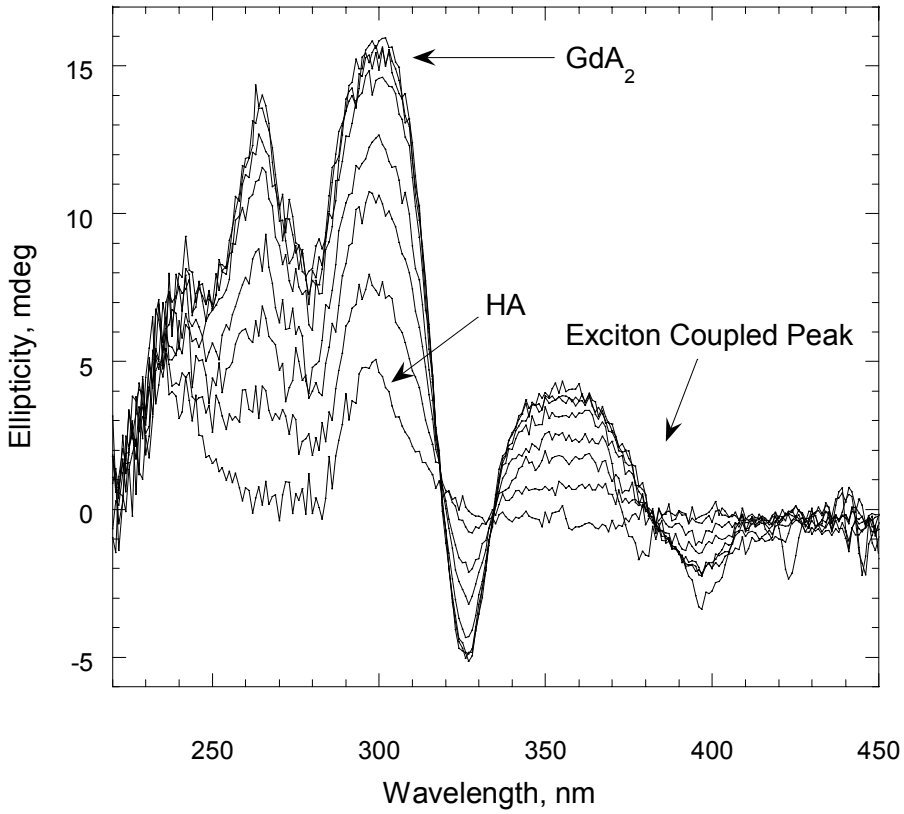

Figure III.13. CD titration of ~50 μM A23187 in 80% CH_3OH/H_2O with Gd^{3+} at pH* 5.0

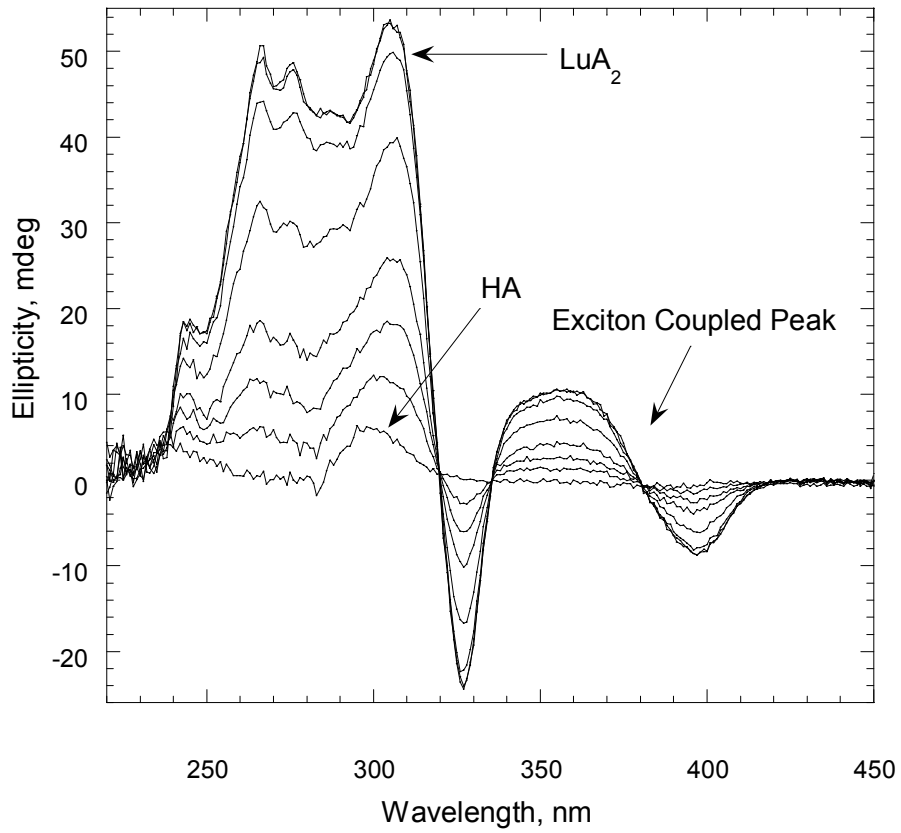

Figure III.14. CD titration of ~50 μM A23187 in 80% CH_3OH/H_2O with Lu^{3+} at pH^* 6.0

The spectra of A23187 titrated with Cu^{2+}, shown in Figure III.15, do not resemble those of any other metal ions tested. There is a large negative peak at ~ 280 nm (where a large positive peak occurs in most metal ions), and the order of the exciton-coupled peaks is reversed relative to those of other metal ions. In this case, the negative peak is at lower wavelength and a positive peak is at higher wavelength, indicating that the absolute stereochemistry about the metal center is opposite to that of other complexes.

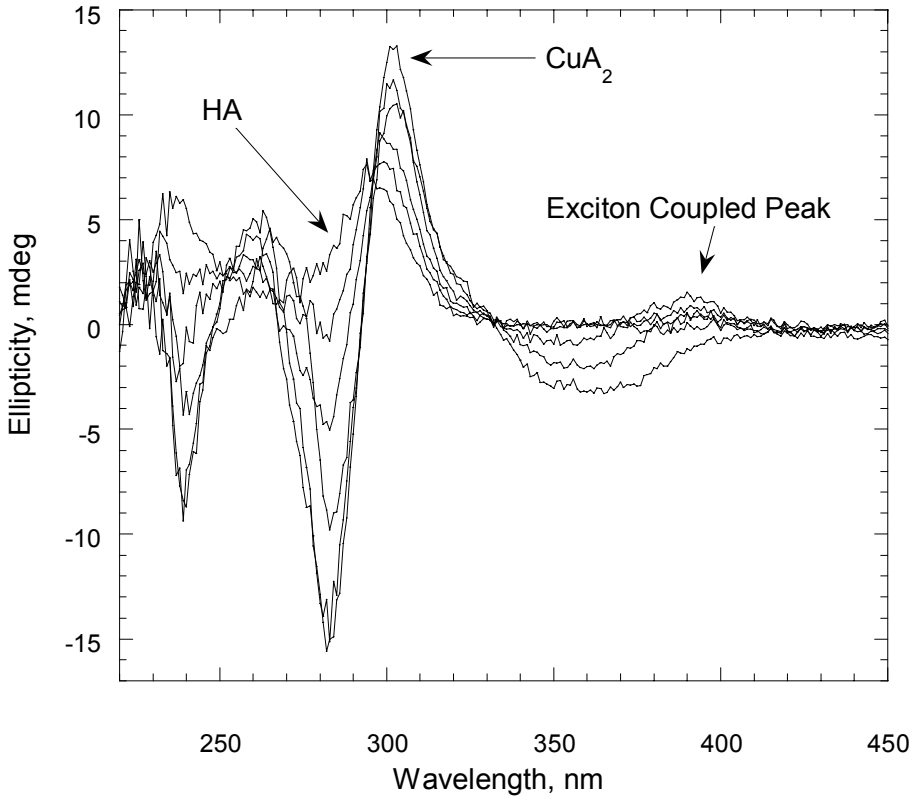

Figure III.15. CD titration of ~50 μM A23187 with Cu^{2+} in 80% CH_3OH/H_2O at pH* 6.5

A titration of A23187 in 80% CH_3OH/H_2O with In^{3+}, shown in Figure III.16, also produces a unique set of spectra. A negative peak that appears at ~ 325 nm is the only significant change observed during the titration. Unlike the spectra of titrations of other metal ions, there are no exciton coupled peaks observed in the wavelength region from 350-410 nm. This indicates that there is no exciton coupling occurring between benzoxazole moieties of two ligand molecules connected by a metal ion, which suggests that indium does not form a 2:1 complex under the reaction conditions.

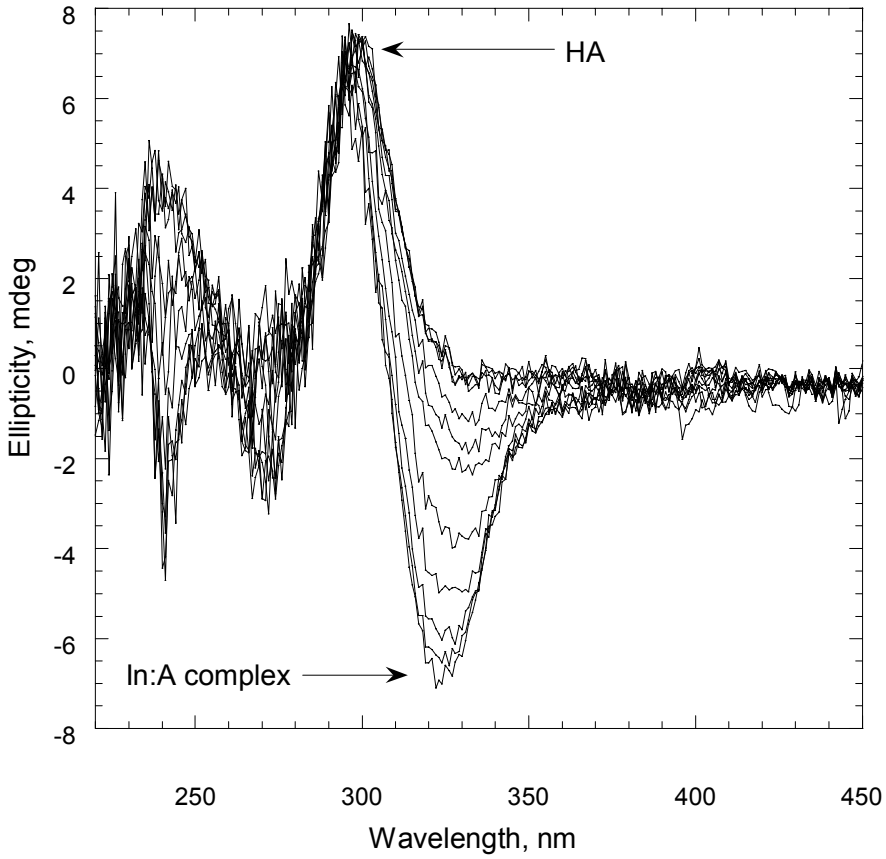

Figure III.16. CD titration of ~50 μM A23187 in 80% CH_3OH/H_2O with In^{3+} at pH^* 5.0

Titrations with several metal ions result in almost no change to the CD spectra, indicating that the metals do not form stable complexes with A23187 under the given titration conditions. Pb^{2+}, Hg^{2+}, Ga^{3+},and Ag^{+} are examples of metals that do not appear to bind well to A23187 in 80% methanol at ~ pH^{*} 5.0. Attempts to increase the solution pH resulted in precipitation of metal cation, which indicates that the binding constant for A23187 and these metals is lower than that of the metal and hydroxide.

2. Solvent Effects on CD spectra of A23187/Metal Complexes

CD spectra of metal-A23187 complexes are also recorded in $CHCl_3$. Each complex is prepared by the extraction method and the CD spectrum collected from 450 nm to 220 nm, as shown in Figure III.17.

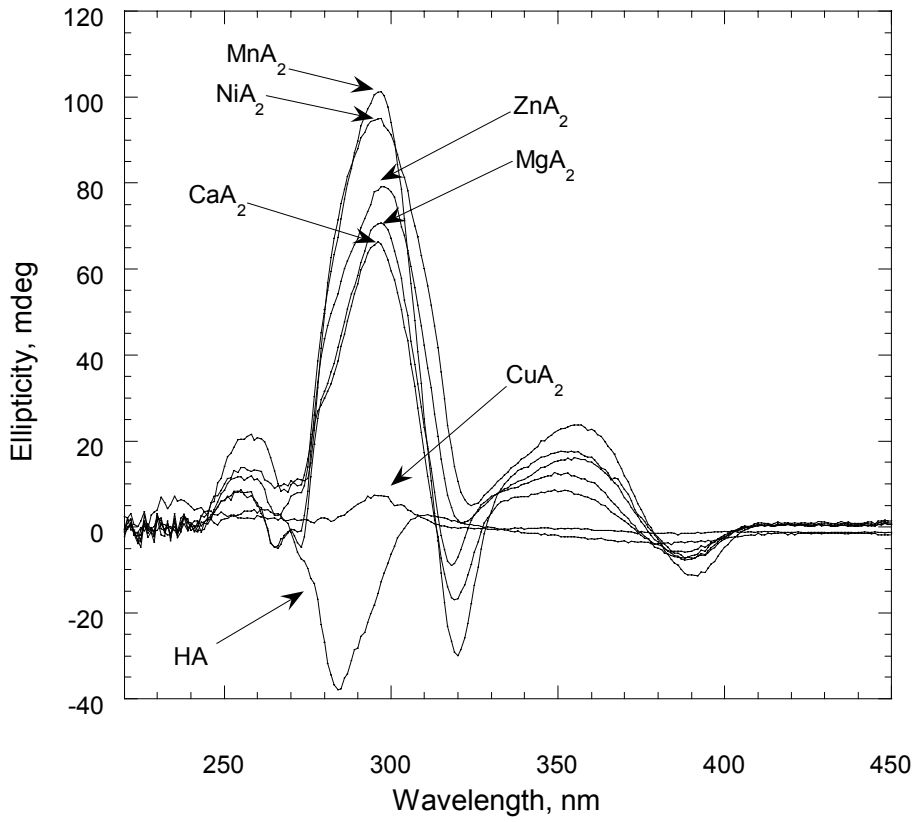

Figure III.17. CD spectra of ~ 50 μM A23187 (HA) and various metal complexes with A23187 (MnA_2, NiA_2, ZnA_2, MgA_2, CaA_2, and CuA_2) in $CHCl_3$

In many cases, the spectrum looks similar to the spectrum of the corresponding metal/A23187 complex in 80% methanol. The spectral features for Zn^{2+}, Cd^{2+}, Mg^{2+}, Ni^{2+}, and Mn^{2+} do not vary significantly in the two solvents except for intensities (mdeg) observed for the peak centered at ~ 290 nm. This difference is likely due to small differences in amount of A23187 used in each case, and the completeness of the extraction process.

However, the CD spectrum of Ca^{2+} resembles those of the 6-coordinate, octahedral complexes when observed in chloroform, but resembles the 7-coordinate complexes when observed in 80% methanol. The differences in the CD spectra of CaA_2 in 80% CH_3OH/H_2O and $CHCl_3$ are shown in Figure III.18. The CD spectra of MgA_2 in 80% CH_3OH/H_2O represents the CD spectrum of a 6-coordinate metal ion:A23187 complex.

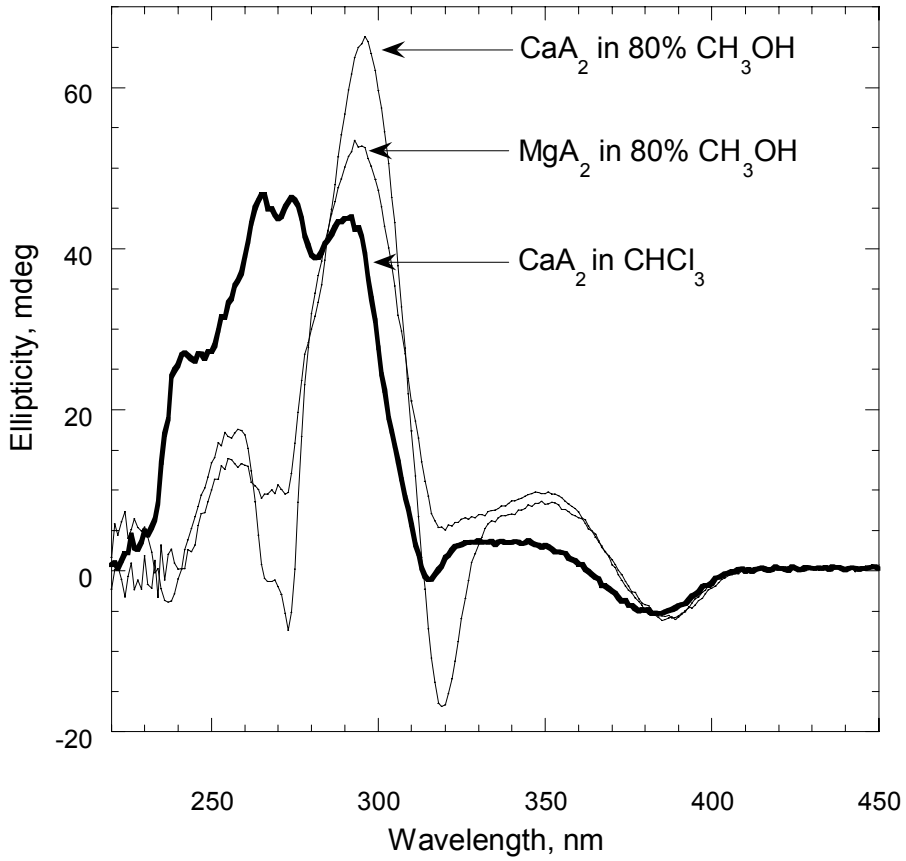

Figure III.18. CD spectra of CaA_2 in 80% CH_3OH/H_2O and $CHCl_3$

These results indicate that the coordination number of the Ca^{2+}/A23187 complex depends on the solvent. In a more polar, coordinating solvent (where donor atoms are available from the solvent), the seventh coordination site is occupied by a solvent molecule, and the complex has a more "open" structure. When in a more non-polar, non-coordinating solvent such as chloroform, only the donor atoms from the A23187

molecules are available, forcing the Ca^{2+} to adopt a coordination number of six because the solvent molecules of chloroform do not have sufficiently polar donor atoms to bind to the Ca^{2+} atom.

Regarding the Cu^{2+} complex, the spectra in $CHCl_3$ do not resemble those of the other metal ion complexes or those of the CuA_2 complex is 80% methanol.

POPC vesicles: Vesicles composed of palmitoyl oleoyl phosphatidyl choline (POPC) were prepared by Thomas et al.[5] to mimic the cell membrane/water interface in which ionophores work. When A23187 was titrated in suspensions of POPC vesicles, Thomas found that both Mg^{2+} and Ni^{2+} displayed spectral characteristics similar to those observed for 80% methanol. This is additional evidence, along with the similarity of metal binding constants in each environment, that 80% methanol is a good model system for the cell membrane-water interface. As shown in Figures III.19a and III.19b, the Mg^{2+} and Ni^{2+} complexes have positive peaks at ~ 290 nm and a set of exciton-coupled peaks centered ~ 350 nm, which are very similar to the spectra observed for each metal titrated with A23187 in 80% methanol. This means the structure of the complex does not change from solution state when partitioned into a vesicle membrane.

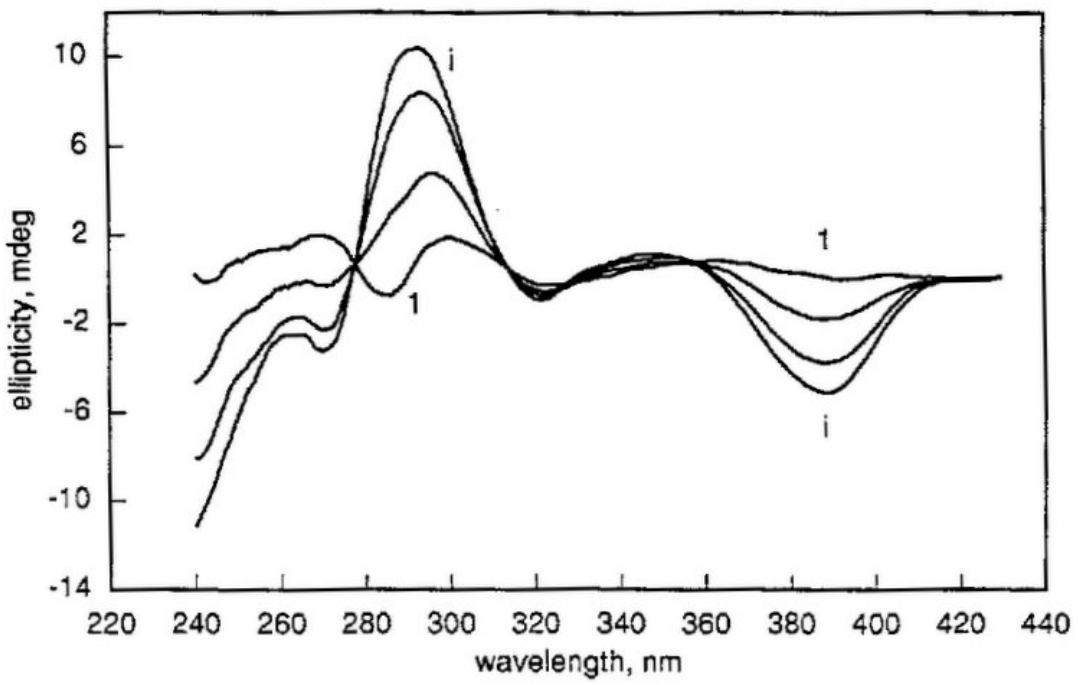

Figure III.19a. CD titration of 50 μM A23187 with Ni^{2+} on POPC vesicles at pH 6.00,[5]

1 = spectrum of HA ($[Ni^{2+}] = 0$), i = spectrum of NiA_2 ($[Ni^{2+}] = 18.7$ μM)

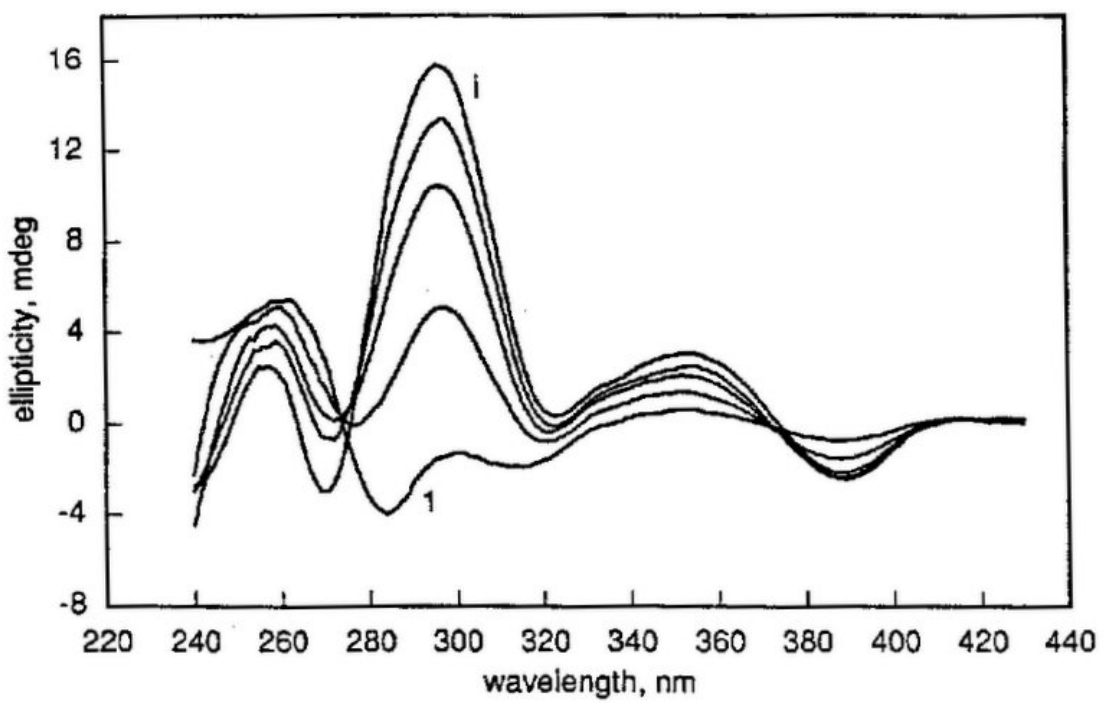

Figure III.19b. CD titration of 50 μM A23187 with Mg^{2+} on POPC vesicles at pH 9.50[5]
1= spectrum of HA ($[Mg^{2+}] = 0$), i = spectrum of MgA_2 ($[Mg^{2+}] = 50$ μM)

The CD spectra of MgA_2 in a POPC vesicle suspension completes a sequence of structural studies that concludes that MgA_2 has the same structure in solid state,[6] $CHCl_3$,[7] 80% CH_3OH/H_2O,[5] and in suspensions of POPC vesicles.[5] The initial MgA_2 data consists of the solid state structure as determined by X-ray crystallography.[6] The complex is found to be 6-coordinate with octahedral geometry. A study of the ^1H NMR spectrum of the MgA_2 complex in $CHCl_3$ compared to the crystal structure indicates that the structures in solid state and in $CHCl_3$ are very similar.[6-7] The CD spectrum of MgA_2 in $CHCl_3$ is therefore labeled as a representative spectrum of a 6-coordinate complex with A23187 that has octahedral geometry. In both 80% CH_3OH/H_2O and in POPC vesicle

suspensions, the CD spectrum of MgA_2 is very similar to the spectrum of MgA_2 in $CHCl_3$, so it can be concluded that the structure of MgA_2 is very similar in all solvents studied.[5] To a limited extent, studies of other metal ion complexes of A23187 rely on this sequence of structural studies to identify the coordination number and geometry of the complex. If the CD spectrum is similar to that of MgA_2, it is assumed to be 6-coordinate with octahedral geometry. If it is not, knowledge of the solid state composition of the complex may aid in determination of the coordination number, such as in the CaA_2 spectra, or similarities between the spectra in question and that of spectra of complexes with known coordination number. Additionally, the spectra can identify the stereochemistry around the metal center if exciton peaks are observed, and the stoichiometry of the complex.

3. X-ray crystallographic Studies of A23187/Metal Complexes

The crystal structures of three metal ion complexes with A23187 had been solved prior to the present study. The structures of CaA_2, MgA_2, and $Fe(II)A_2$ were all found to have three donor atoms per molecule of A23187, head to tail orientation of ionophores, and the appropriate distances and bond angles at the appropriate locations to have one interligand hydrogen bond at each end of the complex.[4,6,8]

The crystal structures presented in this work include an improved structure of the free acid A23187 and the metal ion complexes of Zn^{2+}, Cd^{2+}, Mn^{2+}, Co^{2+}, Ni^{2+}, and Cu^{2+}. The purpose of these studies is to provide background for the wider range of metal ions tested

in transport studies, and for a method of comparison of the solid state structures of metal ion complexes of the parent compound to those of derivatives.

Crystals of several metal/A23187 complexes were grown and analyzed by a Bruker X-ray diffractometer. The crystal structures of several other A23187-metal complexes have been reported previously and those results are included in the present analysis.[4,6,8] When combined with the results of the circular dichroism studies, some interesting correlations are revealed between the coordination number and stereochemistry of the metal center in the solid-state and in solution.

Crystals of A23187 are obtained by dissolving the free acid form of the ligand in 95% CH_3CH_2OH/H_2O followed by slow evaporation. The X-ray structure of the resulting crystal is shown in Figure III.20.

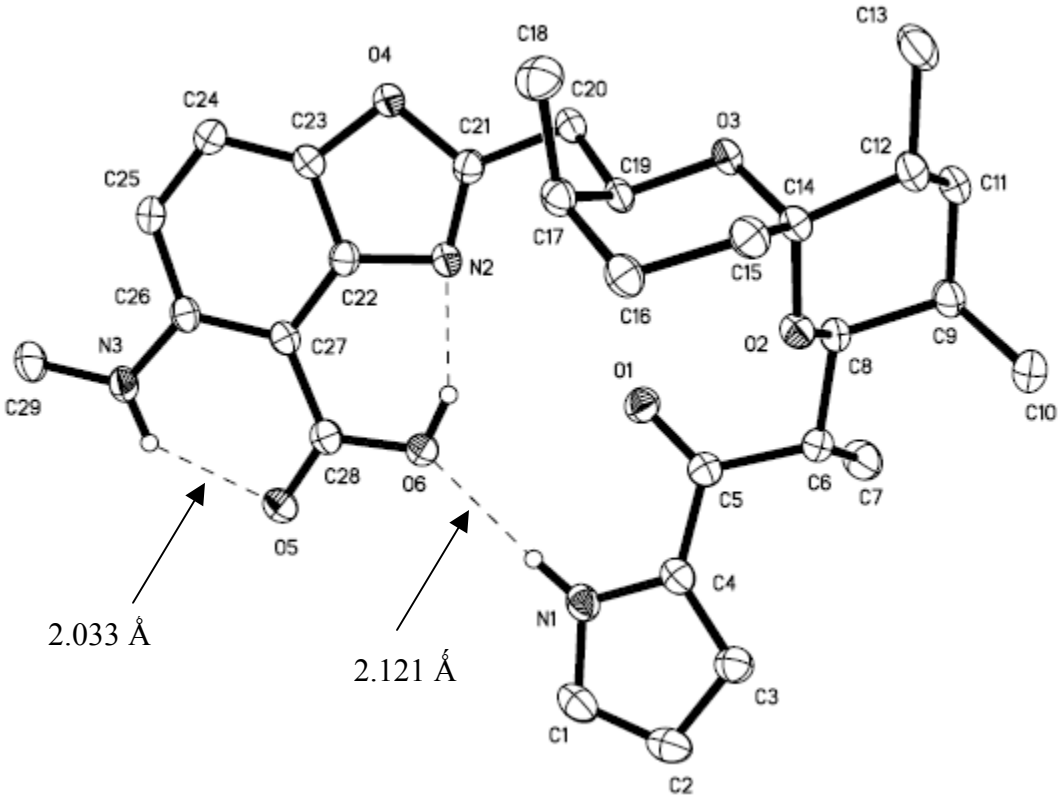

Figure III.20. Crystal structure of A23187

The first crystal structure of A23187, crystallized from acetone, was published in 1974 by Chaney et al.[9] Their results are similar to findings presented here, but do not have the hydrogen atom locations due to poorer resolution (R = 0.063). In that case all hydrogen atoms were placed in idealized positions during refinement.[9] The structure described here is essentially the same as that reported earlier, except that the positions of the hydrogen atoms on the pyrrole nitrogen (N1), methyl amino nitrogen (N3), and carboxyl oxygen (O6) were refined isotropically. This added level of refinement provides a more reliable picture of the hydrogen bond network present in the structure of A23187.

The distance between the methylamino hydrogen and the nearest carboxylic acid oxygen is 2.033 Å and the angle formed between the donor-hydrogen-acceptor atoms (N3-H-O5) is 133.75°. Because hydrogen bonds are likely to form at hydrogen-donor distances of less than 2.7 Å and donor-hydrogen-acceptor angles of over 110°, these measurements indicate the presence of an intraligand hydrogen bond. A second intraligand hydrogen bond is present between the hydrogen attached to the other carboxylic acid oxygen and the benzoxazole nitrogen (O6-H-N2), with a donor-hydrogen distance of 1.833 Å and a bond angle of 153.21°. The distance between the second carboxylic acid oxygen (O6) and the hydrogen atom covalently bonded to the pyrrole nitrogen (N1) is 2.121 Å and the angle formed between the donor-hydrogen-acceptor molecules is 170.20°, which indicates the presence of a third intraligand hydrogen bond between the two ends of the molecule. The closed structure of A23187 in solid state is stabilized by this head-to-tail hydrogen bonding. Additionally, there is no evidence of interligand hydrogen bonding in the solid state structure of the free acid form of A23187.

Zn(A23187)$_2$:

The complex of Zn^{2+} and A23187 is formed by extraction and then crystallized from 95% ethanol. Unless otherwise indicated, all crystalline complexes are formed this way. The structure of the Zn(A23187)$_2$ complex is shown in Figure III.21. A clearer view of the metal center is seen in Figure III.22. The Zn-donor atom distances are shown in Table III.1, and the donor atom-Zn-donor atom bond angles are shown in Table III.2.

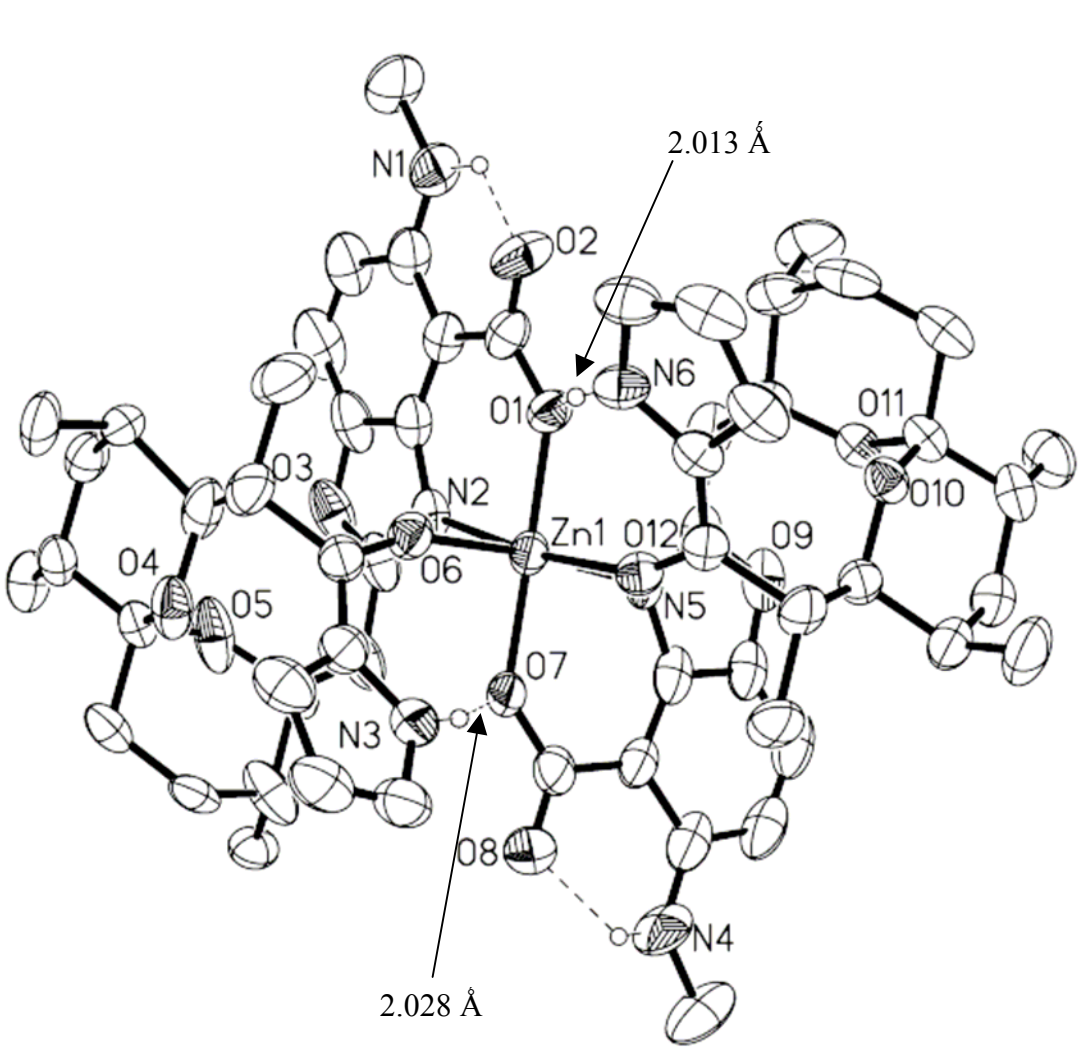

Figure III.21. Crystal structure of Zn(A23187)$_2$ with interligand hydrogen bonds

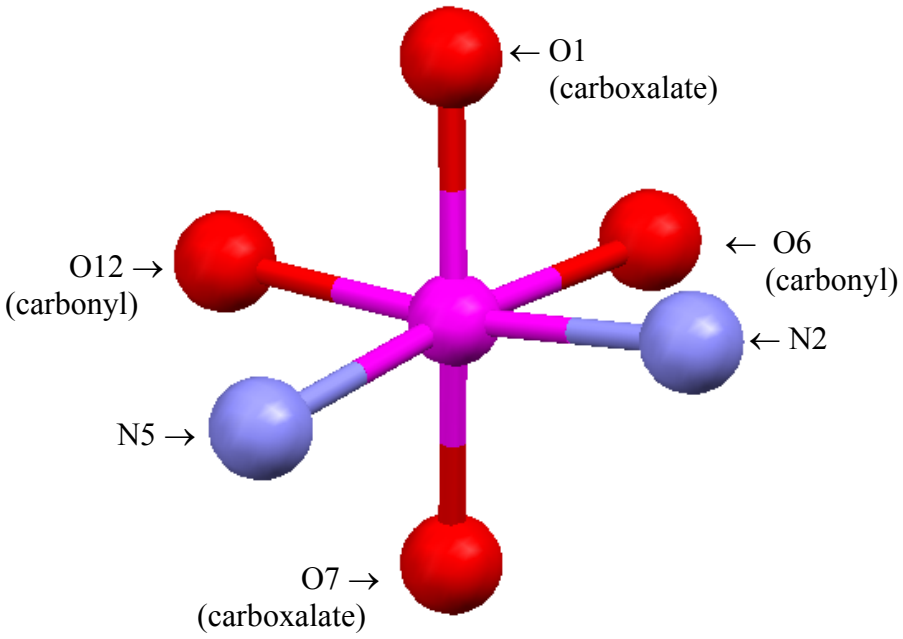

Figure III.22. Metal center of $Zn(A23187)_2$

Metal-Ligand Bond	Distance, Å
Zn-O1 (carboxylate)	1.998
Zn- N2	2.101
Zn-O6 (carbonyl)	2.225
Zn-O7 (carboxylate)	2.010
Zn-N5	2.134
Zn-O12 (carbonyl)	2.150

Table III.1. Metal-ligand distances for $Zn(A23187)_2$

Ligand-Metal-Ligand	Bond Angle, °
N2-Zn-O12 (carbonyl)	85.65
N2-Zn-O1 (carboxylate)	92.34
N2-Zn-O6 (carbonyl)	82.64
N2-Zn-N5	100.02
O1 (carboxylate)-Zn-O6 (carbonyl)	86.95
O1 (carboxylate)-Zn-O12 (carbonyl)	86.29
O1 (carboxylate)-Zn-N2	87.13
O1 (carboxylate)-Zn-N5	101.22
O7 (carboxylate)-Zn-N5	86.42
O7 (carboxylate)-Zn-O6 (carbonyl)	84.94
O7 (carboxylate)-Zn-O12 (carbonyl)	85.79
O7 (carboxylate)-Zn-N2	100.21
O1 (carboxylate)-Zn-O7 (carboxylate)	168.41
N5-Zn-O6 (carbonyl)	172.09
O12 (carbonyl)-Zn-N2	172.46

Table III.2. Bond angles for $Zn(A23187)_2$ metal center

The metal center for the $Zn(A23187)_2$ crystal structure is six-coordinate with octahedral geometry. The two ligands are arranged around the metal center in a head-to-head orientation, with the two benzoxazole nitrogens located cis to one another, the two carbonyl oxygens located cis to one another, and the two carboxylate oxygens located trans to one another. This orientation of the donor atoms is designated as (-), or negative stereochemistry.[2]

Both inter- and intra-molecular hydrogen bonding is observed. The carboxylate oxygen that is not bonded to the zinc atom is engaged in hydrogen bonding to the hydrogen atom covalently bound to the methylamino nitrogen on the same ligand molecule, as found in the free acid form of A23187. These hydrogen bonds are observed for each ligand molecule. The distances between the hydrogen atom and oxygen atom for each ligand is 1.926 Å and 1.962 Å, and the donor-hydrogen-acceptor angles are 134.8° and 130.2°, respectively. The carboxylate oxygen that is bonded to the zinc atom is also engaged in hydrogen bonding to the hydrogen atom that is covalently bound to the pyrrole nitrogen on the opposite end of the second ligand molecule. This interligand hydrogen bonding is observed on both ends of the complex. The distances between the pyrrole hydrogen and oxygen atoms are 2.028 Å and 2.013 Å, and the donor-hydrogen-acceptor angles are 146.80° and 156.73°, respectively. These interligand hydrogen bonds replace the intraligand hydrogen bond observed in the crystal structure of A23187 between the hydrogen attached to the pyrrole nitrogen and one of the carboxylate oxygen atoms.

Cd(A23187)$_2$:

The cadmium/A23187 complex is shown in Figure III.23, and a view of the metal center is shown in Figure III.24. The metal center bond distances and angles are tabulated in Tables III.3-4.

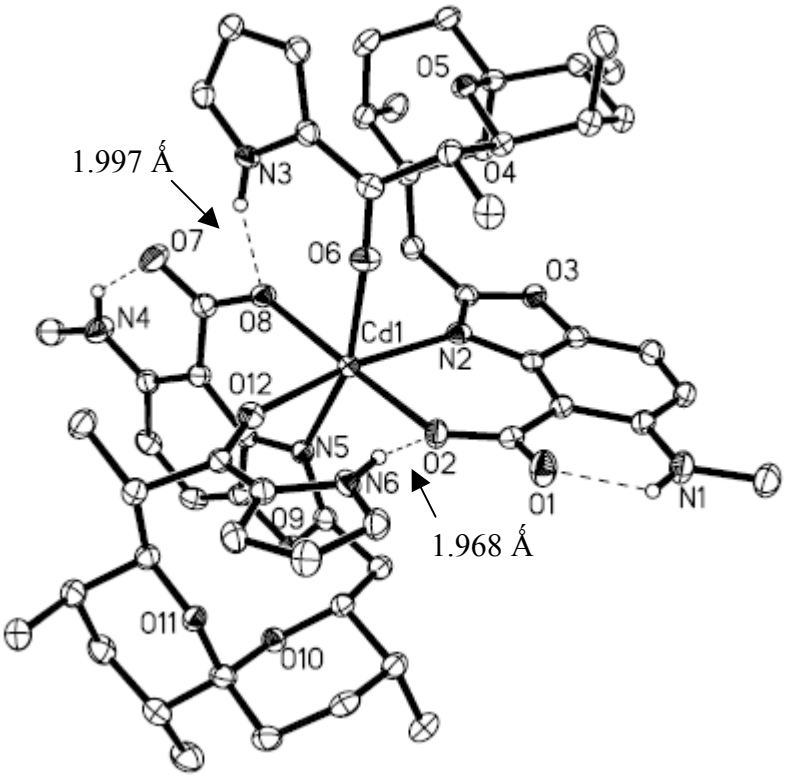

Figure III.23. Crystal structure of Cd(A23187)$_2$ with interligand hydrogen bonds

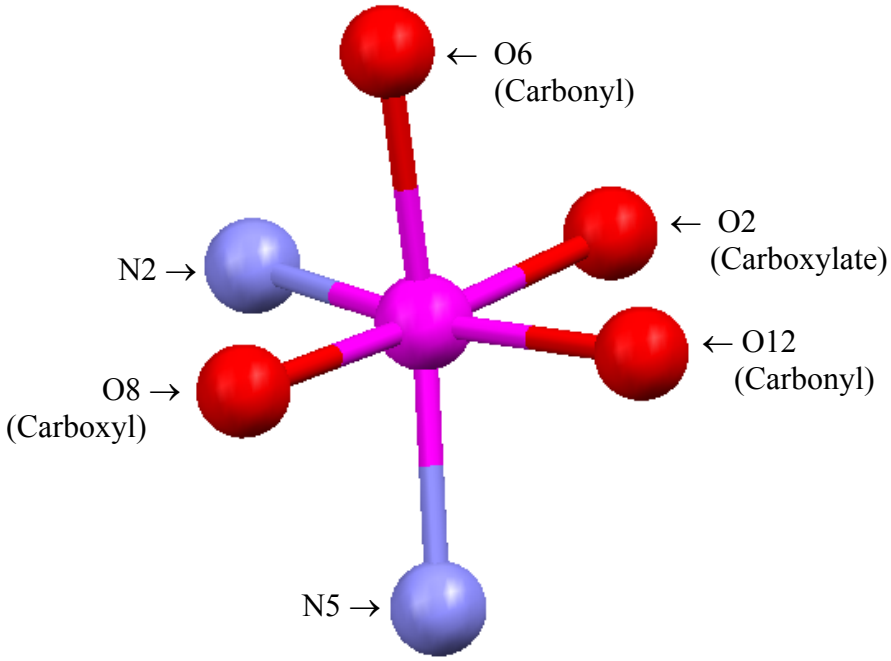

Figure III.24. Metal center of $Cd(A23187)_2$

Metal-Ligand Bond	Distance, Å
Cd-N2	2.305
Cd-O2 (carboxylate)	2.224
Cd-O6 (carbonyl)	2.294
Cd-O12 (carbonyl)	2.310
Cd-N5	2.292
Cd-O8 (carboxylate)	2.225

Table III.3. Metal-ligand distances for $Cd(A23187)_2$

Ligand-Metal-Ligand	Bond Angle, °
O8 (carboxylate)-Cd-N2	102.89
N2-Cd-O2 (carboxylate)	79.40
O2 (carboxylate)-Cd-O12 (carbonyl)	87.85
O12 (carbonyl)-Cd-O8 (carboxylate)	89.73
O6 (carbonyl)-Cd-O8 (carboxylate)	85.81
O6 (carbonyl)-Cd-N2	88.89
O6 (carbonyl)-Cd-O2 (carboxylate)	80.54
O6 (carbonyl)-Cd-O12 (carbonyl)	89.92
N5-Cd-O8 (carboxylate)	80.08
N5-Cd-N2	100.32
N5-Cd-O2 (carboxylate)	104.23
N5-Cd-O12 (carbonyl)	83.79
O6 (carbonyl)-Cd-N5	164.55
O8 (carboxylate)-Cd-O2 (carboxylate)	174.76
N2-Cd-O12 (carbonyl)	167.20

Table III.4. Bond angles for $Cd(A23187)_2$ metal center

The crystal structure of $Cd(A23187)_2$ is very similar to that of $Zn(A23187)_2$. The metal center is approximately octahedral, as indicated by the ~90° and ~180° angles formed by the ligand molecules and the metal center. The hydrogen atoms bonded to each pyrrole nitrogen are 1.997 Å and 1.968 Å from the carboxylate oxygen, of the

opposite ligand molecule, that is bonded to the metal. The angle formed between the donor-hydrogen-acceptor atoms (N-H--O) are 161.00º and 155.75º, respectively. These measurements indicate that the pyrrole hydrogen and carboxylate oxygen of the opposite ligand molecule are involved in hydrogen bonding.

Ni(A23187)$_2$:

The crystal structure of the Ni(A23187)$_2$ complex is shown in Figure III.25 and a view of the metal center is shown in Figure III.26. The metal center bond distances and angles are shown in Tables III.5-6.

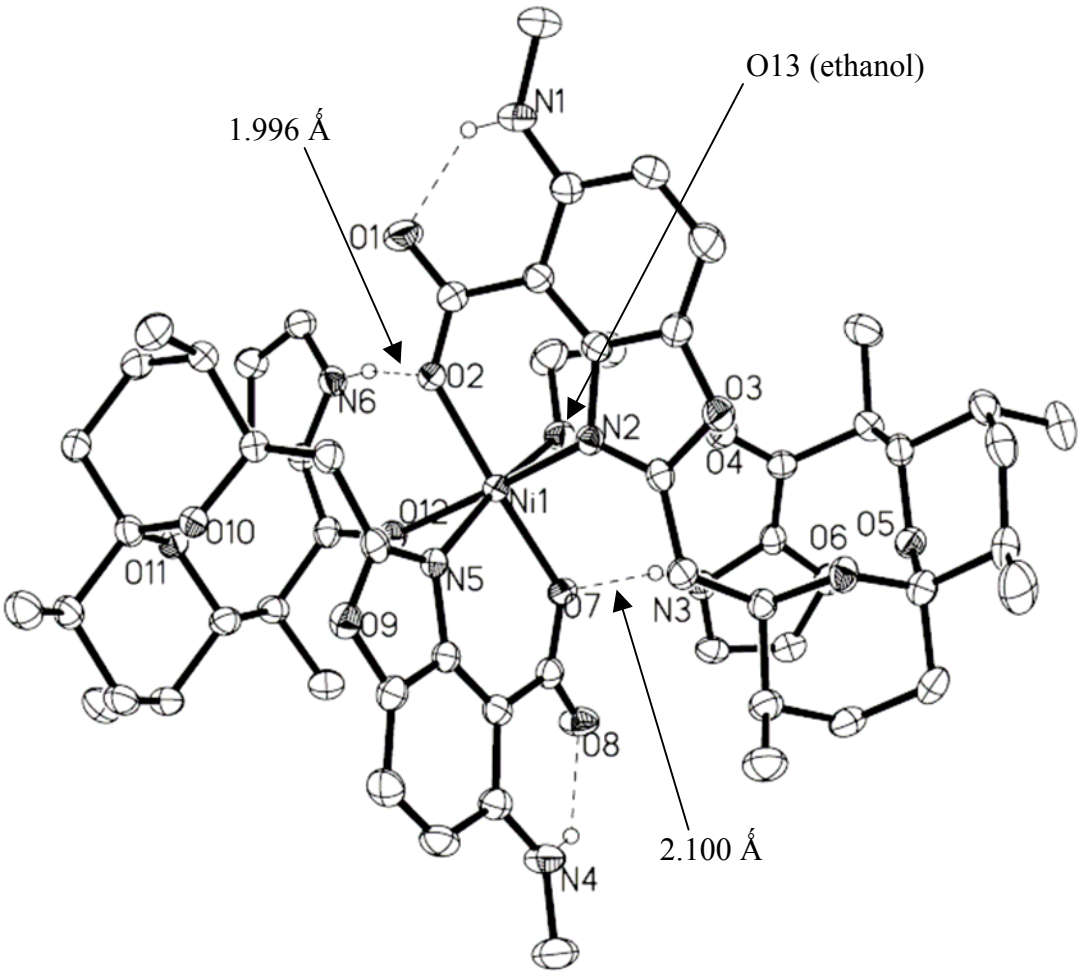

Figure III.25. Crystal structure of Ni(A23187)$_2$ with interligand hydrogen bonds

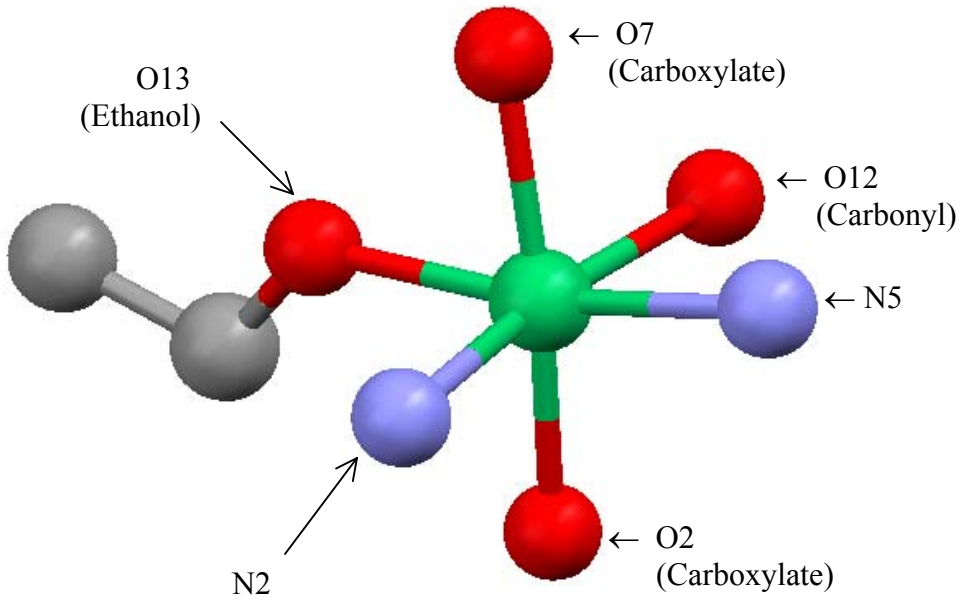

Figure III.26. Metal center of $Ni(A23187)_2$

Metal-ligand Bond	Distance, Å
Ni-O7(carboxylate)	1.998
Ni-N5	2.056
Ni-O12 (carbonyl)	2.162
Ni-O2(carboxylate)	1.992
Ni-N2	2.073
Ni-O13 (EtOH)	2.115

Table III.5. Metal-ligand distances for $Ni(A23187)_2$

Ligand-Metal-Ligand	Bond Angle, °
O2 (carboxylate)-Ni-N5	99.89
N5-Ni-O7 (carboxylate)	89.39
O7 (carboxylate)-Ni- O13 (EtOH)	82.10
O13 (EtOH)-Ni-O2 (carboxylate)	88.33
O1 (carbonyl)-Ni-N5	89.05
O1 (carbonyl)-Ni-O7 (carboxylate)	81.61
O1 (carbonyl)-Ni-O13 (EtOH)	87.68
O1 (carbonyl)-Ni-O2 (carboxylate)	94.60
N2-Ni-O2 (carboxylate)	88.19
N2-Ni-N5	92.00
N2-Ni-O7 (carboxylate)	96.21
N2-Ni-O13 (EtOH)	92.29
O1 (carbonyl)-Ni-N2	172.50
N5-Ni-O13 (EtOH)	170.84
O2 (carboxylate)-Ni-O7 (carboxylate)	169.60

Table III.6. Bond angles for $Ni(A23187)_2$ metal center

The metal center of the $Ni(A23187)_2$ complex is unique among the A23187/metal ion complexes in that it has one tri-dentate and one bi-dentate ligand bound to the metal and a sixth site occupied by a solvent molecule of ethanol. Even with this difference, however, the geometry is octahedral and the stereochemistry (i.e, the arrangement of the

benzoxazole moieties) is comparable to the complexes of Zn^{2+}, Cd^{2+}, Mn^{2+}, Co^{2+}, Mg^{2+}, and Fe^{2+} with A23187.[4,6,8] The pyrrole to carboxylate hydrogen bonds are retained. Hydrogen bonding at either end of the complex is indicated by the distances (2.100 and 1.966 Å) and angles (153.50 and 161.39, respectively) of the donor and acceptor atoms, which are similar to those of the Zn^{2+} and Cd^{2+} complexes. Even though the ketopyrrole oxygen atom is not bound to the metal, the molecule still retains the proper conformation around the metal to keep interligand hydrogen bonds on each side of the complex intact.

Mn(A23187)$_2$:

The crystal structure and metal center of the Mn(A23187)$_2$ complex are shown in Figures III.27-28. The metal-donor atom bond distances and angles are shown in Tables III.7-8.

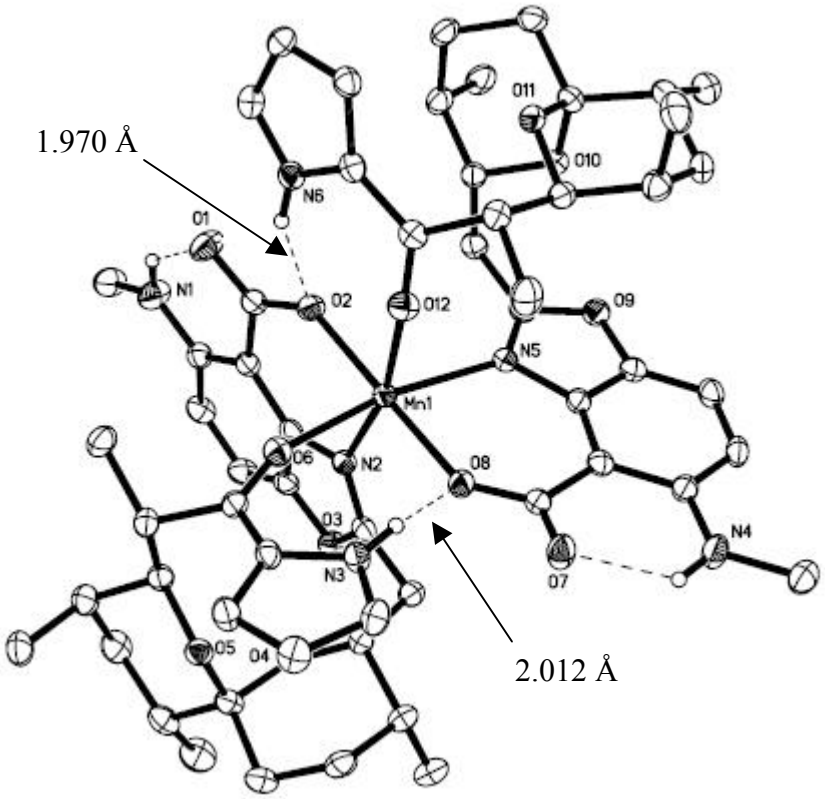

Figure III.27. Crystal structure of Mn(A23187)$_2$ with interligand hydrogen bonds

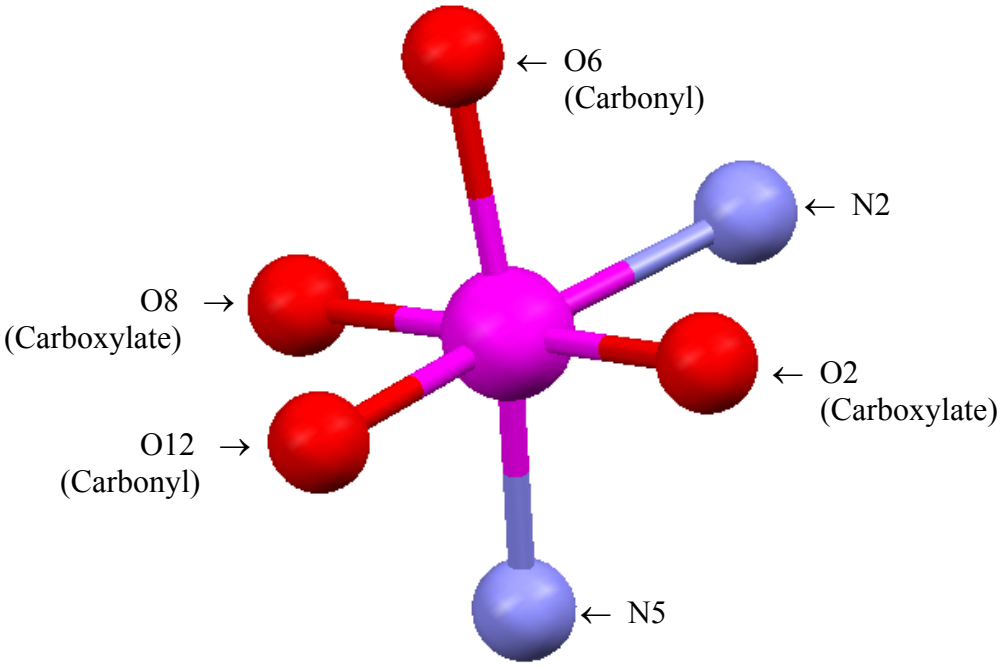

Figure III.28. Metal center of $Mn(A23187)_2$

Metal-Ligand Bond	Distance, Å
Mn-O2 (carboxylate)	2.107
Mn-N2	2.254
Mn-O6 (carbonyl)	2.180
Mn-O8 (carboxylate)	2.109
Mn-N5	2.273
Mn-O12 (carbonyl)	2.171

Table III.7. Metal-ligand distances for $Mn(A23187)_2$

Ligand-Metal-Ligand	Bond Angle, °
O6 (carbonyl)-Mn-O2 (carboxylate)	90.95
O2 (carboxylate)-Mn-N5	100.56
N5-Mn-O8 (carboxylate)	80.32
O8 (carboxylate)-Mn-O6 (carbonyl)	88.22
O12 (carbonyl)-Mn-O2 (carboxylate)	86.44
O12 (carbonyl)-Mn-O6 (carbonyl)	91.61
O12 (carbonyl)-Mn-N5	90.69
O12 (carbonyl)-Mn-O8 (carboxylate)	89.78
N2-Mn-O6 (carbonyl)	86.30
N2-Mn-O2 (carboxylate)	80.88
N2-Mn-N5	95.79
N2-Mn-O8 (carboxylate)	101.92
O12 (carbonyl)-Mn-N2	166.89
O2 (carboxylate)-Mn-O8 (carboxylate)	177.00
N5-Mn-O6 (carbonyl)	168.47

Table III.8. Bond angles for $Mn(A23187)_2$ metal center

The metal center of $Mn(A23187)_2$ consists of two tridentate ligand molecules arranged with octahedral geometry around the metal ion. The stereochemistry matches that of the Zn^{2+}, Cd^{2+}, Ni^{2+}, Ca^{2+}, Mg^{2+}, and Fe^{2+} metal centers.[4,6,8] The distances between the hydrogen attached to the pyrrole nitrogen and the carboxylate oxygen bonded to the

metal for each side of the complex are 2.012 Ǻ and 1.970 Ǻ. The bond angles for each hydrogen bond are 153.81 and 158.8, respectively. The intraligand hydrogen bonding distances between the hydrogen attached to the methylamino nitrogen and the carboxylate oxygen not bound to the metal are 1.975 Ǻ and 1.952 Ǻ. These distances indicate that the complex is stabilized by both inter- and intraligand hydrogen bonds.

Co(A23187)$_2$:

The crystal structure and metal center of Co(A23187)$_2$ are shown in Figures III.29-30. The metal-donor atom bond distances and angles are shown in Tables III.9-10. The methylamino carbon of one ligand is disordered, occupying different positions in the crystal lattice. Additionally, the spiroketal of the opposite ligand is disordered.

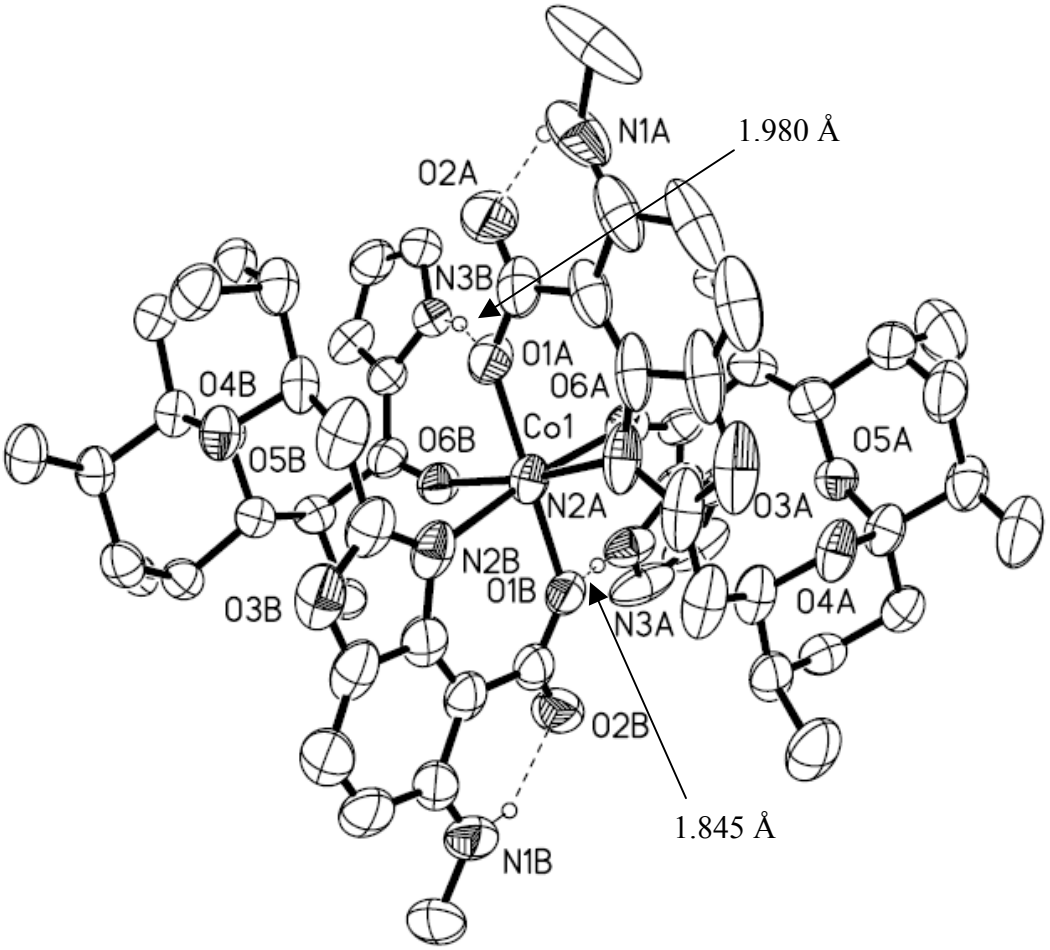

Figure III.29. Crystal structure of CoA$_2$ with interligand hydrogen bonds

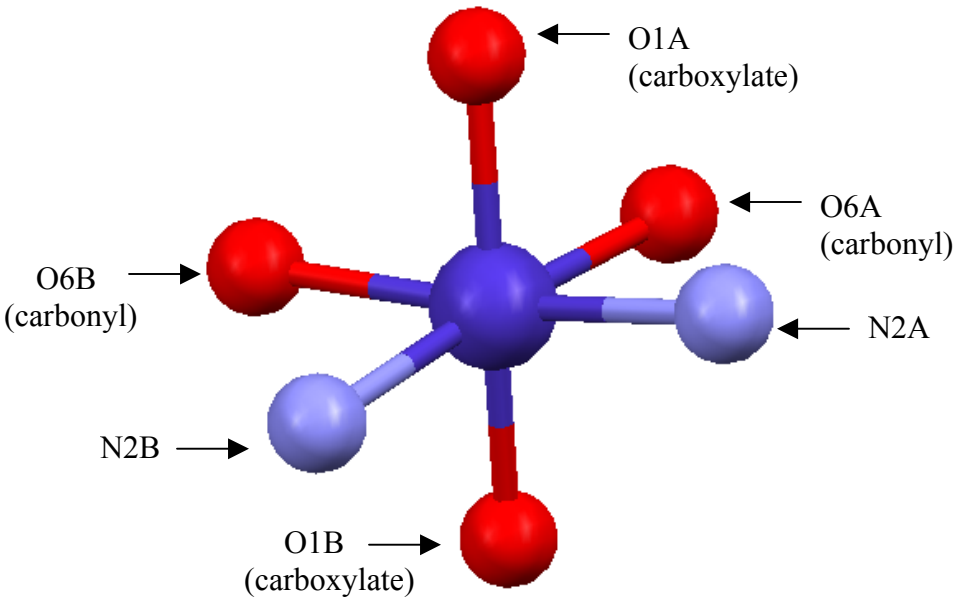

Figure III.30. Metal center of $Co(A23187)_2$

Metal-Ligand Bond	Distance, Å
Co-O1A (carboxylate)	1.993
Co-N2A	2.114
Co-O6A (carbonyl)	2.171
Co-O1B (carboxylate)	2.016
Co-N2B	2.154
Co-O6B (carbonyl)	2.152

Table III.9. $Co(A23187)_2$ metal-ligand distances

Ligand-Metal-Ligand	Bond Angle, °
O1A-Co-N2A	86.42
O1B-Co-N2A	100.52
O1A-Co-O6B	86.85
O1B-Co-O6B	86.00
O1A-Co-N2B	100.10
O1B-Co-N2B	85.23
N2A-Co-N2B	98.65
O6B-Co-N2B	84.12
O1A-Co-O6A	86.74
O1B-Co-O6A	87.99
N2A-Co-O6A	81.71
O6B-Co-O6A	96.30
O1A-Co-O1B	170.60
N2A-Co-O6B	173.08
N2B-Co-O6A	173.16

Table III.10. Bond angles for $Co(A23187)_2$ metal center

The metal center of $Co(A23187)_2$ is very similar to many other complexes of A23187. It consists of a 6-coordinate metal complex with octahedral geometry around the metal ion. It has two interligand hydrogen bonds on either side of the complex.

Cu(A23187)$_2$:

The crystal structure of the Cu(II)/A23187 complex is shown in Figure III.31 and the donor atom geometry around the metal center is shown in Figure III.32. The metal center bond distances and angles are shown in Tables 11-12.

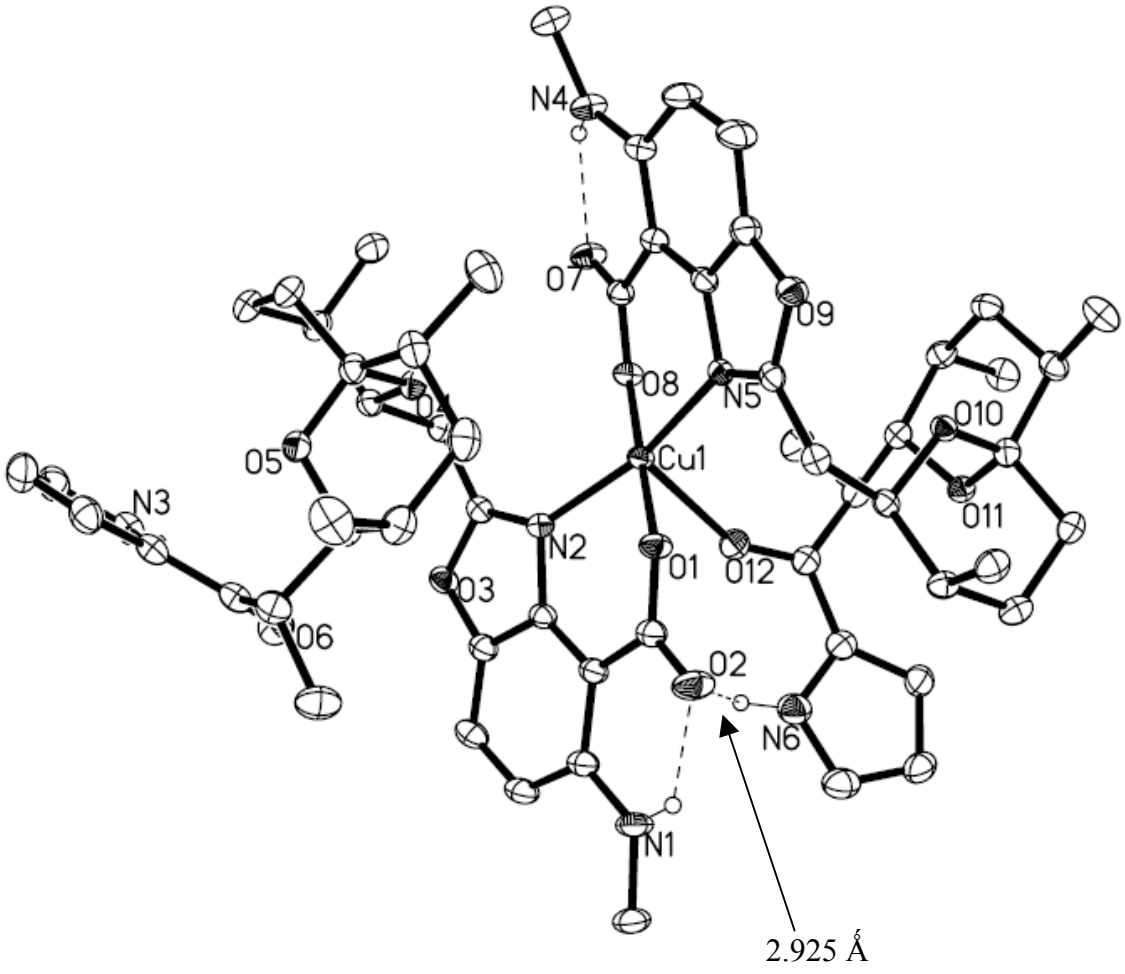

Figure III.31. Crystal structure of Cu(A23187)$_2$ with interligand hydrogen bond

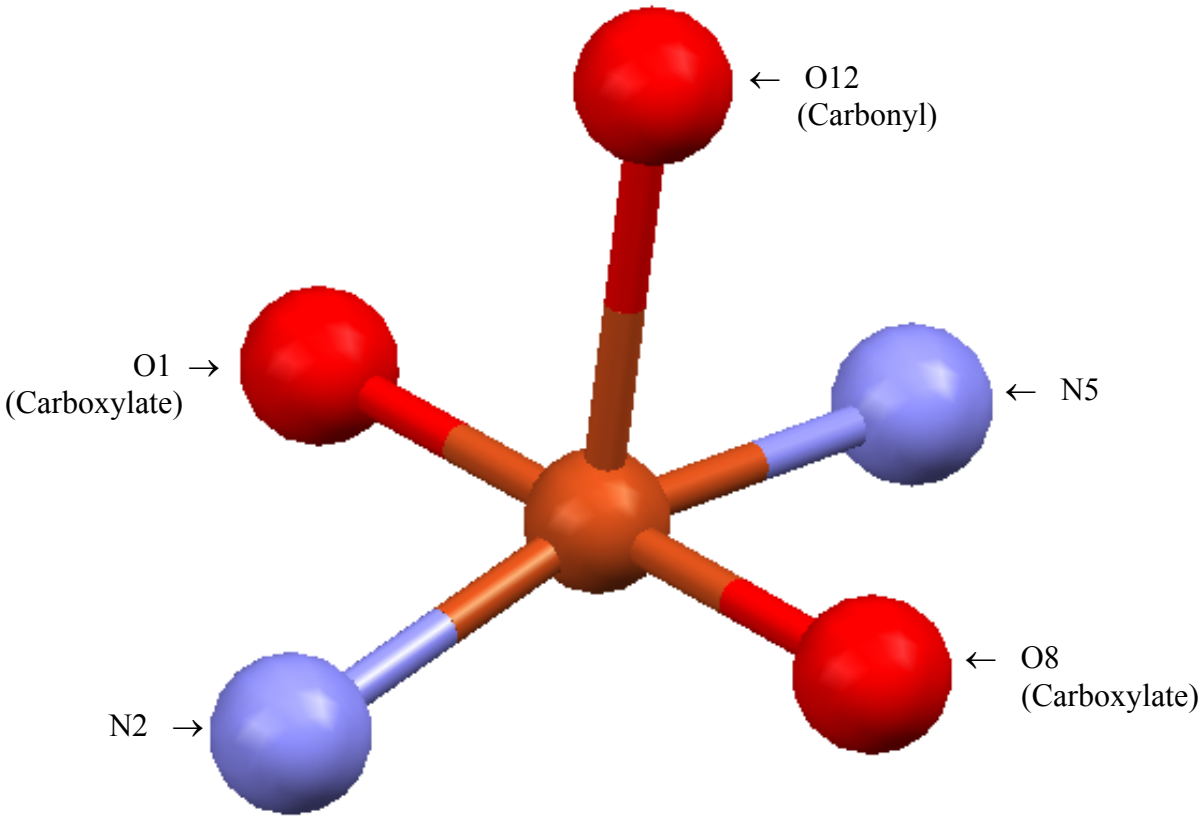

Figure III.32. Metal center of $Cu(A23187)_2$

Metal-Ligand Bond	Distance, Å
Cu-O8 (carboxylate)	1.912
Cu-N5	2.010
Cu-O12 (carbonyl)	2.392
Cu-O1 (carboxylate)	1.914
Cu-N2	1.999

Table III.11. Metal-ligand distances for $Cu(A23187)_2$

Ligand-Metal-Ligand	Bond Angle, °
N5-Cu-O2 (carboxylate)	89.10
O2 (carboxylate)-Cu-N2	89.77
N5-Cu-O8 (carboxylate)	89.62
O8 (carboxylate)-Cu-N5	91.61
O12 (carbonyl)-Cu-N5	89.13
O12 (carbonyl)-Cu-O2 (carboxylate)	86.64
O12 (carbonyl)-Cu-N2	105.84
O12 (carbonyl)-Cu-O8 (carboxylate)	93.08
N5-Cu-N2	164.80
O2 (carboxylate)-Cu-O8 (carboxylate)	179.23

Table III.12. Bond angles for $Cu(A23187)_2$ metal center

The metal center of the $Cu(A23187)_2$ complex differs from all other complexes in several ways. The primary difference is that the metal is bound by five donor atoms rather than six. The ketone of the second ligand molecule does not bind to the metal. While the binding motif of one tridentate and one bidentate ligand is also observed in the nickel complex, the nickel complex incorporates a solvent molecule to preserve the 6-coordinate, octahedral geometry common to other complexes, and retains the two interligand hydrogen bonds that stabilize the complex. The copper complex does not incorporate any solvent donor atoms, and thus has a 5-coordinate, square pyramidal

geometry, with the carboxylate oxygens and the benzoxazole nitrogens serving as the base of the pyramid.

The carbonyl oxygen that does not bind to the copper atom, and the adjoining pyrrole group, are found in a location away from the metal center, rather than close to the position observed in the nickel complex. This results in disruption of part of the hydrogen bonding network common to other complexes. The single interligand hydrogen bond remaining is between the pyrrole hydrogen of the tridentate ligand and the carboxylate oxygen of the bidentate ligand, with a distance of 2.925 Å and a donor-hydrogen-acceptor angle of 122.53°. In this case, the carboxylate oxygen not bound to the metal is involved in the hydrogen bond, whereas in all the other complexes the hydrogen bonding occurs with the carboxylate oxygen bound to the metal. The hydrogen bonding distance is longer than that of other complexes, and has a smaller angle between the donor-hydrogen-acceptor atoms.

The other intraligand hydrogen bonds of $Cu(A23187)_2$ remain intact. For the tridentate ligand, the methylamino hydrogen and carboxylate oxygen are 2.013 Å apart, and for the bidentate ligand the corresponding hydrogen bond is 1.957 Å in length.

The stereochemistry of the metal center is opposite of the metal center stereochemistry of all other known complexes of A23187. The benzoxaxole nitrogens for each ligand are trans to one another, as are the carboxylate oxygens. In most complexes, the carboxylate oxygens are trans to one another, but the benzoxazole nitrogen atoms are cis.

Additional structural information is offered by crystal structures solved by other researchers. Crystal structures of $Ca(A23187)_2$, $Fe(A23187)_2$, and $Mg(A23187)_2$ were solved in 1975, 1983, and 1985, respectively, by Smith and Duax[4], Baker et al.,[8] and Alléaume and Barrans,[6] respectively. The Mg^{2+} and Fe^{2+} complexes are 6-coordinate, octahedral, and identical in stereochemistry to the Zn^{2+}, Cd^{2+}, Mn^{2+}, and Ni^{2+} complexes presented above. The Ca complex is 7-coordinate, with the usual octahedral geometry distorted by a coordinated solvent molecule, and also has stereochemistry similar to the Zn^{2+}, Cd^{2+}, Mn^{2+}, and Ni^{2+} complexes.

B. Protonation and complexation properties of A23187

The protonation and metal complexation properties of A23187 are studied by titrating ~ 50 μM A23187 with the strong base $(CH_3)_4NOH$ (~ 1.3 M). At approximately every 0.5 pH^* unit between pH^* values 3 and 12, the UV-vis spectrum is recorded. Titrations are performed without metal (shown in Figure III.33) to measure protonation constants. Titrations performed with a fixed ratio of either Zn^{2+} or Cd^{2+} are useful for comparison to the spectra of A23187 without metal, and also to gain information about the metal complexation properties of A23187.

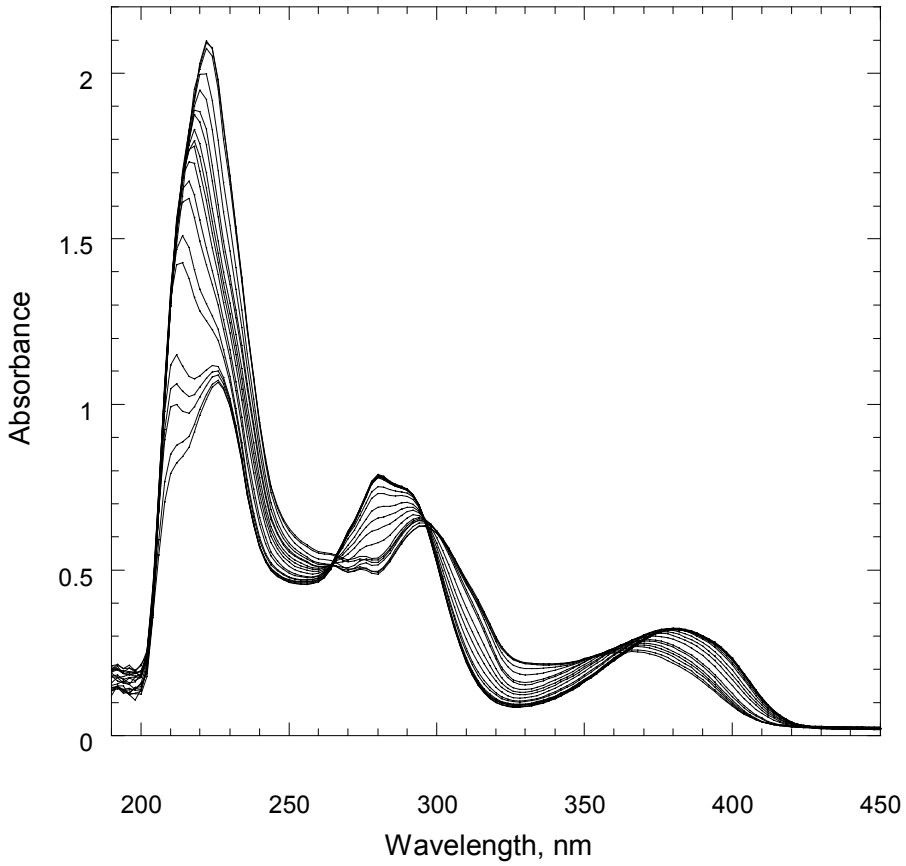

Figure III.33. UV-vis spectra of A23187 titrated with $(CH_3)_4NOH$ in 80% CH_3OH/H_2O

The absorbance at a single wavelength (one which undergoes a relatively large change during the titration) is plotted as a function of pH^*. The number of breaks in the curve are indicative of the number of protonation states the ligand can assume within the pH^* range. The titration is reversible, in that incremental addition of acid after one pH^* titration produces the same absorbance changes at the same pH^* values. Further addition of base results in a repeat of results of the initial low to high pH^* titration. While not all protonation changes may be observed at any single wavelength, the number of

protonation states will not be less than that indicated by such a graph. The plot of absorbance at 382 nm as a function of pH^* is shown in Figure III.34.

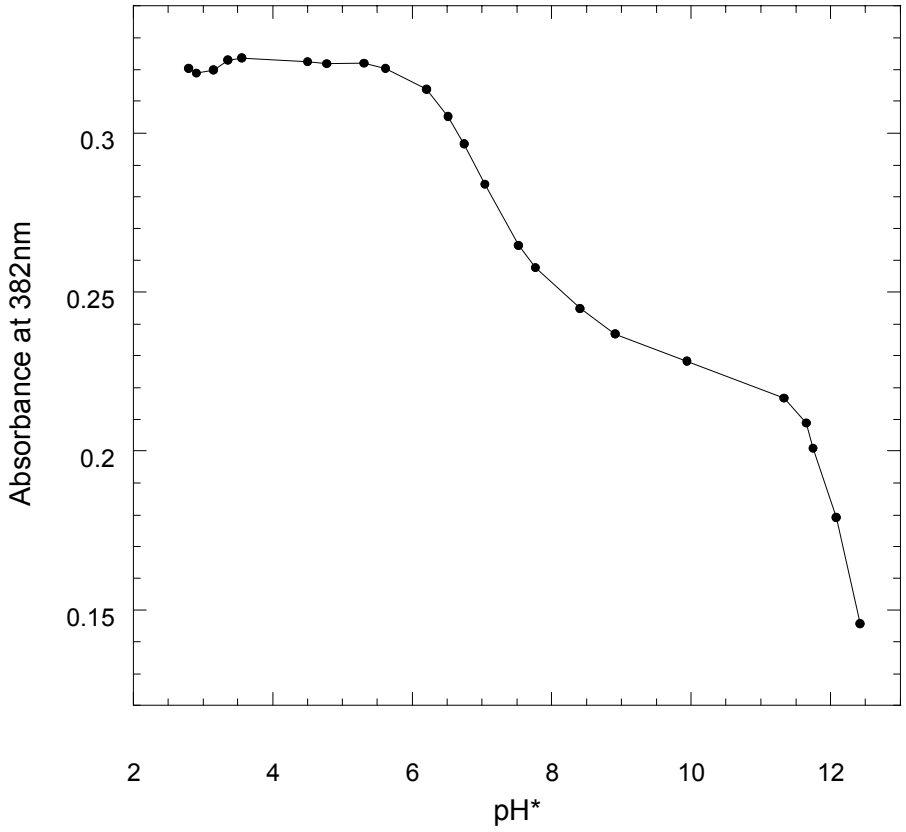

Figure III.34. Absorbance at 382 nm of A23187 in 80% CH_3OH/H_2O titrated with $(CH_3)_4NOH$

This plot indicates that three protonation states (or two changes in protonation states) exist in the pH^* 3-12 range. While the change that occurs around pH^* 7.8 is well known,[10] the change that occurs at pH^* 11.7 has not been previously factored into protonation and complexation schemes for A23187. The lower pK_a is logically assigned to the carboxylic

acid group located on the benzoxazole moiety of A23187.[1] The higher pK_a may be attributed to the loss of the hydrogen attached to the pyrrole nitrogen. The second pK_a becomes important when proposing binding schemes for A23187 and metals. While previous studies concluded that at higher pH, the A23187/metal complex transforms from a MA^+ complex to a MAOH complex,[11] the loss of a second hydrogen on the ligand would also explain the results. A ligand with two hydrogens dissociated would possess a 2- charge, which would neutralize the 2+ charge of a divalent metal. It would also create an additional donor site (the pyrrole nitrogen) that could satisfy the coordination requirements of the majority of divalent metals included in this study. The ligand is flexible enough to achieve such a conformation, as evidenced by the crystal structure of the free acid form of A23187. This 2- ligand could not, however, meet the coordination requirements of calcium without additional solvent binding to the metal. Therefore, a binding scheme accounting for two deprotonation steps would help explain the binding and/or transport selectivity displayed by A23187 in 80% CH_3OH/H_2O.

$\underline{Zn^{2+}}$: The spectra of A23187 in 80% CH_3OH/H_2O with a 1:1 ratio of Zn^{2+} present titrated with the strong base $(CH_4)_3NOH$ are shown in Figure III.35. The spectra are somewhat similar to those in the titration of A23187 without metal (except for the absence of a peak at ~ 325 nm), however, the absorbance change that occurs at λ = 280 nm is more pronounced, and there is an additional large absorbance change at λ = 330 nm. These spectra show an isosbestic point at lower pH^* values, but above pH^* values of 9, the absorbance at this wavelength is lower than at the isosbestic point. In comparison

with the titration of A23187 without metal, the isosbestic point is shifted from ~ 298 nm to ~ 308 nm.

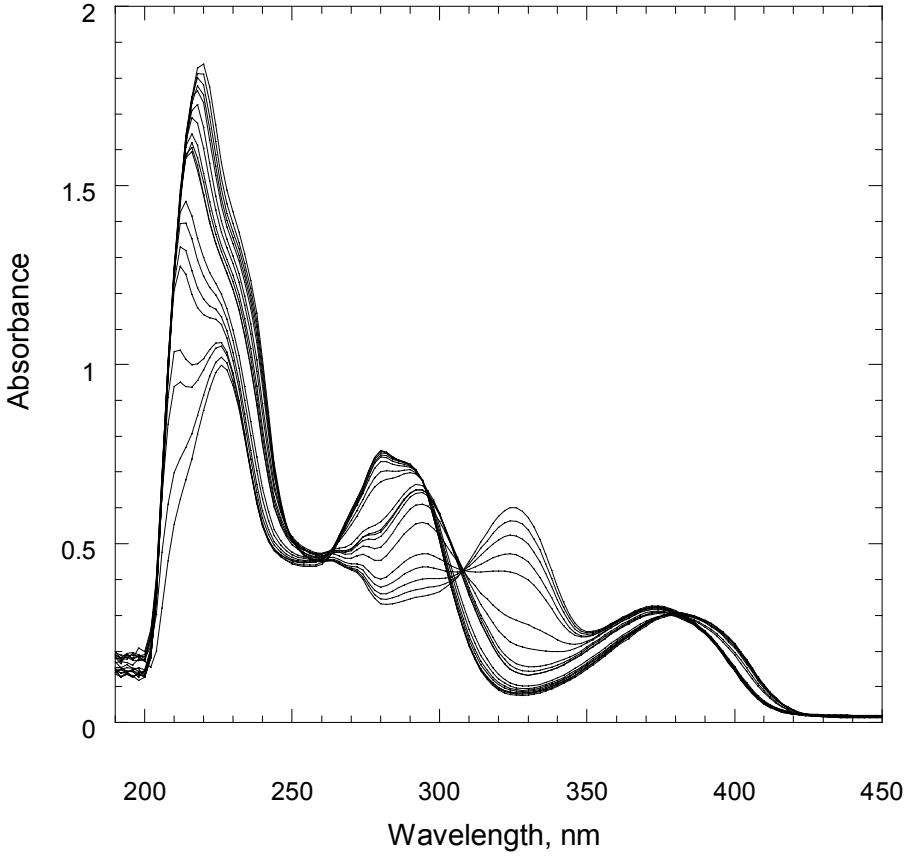

Figure III.35. UV-vis spectra of A23187:Zn^{2+} (1:1) in 80% CH_3OH/H_2O titrated as a function of pH*

When absorbance at 324 nm, a wavelength of relatively large absorbance change, is plotted as a function of pH^* (Figure III.36), two breaks in the titration curve are observed. This indicates two equilibria are represented under titration conditions (50 μM ligand, 1:1 ratio of ligand to metal, and pH^* range 3-12).

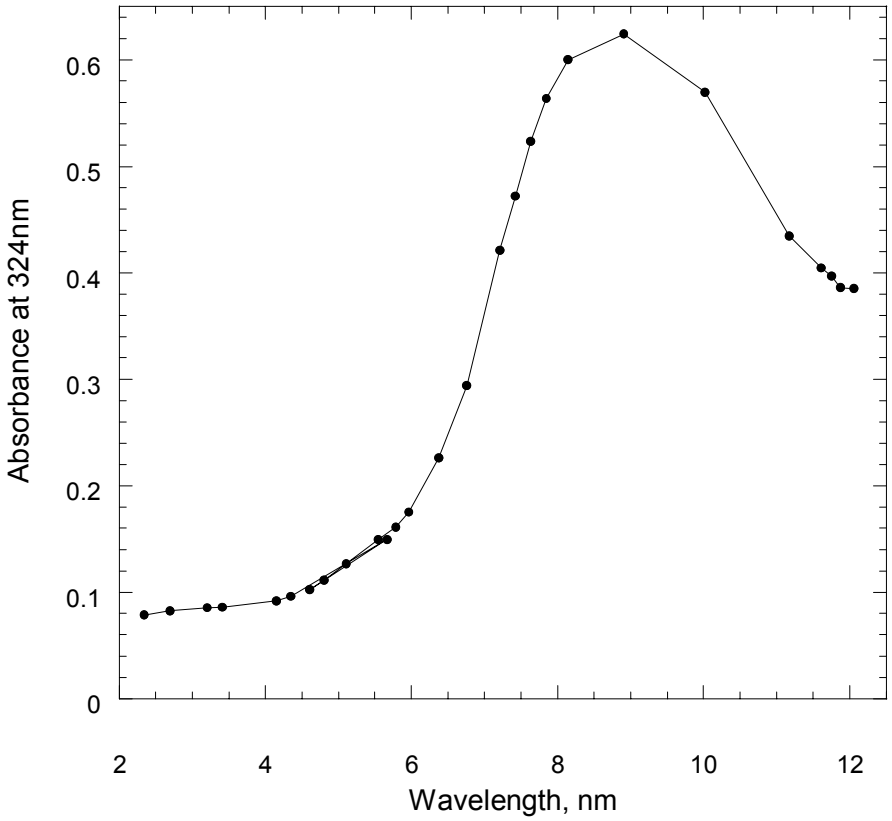

Figure III.36. Absorbance at 324 nm of A23187:Zn^{2+} (1:1) in 80% CH_3OH/H_2O titrated as a function of pH^*

$\underline{Cd^{2+}}$: The titration of A23187 in 80% CH_3OH/H_2O with a 1:1 ratio of Cd^{2+} as a function of pH^* is shown in Figure III.37. The titration does not produce the same smooth spectral changes observed for Zn^{2+}/A23187 and A23187 alone. The absorbance changes at 330 nm and 280 nm are both smaller than observed in the Zn^{2+} titration.

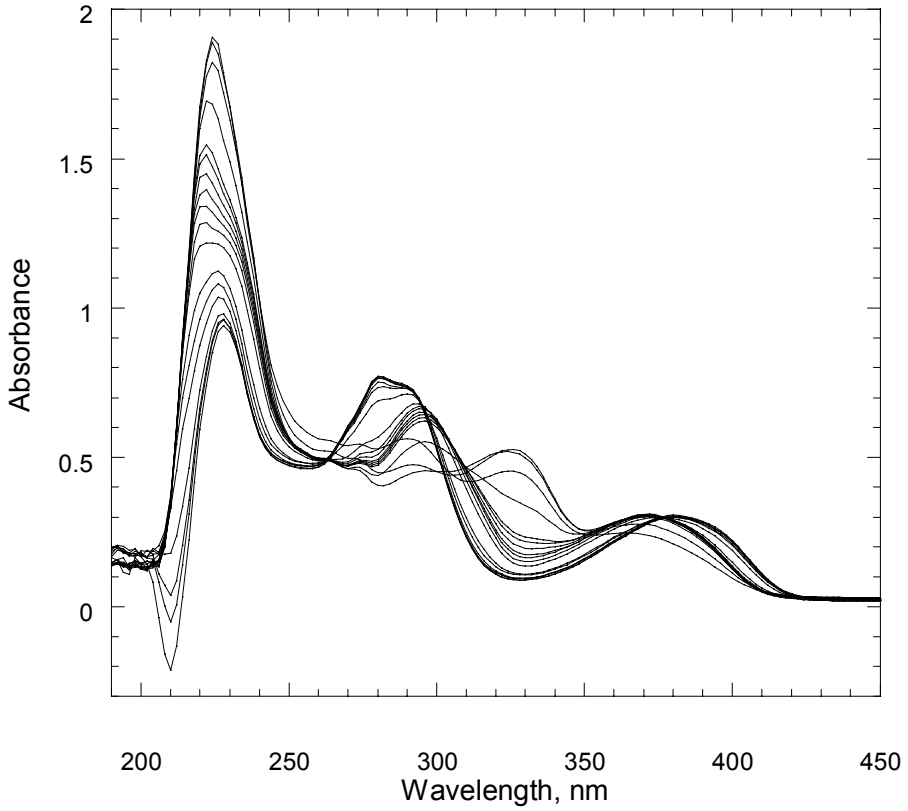

Figure III.37. UV-vis spectra of A23187:Cd^{2+} (1:1) in 80% CH_3OH/H_2O titrated as a function of pH^*

A plot of absorbance at 280 nm as a function of pH*, shown in Figure III.38, indicates that possibly three equilibria are represented in the titration, which explains the lack of clear isosbestic points in the spectral data.

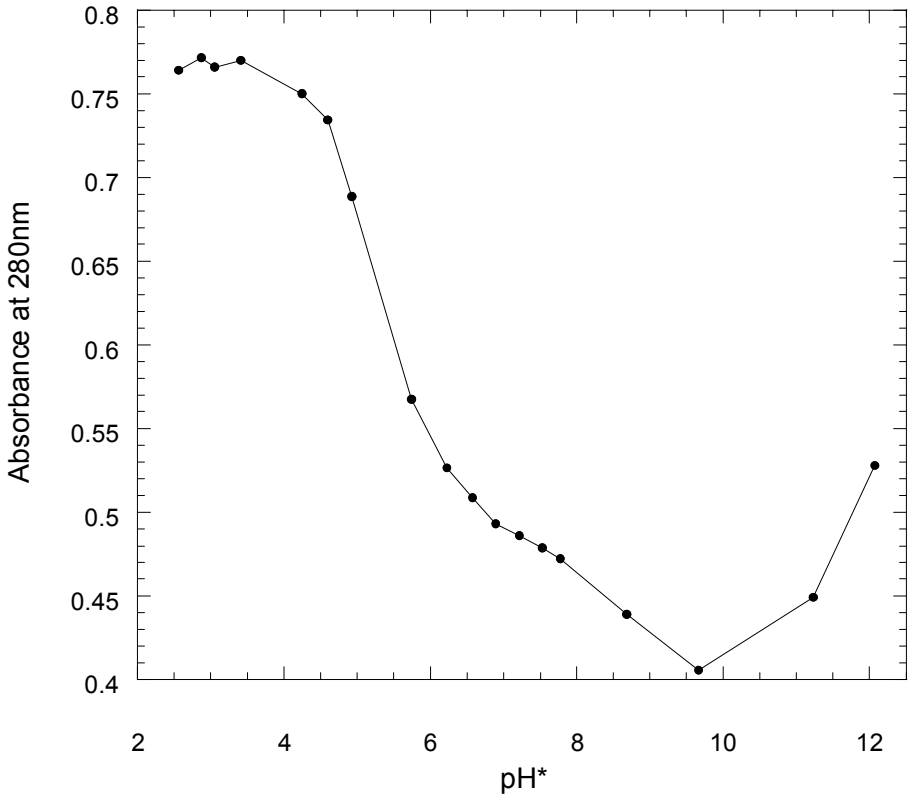

Figure III.38. Absorbance at 280 nm of A23187:Cd^{2+} (1:1) in 80% CH_3OH/H_2O titrated as a function of pH*

C. Summary

Structural Properties: Through analysis of metal/A23187 complex crystal structures, several important features can be observed. In the most common group of A23187/metal structures, a 2:1 ligand:metal ratio is observed, and three donor atoms per ligand are bound to the metal. The stereochemistry about the metal center is the same for all complexes (except CuA_2), with carboxylate functionalites that are trans to one another, and benzoxazole and ketopyrrole moieties that are cis to the equivalent moiety of the opposite ligand. In all structures observed, both donor atoms from the benzoxazole moiety are coordinated to the metal center. Alternate coordination numbers of 5 (CuA_2) and 7 (CaA_2) have been observed, and are due to differences in the participation of the ketopyrrole carbonyl oxygen and/or solvent molecules. Several properties of the metal center, including average cis and trans angles, hydrogen bond distances, and hydrogen bond angle are summarized in Table III.13.

MA_2	C.N*./ Stereo-chem.	CFSE** Δ	Average and range of trans angles (°)	Average and Range of cis angles (°)	Intraligand H-bond Distances (Å) and angles (°)	Interligand H-bond distances (Å) and angles(°)
ZnA_2	6 / -	0	170.9 ± 2.24 (168.41-172.46)	89.9 ± 6.43 (82.64-101.22)	1.962, 1.926 130.21, 134.88	2.013, 2.028 146.80, 156.73
CdA_2	6 / -	0	168.8 ± 5.30 (164.55-174.76)	89.45 ± 8.34 (79.40-104.23)	1.942, 1.965 134.60, 132.39	1.968, 1.997 161.00, 155.75
NiA_2	6 / -	1.2	170.98 ± 1.46 (169.60-172.50)	90.11 ± 5.10 (81.61-99.89)	1.929, 1.947 134.34, 133.69	2.100, 1.996 153.50, 161.39
MnA_2	6 / -	0	170.79 ± 5.43 (166.89-177.00)	90.29 ± 6.43 (80.32-101.92)	1.952, 1.975 134.59, 132.66	1.970, 2.012 158.84, 153.81
CoA_2	6 / -	0.8	172.28 ± 1.45 (170.6-173.16)	90.05 ± 6.78 (81.71-100.52)	1.94, 1.81 138, 134	2.06, 2.03 152, 159
MgA_2[6]	6 / -	0	173.9 ± 4.34 (170.5-178.8)	90.1 ± 4.5 (82.6-96.6)	2.096, 2.032 110.87, 138.53	2.061, 2.072 157.16, 159.91
FeA_2[8]	6 / -	0.4	171.5 ± 1.6 (169.8-173.0)	90.1 ± 5.8 (83.6-100.2)	1.954, 1.894 124.91, 132.67	2.010, 2.022 162.18, 146.95
CaA_2[4]	7 / -		-----	-----	-----	-----
CuA_2	5 / +	0.6	172.015 (164.8-179.23)	91.84875 (86.64-105.84)	2.013, 1.957 130.13, 134.33	2.925 122.53

*C.N. = Coordination number, **CFSE = Crystal field stabilization energy for octahedral complexes

Table III.13. Summary of MA_2 metal center properties[4,6,8]

The stereochemistry of the octahedral metal center is labeled "negative" and is illustrated in Figure III.39.

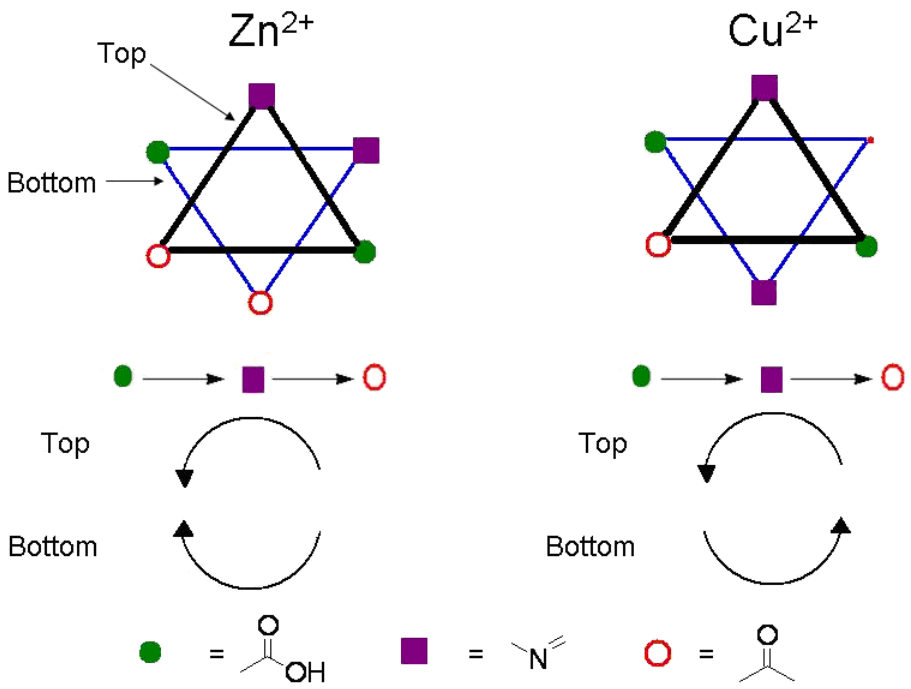

Figure III.39. Diagram of Zn^{2+} and Cu^{2+} metal center stereochemistry in the 1:2 metal/A23187 complex

The orientation of the donor atoms, going from the carboxylate oxygen to the benzoxazole nitrogen, to the ketopyrrole carbonyl, in order, are opposite one another. The MA_2 complexes of Zn^{2+}, Cd^{2+}, Mn^{2+} Co^{2+}, Ni^{2+}, Ca^{2+}, Fe^{2+}, and Mg^{2+} with A23187 have this "negative" stereochemistry. In the case of $Cu(A23187)_2$, the donor atom stereochemistry is "positive". In this case, observed by both X-ray crystallography and CD, the arrangement of donor atoms of each ligand rotate in the same direction.

The stereochemistry of each metal center is also evident in the circular dichroism spectra of each complex in 80% CH_3OH/H_2O. Each complex studied has a set of exciton coupled peaks whose order is indicative of absolute stereochemistry. The complexes whose crystal structure indicates negative stereochemistry have a positive exciton coupled peak at lower wavelength and a negative exciton coupled peak at higher wavelength. Several metal complexes that were not studied by X-ray crystallography also displayed this trend in CD spectra, which indicates their stereochemistry agrees with those whose crystal structures are known. However, the exciton peaks of the Cu^{2+} complex have the reverse order, with the negative peak at lower wavelength and a positive peak at higher wavelength.

The composition of the crystal structure and that observed in solution varies somewhat. While most metal complexes possess octahedral geometry using 3 donor atoms from each of the two ligands in both solid and solution state, the $Ni(A23187)_2$ complex appears to have 6 ligand donor atoms when observed in 80% CH_3OH/H_2O and $CHCl_3$, but 5 ligand donor atoms and one solvent donor atom when observed crystallized from 95% CH_3CH_2OH/H_2O in solid state. The fact that one carbonyl group is not bound in the NiA_2 X-ray structure may be due to packing forces in formation of the crystal and that an ethanol molecule was available from the solution used for growing crystals. The ethanol oxygen takes the place of the carbonyl group so the complex is not destabilized. Growing crystals from a non-coordinating solvent might lead to a complex in which the carbonyl functionality from both ligands were bound to the metal ion. In spite of the presence of a solvent molecule, both interligand hydrogen

bonds are present, because the ligand with the unbound carbonyl group retains the correct position to form a hydrogen bond.

The effect of solvent upon the composition of the complex is also notable: studies of the same complex in both 80% CH_3OH/H_2O, a coordinating polar solvent, and $CHCl_3$, a non-polar, non-coordinating solvent, are presented. Zn^{2+}, Mg^{2+}, Cd^{2+}, Mn^{2+}, Fe^{2+}, Ni^{2+}, and Co^{2+} appear to be 6-coordinate in both solvents. Ca^{2+}, Sr^{2+}, Ba^{2+}, Gd^{3+}, and Lu^{3+}, however, appear to be 7-coordinate or greater in 80% CH_3OH/H_2O, as concluded by the extra peaks at low wavelength in the CD spectra. The X-ray structure of CaA_2 is 7-coordinate with 6 ligand donor atoms and one solvent donor atom. Sr^{2+}, Ba^{2+}, Gd^{3+}, and Lu^{3+} complexes with A23187 have CD spectra in 80% CH_3OH/H_2O similar to that of the complex of Ca^{2+} in the same solvent, so it is reasonable to conclude that they all have a coordination number of 7 in 80% CH_3OH/H_2O. In $CHCl_3$, however, the CD spectrum of Ca^{2+} resembles that of a 6-coordinate metal, indicating that in a non-coordinating solvent of lower polarity, the Ca-complex loses the additional solvent bound to the metal, and is forced into having a lower coordination number than is typical for the metal ion, whose coordination number generally ranges from 7 to 9.[3] The coordination number is not a function of the size of the ion. Both Ca^{2+} and Cd^{2+} have similar ionic radii of ~ 1 Å (for coordination number = 6).[3] There is a point, however, at which the ionic radii becomes too large for two ligands to effectively shield the charge of the ion from the environment. The ligands do not enclose the metal ion completely, thus leaving room for one or more solvent molecules to bind to the ion and further inhibit transport across a membrane.

REFERENCES:

1. Pfeiffer, D. R., Reed, P. W., and Lardy, H. A. *Biochemistry*, **1974**, *13*, 4007-4013.

2. Charney, E. *The Molecular Basis of Optical Activity: Optical Rotatory Dispersion and Circular Dichroism*; Wiley: New York **1979**.

3. Painter, G. R. and Pressman, B. C. in *Metal Ions in Biological Systems*; Sigel, H., Ed; Marcel Dekker: New York **1973**; Vol. 19.

4. Smith, G. D. and Duax, W. L. *J. Am. Chem. Soc*. **1976**, *98*, 1578-1580

5. Thomas, T. P. *Ph.D Dissertation* **1991**, University of Oklahoma, Norman, OK.

6. Alleaume, M., and Barrans, Y. *Can. J. Chem.* **1985**, *63*, 3482-3485.

7. D. R., Reed, P. W., and Lardy, H. A. *Biochemistry*, **1974**, *13*, 4007-4014

8. Baker, E., Maslen, E. N., Watson, K. J., and White, A. H. *J. Am. Chem. Soc*. **1984**, *106*, 2860-2864.

9. Chaney, M. O., Demarco, P. V., Jones, N. D., and Occolowitz, J. L. *J. Am. Chem. Soc*., **1974**, *96*, 1932-1933

10. D. R., Taylor, R. W., and Lardy, H. A. *Ann. N. Y. Acad. Sci*. **1978**, *307*, 402-423.

11. Chapman, C. J., Puri, A. K., Taylor, R. W., and Pfeiffer, D. R. *Biochemistry*, **1987**, *26*, 5009-5018.

CHAPTER IV

RESULTS: 4-ClA23187

Structural and binding properties of 4-ClA23187 were studied and compared with those of the parent compound A23187. The crystal structure of $Mg(4\text{-ClA23187})_2$ was analyzed by X-ray crystallography, and the binding properties analyzed by titrations followed by UV-vis spectroscopy. Two forms of titrations, at fixed pH^* as a function of metal ion concentration, and at a fixed metal ion:4-ClA23187 ratio as a function of pH^* were performed. Titrations at fixed pH^* provide, in some cases, information about the stoichiometry of the metal ion:4-ClA23187 complex. Data from titrations at fixed metal ion:4-ClA23187 ratio were fit by the program SPECFIT to gain pH^* independent protonation and metal binding constants for the ionophore.

A. Structural Properties of 4-ClA23187

1. Solid state structure of $Mg(4\text{-}ClA23187)_2$

The $Mg(4\text{-}ClA23187)_2$ complex was dissolved in 95% C_2H_5OH/H_2O. Slow evaporation produced yellow, needlelike crystals that were suitable for X-ray analysis. The metal center is octahedral in geometry, with three donor atoms per molecule of 4-ClA23187. The donor atoms in each ligand are a carboxylic acid oxygen, the benzoxazole nitrogen, and the ketopyrrole carbonyl oxygen. The stereochemistry around the metal center is similar to that found for many of the divalent metal ion complexes of A23187. The crystal structure is illustrated in Figure IV.1.

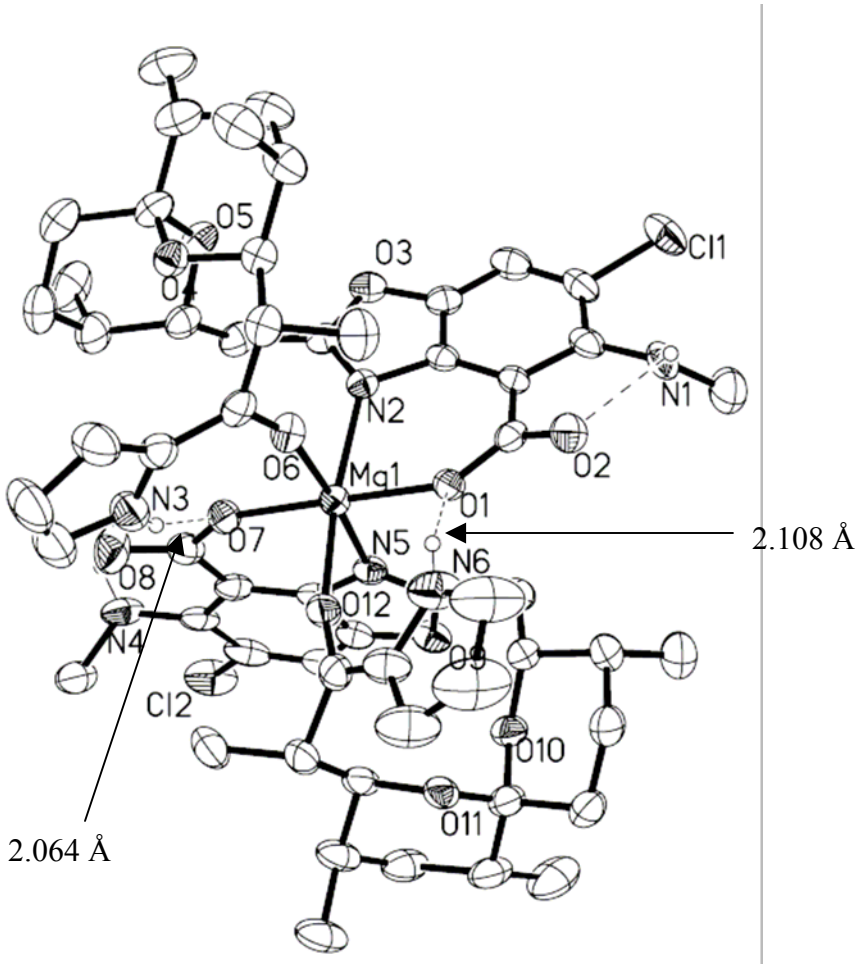

Figure IV.1. Crystal structure of Mg(4-ClA23187)$_2$ with interligand hydrogen bonds

The metal center of the complex, formed by three donor atoms per ligand, has octahedral geometry. It is illustrated in greater detail in Figure IV.2.

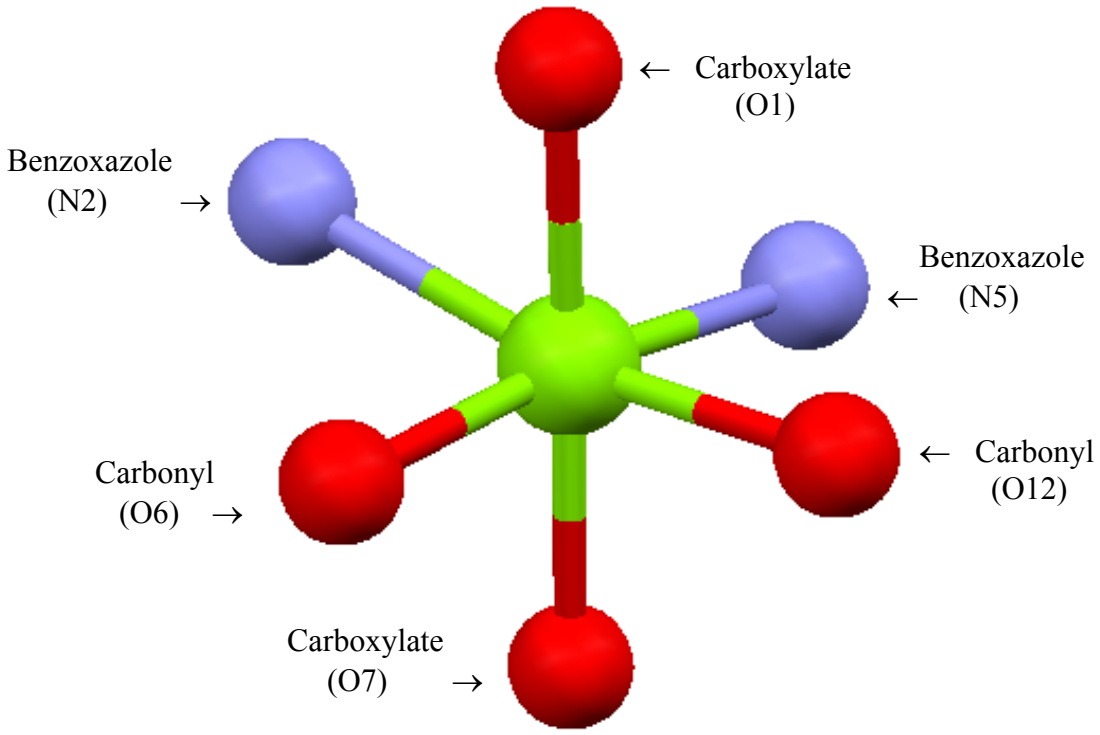

Figure IV.2. Metal center of $Mg(4\text{-}ClA23187)_2$

The distances between each donor atom and the metal are listed in Table IV.1, while the angles formed between every pair of donor atoms and the metal are listed in Table IV.2.

Metal-Ligand Bond	$Mg(4\text{-}ClA)_2$ Distance, Å	MgA_2 Distance, Å
Mg-O1 (carboxylate)	2.002	1.996
Mg-N2	2.181	2.135
Mg-O6 (carbonyl)	2.084	2.064
Mg-O7 (carboxylate)	2.018	1.990
Mg-N5	2.219	2.228
Mg-O12 (carbonyl)	2.033	2.06

Table IV.1. Metal-ligand bond distances of $Mg(4\text{-}ClA23187)_2$ and $Mg(A23187)_2$[1] Bond distance measurement errors range from 0.02 to 0.03 Å.

Ligand-Metal-Ligand	$Mg(4\text{-}ClA)_2$ Bond Angle, °	MgA_2 Bond Angle, °
N2-Mg-O6 (carbonyl)	87.72	86.7
O1-Mg-O12 (carbonyl)	93.65	90.7
O12 (carbonyl)-Mg-N5	89.17	88.3
N5-Mg-N2	99.05	95.4
O7 (carboxylate)-Mg-N2	100.77	96.6
O7 (carboxylate)-Mg-O6 (carbonyl)	89.20	89.9
O7 (carboxylate)-Mg-O12 (carbonyl)	88.04	92.5
O7 (carboxylate)-Mg-N5	80.81	82.6
O1 (carboxylate)-Mg-N2	82.89	82.7
O1 (carboxylate)-Mg-O6 (carbonyl)	89.64	91.0
O1 (carboxylate)-Mg-O12 (carbonyl)	88.83	88.2
O1 (carboxylate)-Mg-N5	100.53	96.5
O7 (carboxylate)-Mg-O1 (carboxylate)	176.11	178.8
N5-Mg-O1	169.53	172.4
O12 (carbonyl)-Mg-N2	171.11	170.5

Table IV.2. Bond angles of $Mg(4\text{-}ClA23187)_2$ and $Mg(A23187)_2$ metal centers[1]

Bond angle measurement errors range from 0.02 to 0.1°

The bond angles of the metal center are consistent with octahedral geometry. The distances between the pyrrole hydrogen atom and the carboxylate oxygen atom in the interligand hydrogen bonds, thought to contribute to complex stability, are 2.108 Å and 2.064 Å.

The crystal structure of $Mg(4\text{-}ClA23187)_2$ is similar to that of many A23187-metal complexes, including magnesium, zinc, cadmium, cobalt, iron II, and manganese complexes. This indicates that in solid state, the presence of a bulky, electronegative atom at the 4 position of the benzoxazole ring does not prohibit binding to the metal or of a second molecule of 4-ClA23187.

A comparison of the magnesium complexes of 4-ClA23187 and the parent compound A23187 is summarized in Tables IV.3-IV.5. The interligand hydrogen bonds that stabilize the 2:1 complex are compared in Table IV.3, and other bond lengths and angles that characterize the complexes are listed in Tables IV.4-IV.5.

	Interligand H-bond Distances, Å	Donor-H-acceptor Angles, °
$Mg(4\text{-}ClA23187)_2$	2.108, 2.064	150.75, 154.61
$Mg(A23187)_2$	2.061, 2.072	157.16, 159.91

Table IV.3. Hydrogen bond distances and angles of $Mg(A23187)_2$ and $Mg(A23187)_2$[1]

	$Mg(A23187)_2$	$Mg(4\text{-}ClA23187)_2$
Range of cis angles	82.6-96.6	80.8-100.8
Avg. of cis angles	90.9 ± 6.6	90.86 ± 6.57
Range of trans angles	170.8-178.8	169.8-176.1
Avg. of trans angles	173.9 ± 4.3	172.2 ± 3.4
Range of Benz. N - Mg distances	2.235, 2.228	2.181, 2.219
Avg. of Benz. N - Mg distances	2.232	2.200
Range of Carboxylate O - Mg distances	1.996, 1.990	2.002, 2.018
Avg. of Carboxylate O - Mg distances	1.993	2.010
Range of Carbonyl O - Mg distances	2.064, 2.060	2.084, 2.033
Avg. of Carbonyl O - Mg distances	2.062	2.058

Table IV.4. Comparison of metal-donor atom bond distances (Å) and angles (°) for magnesium complexes of 4-ClA23187 and A23187[1]

Both complexes are 6-coordinate, with octahedral geometry. The arrangement of the donor atoms around the metal center is similar for both complexes: the carboxylate oxygens are in trans positions relative to one another, with an angle of ~ 180°. The benzoxazole nitrogens are arranged cis to one another, as are the carbonyl oxygens of the two ligand molecules, which are indicated by the ~ 90° angles. Interligand and intraligand hydrogen bonding is observed in the $Mg(4\text{-}ClA23187)_2$ and $Mg(A23187)_2$ complexes.

The presence of a chlorine atom in the 4 position of the benzoxazole ring affects the torsion angles depicted in Figure IV.3, which may affect the ability of the ligand to bind to metal ions.

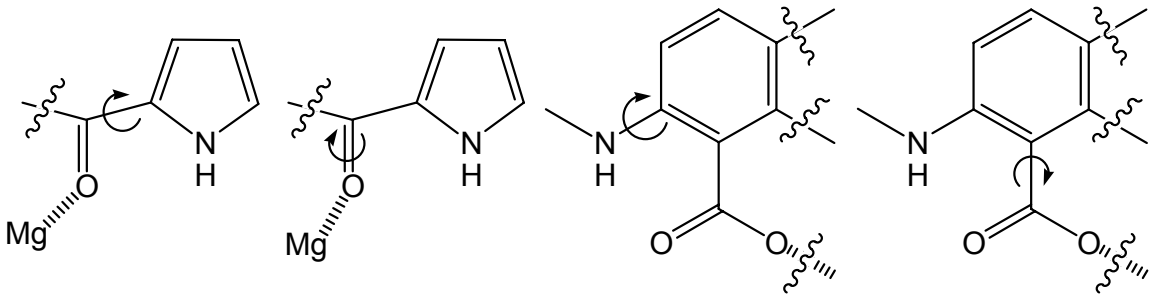

1 2 3 4

Figure IV.3. Torsion angles of magnesium complexes of A23187 and derivatives

A comparison of the torsion angles shown in Figure IV.4 for the magnesium complexes of 4-ClA23187 and the parent compound A23187 are listed in Table IV.5.

Location	Ligand	Atoms involved	$Mg(4\text{-}ClA)_2$ Torsion angle, °	MgA_2 Torsion angle,°
1. Pyrrole	1	O12-C54-C55-N6	-8.4	-11.19
	2	O6-C25-C26-N3	-10.99	-10.22
2. Pyrrole	1	Mg1-O12-C54-C55	+20.7	+31.79
	2	Mg1-O6-C25-C26	+1.76	+31.63
3. Benzoxazole	1	C30-N4-C31-C36	-131.1	+173.00
	2	C1-N1-C2-C7	+124.75	+174.30
4. Benzoxazole	1	O7-C37-C36-C31	-176.7	+171.72
	2	O1-C8-C7-C2	+160.46	+171.54

Table IV.5. Torsion angles of $Mg(4\text{-}ClA23187)_2$ and $Mg(A23187)_2$[1]

Unlike studies of A23187, comparison of the stereochemistry of the metal complex as observed by X-ray crystallography in the solid state and circular dichroism (CD) in solution is not possible with 4-ClA23187. The spectra do not change significantly with the addition of metal to solutions of 4-ClA23187 in 80% CH_3OH/H_2O as they do when similar titrations were carried out with A23187.

B. Protonation and Complexation Properties of 4-ClA23187

The protonation (or acid dissociation) constants for 4-ClA23187 were measured in 80% CH_3OH/H_2O using both potentiometric and spectrophotometric titrations. The complex formation (or complexation) constants of 4-ClA23187 with selected divalent cations (Zn^{2+}, Cd^{2+}, Ca^{2+}, Mg^{2+}, and Ni^{2+}) were measured in 80% CH_3OH/H_2O by spectrophotometric titrations. In potentiometric titrations, 6 mL of solution of ~ 1 mM ligand in 80% CH_3OH/H_2O with ionic strength of 0.05 M is titrated with ~ 10 mM $(CH_3)_4NOH$ (also in 80% CH_3OH/H_2O with ionic strength of 0.05 M). The pH^* of the solution is measured after each addition of base and a pH^* curve is generated. The point at which the slope is greatest is the equivalence point, at which the moles of acid and base present are equal. The pK_a is estimated by finding the pH^* at which the volume is half that required to reach the equivalence point. The pK_a of the ligand is found more precisely by fitting the data using the program PKAS.[2]

For protonation constants measured spectrophotometrically, 2 mL of a solution of 4-ClA23187 (~ 50 μM) is titrated with the strong base $(CH_3)_4NOH$. The pH^* of the ligand solution is measured potentiometrically after each addition of base, and the UV-vis spectrum is recorded. For metal complexation constants, spectrophotometric titrations are performed at either a constant pH^* as a function of metal concentration or at a constant [metal]:[4-ClA23187] ratio as a function of pH^*. Data from titrations at fixed pH^* (typically 5.5, 7.0, and 10.0) are used to determine stoichiometry of complexes. Data from titrations at fixed [metal ion]:[4-ClA23187] ratio are fit with SPECFIT to determine binding constants that are pH^*-independent.

1. Protonation constants of 4-ClA23187 in 80% CH_3OH/H_2O

The potentiometric titration of 4-ClA23187 with $(CH_3)_4NOH$ results in a titration curve with one equivalence point. The plot of experimental and calculated (fit) data is shown in Figure IV.4. Visual inspection of the curve indicates that the pK_a is approximately 6. Using the program PKAS, which corrects for the difference in pH observed (using a meter standardized with aqueous buffers) and pH^*, the pK_a is determined to be 5.90 ± 0.02.

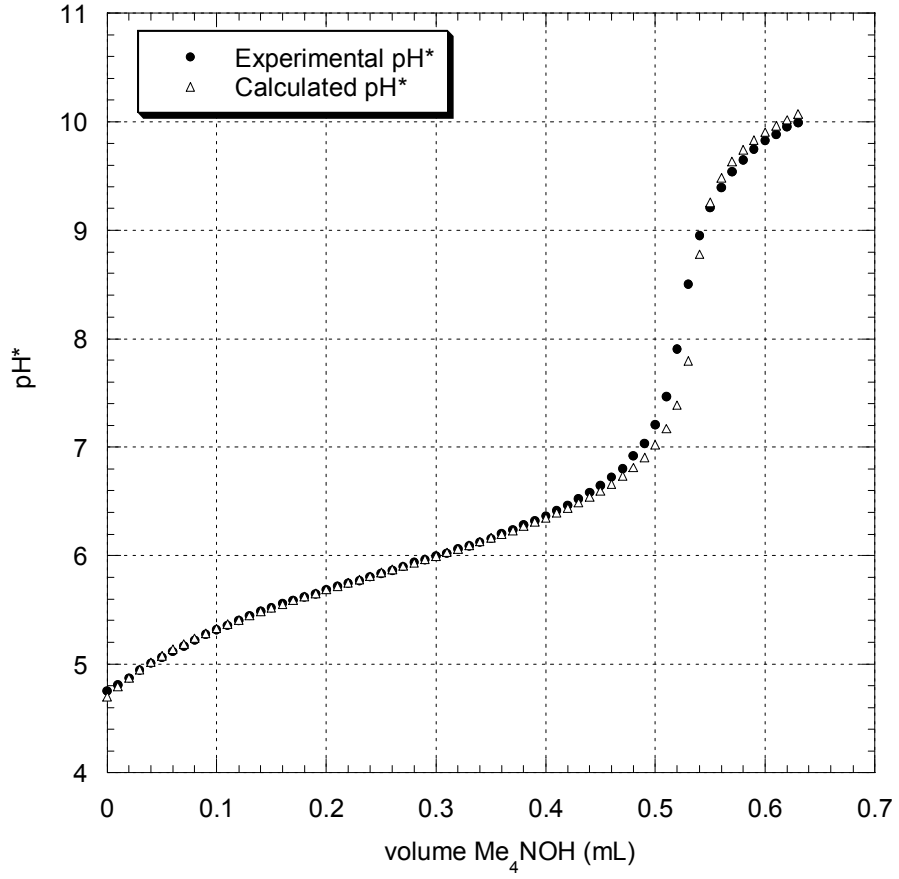

Figure IV.4. Potentiometric titration of ~ 1 mM 4-ClA23187 in 80% CH_3OH/H_2O, I = 0.05 TEAP, 25 °C

The UV-vis spectra of 4-ClA23187 titrated with $(CH_3)_4NOH$, shown in Figure IV.5, have several wavelengths at which the absorbance changes significantly. At lower pH^* values, an isosbestic point is located around 252 nm. Absorbance at wavelengths 290 nm and 330 nm change as a function of pH^*.

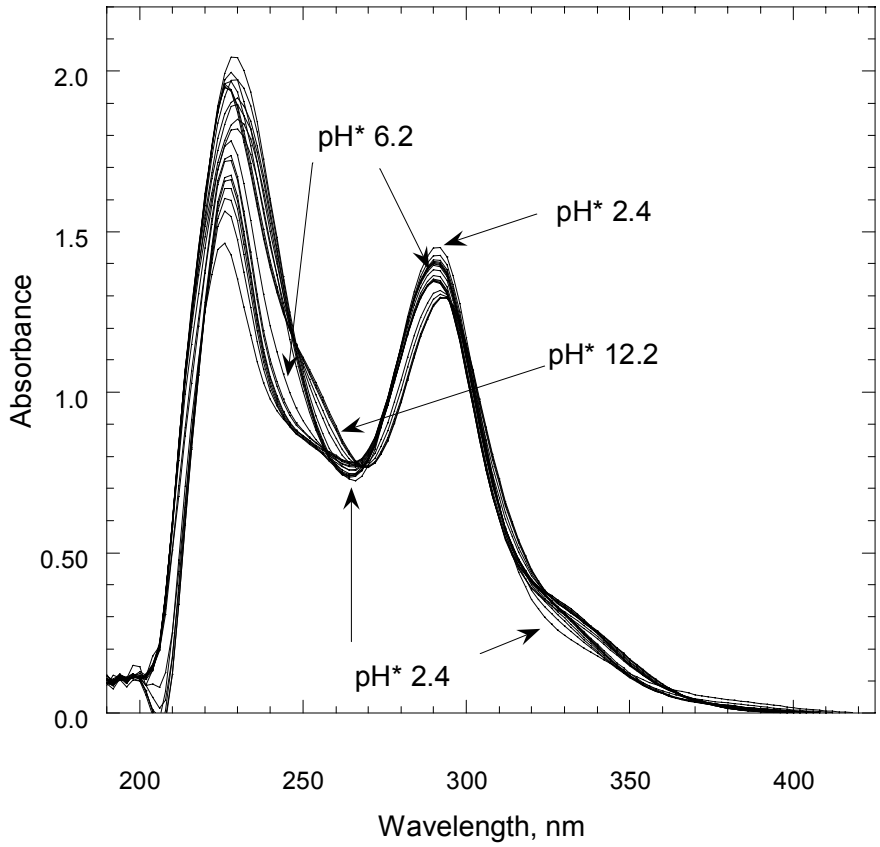

Figure IV.5. UV-vis spectra of 67.7 μM 4-ClA23187 in 80% CH_3OH/H_2O as a function of pH^*

The CD spectra of 4-ClA23187 titrated with base in 80% CH_3OH/H_2O resulted in a small change in ellipticity around 290 nm, shown in Figure IV.6, which is not sufficient for determination of protonation constants. The remainder of the spectra remained unchanged as the pH^* was varied, except for the large changes at very low wavelength (220-250 nm) due to inert components unrelated to the ligand.

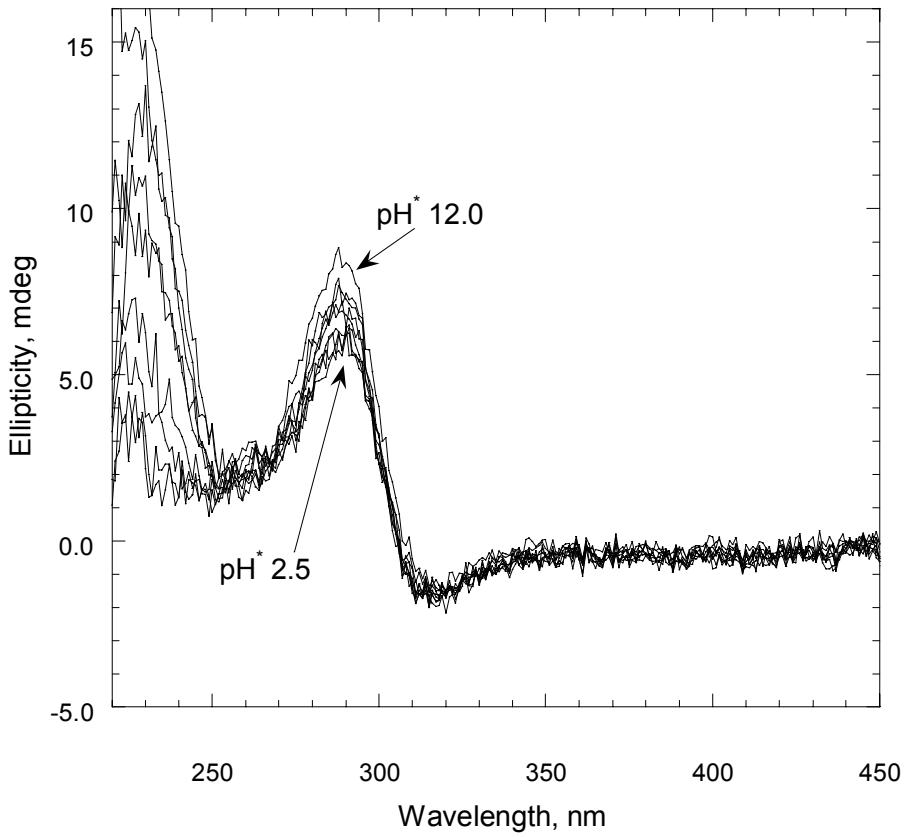

Figure IV.6. CD spectra of 51.7 μM 4-ClA23187 pH titration in 80% CH_3OH/H_2O

Two protonation equilibria are observed in a plot of UV-vis absorbance at 348 nm as a function of pH^*, which is shown in Figure IV.7.

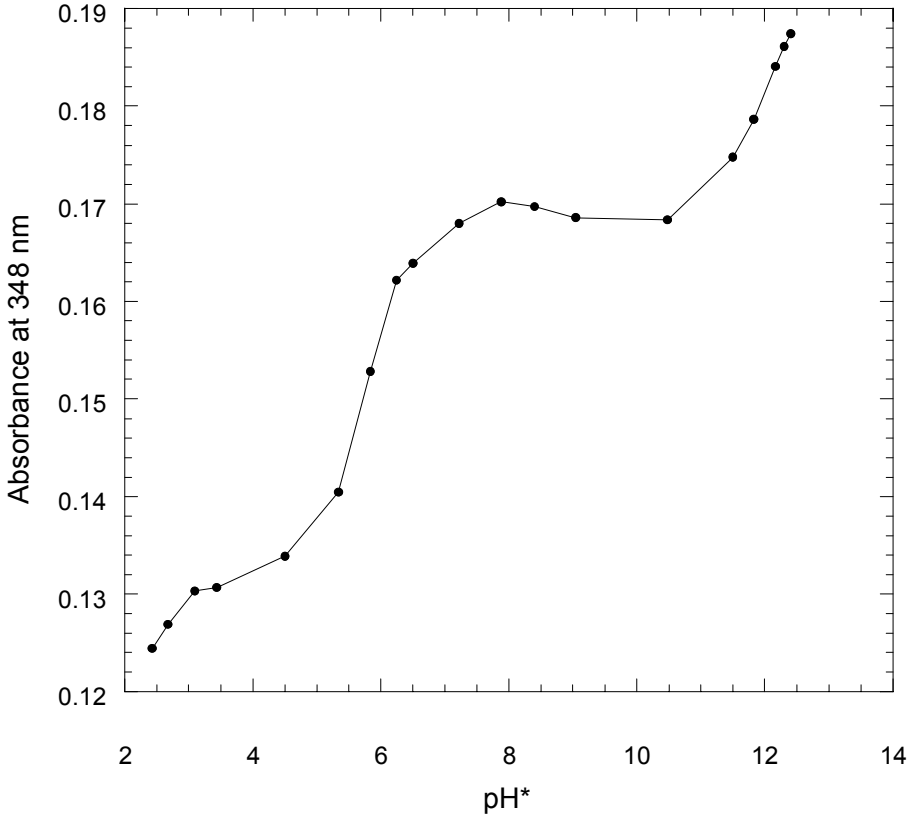

Figure IV.7. UV-vis absorbance at 348 nm of a pH titration of 67.7 μM 4-ClA23187 in 80% CH_3OH/H_2O

This graph shows that two equilibria are involved in the titration. These equilbria represent the acid dissociation reactions described in Equations IV.1-4.

$$H_2(4\text{-ClA23187}) \leftrightarrows H^+ + H(4\text{-ClA23187})^- \qquad \text{Eq. IV.1}$$

$$K_{a1} = \frac{[H^+][H(4\text{-ClA23187})^-]}{[H_2(4\text{-ClA23187})]} \qquad \text{Eq. IV.2}$$

$$H(4\text{-ClA23187})^- \leftrightarrows H^+ + (4\text{-ClA23187})^{2-} \qquad \text{Eq. IV.3}$$

$$K_{a2} = \frac{[H^+][(4\text{-ClA23187})^{2-}]}{[H(4\text{-ClA23187})^-]} \qquad \text{Eq.IV.4}$$

The pH^* values at which these inflection points occur represent the negative log function of the K_{a1} and K_{a2} values, or pK_{a1} and pK_{a2}, respectively. The best fit for the K_a values, found by use of the program SPECFIT, indicates that the value of pK_{a1} (which represents the loss of hydrogen at the carboxylic acid functional group) is 5.90, which agrees with the pK_{a1} obtained by potentiometric titration. The value of pK_{a2} found by SPECFIT is 11.4, however, because completion of this equilibrium step is not achieved (the pH^* is limited by the conditions of the titrations to ~ 12.5) this pK_a is somewhat underapproximated.

The value for pK_{a1} is substantially lower than the pK_{a1} for the parent compound A23187, which is 7.85 under the same conditions.[3] Inductive effects due to the presence of an electon-withdrawing halogen on an aromatic ring, illustrated in Figure IV.8, explain the lower value of pK_{a1}.

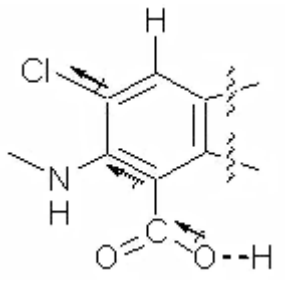

Figure IV.8. Inductive effect of chlorine at 4 position of benzoxazole ring of A23187

The presence of the electron-withdrawing chlorine atom pulls electron density away from the carbon atom it is bound to, making it more electropositive. This affects the aromatic ring the carbon is a part of, which ultimately causes the carbon of the carboxylate moiety to become more electronegative and the oxygen atoms of the carboxylate moiety to become less electronegative. It is easier for bound hydrogen to dissociate from an oxygen atom with lower electronegativity, resulting in a lower pK_a.

The inflection point at $pH^* \geq 10.3$ indicates another process that cound represent a second ionization step, perhaps dissociation of the pyrrole hydrogen. Similar pH^* absorbance behavior is observed with the parent compound A23187 which is consistent with the fact that the pyrrole moiety is not altered.

2. 4-ClA23187 titrated with Zn^{2+} at fixed pH^* (5.5, 7.0, and 10.0)

Solutions of 50 μM 4-ClA23187 in 80% CH_3OH/H_2O were titrated with Zn^{2+} at pH^* values 5.5, 7.0, and 10.0. The pH^* of solutions of analyte and blank were buffered with the appropriate buffer, and the pH^* of the blank, analyte, and metal ion solutions were measured by pH meter prior to titration.

a. pH^* 7.0: The spectra of 4-ClA23187 at pH^* 7.0 do not show the large changes in absorbance observed in spectra of A23187 during metal ion complexation, but do contain significant changes that reflect the change associated with complexation. At pH^* 7.0, the largest changes in absorbance occur near wavelengths 295 nm and 335 nm, as seen in Figure IV.9.

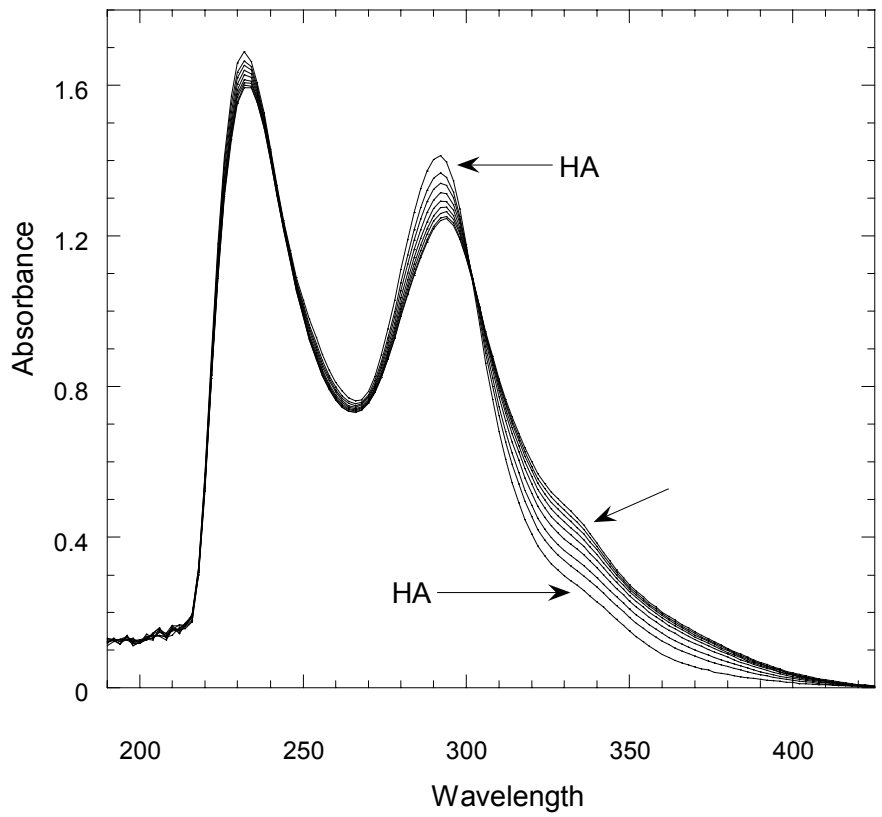

Figure IV.9. UV-Vis spectra of 51.7 μM 4-ClA23187 in 80% CH_3OH/H_2O titrated with Zn^{2+} at pH* 7.0

When the data is plotted as absorbance as a function of amount of Zn^{2+} added, it is apparent that the largest changes in absorbance occur at the beginning of the titration, and decrease as more Zn^{2+} is added. It takes a large excess of Zn^{2+} (20 or 30 times the amount of ligand) to achieve a plateau, where ligand is saturated with metal ion, as observed in Figure IV.10.

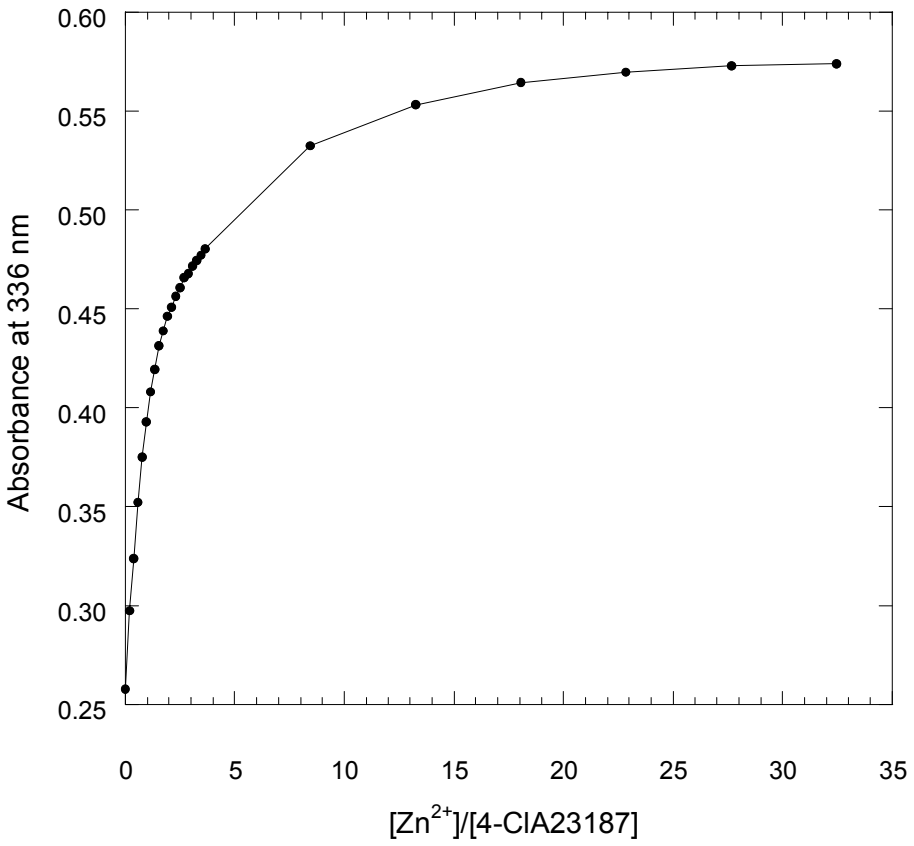

Figure IV.10. UV-vis absorbance at 336 nm of 51.7 μM 4-ClA23187 titrated with Zn^{2+} at pH^* 7.0.

b. pH^* 10.0 At pH^* 10.0, the spectra of 4-ClA23187 titrated with Zn^{2+} are similar to those for same titration conducted at pH^* 7.0. A plot of absorbance at 336 nm as a function of $[Zn^{2+}]/[4\text{-ClA23187}]$ (Figure IV.11) is virtually indistinguishable between the titrations at pH^* 7.0 and 10.0. In titrations at both pH^* values, stoichiometric complexation is not observed, unlike the parent compound at pH^* 7.0 titrated with Zn^{2+}. This indicates that the complexation constant(s) for 4-ClA23187 and Zn^{2+} are much lower than those for A23187.

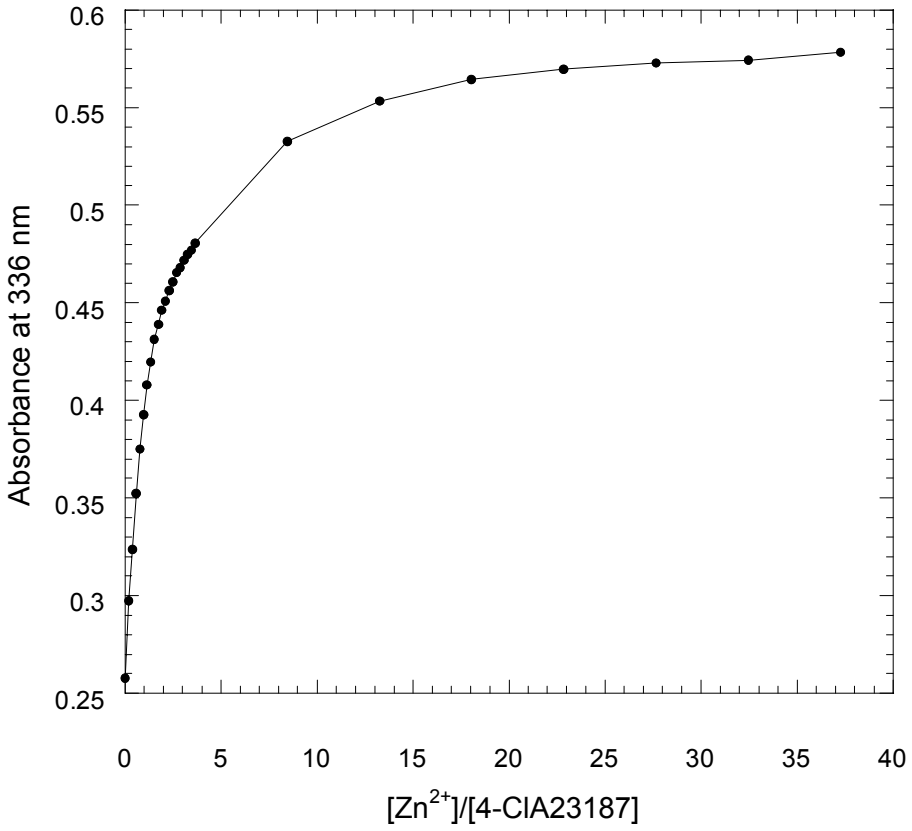

Figure IV.11. UV-vis absorbance at 336 nm of 51.7 μM 4-ClA23187 in 80 % CH_3OH/H_2O titrated with Zn^{2+} at pH^* 10.0

c. pH^* 5.5: Titrations of 4-ClA23187 with Zn^{2+} at pH^* 5.5 did not produce any observable spectral changes.

3. 4-ClA23187 Titrated with Cd^{2+} at fixed pH^* (5.5, 7.0, and 10.0)

a. pH^* 7.0 The titration of 4-ClA23187 in 80% CH_3OH/H_2O with Cd^{2+} at pH^* 7.0 does not produce any significant UV-vis spectral changes, as shown in Figure IV.12. This either means that Cd^{2+} does not bind to the ligand to any appreciable extent at this pH^*, or the spectra of bound and unbound ligand are identical. Because the spectra of this ligand titrated with Zn^{2+} at pH^* 7.0 does produce observable spectral changes, it can be reasonably concluded that Cd^{2+} does not bind to 4-ClA23187 at this pH^*. Additionally, A23187 titrated with Cd^{2+} under these conditions does produce observable spectral changes.

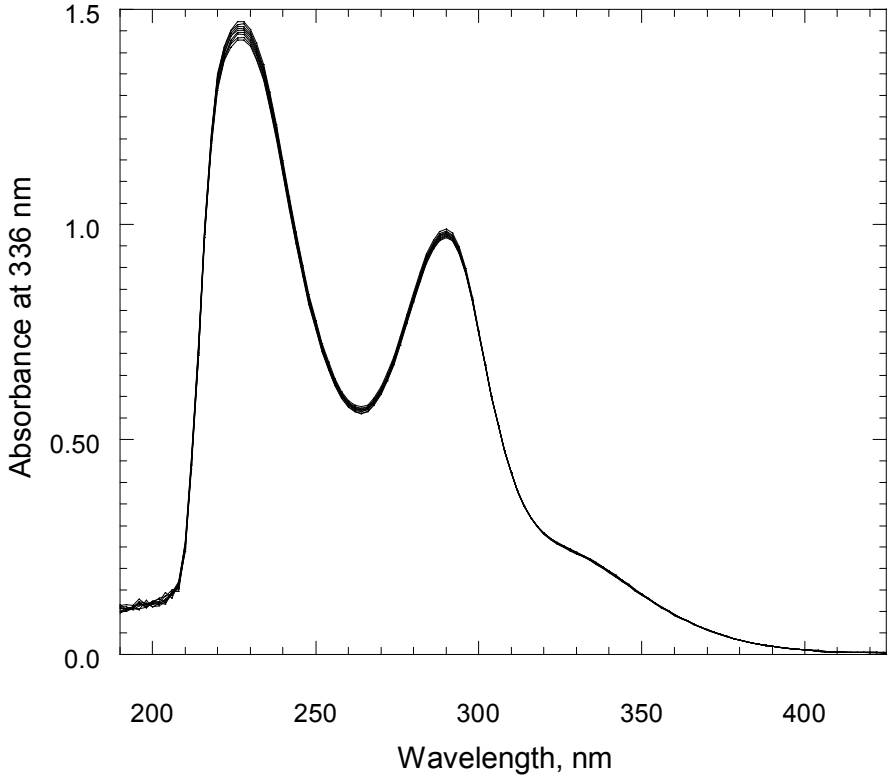

Figure IV.12. UV-vis spectra of 67.7 μM 4-ClA23187 in 80% CH_3OH/H_2O titrated with Cd^{2+} at pH^* 7.0

b. pH* 10.0 The UV-vis spectra of 4-ClA23187 in CH_3OH/H_2O titrated with Cd^{2+} at pH* 10.0 does produce small, but observable spectral changes as seen in Figure IV.13. The absorbance at 336 nm increases upon ligand binding to Cd^{2+}.

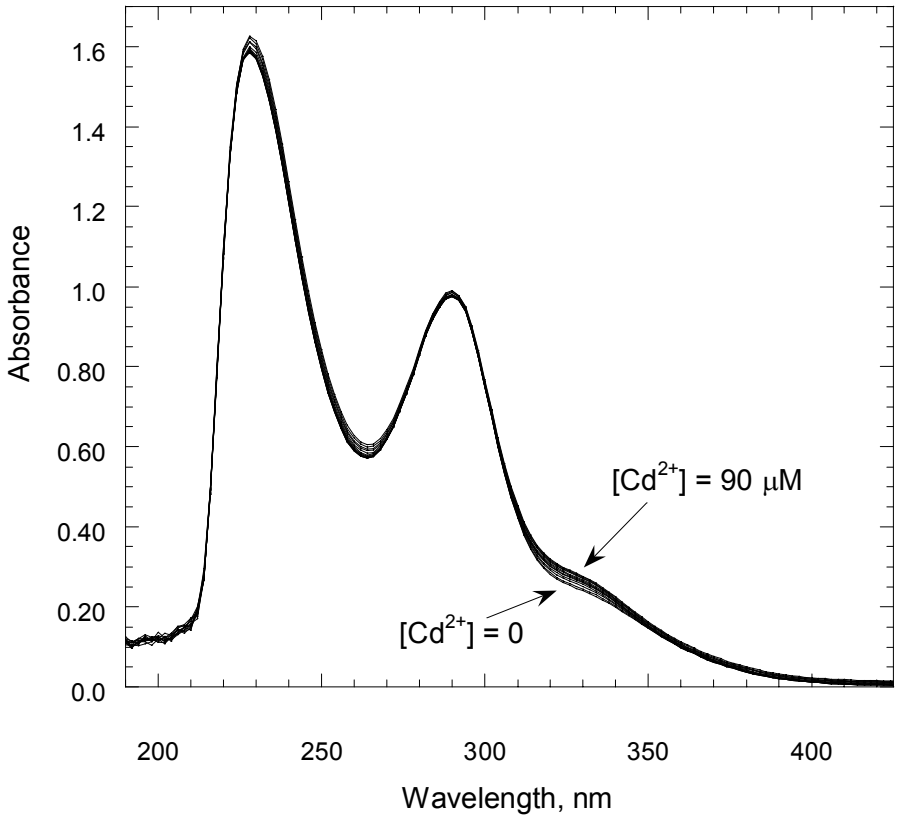

Figure IV.13. UV-vis spectra of 67.7 μM 4-ClA23187 in 80% CH_3OH/H_2O titrated with Cd^{2+} at pH* 10.0

When plotted as a function of $[Cd^{2+}]/[4\text{-ClA23187}]$, as shown in Figure IV.14, the absorbance increases somewhat linearly past a metal:ligand ratio of 1. It was not possible to titrate to a point of excess of Cd^{2+} due to the low solubility of $Cd(OH)_2$ that formed beyond that point.

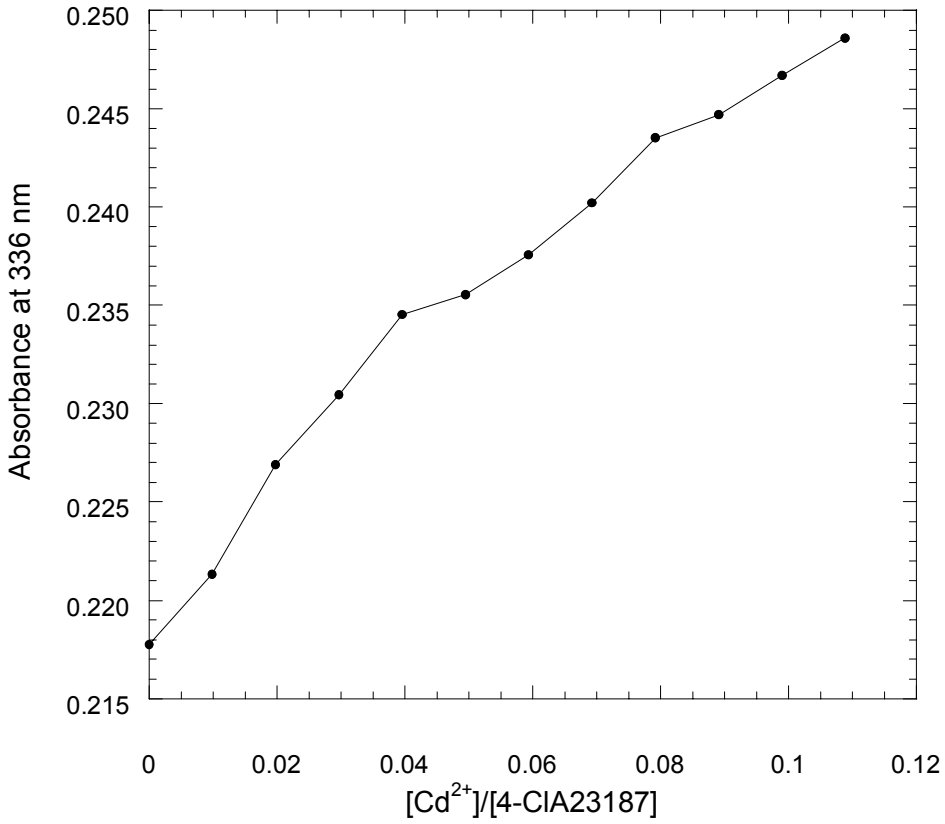

Figure IV.14. UV-vis absorbance at 336 nm of 67.7 μM 4-ClA23187 at 80% CH_3OH/H_2O titrated with Cd^{2+} at pH^* 10.0

c. pH^* 5.5: Titrations of 4-ClA23187 with Cd^{2+} at pH^* 5.5 did not produce any observable spectral changes.

4. 4-ClA23187 titrated with Ni^{2+} at fixed pH^* (5.5, 7.0, and 10.0)

a. pH^* 7.0 UV-vis spectra of 4-ClA23187 titrated with Ni^{2+} at pH^* 7.0 shows very small changes in absorbance at wavelengths 330 nm and 290 nm, as shown in Figure IV.15.

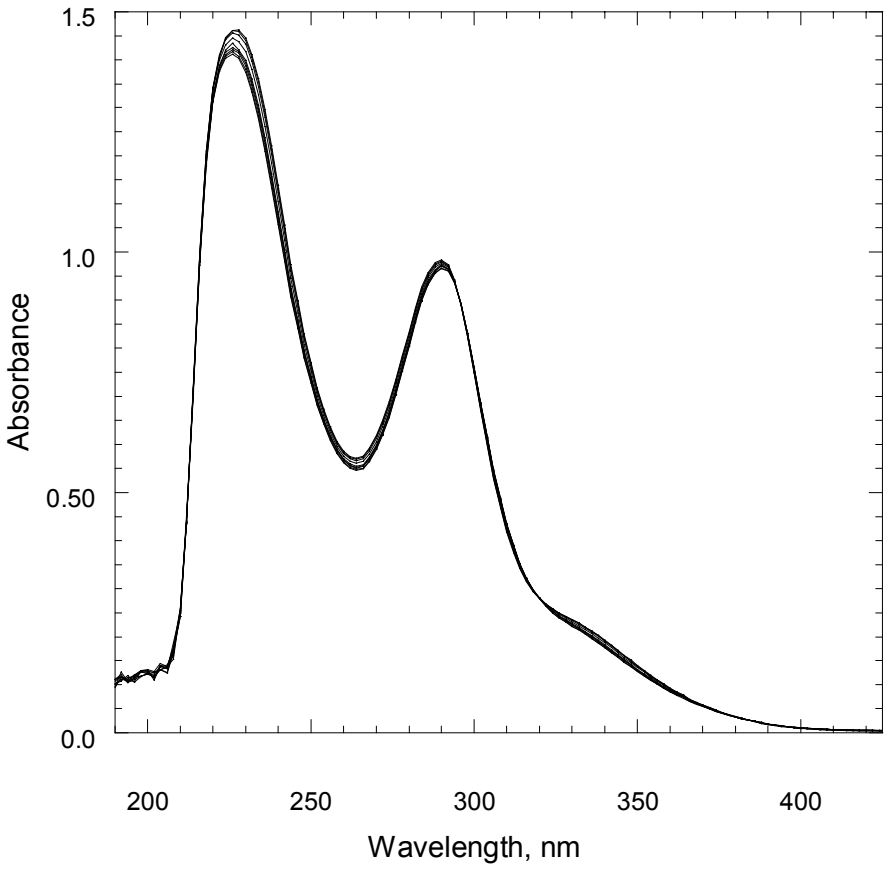

Figure IV.15. UV-vis spectra of 67.7 μM 4-ClA23187 in 80% CH_3OH/H_2O titrated with Ni^{2+} at pH^* 7.0

A plot of absorbance at 336 nm as a function of $[Ni^{2+}]/[4\text{-ClA23187}]$ is shown in Figure IV.16. A large excess of Ni^{2+} is required to approach a plateau in absorbance at this wavelength, indicating that 4-ClA23187 does not bind Ni^{2+} well at this pH^*.

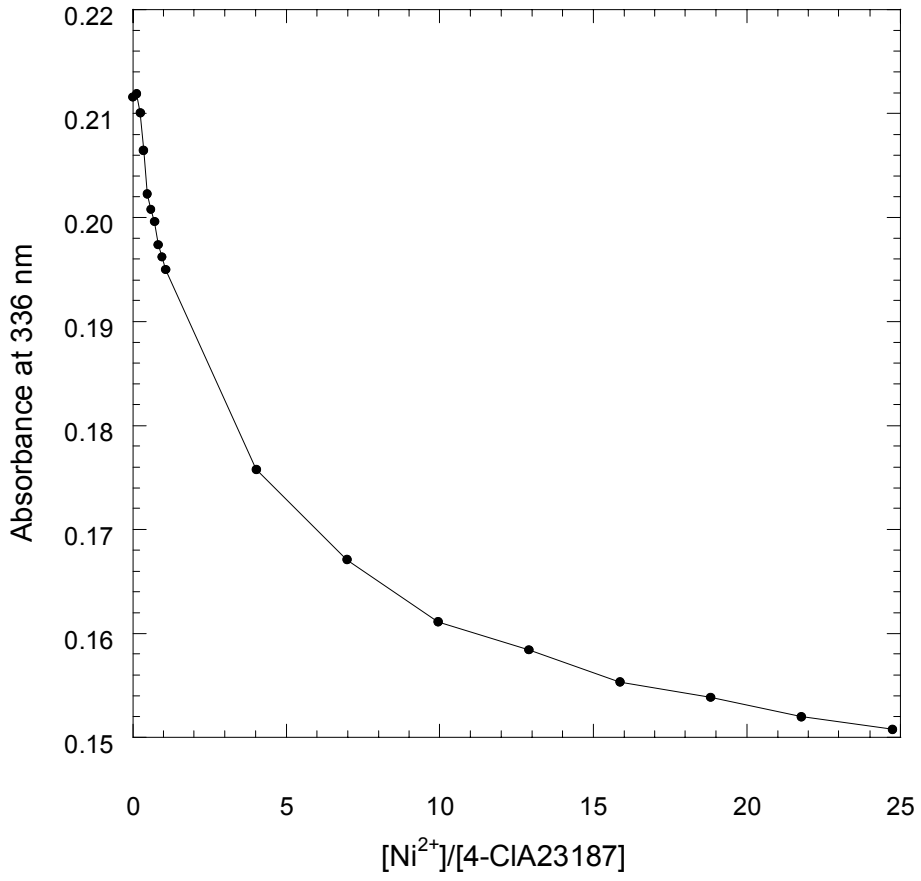

Figure IV.16. UV-vis absorbance at 336 nm of 67.7 μM 4-ClA23187 titrated with Ni^{2+} at pH^* 7.0

b. pH*10.0 At pH* 10.0, 4-ClA23187 produces larger spectral changes when titrated with Ni^{2+} than it does when titrated with this metal at pH* 7.0. The changes in absorbance at 330 and 290 nm are more pronounced, as seen in Figure IV.17.

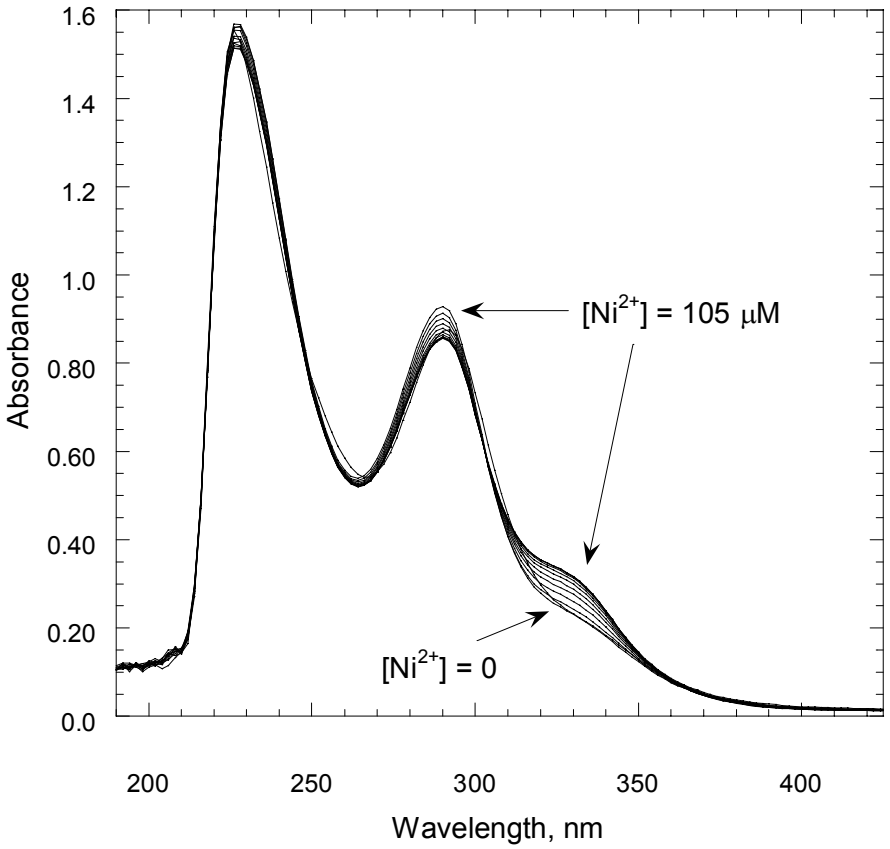

Figure IV.17. UV-vis spectra of 50 μM 4-ClA23187 in 80% CH_3OH/H_2O titrated with Ni^{2+} at pH* 10.0

When absorbance at 336 nm is plotted as a function of pH* (Figure IV.18) it is apparent that a much smaller amount of metal is required to reach a plateau in absorbance

at this pH*. Absorbance begins to level off at a ratio of Ni^{2+} to ligand that is between 2;1 and 1:1, indicating a mixed complex stoichiometry. The complexation observed indicates that the complexation constant(s) for 4-ClA23187 and Ni^{2+} at pH* 10.0 are higher than those for 4-ClA23187 and Zn^{2+} or Cd^{2+} at the same pH*.

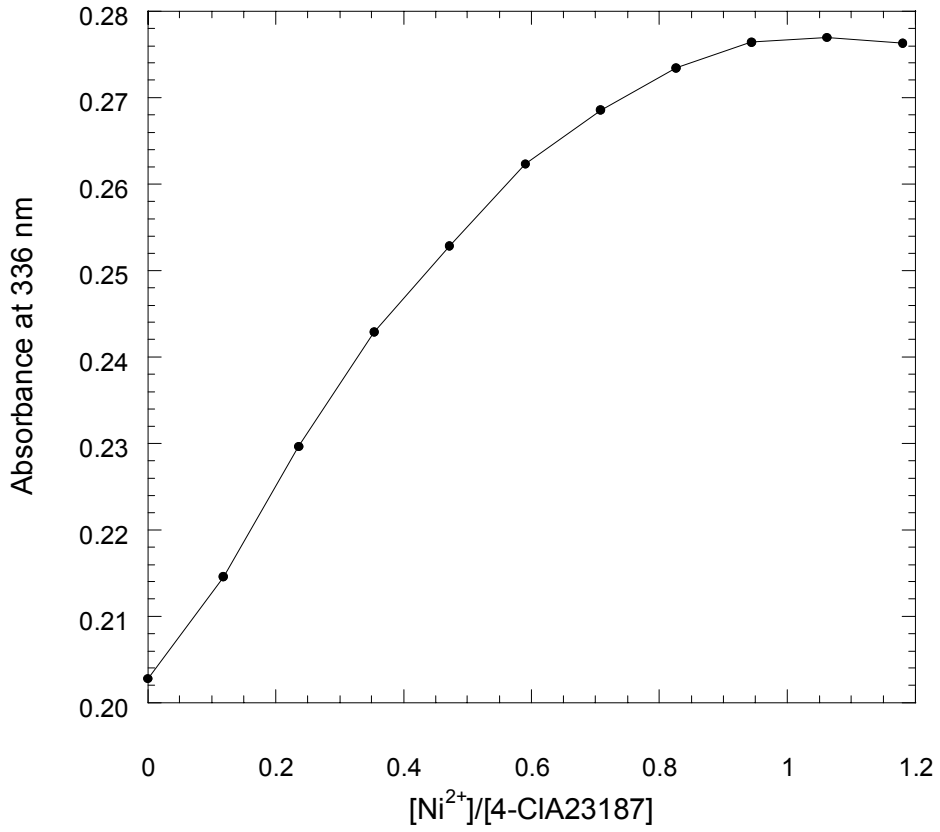

Figure IV.18. UV-vis absorbance at 336 nm of 50 μM 4-ClA23187 in 80% CH_3OH/H_2O titrated with Ni^{2+} at pH* 10.0

c. pH* 5.5: Titrations of 4-ClA23187 with Ni^{2+} at pH* 5.5 did not produce any observable spectral changes.

5. 4-ClA23187 titrated with Ca^{2+} at fixed pH^* (5.5, 7.0, and 10.0)

Titrations of 4-ClA23187 at pH^* 5.5, pH 7.0, and pH 10.0 with Ca^{2+} did not produce observable spectral changes, shown in Figure IV.19 for pH^* 10.0.

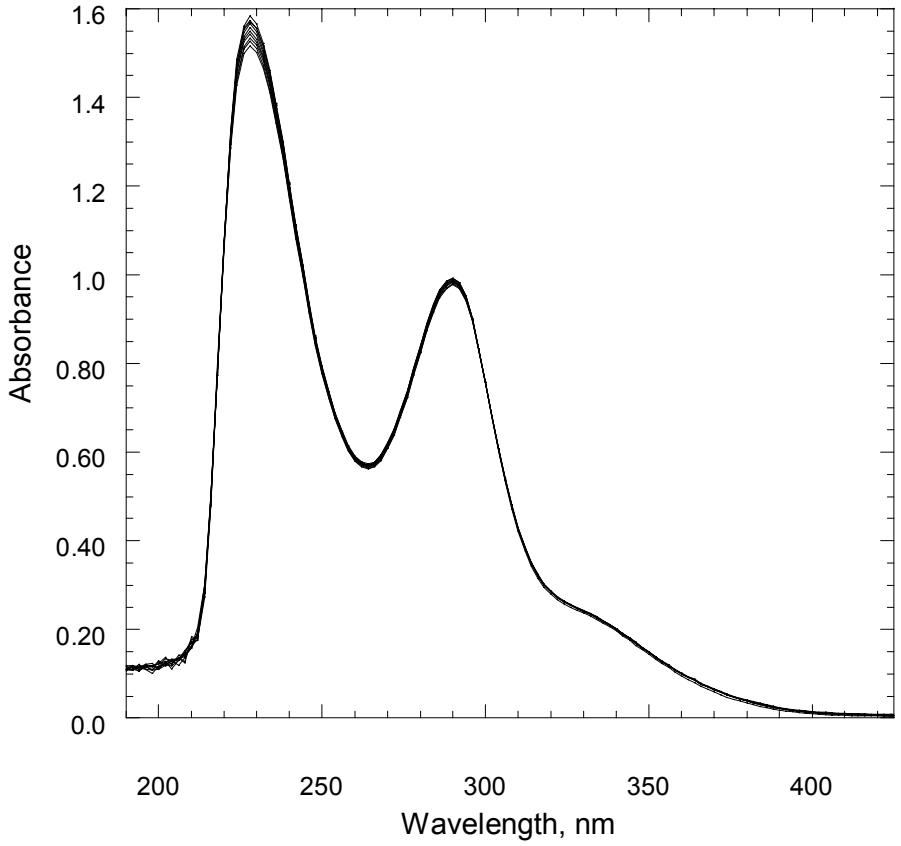

Figure IV.19. UV-vis spectra of 67.7 μM 4-ClA23187 in 80% CH_3OH/H_2O titrated with Ca^{2+} at pH^* 10.0

6. 4-ClA23187 titrated with Mg^{2+} at fixed pH^* (5.5, 7.0, and 10.0)

Titrations of 4-ClA23187 in CH_3OH/H_2O with Mg^{2+} at pH^* 5.5, 7.0, or 10.0 resulted in no UV-vis spectral changes. This indicates that regardless of pH^*, 4-ClA23187 binds very poorly to Mg^{2+}.

7. Titrations with $(CH_3)_4NOH$ of solutions containing a fixed ratio of Zn^{2+}:4-ClA23187

a. 1:1 ratio of 4-ClA23187 to Zn^{2+}: Changes in the UV-vis spectra of a solution containing a 1:1 mixture of 4-ClA23187 and Zn^{2+} (~ 50 μM) in 80% CH_3OH/H_2O as a function of pH^*, shown in Figure IV.20, are similar to those of 4-ClA23187 titrated without metal. Changes in absorbance are observed at 265 nm, 298 nm, and 350 nm. Isosbestic points are observed at 258 nm and 328 nm.

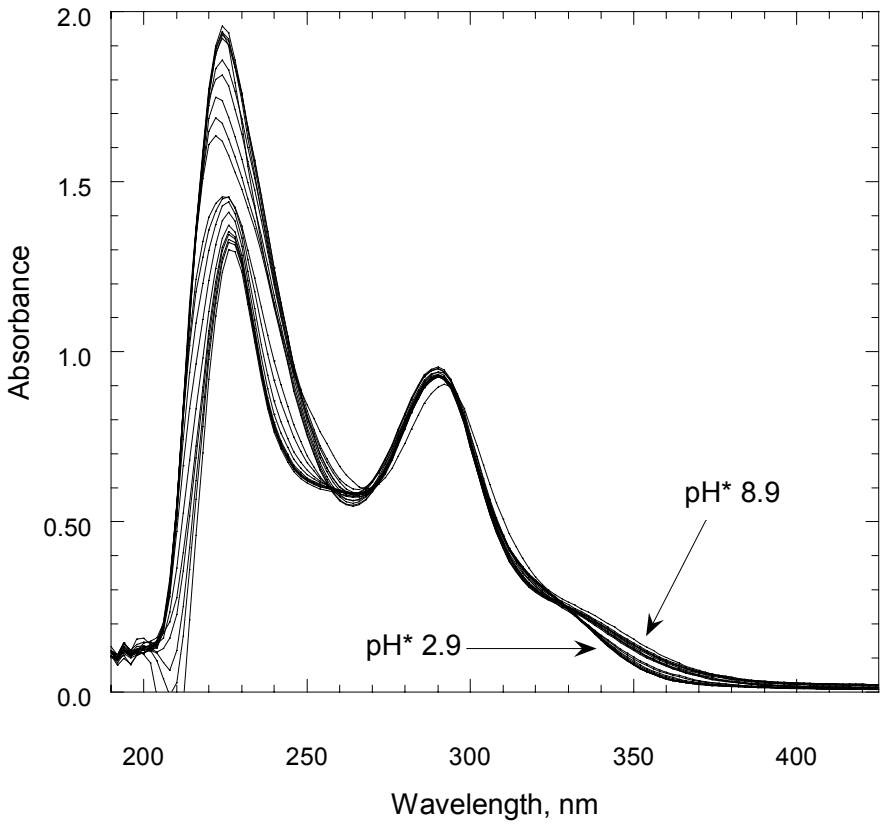

Figure IV.20. 51.7 μM 4-ClA23187:Zn^{2+} (1:1) pH^{*} titration in 80% CH_3OH/H_2O

When absorbance values at 348 nm are plotted as a function of pH^*, as seen in Figure IV.21, two main inflection points are observed, at pH^* values of ~ 6.0, and ~ 12.0. These points are similar to those observed in titrations of the ligand in the absence of metal ion; therefore it is likely that spectral changes are due to primarily acid dissociation.

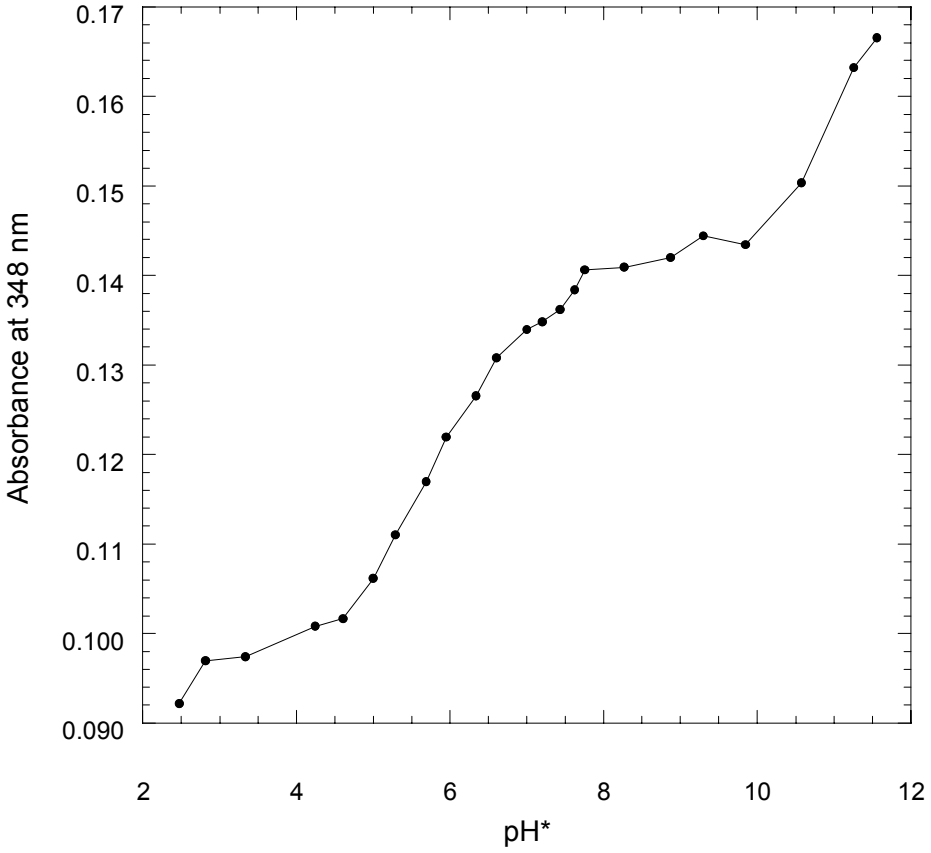

Figure IV.21. UV-vis absorbance at 348 nm of 51.7 μM 4-ClA23187:Zn^{2+} (1:1) pH^* titration. Solid line thorough data points is a visual aid only, and does not represent fit data

The pH^* at which these inflection points occur may reflect a combination of complexation and acid dissociation. These equations are described by equations IV.5-

IV.10. Equations IV.5 through IV.8 describe deprotonation reactions and equations IV.9 and IV.10 describe metal ion complexation reactions.

$$H_2(4\text{-ClA23187}) \leftrightarrows [H(4\text{-ClA23187})]^- + H^+ \qquad \text{Eq. IV.5}$$

$$K_{a1} = \frac{[H(4\text{-ClA23187})^-][H^+]}{[H_2(4\text{-ClA23187})]} \qquad \text{Eq. IV.6}$$

$$H(4\text{-ClA23187})^- \leftrightarrows 4\text{-ClA23187}^{2-} + H^+ \qquad \text{Eq. IV.7}$$

$$K_{a2} = \frac{[4\text{-ClA23187}^{2-}][H^+]}{[H(4\text{-ClA23187})^-]} \qquad \text{Eq. IV.8}$$

The potential metal ion complexation steps are described by Equations IV.9-IV.10.

$$[H(4\text{-ClA23187})^-] + Zn^{2+} \leftrightarrows [H(4\text{-ClA23187})Zn^+] \qquad \text{Eq. IV.9}$$

$$K_{HML} = \frac{[H(4\text{-ClA23187})Zn^+]}{[H(4\text{-ClA23187}^-)][Zn^{2+}]} \qquad \text{Eq. IV.10}$$

$$H(4\text{-ClA23187})Zn^{+} \leftrightarrows (4\text{-ClA23187})Zn + H^{+} \qquad \text{Eq. IV.11}$$

$$K_{ML} = \frac{[(4\text{-ClA23187})Zn][H^{+}]}{[H(4\text{-ClA23187})Zn^{+}]} \qquad \text{Eq. IV.12}$$

Other possible reactions, including the binding of a second mono-protonated ligand to the [H(4-ClA23187)Zn] complex, did not fit the data well in SPECFIT. The reactions in Equations IV.5-IV.12 represent parts of the model that produced the best fit using SPECFIT.

b. 2:1 ratio of 4-ClA23187 and Zn^{2+}: The spectral features of ~ 50 μM 4-ClA23187 in the presence of Zn^{2+} in a 2:1 ratio titrated with $(CH_3)_4NOH$ in CH_3OH/H_2O are somewhat similar to those of a titration of a 1:1 ratio of ligand to metal. However, in the titration of 1:1 ratio of ligand to metal, a larger absorbance change is observed at 335 nm. Additonally, the pH^* at which these absorbance changes occur is different in the titration of 1:1 ratio of metal ion to ligand. A graph of absorbance at 332 nm as a function of pH^* (Figure IV.22) indicates the presence of two equilibria.

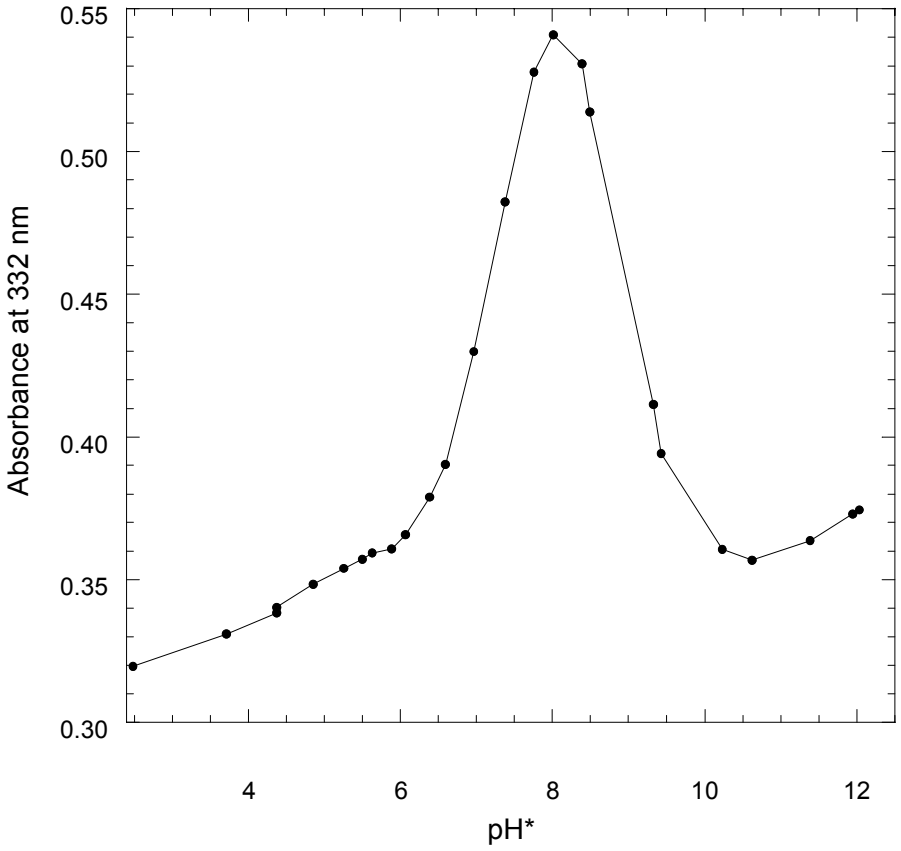

Figure IV.22. UV-vis absorbance at 332 nm of 67.6 μM 4-ClA23187:33.8 μM Zn^{2+} pH^* titration

8. Titrations with $(CH_3)_4NOH$ of solutions containing a fixed ratio of Cd^{2+}:4-ClA23187

a. 1:1 ratio of 4-ClA23187 and Cd^{2+}: All of the titrations of this type with 4-ClA23187 and Cd^{2+} resulted in somewhat poor data. The combination of low affinity of ligand for Cd^{2+} and the occurrence of precipitation of Cd^{2+} at relatively modest pH^* values is a likely cause. However, some information can still be obtained from these titrations.

The pH^* titration of 4-ClA23187 and Cd^{2+} (1:1) is shown in Figure IV.23. An isosbestic point is observed at lower pH^* values at 335 nm. A significant increase in absorbance at all wavelengths is visible at pH^* values above 10. This indicates that it is due to precipitation formation rather than a change in binding state. The most likely reaction to account for the precipitation is formation of $Cd(OH)_{2(s)}$. In H_2O (at 25 °C), a solution of 50 μM Cd^{2+} (for most titrations, this concentration is ≈ [ligand]) will form precipitate past a pH value of 9.35.[4] In the (2:1) titration, however, this precipitation is not observed within the pH^* values of the titration. At values above pH^* 10.0, the absorbance stops changing. This indicates that a 2:1 ratio of ligand to Cd^{2+} is sufficient to bind all the Cd^{2+} strongly enough to prevent precipitation at pH^* values up to 11.

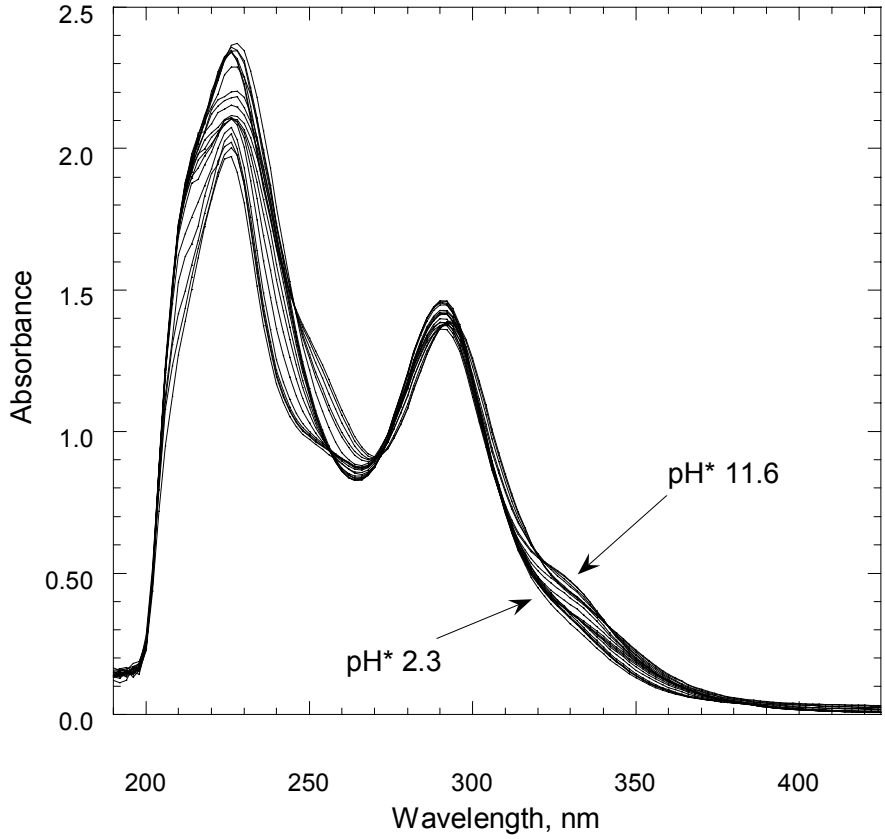

Figure IV.23. UV-vis spectra of 51.7 μM 4-ClA23187: 51.7 μM Cd^{2+} pH^{*} titration

The graph of absorbance at 348 nm as a function of pH^* (Figure IV.24) shows two equilibria present at this pH^* range. However, the second is somewhat obscured by the increase in absorbance due to precipitation of $Cd(OH)_{2(s)}$.

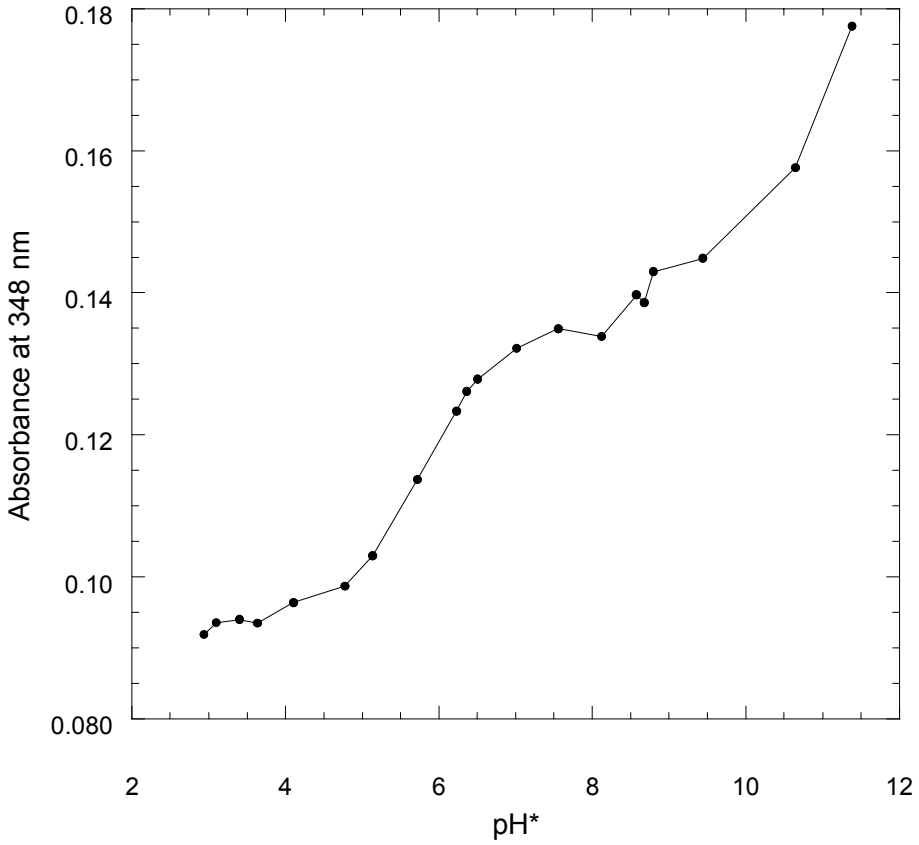

Figure IV.24. UV-vis absorbance at 348 nm of 51.7 μM 4-ClA23187: 51.7 μM Cd^{2+} pH^* titration

b. 2:1 ratio of 4-ClA23187/Cd^{2+}: The graph of absorbance at 336 nm as a function of pH^* is shown in Figure IV.25. The precipitation observable in the 1:1 4-ClA23187:Cd^{2+} titration is not apparent in this titration, due to the fact that weak binding is overcome by the excess of ligand present.

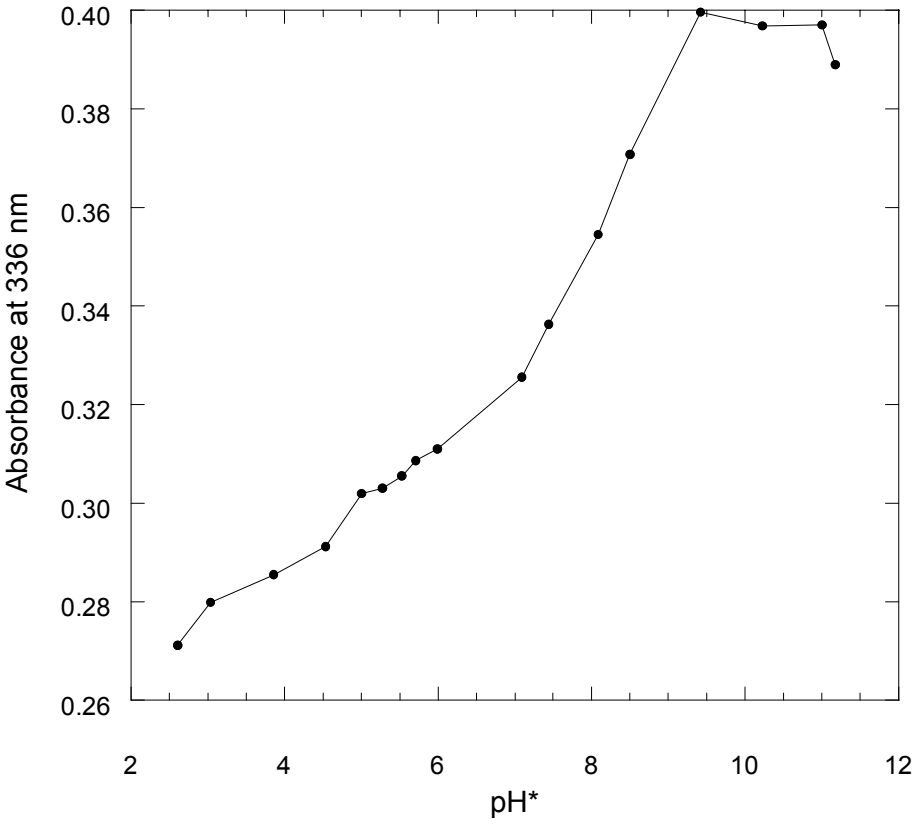

Figure IV.25. UV-vis absorbance at 336 nm of 51.7 μM 4-ClA23187:25.85 μM Cd^{2+} pH^* titration

9. Titrations with $(CH_3)_4NOH$ of solutions containing a fixed ratio of Ca^{2+}:4-ClA23187

a. 1:1 ratio of 4-ClA23187 to Ca^{2+}: The pH^* titration of 4-ClA23187:Ca^{2+} (1:1), shown in Figure IV.26, is very similar to both the pH^* titration of 4-ClA23187 without metal and to the pH^* titrations of 4-ClA23187 with other metal ions present. It is also similar to the pH^* titration of 4-ClA23187:Ca^{2+} (2:1 ratio). An increase in absorbance at several wavelengths at higher pH^* values is observed. However, the increase in absorbance is not due to precipitation for two reasons: the increase is not observed at all wavelengths (and was not observed visually) and the pH^* at which 50 μM Ca^{2+} forms $Ca(OH)_{2(s)}$ is higher than that for Cd^{2+}, at 13.52 in H_2O (at 25 °C).[4]

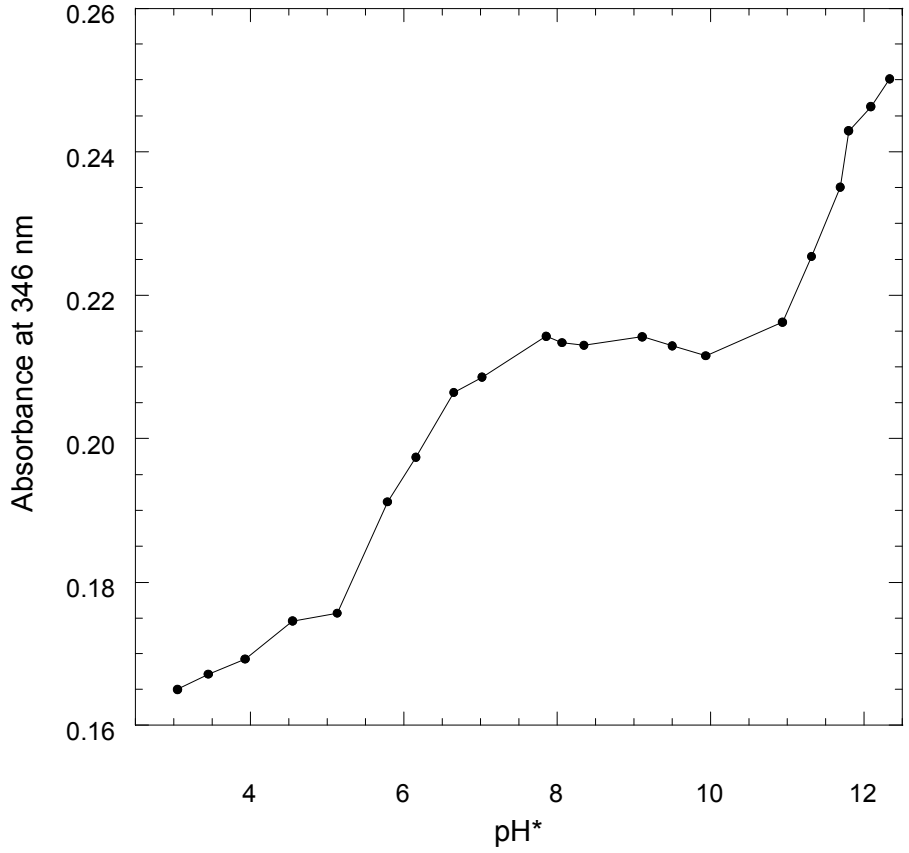

Figure IV.26. UV-vis absorbance at 348 nm of 51.7 μM 4-ClA23187: 51.7 μM Ca^{2+} pH^* titration

A plot of absorbance at 346 nm plotted as a function of pH^* indicates that there are two inflection points in the titration of 4-ClA23187 and Ca^{2+} with base. This graph is shown in Figure IV.27.

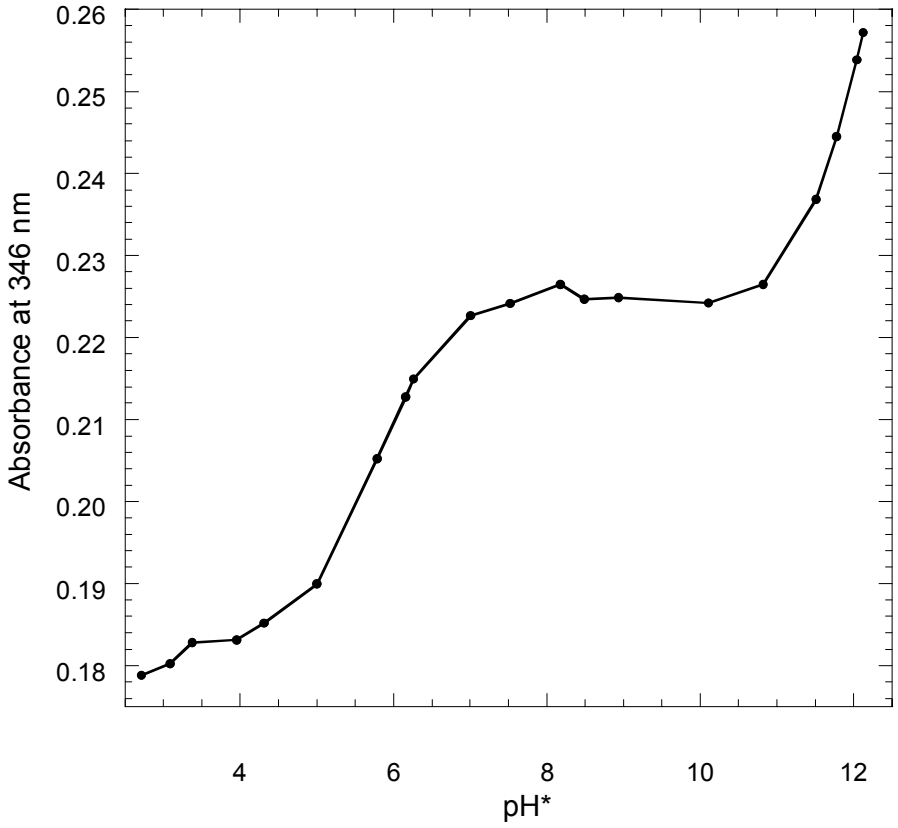

Figure IV.27. UV-vis absorbance at 346 nm of 51.7 μM 4-ClA23187: 51.7 μM Ca^{2+} pH^* titration

b. 2:1 ratio of 4-ClA23187 to Ca^{2+}: The pH^* titration of Ca^{2+}:4-ClA23187 (1:1 ratio) produced the same spectral changes at the same pH^* values as the 2:1 titrations.

10. Titrations with $(CH_3)_4NOH$ of solutions containing a fixed ratio of Mg^{2+}:4-ClA23187

Both the 2:1 and 1:1 (4-ClA23187:Mg^{2+}) pH^* titrations indicate that precipitation of Mg^{2+} occurs at pH^* above 10.0. The difference between the Ca^{2+} and Mg^{2+} may be due primarily to the pH* at which hydroxide precipitate forms. A solution of 50 μM Ca^{2+} in H_2O forms precipitate above pH^* 13.52, while a solution of 50 μM Mg^{2+} begins to form hydroxide precipitate above pH^* 10.78.[4] However, the data at pH^* values below 10 offer some insight into the binding properties of this metal. The spectra of the pH^* titration of 4-ClA23187 and Mg^{2+} is shown in Figure IV.28.

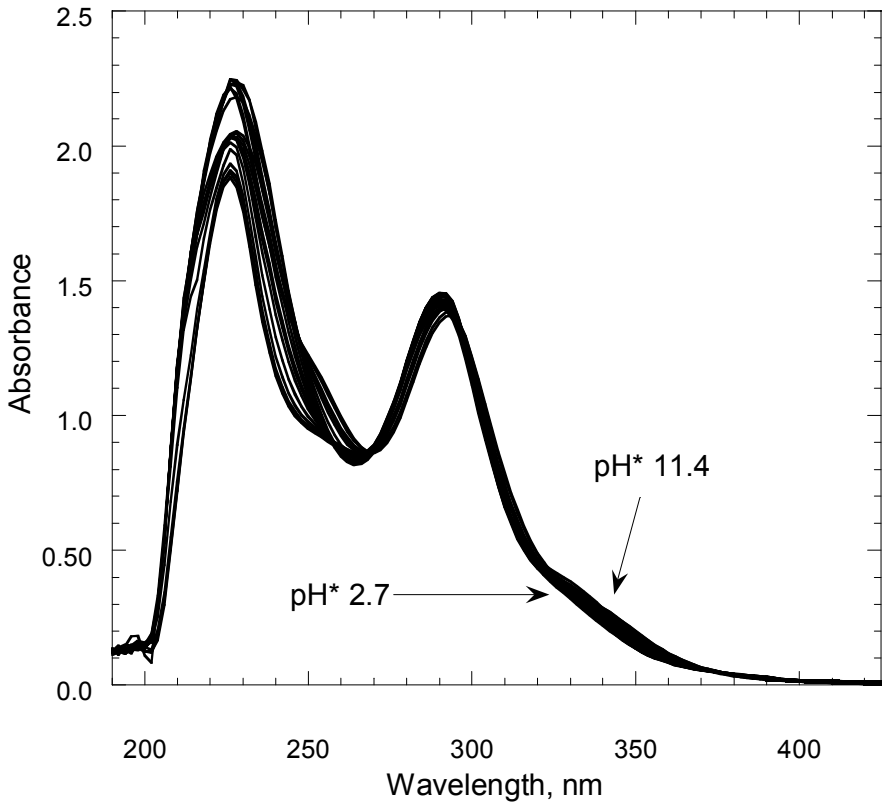

Figure IV.28. UV-vis spectra of 67.6 μM 4-ClA23187:33.8 μM Mg^{2+} pH^* titration in 80% CH_3OH/H_2O

A plot of absorbance at 346 nm as a function of pH^* indicates that there is one inflection point in the titration of 4-ClA23187 and Mg^{2+} (1:1 ratio) with base before precipitation occurs. This plot is shown in Figure IV.29. The corresponding plot for the titration of a 2:1 ligand:metal ion mixture also shows precipitation at a pH^* of approximately 10.0 (Figure IV.30). These graphs illustrate how poorly the ligand binds Mg^{2+}: above the pH^* at which $Mg(OH)_2$ is soluble, the metal precipitates rather than bind with ligand, even when there is a two-fold excess of ligand.

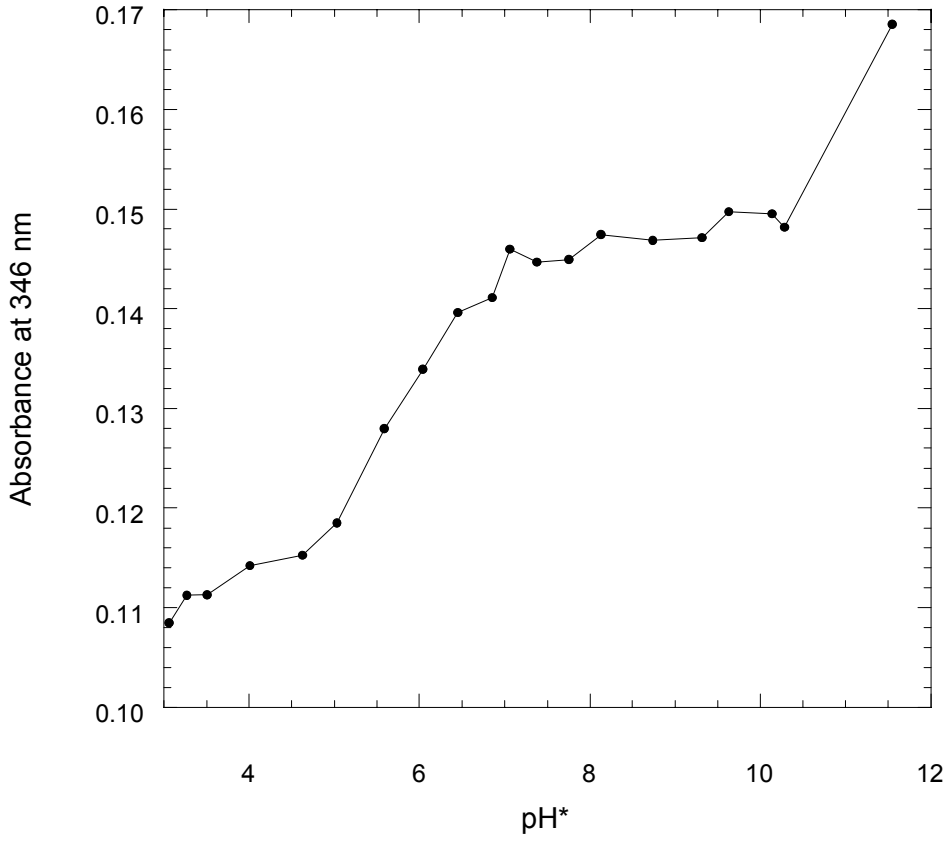

Figure IV.29. UV-vis absorbance at 346 nm of 67.6 μM 4-ClA23187: 67.6 μM Mg^{2+} pH^* titration

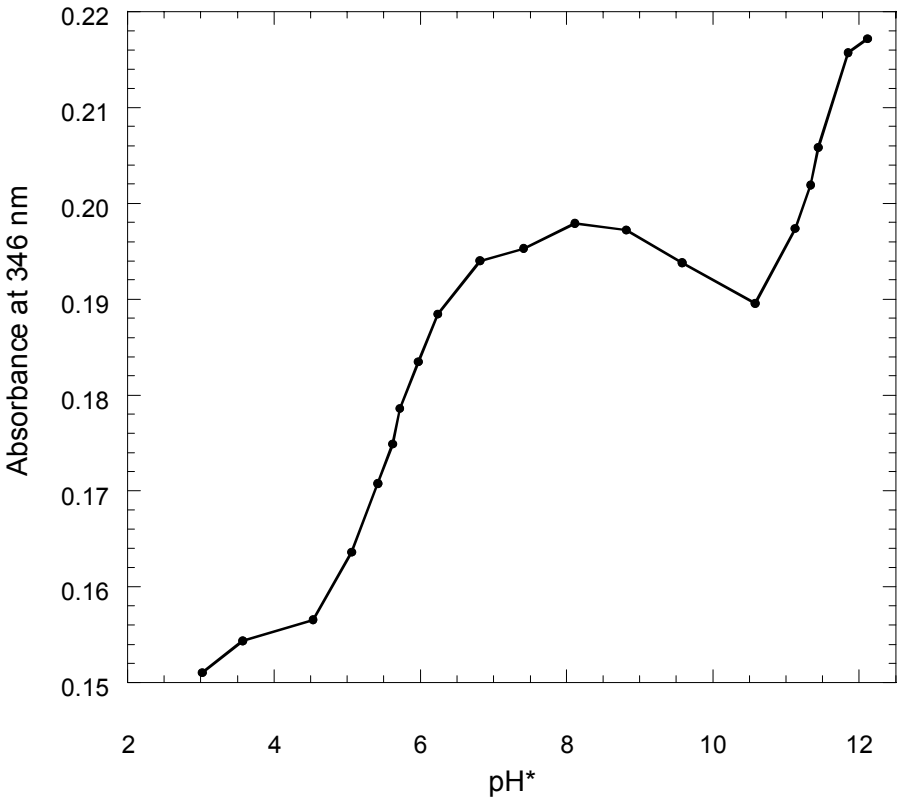

Figure IV.30. UV-vis absorbance at 346 nm of 67.6 μM 4-ClA23187:33.8 μM Mg^{2+} pH^{*} titration

11. Titrations with $(CH_3)_4NOH$ of solutions containing a fixed ratio of Ni^{2+}:4-ClA23187

The titrations of 4-ClA23187 with Ni^{2+} at (1:1) or (2:1) ratios as a function of pH^* show one inflection point at lower pH^* values, and precipitation of the metal hydroxide at pH^* values above 8. The plots of absorbance at 318 nm, and 330 nm are shown as a function of pH^* for the titration with a 1:1 or 2:1 ratio of ligand to metal, respectively. These plots are shown in Figures IV.31-32.

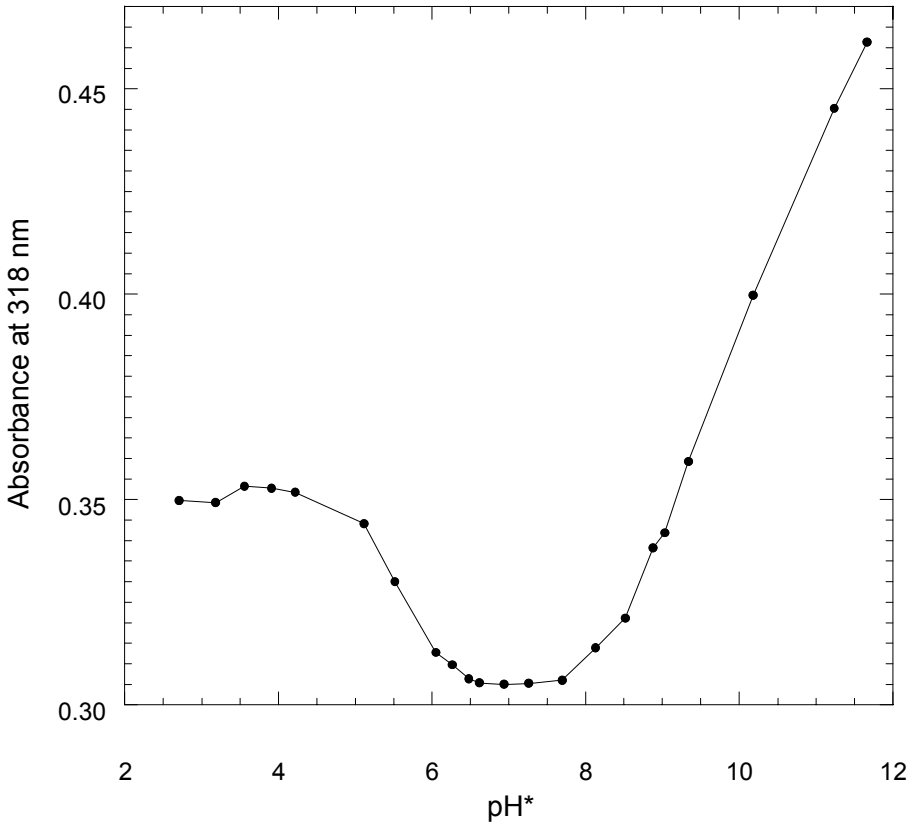

Figure IV.31. UV-vis absorbance at 318 nm of 52 μM 4-ClA23187: 52 μM Ni^{2+} pH^* titration

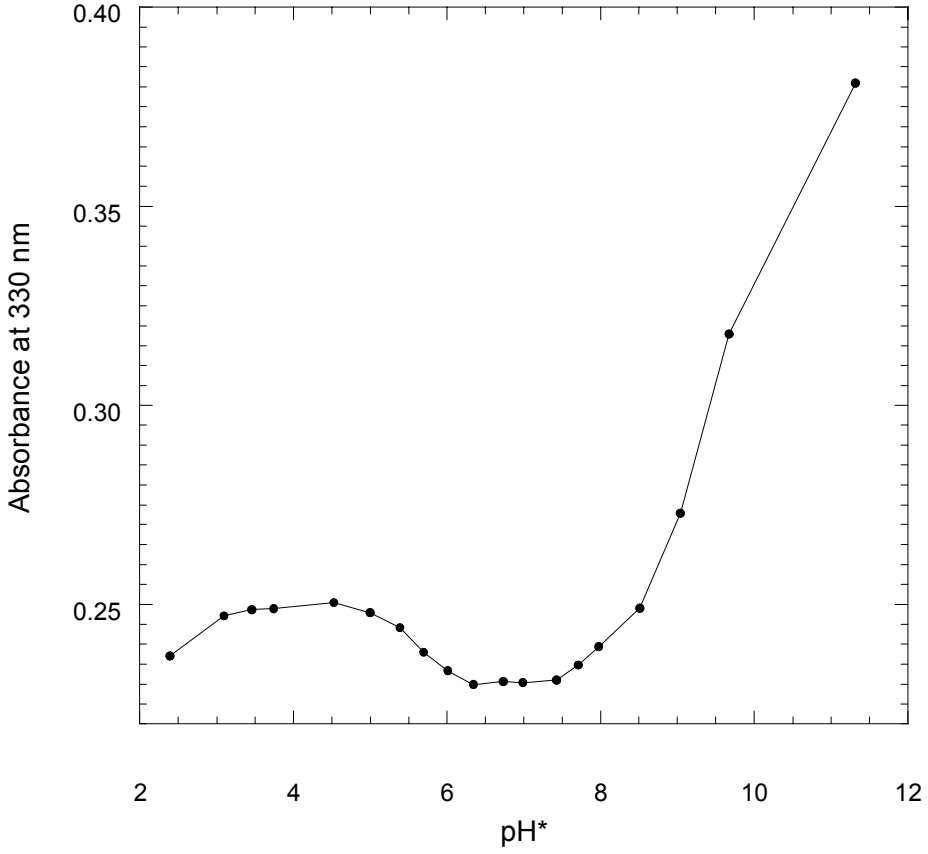

Figure IV.32. UV-vis absorbance at 330 nm of 52 μM 4-ClA23187:26 μM Ni^{2+} pH^{*} titration

12. Determination of protonation and complexation constants by spectroscopic data

The protonation and complexation constants derived from the pH^* titrations of each metal ion at a fixed molar ratios of 2:1 or 1:1 for [4-ClA23187]:[M^{2+}] are determined by fitting the data with the SPECFIT program. The protonation constants, determined by spectroscopic titration, are included in each model and held at fixed values when fitting metal complexation data. Various models are tried that include every combination of the complexation constants K_{HMA} and K_{MA} as well as the constants for formation of possible complexation species MA_2, MA_2H_2, and MA_2H. These complexation and protonation equilibria are listed in Table IV.6.The best fit occurred with the model that included the protonation constants and complexation constants for formation of only the species HMA and MA. The formation constants for K_{HMA} and K_{MA} for 4-ClA23187 are listed in Table IV.7, along with the formation constants for K_{HMA} for A23187.[5]

Reaction	Equilibrium Constant, K
$H_2A \leftrightarrows H^+ + HA^-$	$K_{a1} = \frac{[H^+][HA^-]}{[H_2A]}$
$HA^- \leftrightarrows H^+ + A^{2-}$	$K_{a2} = \frac{[H^+][A^{2-}]}{[HA^-]}$
$M^{2+} + HA^- \leftrightarrows (M)AH^+$	$K_{HMA} = \frac{[(M)AH^+]}{[M^{2+}][HA^-]}$
$M^{2+} + A^{2-} \leftrightarrows MA$	$K_{MA} = \frac{[MA]}{[M^{2+}][A^{2-}]}$

Table IV.6. Complexation equilibria and associated constants for 4-ClA23187

	Log K_{HMA}	Log K_{HMA}	Log K_{MA}
Metal	A23187[5]	4-ClA23187	4-ClA23187
Zn^{2+}	6.79	3.8 ± 0.3	5.1 ± 0.2
Cd^{2+}	6.48	4.5 ± .07	8.0 ± 0.1
Ca^{2+}	4.5	3.7 ± 0.2	6.1 ± 0.2
Mg^{2+}	4.55	4.1 ± 0.2	4.69 ± 0.3
Ni^{2+}	7.54	no data	no data

Table IV.7. Metal complexation constants for 4-ClA23187 in 80% CH_3OH/H_2O

The binding constants for formation of the 1:1 complex are lower for every metal studied when compared to the parent compound. This indicates that the presence of the halogen affects the ability of the ligand to bind to metals in general. The selectivity observed in the transport data is not reflected in the binding constants.

C. Transport Studies

The transport behavior of nine divalent cations by 4-ClA23187 into POPC vesicles was studied by collaborators at The Ohio State University. The rates of transport of Zn^{2+}, Mn^{2+}, Cd^{2+}, Pb^{2+}, Co^{2+}, Ni^{2+}, Cu^{2+}, Ca^{2+}, and Sr^{2+} into vesicles were monitored by changes in the UV-vis absorbance of the indicator dye Quin-2.[6] Measurements were taken approximately once per second for approximately 14 minutes. The transport results are shown in Figure IV.33.

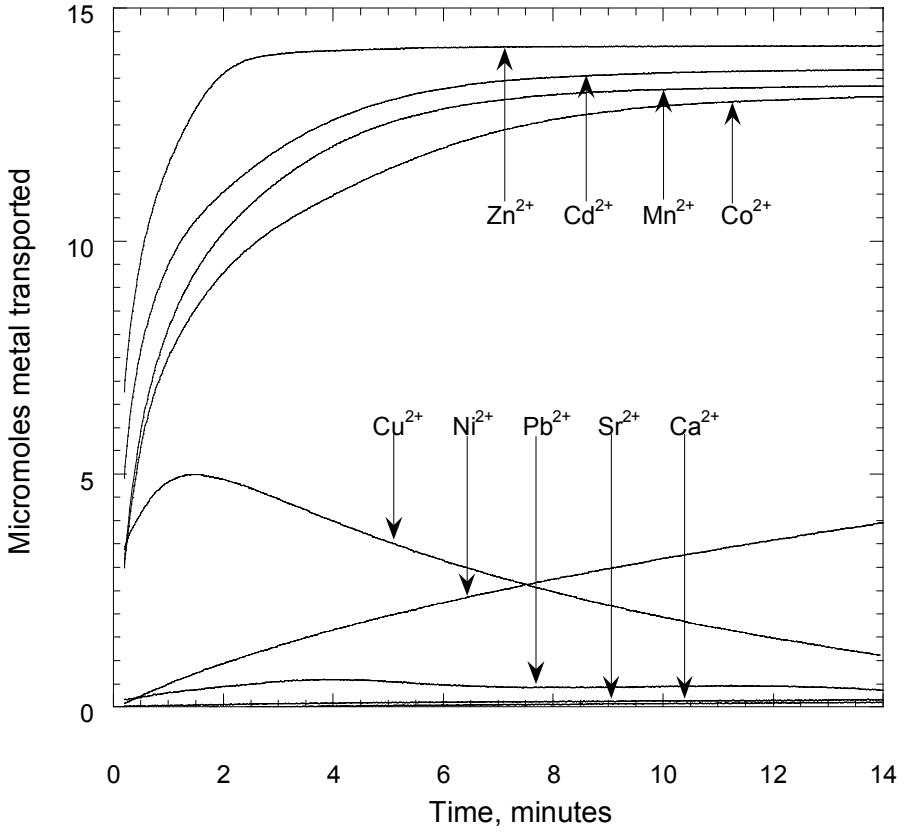

Figure IV.33. Transport kinetics for 4-ClA23187 and several divalent cations

The transport data show that under the given conditions, 4-ClA23187 transports Zn^{2+} at the highest rate, followed closely by Cd^{2+}, Mn^{2+}, and Co^{2+}. Transport of Cu^{2+} has a very high initial rate, but after ~ 90 seconds, the concentration of Cu^{2+} within the vesicle decreases. The loss of absorbance is possibly due to either precipitation of the Cu^{2+}:Quin-2 complex, or due to a change in the stoichiometry of the complex (from 1:1 to 2:1 metal:ligand ratio) that has different spectral properties than the expected 1:1 complex.[7] Transport of Pb^{2+} also displays behavior that may be the result of the same type of events as observed with Cu^{2+}, or by a complex that forms between Pb^{2+} and ionophore that results in a stable, non-transporting species.[7] The transport of Ni^{2+} occurs slowly but steadily throughout the experiment. It does not reach a plateau as other metals do due to the low speed of transport.

The basis for the transport selectivity displayed by 4-ClA23187 may be due to the ability of the 1:1 metal-ligand complex to lose the proton attached to the pyrrole nitrogen. The zinc, manganese, cadmium, and cobalt metal ions are more likely to be transported as a one metal ion- one ligand complex in which the pyrrole proton has been dissociated than calcium ions (which would require more than the four available donor atoms from the ligand and would have additional binding sites occupied by water molecules).

D. Summary

The crystal structure of the magnesium complex of 4-ClA23187 shows that addition of a halogen to the 4 position of the benzoxazole ring of A23187 does not prohibit the derivative from forming the 2:1 ligand:metal complex. The $Mg(4\text{-}ClA23187)_2$ complex has three donor atoms per ligand and two interligand pyrrole hydrogen/carboxylate oxygen hydrogen bonds, which is similar to most metal complexes observed for A23187.

Although the $Zn(4\text{-}BrA23187)_2$ crystal structure[8] is shown to have one ketopyrrole oxygen displaced from the metal center by a solvent molecule, this is not directly due to the addition of a halogen to the 4 position of the benzoxazole ring. The crystal structure of $Mg(4\text{-}ClA23187)_2$ is evidence against the theory that a halogenated 4 position is sufficient to disrupt traditional binding patterns observed with the parent compound.

The crystal structure of $Ni(A23187)_2$, which also features a solvent molecule that has displaced a ketopyrrole oxygen from the metal center, refutes the theory that a halogen at the 4 position on the benzoxazole ring is necessary to disrupt traditional binding properties of A23187.

Studies of binding properties of 4-ClA23187 led to the discovery of two relevant pK_a's for the ligand. UV-vis spectroscopy and potentiometric titrations revealed one pK_a at 5.90, and UV-vis spectroscopy titrations revealed an additional pK_a at 11.3 in 80% CH_3OH/H_2O. The pK_a of 5.90 reflects the deprotonation of the carboxylate moiety. For the parent compound, the pK_a for this hydrogen is 7.8 in 80% CH_3OH/H_2O. The lower pK_a of 4-ClA23187 is expected due to the inductive effect of an electron withdrawing group at the 4 position of the benzoxazole ring. The second pK_a, presumably due to the

loss of hydrogen at the pyrrole nitrogen, is approximately 11.3 for both 4-ClA23187 and parent compound A23187.

The metal complexation properties of 4-ClA23187 as observed by UV-vis spectroscopy indicate that the presence of the chlorine does alter the binding observed with the parent compound A23187. The binding constant for formation of all $M(HL)^+$ complexes studied (M = Zn^{2+}, Cd^{2+}, Ca^{2+}, and Mg^{2+}) are lower for 4-ClA23187 than for A23187. The best fit for all pH^* titrations of 4-ClA23187 with metal present is a model that includes the formation of the 1:1 metal:ligand complex at lower pH^* values, and the deprotonation of the pyrrole nitrogen of the complex at higher pH^* values. The loss of this hydrogen results in a ligand with 4 donor atoms and a -2 charge which gives a neutral complex when bound to a divalent metal ion. If the ligand of this complex is able to suitably wrap around the metal ion (i.e., if the metal ion is small and can have a coordination number of 4), it can potentially shield it from hydrophobic environments, thus increasing the ability to transport the metal across a cell membrane. The ability of the ligand to do this for any particular metal ion may affect transport selectivity.

Transport data for 4-ClA23187 is very similar to transport data for 4-BrA23187.[5] Zn^{2+}, Co^{2+}, and Mn^{2+} are transported with high selectivity over Ca^{2+} and Mg^{2+}, as seen in transport data for 4-BrA23187. Ni^{2+} is transported with slightly higher selectivity than Ca^{2+} or Mg^{2+}. Selectivity of transport may be due to either the increased ability to wrap around smaller metal ions, or in the ability of the metal ion that is bound to the ligand to induce deprotonation of the pyrrole nitrogen, thus creating a 4^{th} donor atom and -2 charge to neutralize the complex. Additionally, the transport data may reflect the ability of the ligand to form overly stable complexes with metal ions that result in slow transport due to

poor dissociation between the metal ion and ligand. In the case of Ni^{2+}, transport may be impeded due to the affinity of the metal ion for the ligand. The metal ions that transport at the highest rates have median complexation constants, and can associate and dissociate with the ligand with equal ease.

REFERENCES:

1. Alleaume, M., and Barrans, Y. *Can. J. Chem.* **1985**, *63*, 3482-3485

2. Martell, A. E. and Motekaitis, R. J. *Determination and Use of Stability Constants*, 2nd Ed., VCH Publishers, Inc.: New York, **1992**.

3. Pfeiffer, D. R., Taylor, R. W., and Lardy, H. A. *Ann. N. Y. Acad. Sci*. **1978**, *307*, 402-423.

4. Basolo, F. and Johnson, R. *Coordination Chemistry: The Chemistry of Metal Complexes*; Johnsen, R., Ed.; W. A. Benjamin, Inc.: New York **1964**.

5. Chapman, C. J., Puri, A. K., Taylor. R. W., and Pfeiffer, D. R. *Biochemistry*, **1987**, *26*, 5009-5018.

6. Erdahl, W. L., Chapman, C. J., Wang, E., Taylor, R. W., and Pfeiffer, D. R. *Biochemistry*, **1996**, *35*, 13817-13825.

7. Yuchi, A., Tanaka, A., Hirai, M., Yasui, T., Wada, H., and Nakagawa, G. *Bull. Chem. Soc. Jpn*., **1993**, *66*, 3377-3381.

8. Vila, S., Canet, I., Guyot, J., Jeminet, G., and Pointud, Y. *New J. Chem.*, **2003**, *27*, 1246-1250.

CHAPTER V

STRUCTURAL AND BINDING PROPERTIES OF 23,24-Br_2A23187

Structural and binding properties of 4-ClA23187 were studied and compared with those of 4-ClA23187 and parent compound A23187. The crystal structure of Mg(23,24-Br_2A23187) was analyzed by X-ray crystallography, and the binding properties analyzed by spectrophotometric titrations. Two forms of titrations, at fixed pH^* as a function of metal ion concentration, and at fixed metal ion:23,24-Br_2A23187 ratio as a function of pH^* were performed. Titrations at fixed pH^* are used to determine the stoichiometry of the complex. Titrations at fixed metal ion:23,24-Br_2A23187 ratio were fit by the program SPECFIT to gain pH^* independent protonation and complexation constants for the ionophore.

A. Structural Properties

1. Crystal structure of Mg(23,24-Br_2A23187)$_2$

The Mg complex of 23,24-Br_2A23187 is formed by extraction of Mg^{2+} from aqueous solution into a solution of 23,24-Br_2A23187 in $CHCl_3$. Solvent is removed by vacuum and crystals are formed by evaporation from 95% CH_3CH_2OH/H_2O. The resulting crystal is analyzed by X-ray diffractometer and is shown in Figures V.1 and V.2.

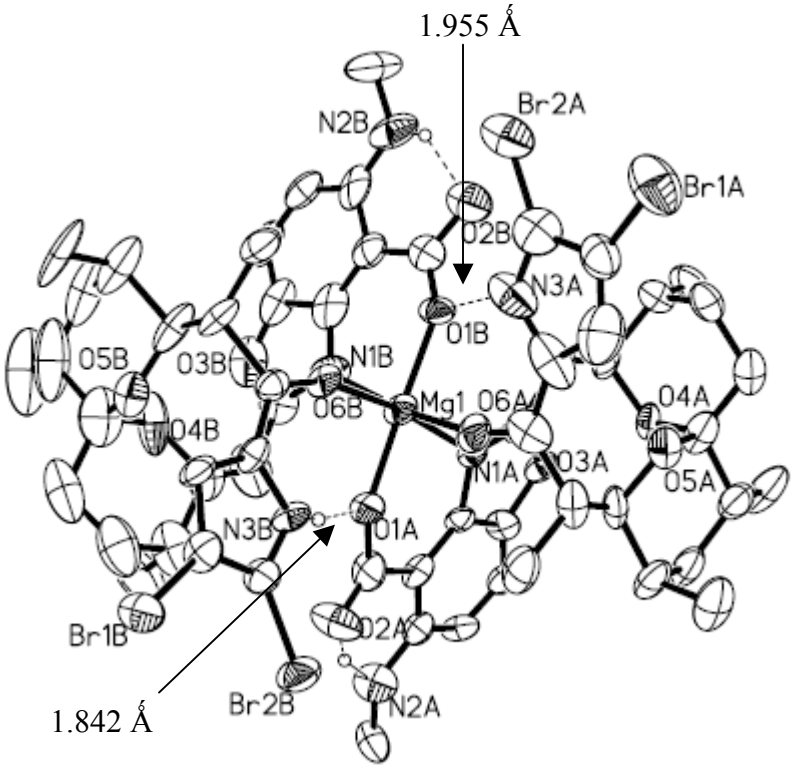

Figure V.1. Crystal structure of Mg(23,24-Br_2A23187)$_2$

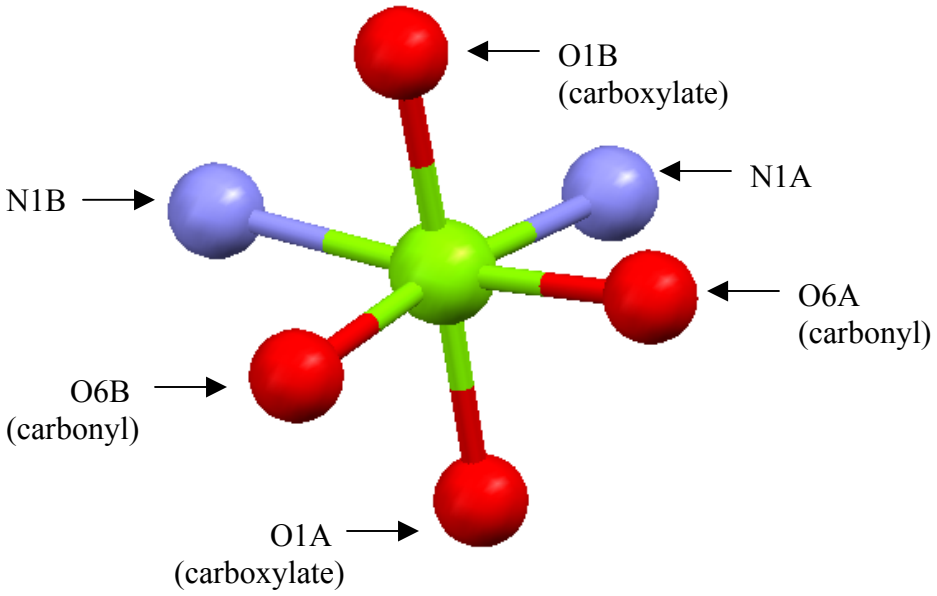

Figure V.2. Metal center of $Mg(23,24\text{-}Br_2A23187)_2$

The metal center of the complex (6-coordinate with octahedral geometry) is similar to those of most complexes of A23187. It is comprised of three donor atoms of each ligand: a carboxylate oxygen, a benzoxazole nitrogen, and a ketopyrrole oxygen. The donor atom-metal bond distances are listed in Table V.1.

Metal-Ligand Bond	$Mg(23,24\text{-}Br_2A)_2$ Bond Length, Å	MgA_2 Bond Length[x], Å
Mg1-O1A (carboxylate)	1.993	1.996
Mg1-O6A (carbonyl)	2.060	2.064
Mg1-N1A	2.186	2.235
Mg1-O1B (carboxylate)	1.970	1.990
Mg1-N1B	2.201	2.228
Mg1-O6B (carbonyl)	2.060	2.060

Table V.1. Metal ligand bond distances of donor atoms in metal center of $Mg(23,24\text{-}Br_2A23187)_2$ compared to $Mg(A23187)_2$[1]

The stereochemistry of the metal center is also similar to all complexes except that found for $Cu(A23187)_2$. The carboxylate oxygens of each ligand are trans to one another, the ketopyrrole oxygens are cis to one another, and the benzoxazole nitrogens are cis to one another. The bonding angles that support this observation are listed in Table V.2. This orientation is labeled as negative stereochemistry.[2]

Donor Atom-Mg-Donor Atom	$Mg(23,24\text{-}Br_2A)_2$ Angle, °	MgA_2 Angle, °
O1A (carboxylate)-Mg1-O6A (carbonyl)	90.01	91.0
O6A (carbonyl)-Mg1-O1B (carboxylate)	80.47	88.9
O1B (carboxylate)-Mg1-N1B	83.58	82.6
N1B-Mg1-O1A (carboxylate)	97.93	96.5
N1A-Mg1-O1A (carboxylate)	84.33	82.7
N1A-Mg1-O6A (carbonyl)	88.12	86.7
N1A-Mg1-O1B (carboxylate)	99.38	96.6
N1A-Mg1-N1B	93.13	95.4
O6B (carbonyl)-Mg1-O1A (carboxylate)	88.59	88.2
O6B (carbonyl)-Mg1-O6A (carbonyl)	89.93	90.7
O6B (carbonyl)-Mg1-O1B (carboxylate)	87.64	92.5
O6B (carbonyl)-Mg1-N1B	89.78	88.3
O1A (carboxylate)-Mg1-O1B (carboxylate)	175.94	178.4
O1 (carbonyl)-Mg1-N2	172.05	172.4
N1A-Mg1-O6B (carbonyl)	172.65	170.5

Table V.2. Bond angles (ligand-metal-ligand) of metal center of $Mg(23,24\text{-}Br_2A23187)_2$

Error associated with measurement of bond angles ranges from ± 0.02 to 0.1.

The hydrogen bond network observed in complexes of A23187 is observed in this complex as well. Intraligand hydrogen bonding is observed between the methylamino proton and the carboxylate oxygen not bound to the metal. This bond length is 1.856 Å for one ligand and 1.838 Å for the second. Interligand hydrogen bonding is observed between the pyrrole nitrogen proton and the carboxylate oxygen of the opposite ligand that is bound to the metal. These hydrogen bonds, which lend stability to the complex, are measured to be 1.955 and 1.842 Å. Compared to the magnesium complex of 4-ClA, which has interligand hydrogen bond distances of 2.064 and 2.108 Å, the bonds of 23,24-Br_2(A23187)$_2$ are somewhat shorter. The presence of two bromine molecules on each pyrrole ring does not have an effect upon the formation of these hydrogen bonds in the solid state.

2. Structural Studies by Circular Dichroism

a. Protonation equilibrium

The CD spectra of $Br_2A23187$ in CH_3OH/H_2O titrated with the strong base $(CH_3)_4NOH$, shown in Figure V.3, develop peak centered at ~ 298 nm that increases until ~ pH^* 8.5, then decreases. Other features of the spectra are a negative peak centered at ~ 335 nm that increases with an increase in pH^*, and a smaller, second positive peak centered at ~ 370 nm.

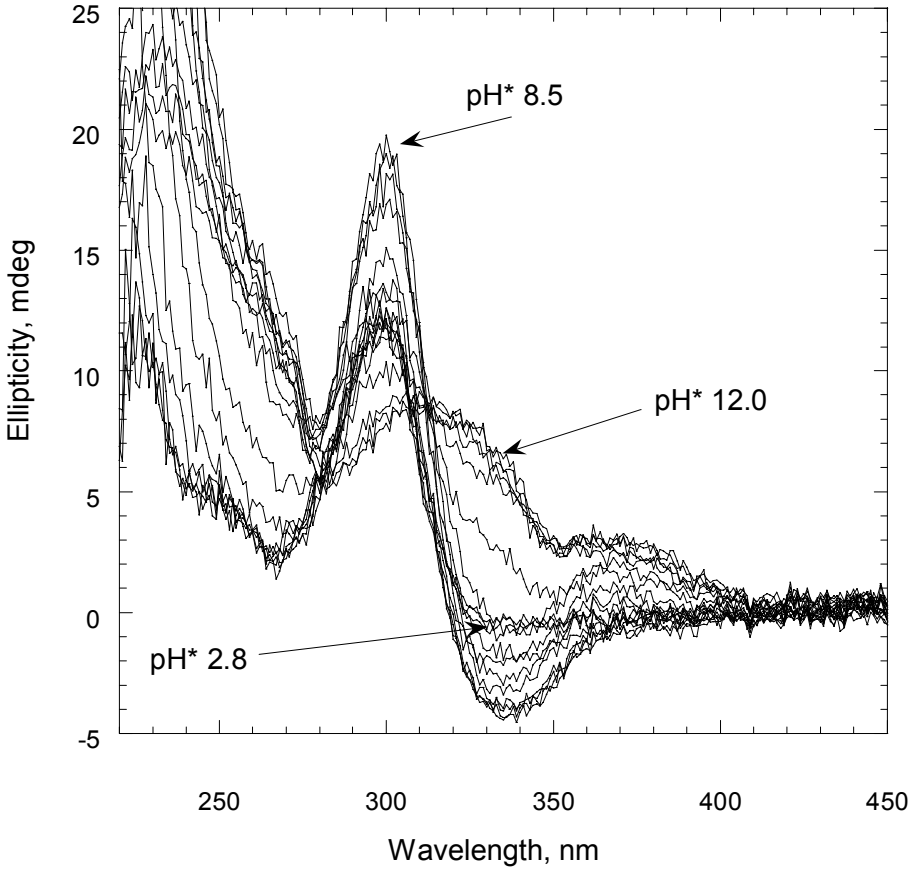

Figure V.3. CD spectra of Br_2A in 80% CH_3OH/H_2O titrated with $(CH_3)_4NOH$

Ellipticity at 290 nm plotted as a function of pH^* (Figure V.4) shows that two equilibria are present during the titration. This is evidence there are two deprotonation steps occurring during the course of the pH^* titration of 23,24-Br_2A23187.

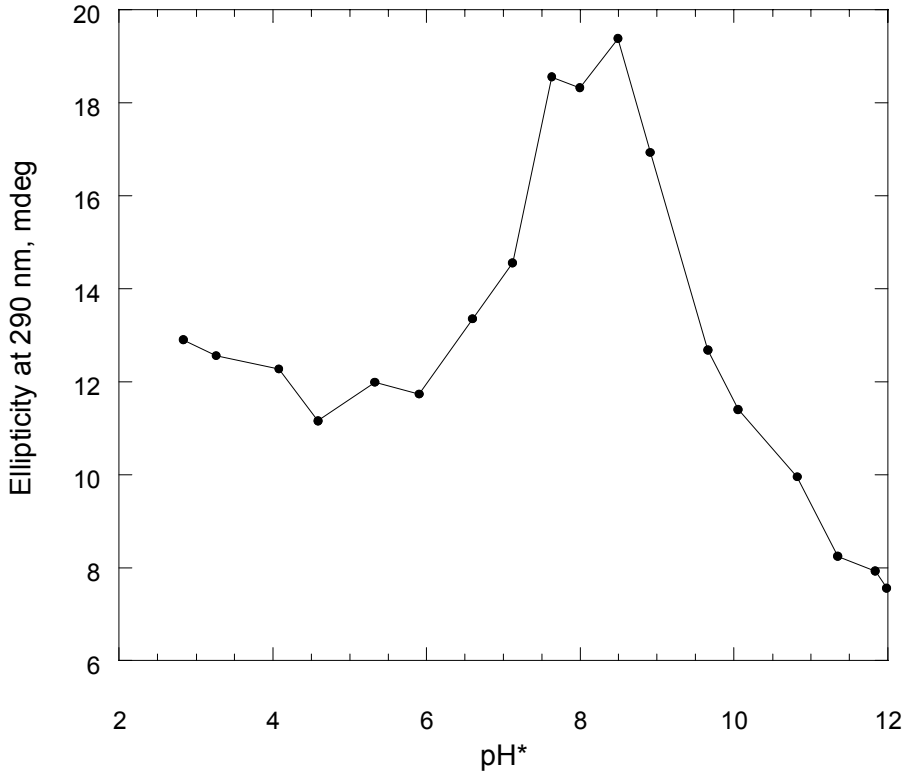

Figure V.4. Ellipticity at 290 nm of 23,24-Br_2A23187 titrated with $(CH_3)_4NOH$

b. CD titrations of 23,24-Br_2A23187 with metal ions at fixed pH^*

1. 23,24-Br_2A23187 titrated with Zn^{2+}

The CD spectra of 23,24-Br_2A23187 titrated with Zn^{2+} at pH^* 7.0 has two main spectral features, shown in Figure V.5. A positive peak develops at 300 nm and a negative peak develops at 340 nm. The exciton coupling involving the benzoxazole moiety is not observed. However, the large negative peak at ~ 340 nm overlaps the benzoxazole region and this may obscure the lower wavelength portion of a possible exciton split peak.

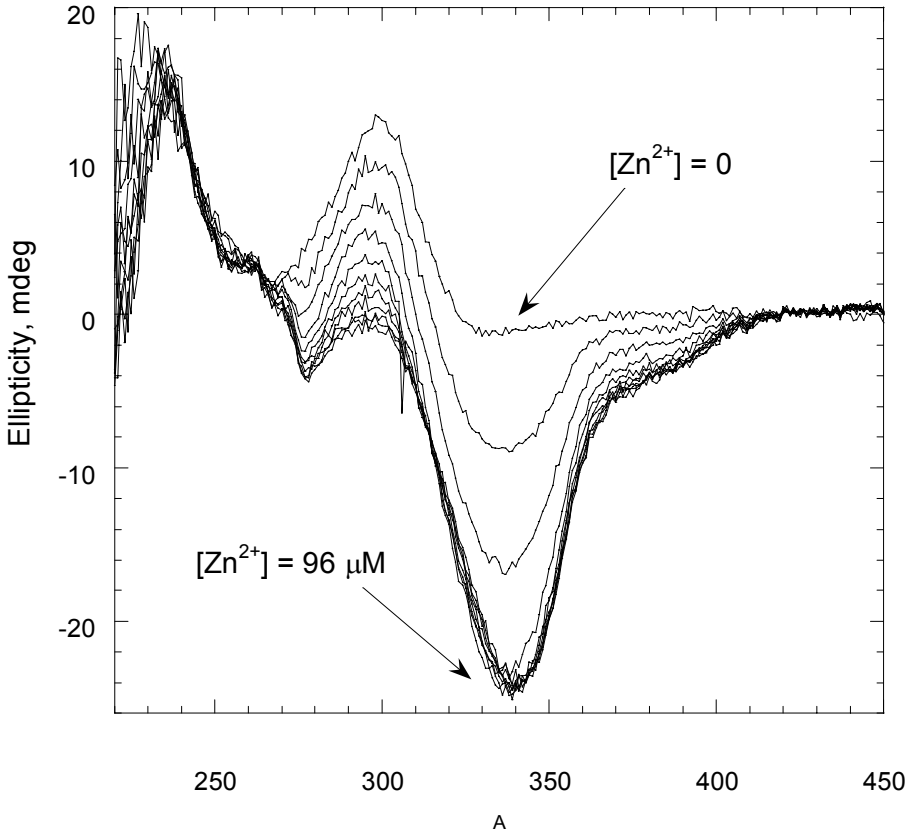

Figure V.5. CD spectra of 43.9 μM 23,24-Br_2A23187 titrated with Zn^{2+} at pH^* 7.0

Plotting ellipticity at 336 nm as a function of pH^* results in the graph shown in Figure V.6. This graph shows that change occurs linearly until the maximum amount of 2:1 ligand:metal complex has been formed. After this point, ellipticity at 336 nm ceases to change. Additional Zn^{2+} added after the conversion of all ligand into the 2:1 complex results in reaction V.1.

$$MA_2 + M^+ \leftrightarrows 2MA^+ \qquad \text{Eq. V.1}$$

This shift from 2:1 complex to a mixture of 2:1 and 1:1 is not observed by CD. Due to a lack of exciton coupling in the spectra of MA_2, further conversion to MA^+, in which exciton coupling would not be observed, is undetectable.

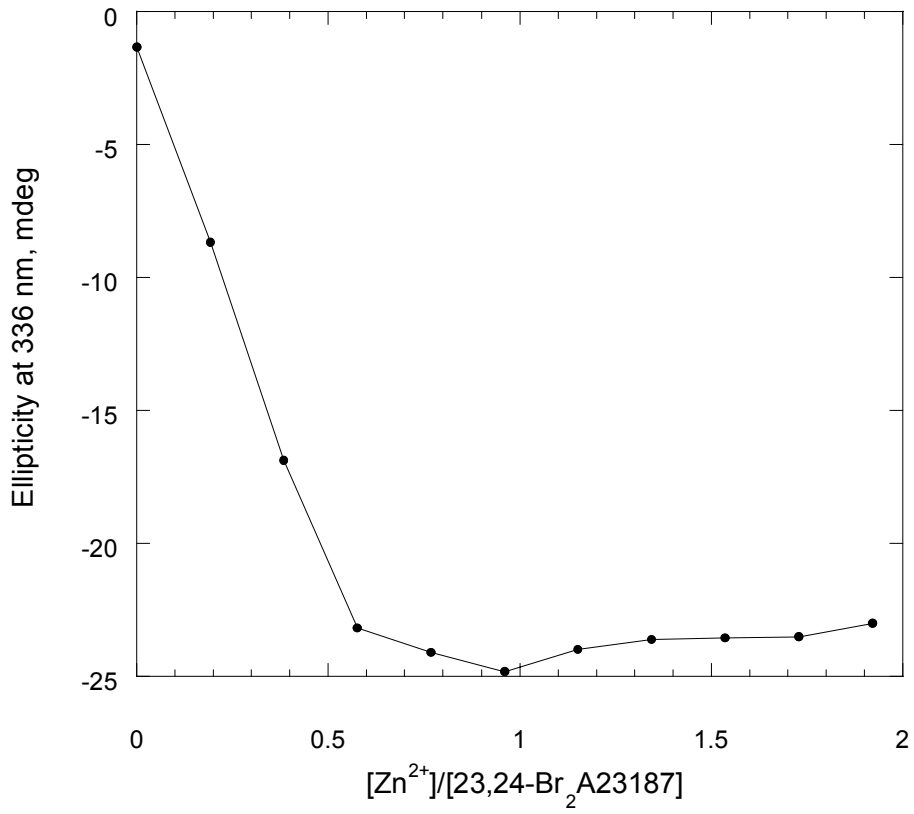

Figure V.6. Ellipticity at 336 nm of 23,24-Br_2A23187 titrated with Zn^{2+} at pH^* 7.0

2. 23,24-Br_2A23187 titrated with Cd^{2+}

The CD spectra of 23,24-Br_2A23187 titrated with Cd^{2+} at pH^* 7.0, shown in Figure V.7, is very similar in appearance to that of the ligand titrated with Zn^{2+} at the same pH^*.

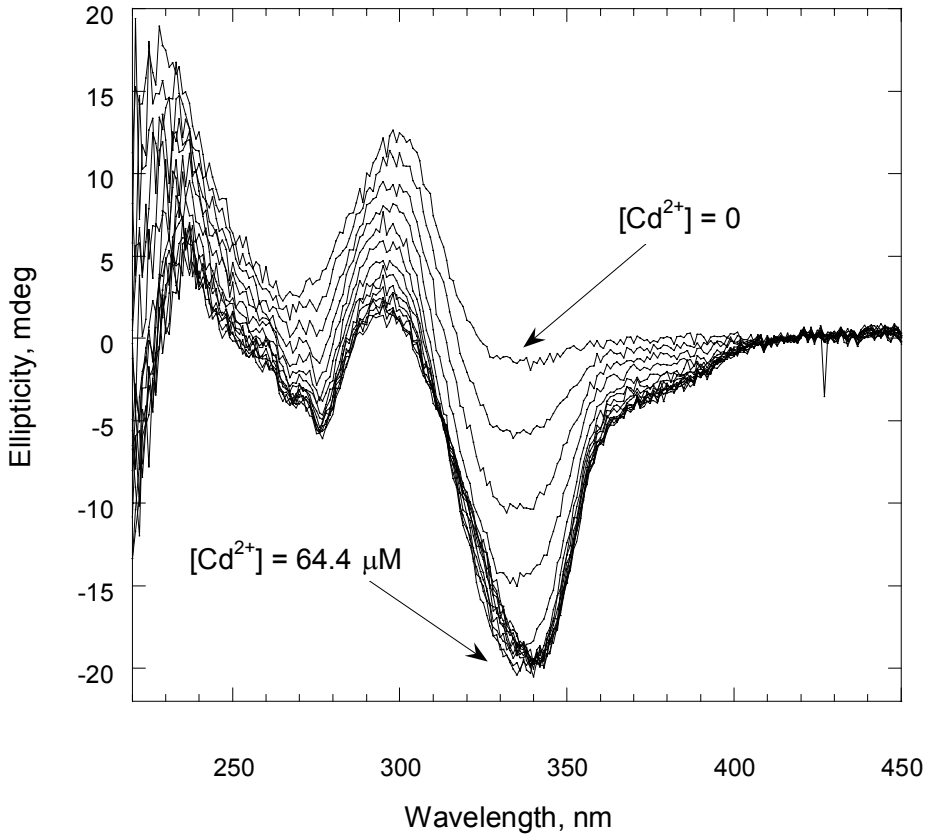

Figure V.7. CD spectra of 50 μM 23,24-Br_2A23187 in 80% CH_3OH/H_2O titrated with Cd^{2+} at pH^* 7.0

Like the Zn^{2+} titration, the Cd^{2+} titration produces ellipticity at ~330 nm as a function of metal:ligand ratio that changes linearly until the point where enough metal has been added to completely form 2:1 ligand:metal complex with 23,24-Br_2A23187. After this point, no further changes are observed, as seen in Figure V.8.

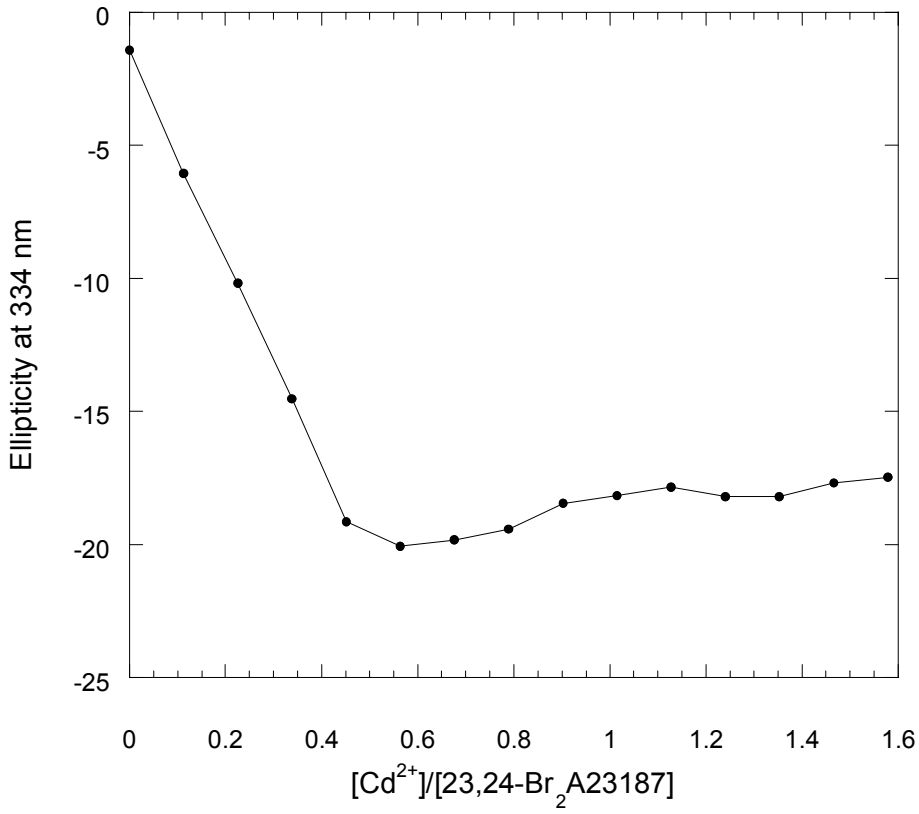

Figure V.8. Ellipticity at 334 nm of 50 μM 23,24-Br_2A23187 titrated with Cd^{2+} at pH* 7.0

3. 23,24-Br_2A23187 titrated with Ca^{2+}

The spectra of 23,24-Br_2A23187 titrated with Ca^{2+} at pH^* 7.0, shown in Figure V.9, produced no observable changes in ellipticity at any wavelength between 220 and 450 nm. Either no complexation is occurring, or the complexation does not result in a conformational change that is observed by CD in this wavelength range.

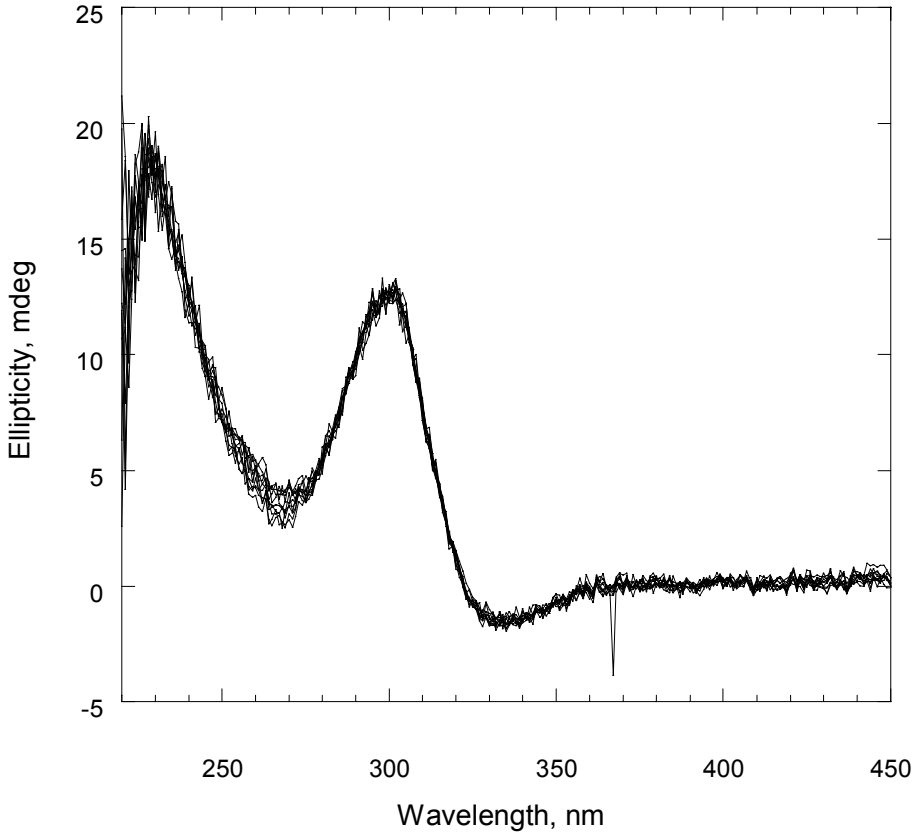

Figure V.9. CD spectra of 50 μM 23,24-Br_2A23187 in 80% CH_3OH/H_2O titrated with Ca^{2+} at pH^* 7.0

4. 23,24-Br_2A23187 titrated with Mg^{2+}

Like the titration with Ca^{2+}, the titration of 23,24-Br_2A23187 with Mg^{2+} produced no observable CD spectral changes, as seen in Figure V.10.

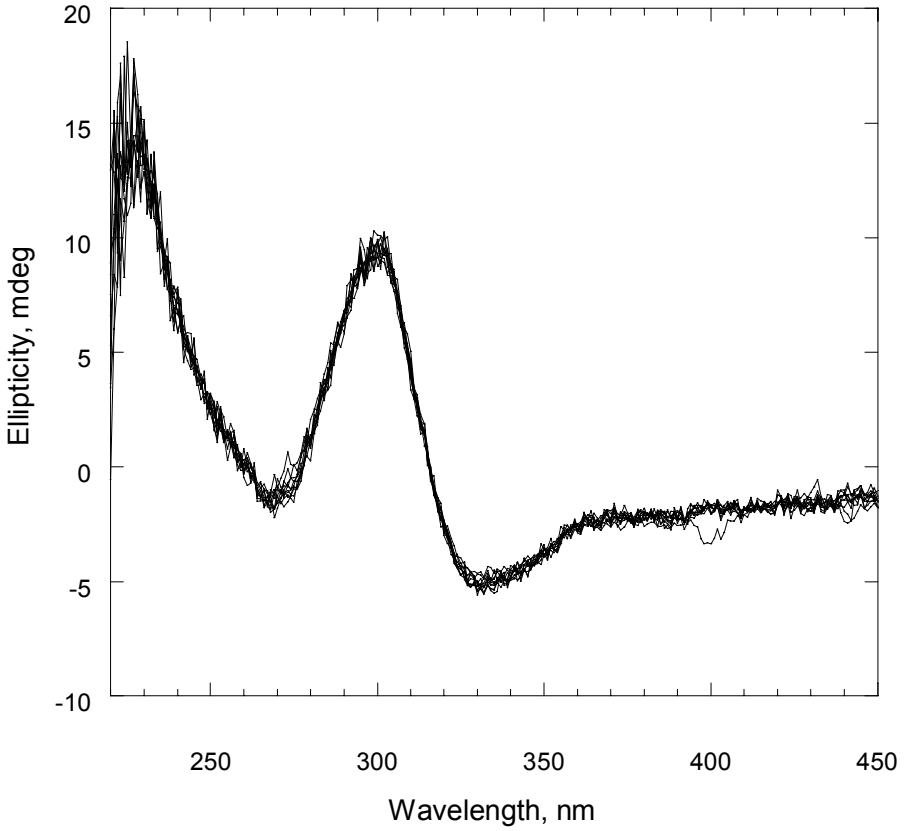

Figure V.10. CD spectra of 50 μM 23,24-Br_2A23187 in 80% CH_3OH/H_2O titrated with Mg^{2+} at pH^* 7.0

5. 23,24-Br_2A23187 titrated with Ni^{2+}

The titration of 23,24-Br_2A23187 with Ni^{2+} at pH^* 7.0 resulted in spectra that are similar in appearance to those in titrations of ligand with Zn^{2+} and Cd^{2+} at pH^* 7.0. The spectra for this titration are shown in Figure V.11.

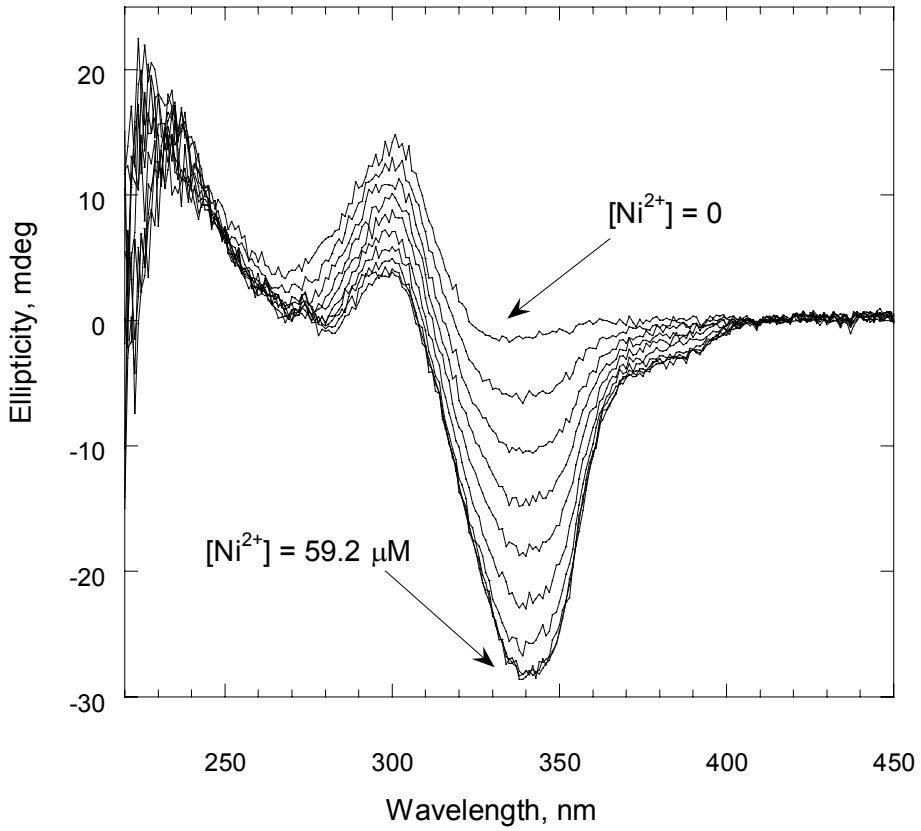

Figure V.11. CD spectra of 50.5 μM 23,24-Br_2A23187 in 80% CH_3OH/H_2O titrated with Ni^{2+} at pH^* 7.0

Unlike the titrations with Zn^{2+} and Cd^{2+}, however, in the titration of 23,24-Br_2A23187 with Ni^{2+} the ellipticity at 337 nm does not reach a minimum at a ratio of $[M^{2+}]$/[23,24-Br_2A23187] = 0.5. The ellipticity at 337 nm as a function of metal:ligand ratio, shown in Figure V.12, changes linearly until a ratio between 0.8 and 0.9 is reached. The graph then levels off for the remainder of the titration.

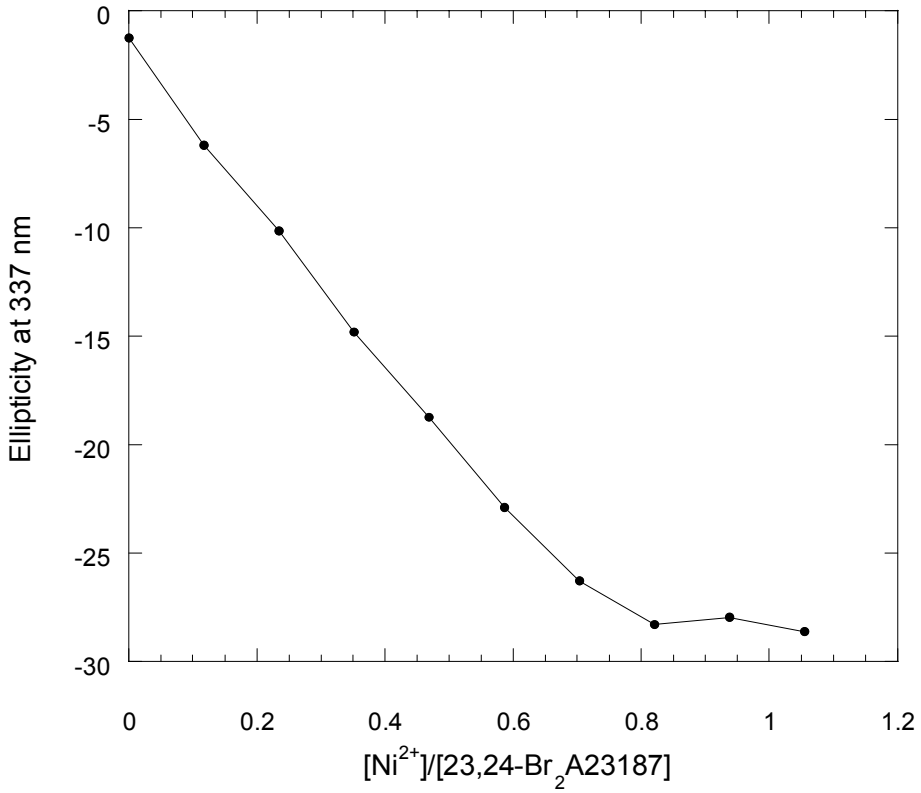

Figure V.12. Ellipticity at 337 nm of 23,24-Br_2A23187 titrated with Ni^{2+} at pH* 7.0

c. Solvent effects on structure of $M(Br_2A23187)_2$:

23,24-Br_2A23187 was extracted with aqueous solutions of metal (Zn^{2+}, Cd^{2+}, Mg^{2+}, Ca^{2+}, and Ni^{2+}) and the CD spectrum of each $M(Br_2A)_2$ complex in $CHCl_3$ recorded. The results are shown in Figure V.13.

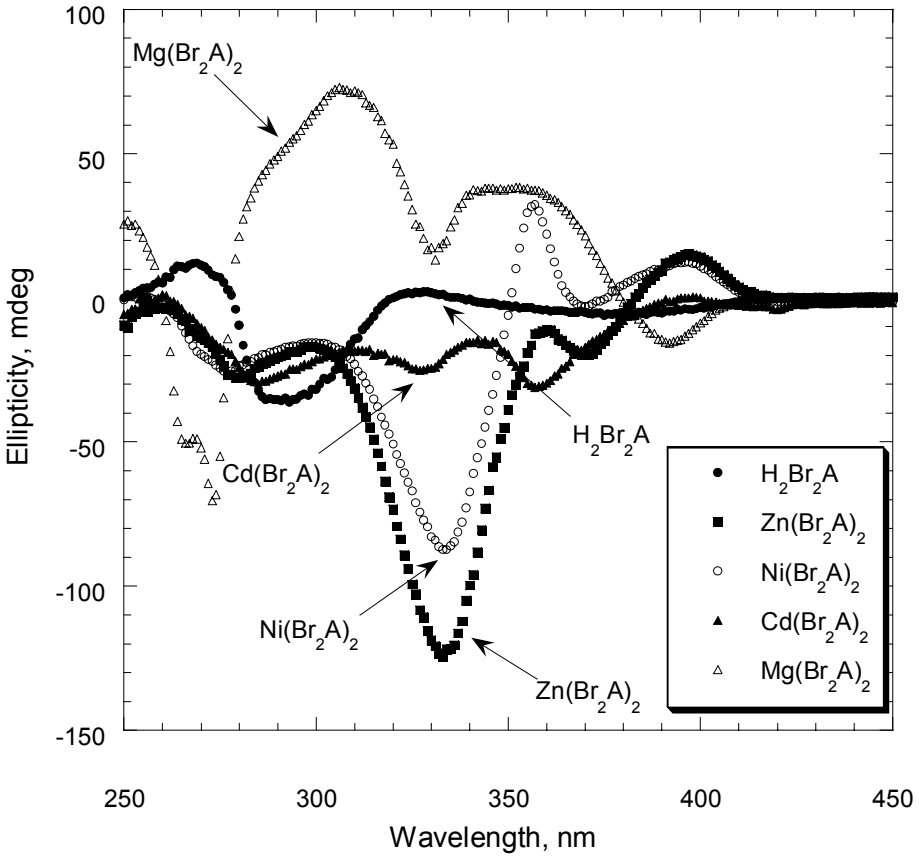

Figure V.13. CD spectra of $M(Br_2A)_2$ complexes in $CHCl_3$

Compared to the free acid form of 23,24-Br_2A23187, the zinc and nickel complexes have a large negative peak centered at ~ 330 nm, a small negative peak centered at ~ 370 nm, and a peak centered at ~ 390 nm. A small positive peak is also observed at ~ 355 nm. The cadmium complex, which is expected to behave like the zinc complex, has only a small negative peak centered at 330 nm and a small negative peak analogous to the ~ 370 nm-centered peak of the zinc and nickel complexes that is shifted by about 15 nm to the left. It also has a positive peak centered at ~ 390 nm, but it is lower in intensity than those of the zinc or nickel complexes. While these observations might indicate that the cadmium complex is different in structure than the nickel or zinc complexes, it is more likely that the extraction process used to form the cadmium complex is not complete. This would mean the CD spectrum of the cadmium complex represents a mixture of complexed and uncomplexed ligand. The peaks are all of the same sign when compared to the peaks of the zinc and nickel complexes. These spectra, like those of CD titrations of A23187 with many divalent cations, indicate the same negative stereochemistry observed for the parent compound.

The CD spectrum of the magnesium complex of Br_2A23187 is different than those of the zinc, nickel, and cadmium complexes. Compared to the spectrum of the free acid form of Br_2A23187, the spectrum of the magnesium complex has two large positive peaks centered at 305 and 350 nm. Between them is a region that appears to be a negative peak, but does not go below the x-axis. This “negative” peak lines up well with the negative peaks of other complexes. A negative peak at ~ 390 nm is observed as well, which is in constrast to the positive peak at this wavelength observed for other

complexes. It is clear from the CD data that magnesium complex of Br_2A23187 is significantly different structurally than the complexes of zinc, nickel, or cadmium.

B. Protonation and Complexation Properties of 23,24-Br_2A23187

1. Protonation Constants of 23,24-Br_2A23187

The potentiometric titration of 6 mLs of ~ 1 mM 23,24-Br_2A23187 with ~ 10 mM $(CH_3)_4NOH$ in 80% CH_3OH/H_2O is used to determine the pK_a of the carboxylic acid group of the ligand. Base is added to the ligand in 0.02 mL increments, and the pH^* recorded after each addition. The data is fit by PKAS,[3] which also accounts for the difference in solvent between CH_3OH/H_2O and H_2O. This difference is accounted for by using the "δ" factor, obtained from titration of acetic acid in 80% CH_3OH/H_2O after standardizing the pH meter using aqueous standard buffers. Figure V.14 shows the experimental data and data fit by PKAS. The pK_a is determined to be 7.64 ± 0.02.

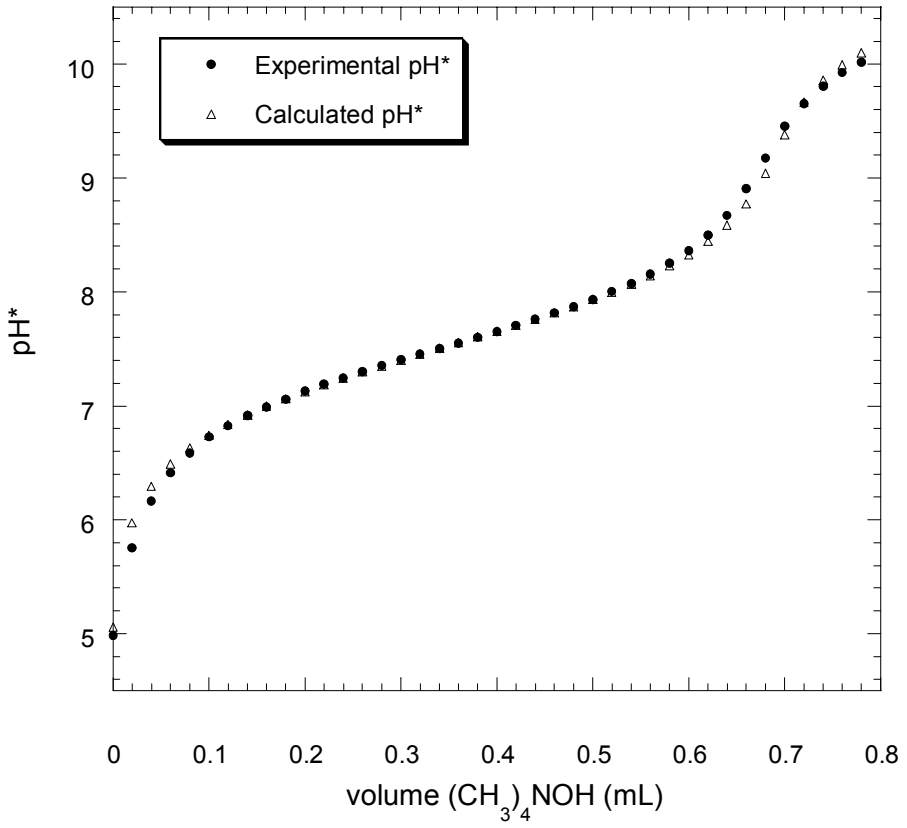

Figure V.14. Potentiometric titration of ~ 1 mM 23,24-Br_2A23187 with $(CH_3)_4NOH$ in 80% CH_3OH/H_2O

The UV-vis spectra of 23,24-Br_2A23187 titrated as a function of pH^* (by incremental additions of $(CH_3)_4NOH$) are shown in Figure V.15. A large change in absorbance is observed at wavelength ~330 nm, and smaller changes in absorbance are seen at wavelengths 250 nm, 280 nm, 300 nm, and 380 nm. Isosbestic points are seen (for at least part of the titration) at ~ 262 nm, 310 nm, and 358 nm.

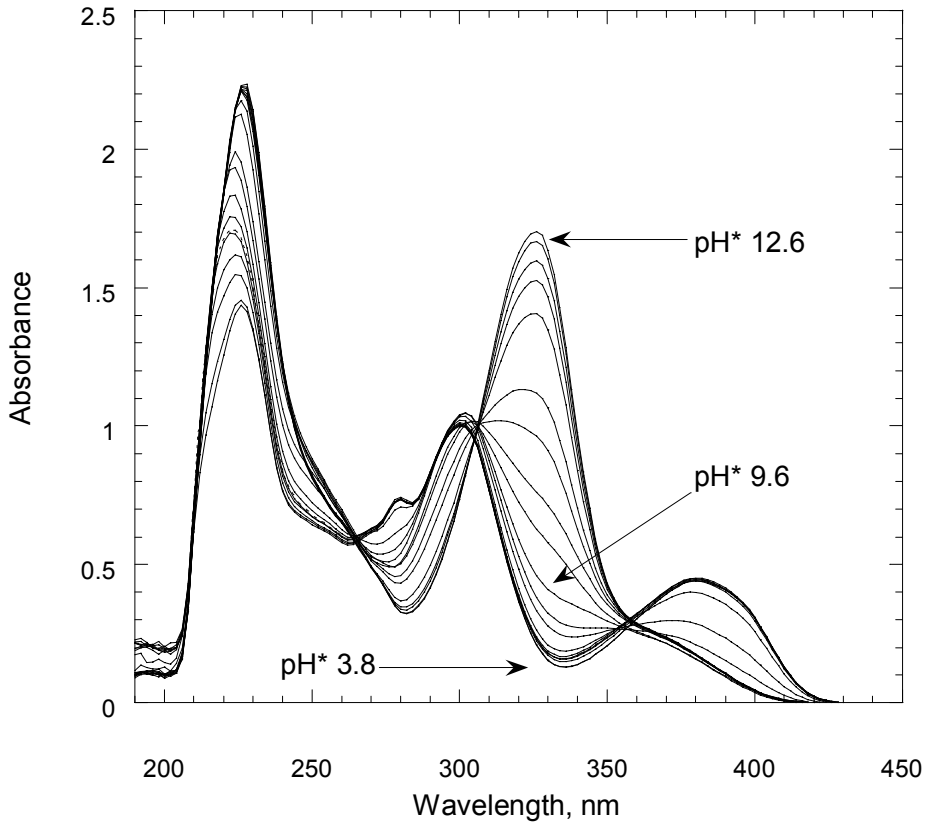

Figure V.15. UV-vis spectra of 50 μM 23,24-Br_2A23187 titrated with $(CH_3)_4NOH$

A plot of absorbance at 280 nm as a function of pH^*, shown in Figure V.16, indicates that two protonation equilibria are present in the pH^* range covered. The inflection points in the pH^* regions 7.0-9.0 and 10.5-12.5 provide estimates of pK_{a1} and pK_{a2}, respectively for the curve fitting program SPECFIT. Analysis of the spectra using this program gives values of 7.8 and 11.4 for pK_{a1} and pK_{a2}, respectively.

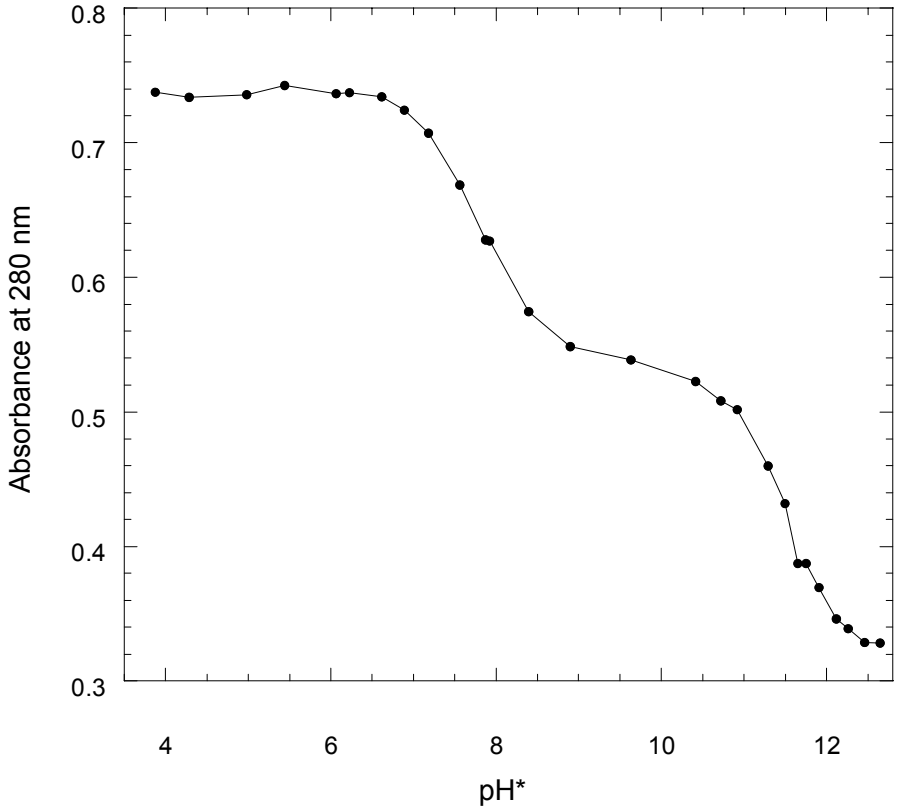

Figure V.16. Absorbance at 280 nm of 50 μM 23,24-Br_2A23187 titrated with $(CH_3)_4NOH$

Plots of absorbance at two other wavelengths, 384 and 302 nm (Figures V.17 and V.18), reflect primarily pK_{a1} and pK_{a2}, respectively. In the parent compound, the absorbance peak centered at 350 nm has been determined to reflect the benzoxazole moiety.[3] Because the spectra of 23,24-Br_2A23187 are similar to those of the parent compound when titrated as a function of pH^*, it can be concluded that the changes observed in the absorbance of 23,24-Br_2A23187 at 384 nm as a function of pH^* (labeled pK_{a1}) are due to the deprotonation step that occurs on the benzoxazole ring. This provides further evidence that pK_{a1} represents the deprotonation step at the carboxylic acid of A23187 and similar derivatives.

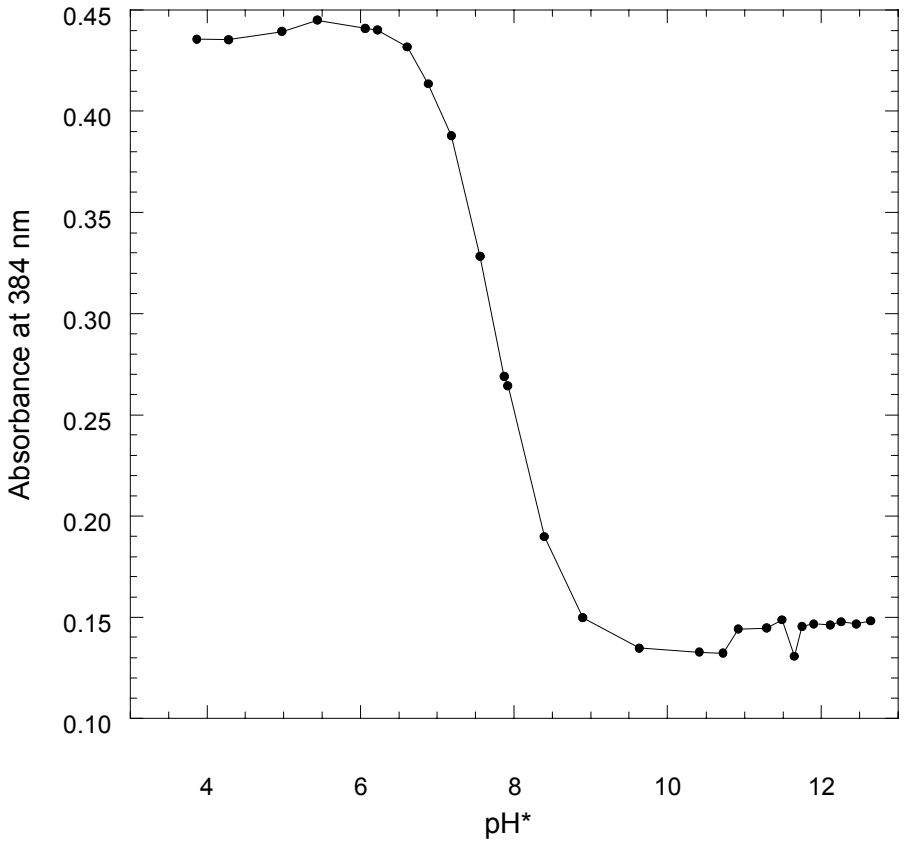

Figure V.17. Absorbance at 384 nm of 50 μM 23,24-Br_2A23187 in 80% CH_3OH/H_2O titrated with $(CH_3)_4NOH$

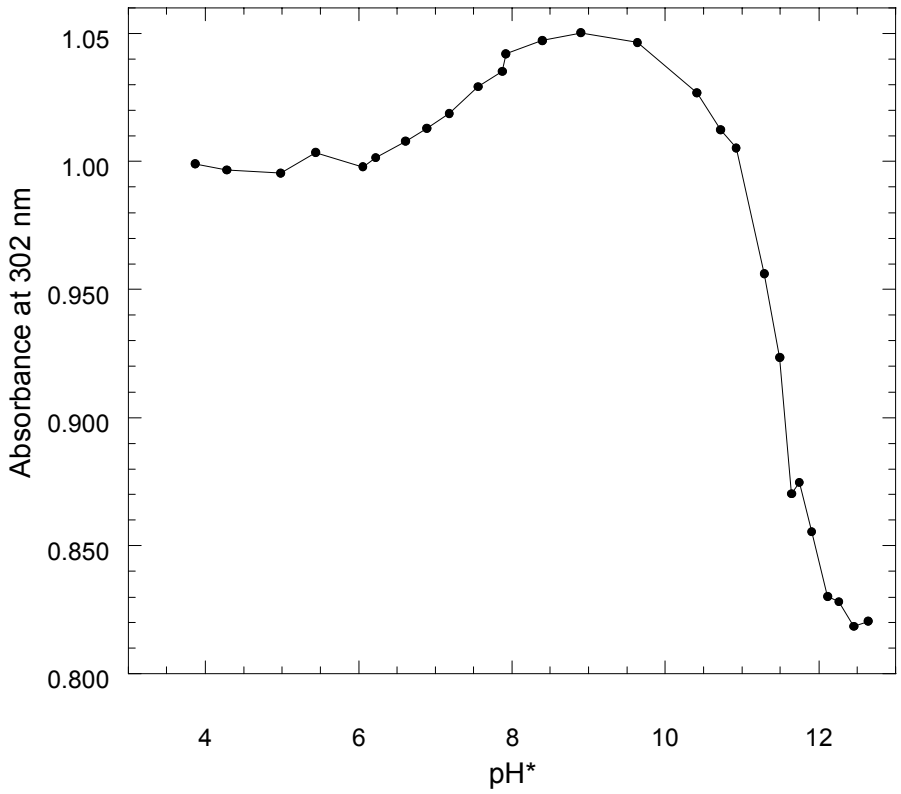

Figure V.18. Absorbance at 302 nm of 50 μM 23,24-Br_2A23187 in 80% CH_3OH/H_2O titrated with $(CH_3)_4NOH$

2. Metal complexation titrations at fixed pH^*

a. Titrations of 23,24-Br_2A23187 with Zn^{2+} at fixed pH^*

Titrations of 23,24-Br_2A23187 in 80% CH_3OH/H_2O with Zn^{2+} at pH^* 5.5 results in a UV-vis spectra with large peaks at wavelengths 302 nm and 345 nm, shown in Figure V.19. The absorbance at 302 nm goes down with increasing amounts of Zn^{2+}, while the peak at 345 nm increases. These spectra show a single set of isosbestic points, indicating that a single complexation equilibrium is occurring during the titration. This equilibrium is presumably between unbound, partially protonated ligand (at pH^* 5.5, the ligand is approximately 99.5% protonated) and a 1:1 ligand:metal complex. This reaction is shown in Equations V.1-2.

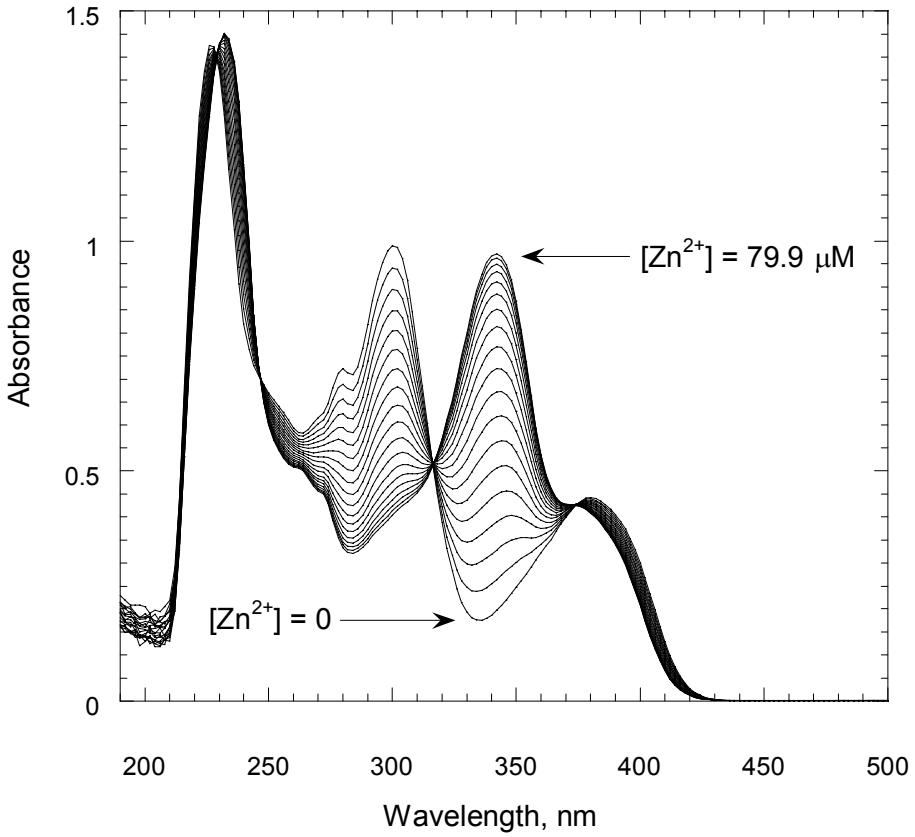

Figure V.19. UV-vis spectra of 50 μM 23,24-Br_2A23187 titrated with Zn^{2+} at pH^* 5.5

$$H_2(23,24\text{-}Br_2A23187) + Zn^{2+} \leftrightarrows [H(23,24\text{-}Br_2A23187)Zn]^+ + H^+ \qquad \text{Eq.V1}$$

$$K_{HML} = \frac{[H(23,24\text{-}Br_2A23187)Zn^+]\,[H^+]}{[H_2(23,24\text{-}Br_2A23187)][\,Zn^{2+}]} \qquad \text{Eq.V2}$$

When plotted as a function of $[Zn^{2+}]/[23,24\text{-}Br_2A23187]$, the absorbance of this titration at 338 nm, shown in Figure V.20, shows the progress of the complexation reaction described in Equation V1. A plateau gradually emerges beginning near a metal/ligand ratio of 1. This is further evidence that at this pH^*, the species formed in this titration is composed of one ligand and one metal.

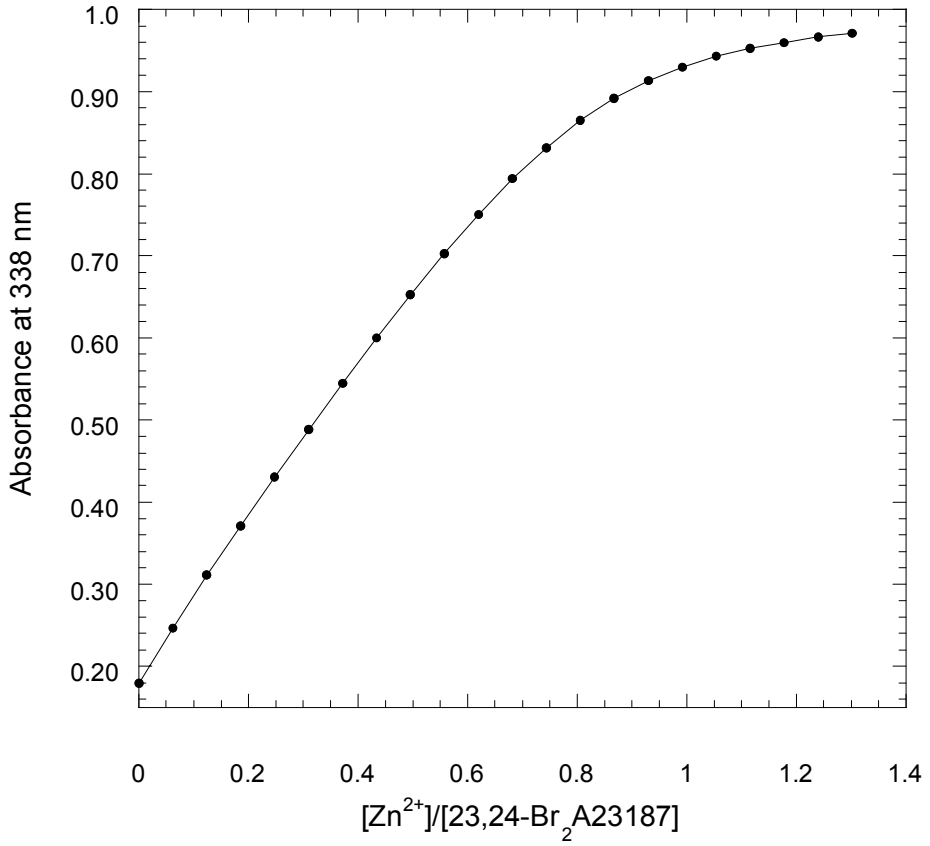

Figure V.20. Absorbance at 338 nm of 50 μM 23,24-Br_2A23187 titrated with Zn^{2+} at pH^* 5.5

At pH* 7.0, a titration of 23,24-Br_2A23187 with Zn^{2+} produces the same spectral changes with a single set of isosbestic points, but reaches a plateau more sharply. As shown in Figure V.21, the region between metal/ligand ratio 0 to 1 is linear, and levels off quickly past a metal/ligand ratio of 1. The reaction becomes complete at lower Zn^{2+} levels due to reduced competition for binding to ligand by protons.

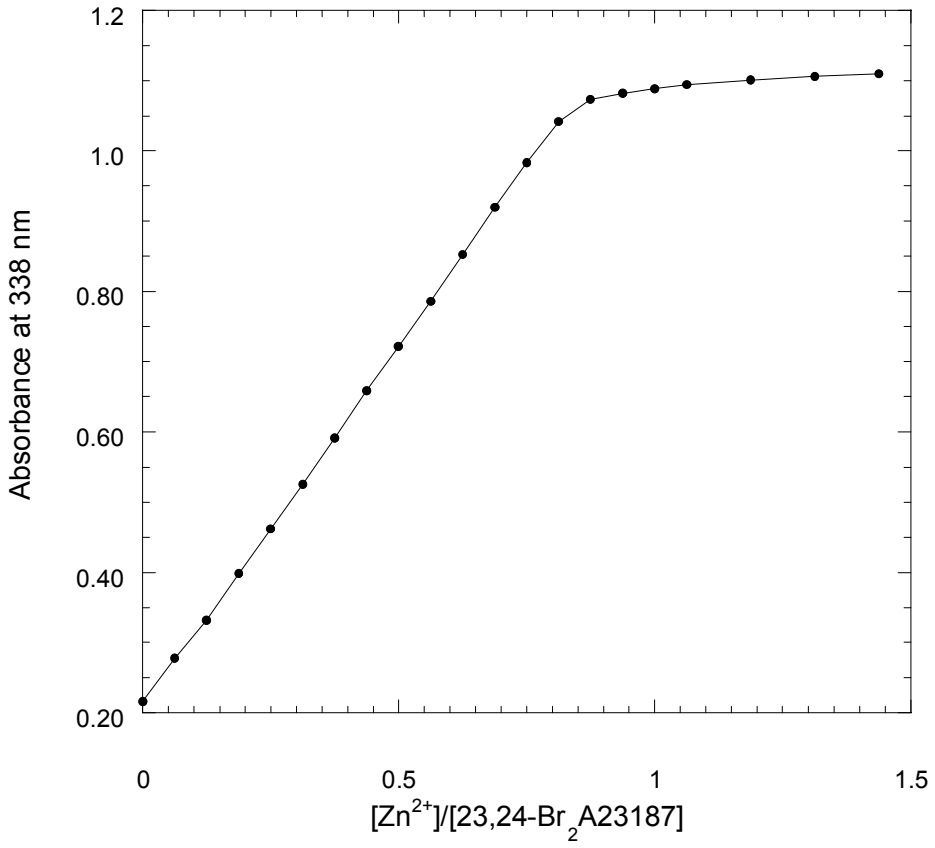

Figure V.21. UV-vis absorbance at 338 nm of 50 μM 23,24-Br_2A23187 titrated with Zn^{2+} at pH* 7

When titrated at pH* 10.0, however, the sharp change between the linearly increasing segment of the graph and the plateau region is not as visible. A graph of absorbance at 338 nm as a function of $[Zn^{2+}]/[23,24\text{-}Br_2A23187]$ is shown in Figure V.22.

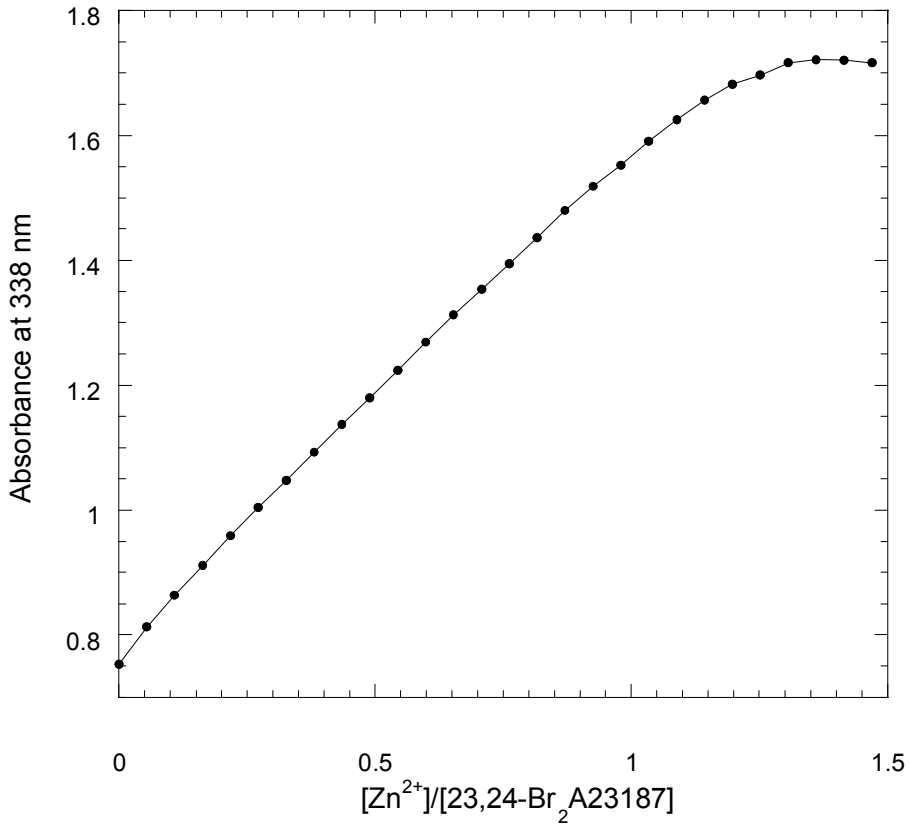

Figure V.22. Absorbance at 338 nm of 50 μM 23,24-Br_2A23187 titrated with Zn^{2+} at pH* 10.0

b. Titrations of 23,24-Br_2A23187 with Cd^{2+} at fixed pH^*

Solutions of 23,24-Br_2A23187 in 80% CH_3OH/H_2O titrated with Cd^{2+} have spectral features similar to those of titrations of the ligand with Zn^{2+}. As shown in Figure V.23, the same large changes in absorbance are seen at the same wavelengths as in the Zn^{2+} titrations. The isosbestic point near 310 nm shifts slightly near the end of the titration. This indicates formation of a third species, in addition to the free ligand and CdA (or $HCdA^+$), in the presence of excess metal.

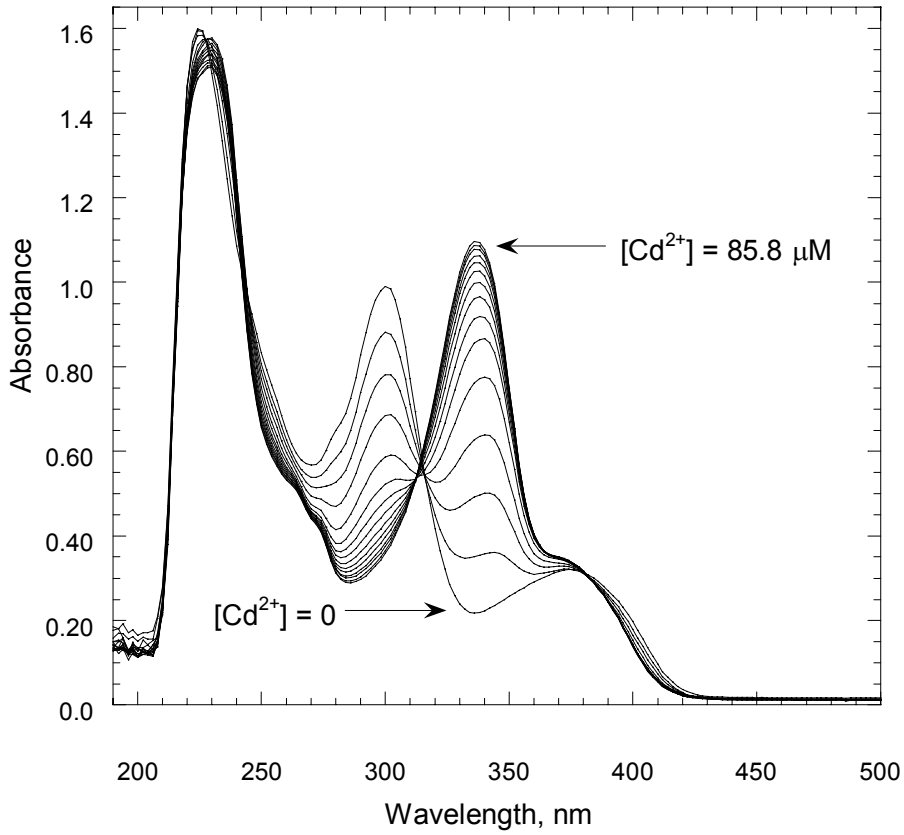

Figure V.23. UV-vis spectra of 50 μM 23,24-Br_2A23187 titrated with Cd^{2+} at pH^* 7.0

A curved graph is observed when absorbance at 336 nm is plotted as a function of metal/ligand ratio at pH* 5.5 (Figure V.24). However, a distinct plateau is not observed for the $[Cd^{2+}]$:$[Br_2A]$ ratios measured in this titration.

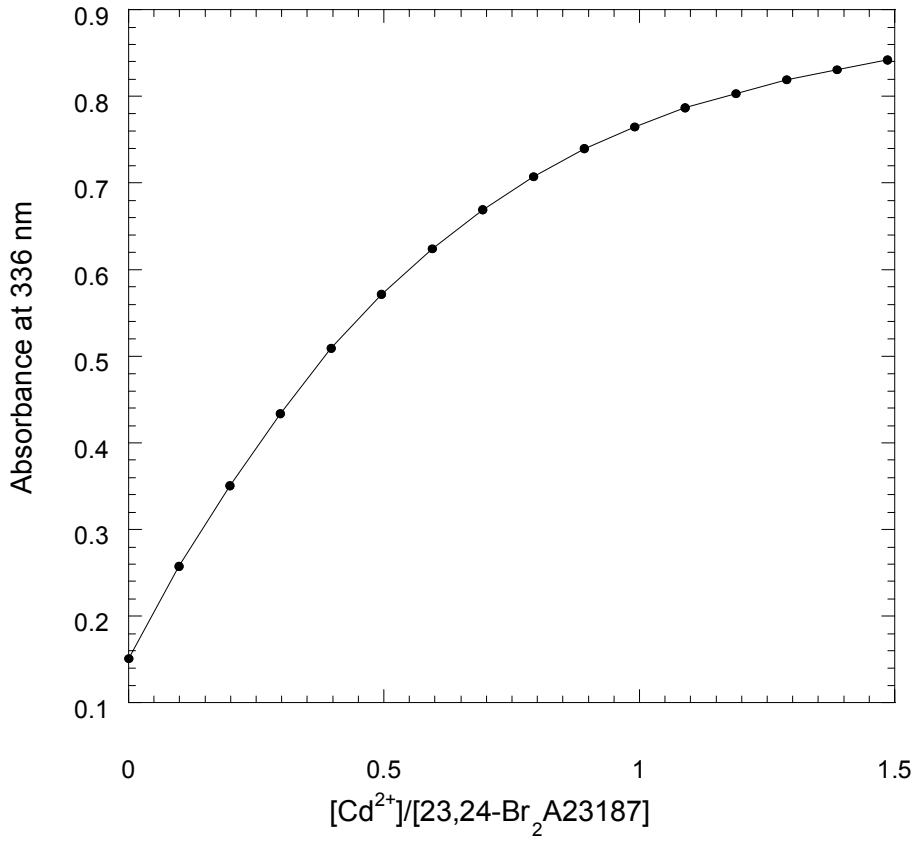

Figure V.24. Absorbance at 336 nm of 50 μM 23,24-Br_2A23187 titrated with Cd^{2+} at pH* 5.5

At pH* 7.0, the plot is linear below the metal:ligand ratio of 0.5 (Figure V.25). The slope of the graph decreases greatly at a metal:ligand ratio of 0.5 (respresenting the point in the titration where the ligand is present primarily as the 2:1 complex). After this point, however, the absorbance continues to increase, which indicates that another reaction occurs after this point is reached.

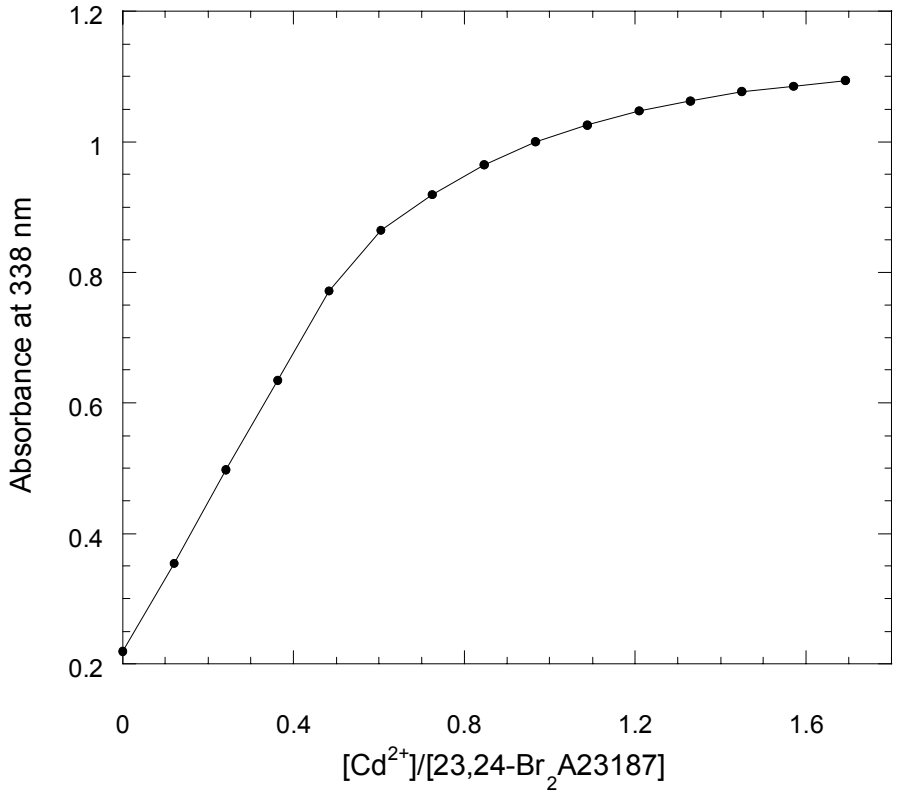

Figure V.25. Absorbance at 338 nm of 50 μM 23,24-Br_2A23187 titrated with Cd^{2+} at pH* 7.0

Absorbance at 336 nm of 23,24-Br_2A23187 titrated with Cd^{2+} at pH^* 10.0 (Figure V.26) is also linear at lower titration points, but continues the linearity until a metal:ligand ratio of close to 1.

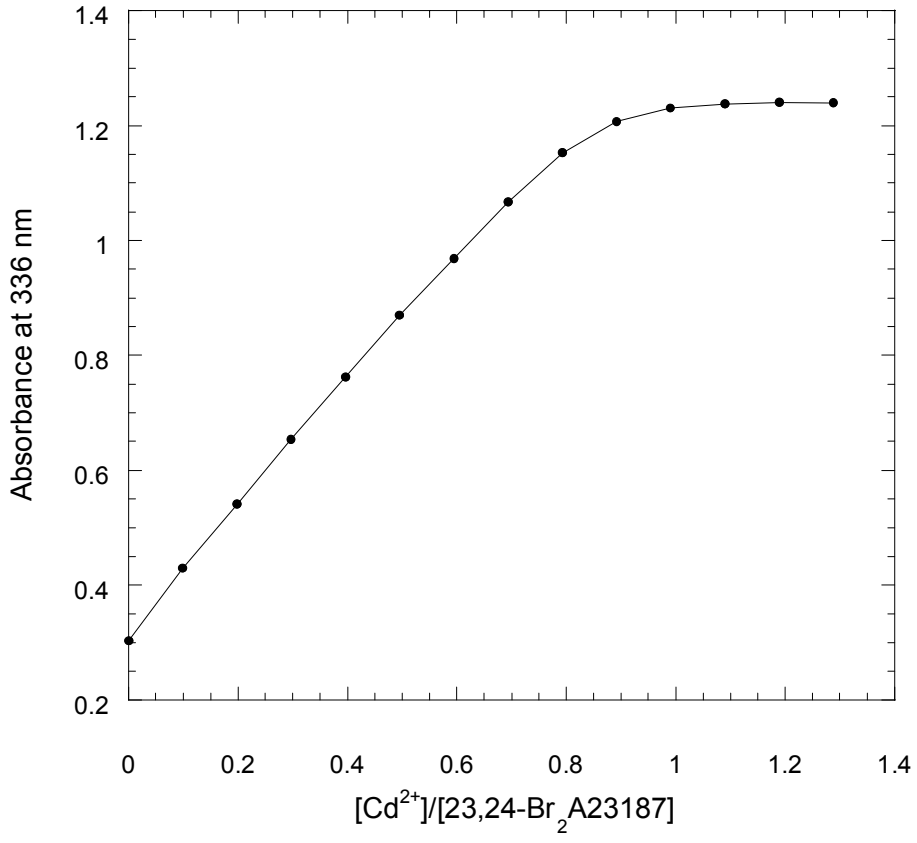

Figure V.26. Absorbance at 336 nm of 50 μM 23,24-Br_2A23187 titrated with Cd^{2+} at pH^* 9.0

c. Titrations of 23,24-Br_2A23187 with Ca^{2+} at fixed pH^*

Titrations of 23,24-Br_2A23187 with Ca^{2+} at any pH^* appear significantly different than those of titrations with Zn^{2+} or Cd^{2+}. At pH^* 5.5, the spectra did not change appreciably. At pH^* 7.0, the spectra (Figure V.27) showed absorbance changes at 280 nm, 300 nm, and 330 nm. A set of isosbestic points is observed at 310 nm, 370nm, and 260 nm.

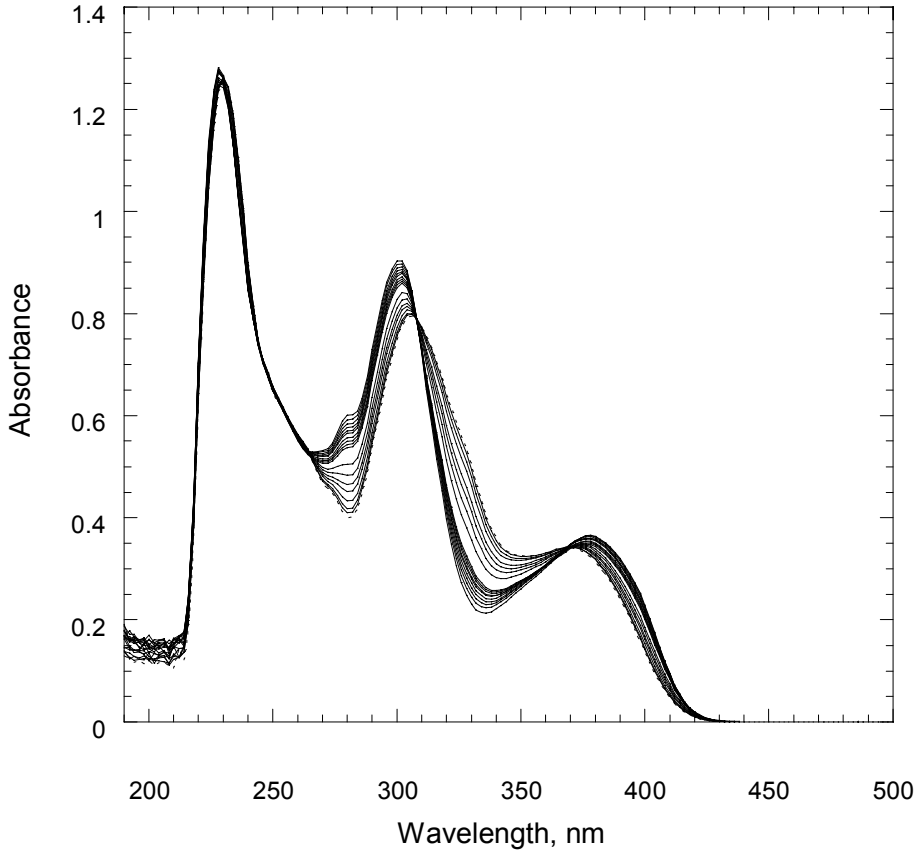

Figure V.27. UV-vis spectra of 50 μM 23,24-Br_2A23187 titrated with Ca^{2+} at pH^* 7.0

The absorbance at 336 nm, plotted as a function of metal:ligand ratio in Figure V.28, increases sharply up to a metal to ligand ratio of 2, and then increases much more gradually.

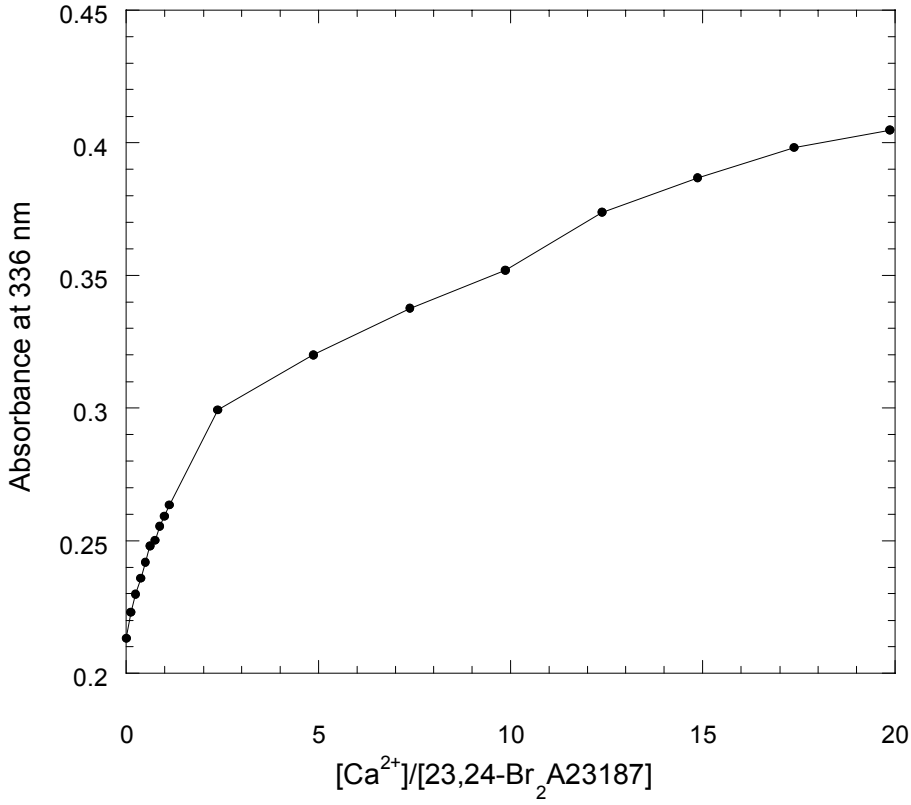

Figure V.28. Absorbance at 336 nm of 50 μM 23,24-Br_2A23187 titrated with Ca^{2+} at pH^* 7.0

As shown in Figure V.29, titrating 23,24-Br_2A23187 with Ca^{2+} at pH^* 10.0 produces a much different set of UV-vis spectra than the same titration conducted at pH^* 7.0. In this case there are large absorbance changes at 305 nm and 330 nm similar to those observed for titrations with Zn^{2+} or Cd^{2+}. Between these wavelengths there is a clean isosbestic point at 315 nm.

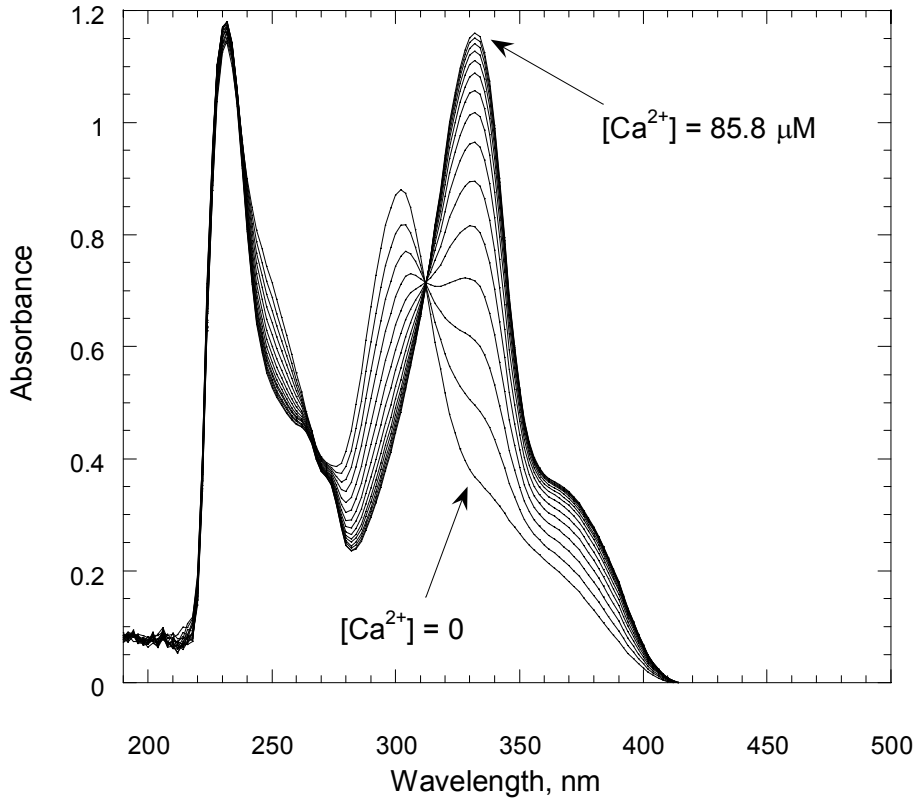

Figure V.29. UV-vis spectra of 50 μM 23,24-Br_2A23187 titrated with Ca^{2+} at pH^* 10.0

The difference in appearance of the spectra of 23,24-Br_2A23187 titrated with Ca^{2+} at pH^* 7.0 and 10.0 indicates that at these pH^* values, different metal:ligand species are formed.

As shown in Figure V.30, a plot of absorbance at 336 nm as a function of $[Ca^{2+}]$/[23,24-Br_2A23187] results in a curve that suggests the predominant metal:ligand stoichiometry is 1.

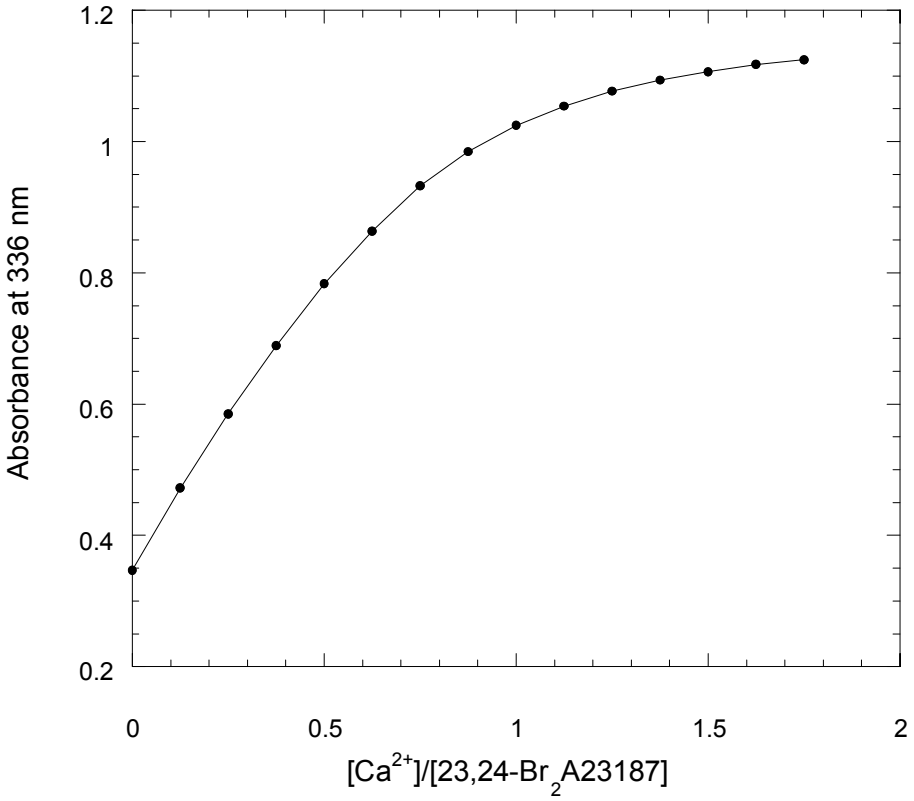

Figure V.30. Absorbance at 336 nm of 50 μM 23,24-Br_2A23187 titrated with Ca^{2+} at pH^* 10.0

d. Titrations of 23,24-Br_2A23187 with Mg^{2+} at fixed pH^*

Titrations of 23,24-Br_2A23187 titrated with Mg^{2+} are similar to those titrated with Ca^{2+} At pH^* 5.5, no spectral changes are observed. At pH^* 7.0, spectral changes similar to those of 23,24-Br_2A23187 titrated with Ca^{2+} at the same pH^* are observed (Figure V.31).

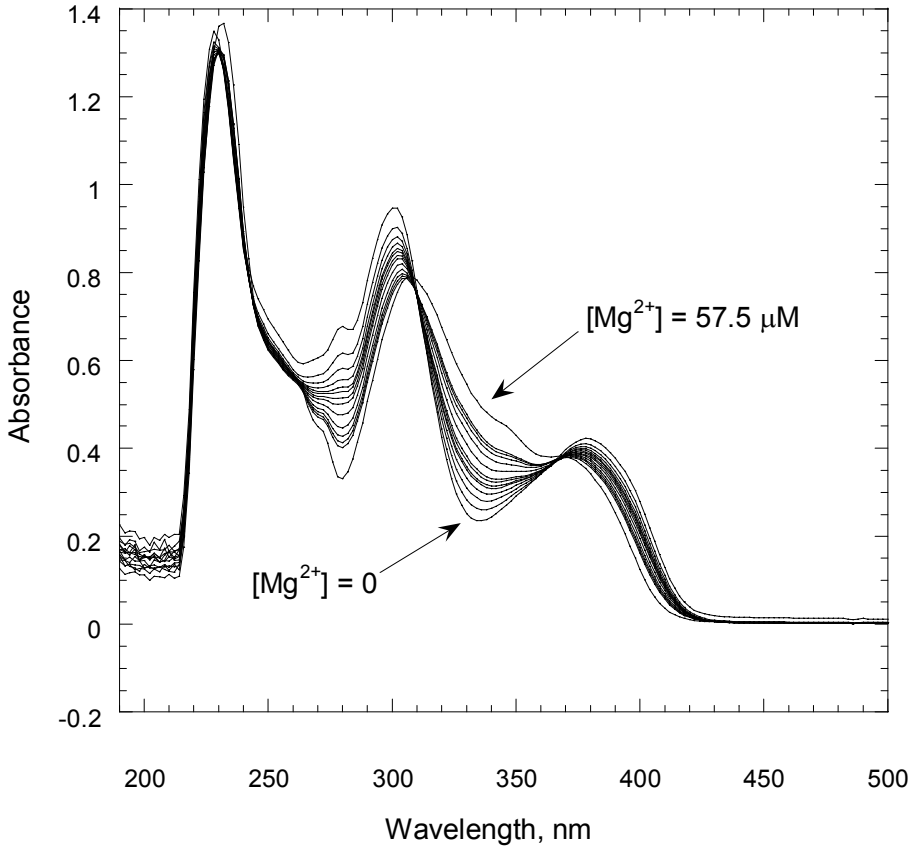

Figure V.31. UV-vis spectra of 50 μM 23,24-Br_2A23187 titrated with Mg^{2+} at pH^* 7.0

The plot of absorbance at 338 nm as a function of $[Mg^{2+}]/[23,24\text{-}Br_2A23187]$, as seen in Figure V.32, is a curved line without a distinct plateau.

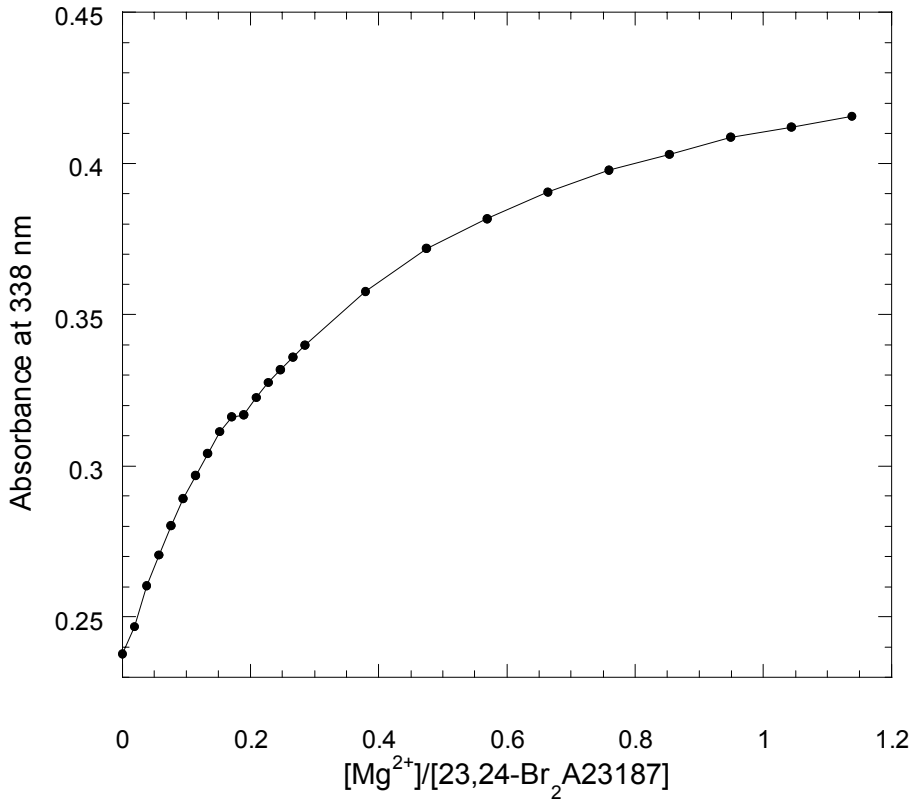

Figure V.32. Absorbance at 338 nm of 50 μM 23,24-Br_2A23187 titrated with Mg^{2+} at pH* 7.0

The spectra of 23,24-Br_2A23187 titrated with Mg^{2+} at pH^* 10.0 closely resembles that of the same ligand titrated with Ca^{2+} at pH^* 10.0 (Figure V.33).

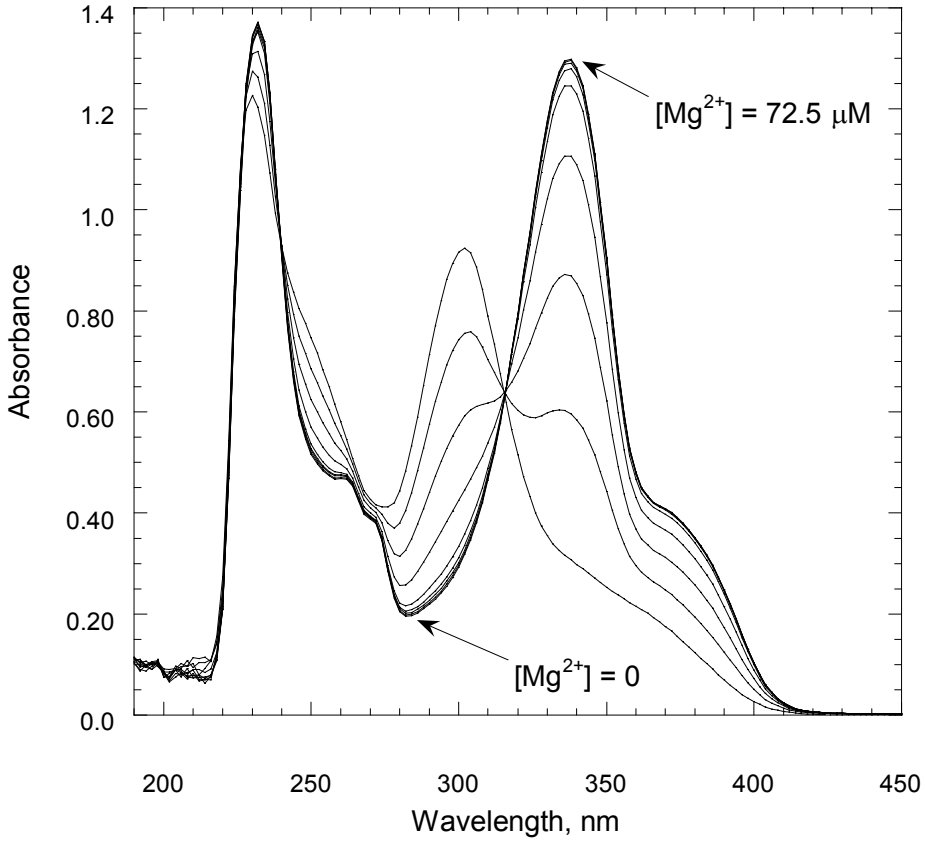

Figure V.33. UV-vis spectra of 50 μM 23,24-Br_2A23187 titrated with Mg^{2+} at pH^* 10.0

The plot of absorbance at 338 nm as a function of metal:ligand ratio, shown in Figure V.34, illustrates a clear linear relationship up to $[Mg^{2+}]/[23,24\text{-}Br_2A23187] = 0.5$. This indicates that the species being formed up to this point in the titration is the 2:1 ligand:metal complex. After this point, absorbance levels off, indicating that further reaction does not occur.

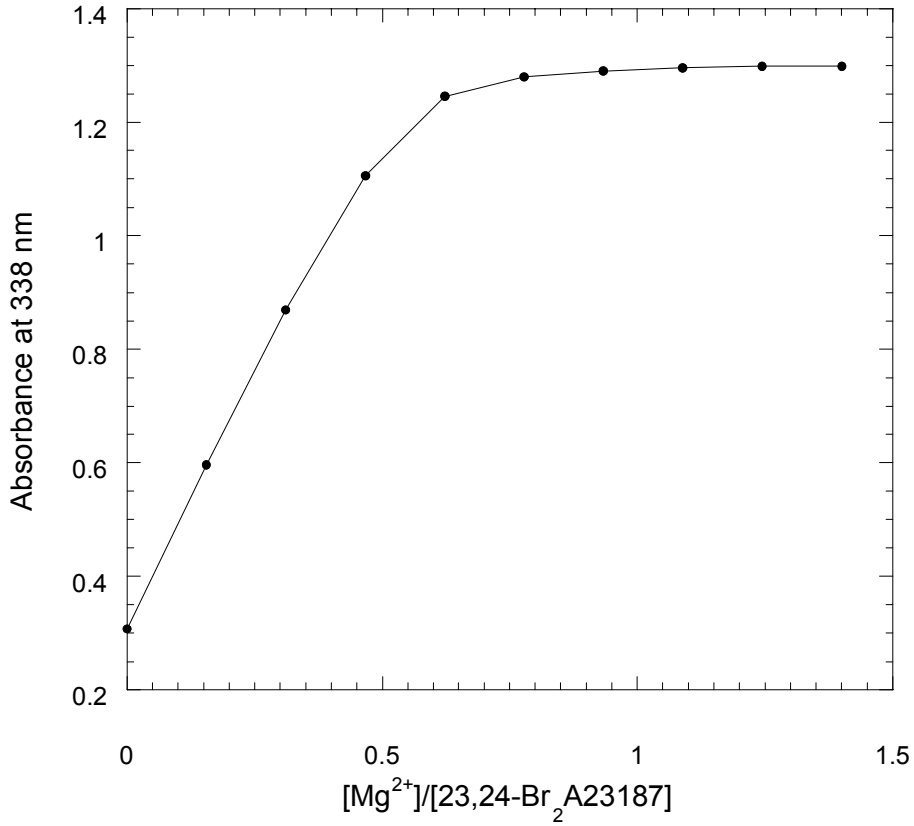

Figure V.34. Absorbance at 338 nm of 50 μM 23,24-Br_2A23187 titrated with Mg^{2+} at pH^* 10.0

e. Titrations of 23,24-Br_2A23187 with Ni^{2+} at fixed pH^*

The titration of 23,24-Br_2A23187 with Ni^{2+} at pH^* 5.5 results in the spectra shown in Figure V.35. They appear to be similar to titrations of Zn^{2+} and Cd^{2+} at pH^* 7.0 initially, but do not have the same peak intensity at higher [Ni^{2+}]/[23,24-Br_2A23187] values than those spectra.

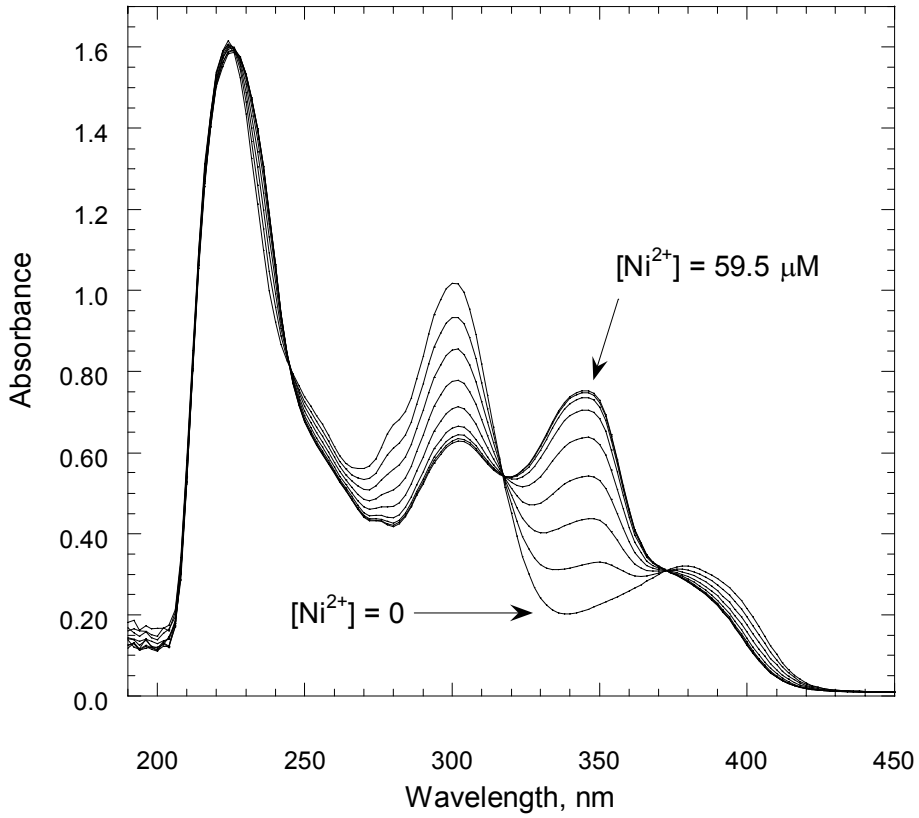

Figure V.35. UV-vis spectra of 50 μM 23,24-Br_2A23187 titrated with Ni^{2+} at pH^* 5.5

A plot of absorbance at 348 nm as a function of $[Ni^{2+}]/[23,24\text{-}Br_2A23187]$ (Figure V.36) shows a plateau that occurs near the 0.7 metal:ligand ratio. The linear portions of the graph intersect near a metal:ligand ratio of 0.5.

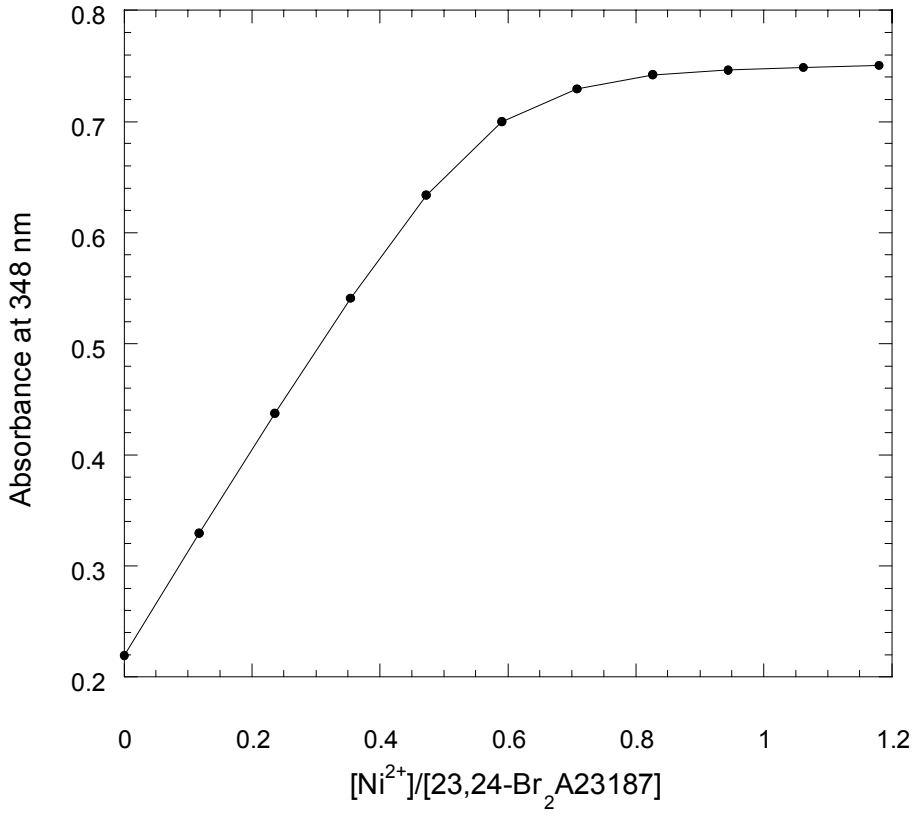

Figure V.36. Absorbance at 348 nm of 50 μM 23,24-Br_2A23187 titrated with Ni^{2+} at pH* 5.5

A titration of Ni^{2+} with ligand at pH^* 7.0 results in spectra that are very similar to those of titrations with Zn^{2+} or Cd^{2+}. The same large absorbance changes and isosbestic points are present, as seen in Figure V.37. The changes in absorbance at 338 nm increase linearly to the point where $[Ni^{2+}]$:[23,24-Br_2A23187] = 1, then level off as shown in Figure V.32. This behavior differs from that observed at pH^* 5.5 where the predominant metal complex species appeared to have a stoichiometry of 2:1 (metal:ligand).

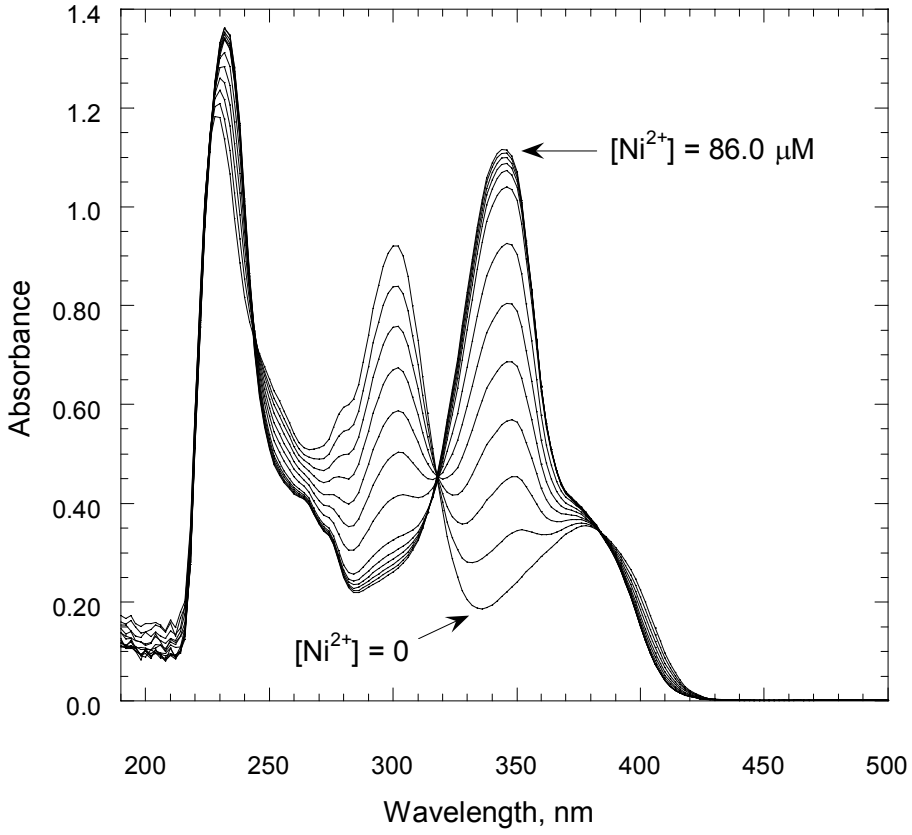

Figure V.37. UV-vis spectra of 50 μM 23,24-Br_2A23187 titrated with Ni^{2+} at pH^* 7.0

The plot of absorbance at 338 nm as a function of $[Ni^{2+}]/[23,24\text{-}Br_2A23187]$ shows the absorbance change continuing linearly until a ratio of 1 is reached, at which point it reaches a plateau. This plot is illustrated in Figure V.38.

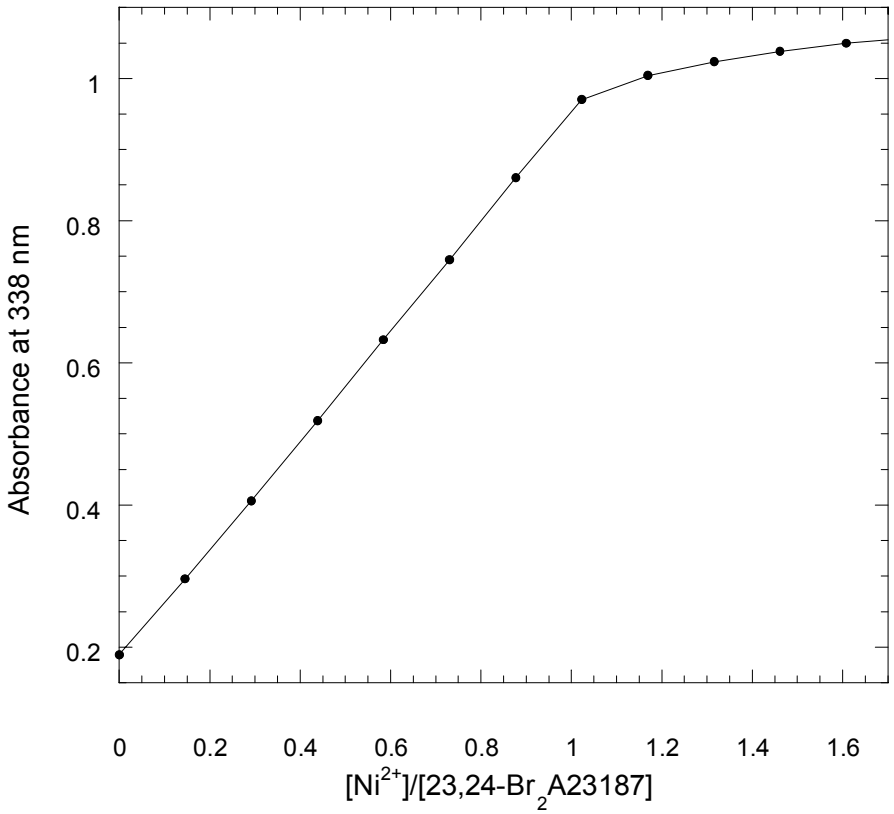

Figure V.38. Absorbance at 338 nm of 50 μM 23,24-Br_2A23187 titrated with Ni^{2+} at pH^* 7.0

The spectra of 23,24-Br_2A23187 titrated with Ni^{2+} at pH^* 10.0 have unique characteristics. At lower concentrations of metal (up to $[Ni^{2+}]$:[ligand] = 1), they appear identical to spectra at pH^* 7.0. However, at higher amounts of metal ion, the isosbestic point at ~ 318 nm is lost and a new one appears at ~ 310 nm. This indicates that two equilibria occur under the titration conditions. The first, at lower metal concentrations, is likely the same one observed at lower pH^* values. The second, however, appears unique to the high pH^* region of the Ni^{2+} titration. These spectra are observed in Figure V.39.

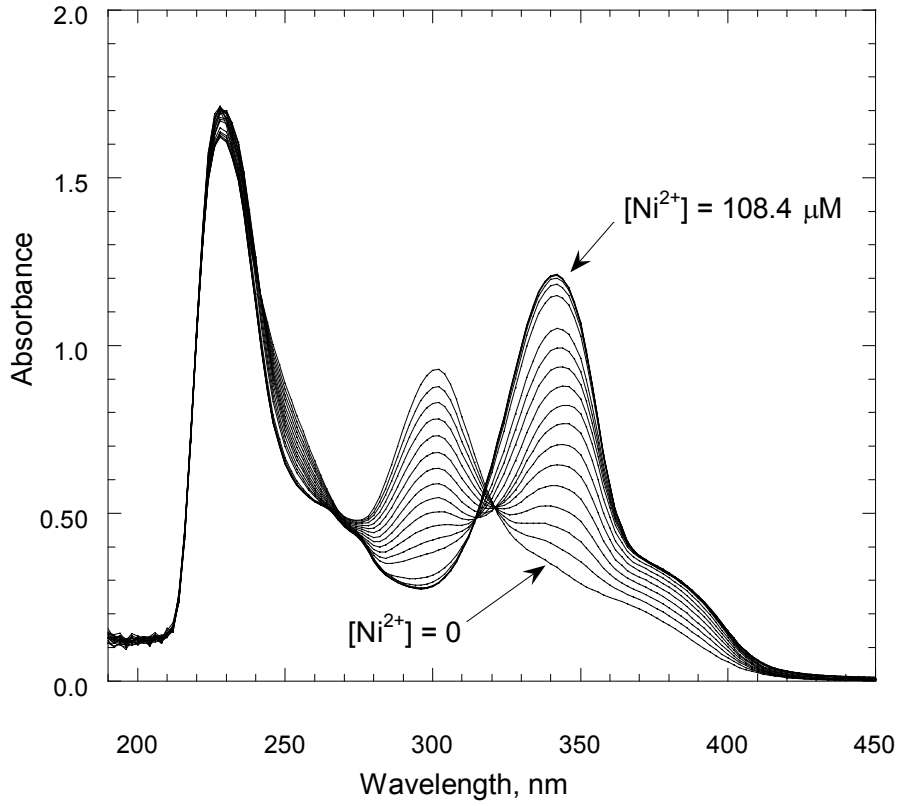

Figure V.39. UV-vis spectra of 50 μM 23,24-Br_2A23187 titrated with Ni^{2+} at pH^* 10.0

As shown in Figure V.40, the plot of absorbance at 344 nm as a function of $[Ni^{2+}]/[23,24\text{-}Br_2A23187]$ is linear up to a metal:ligand ratio of 1.5. After this point the absorbance reaches a plateau.

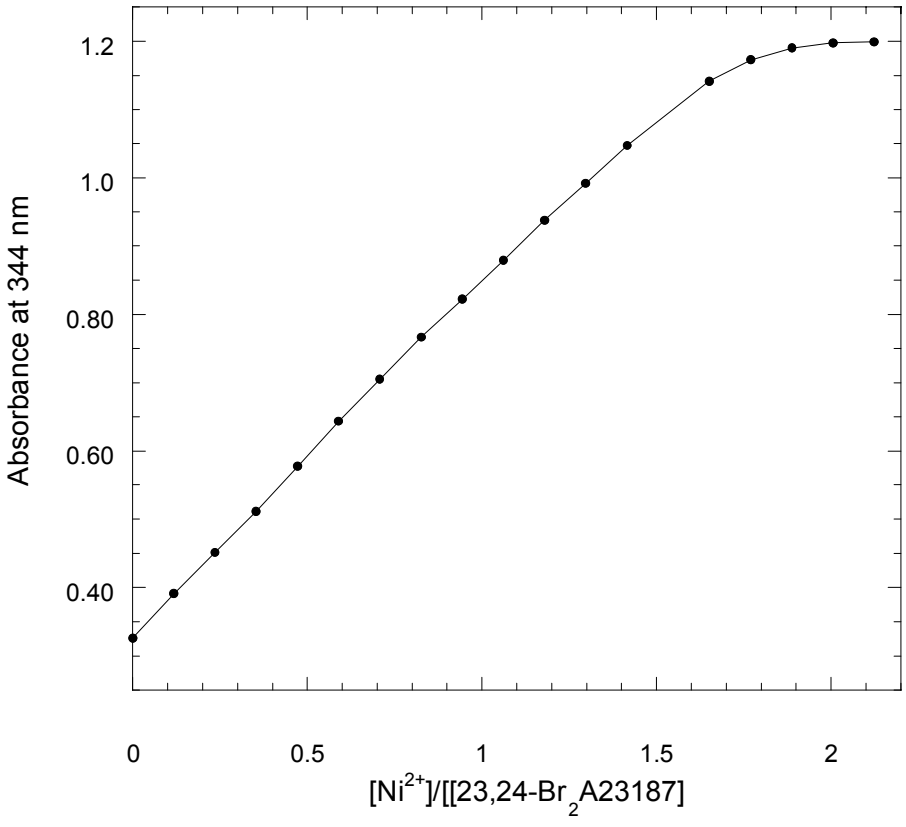

Figure V.40. Absorbance at 344 nm of 50 μM 23,24-Br_2A23187 titrated with Ni^{2+} at pH* 10.0

3. Titrations of 23,24-Br_2A23187 at fixed [M^{2+}] as a function of pH^*

a. Titrations of 23,24-Br_2A23187:Zn^{2+} as a function of pH^*

The pH^* titration of 23,24-Br_2A23187 in the presence of an equivalent amount of Zn^{2+} produces UV-vis spectra with absorbance peaks that are in similar locations as those of the pH^* titration without metal (Figure V.41). It also shares characteristics with the spectra of the titration of ligand with Zn^{2+} at fixed pH^*. At high pH^* values (over 10.0) a blue shift occurs in the peak centered at 340 nm.

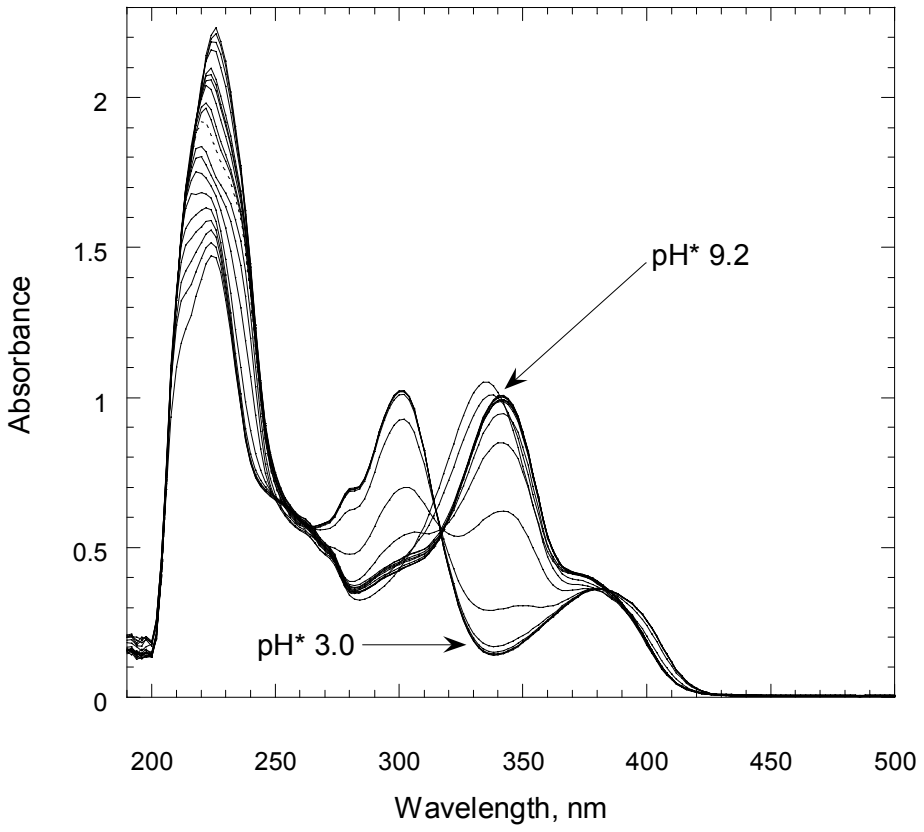

Figure V.41. UV-vis absorbance of pH^* titration of 23,24-Br_2A23187:Zn^{2+} (1:1)

A graph of absorbance at 342 nm as a function of pH^* shows one large change in absorbance centered at approximately pH^* 5, shown in Figure V.42.

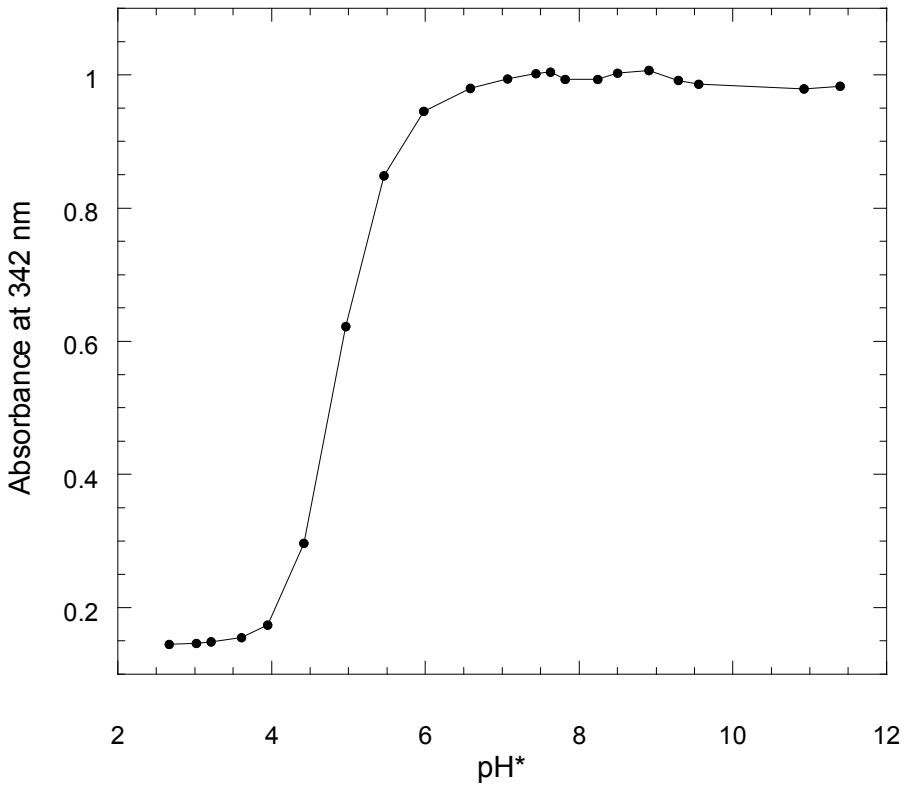

Figure V.42. Absorbance at 342 nm of pH^* titration of 23,24-Br_2A32187:Zn^{2+} (1:1)

b. Titrations of 23,24-Br_2A23187:Cd^{2+} as a function of pH^*

The spectra of 23,24-Br_2A23187:Cd^{2+} (1:1) titrated with $(CH_3)_4NOH$ are shown in Figure V.43. The behavior is similar to that observed for Zn^{2+} with the ligand. A similar red shift is observed in the peak centered at 340 nm, which occurs simultaneously with a disappearance of the isosbestic point at 320 nm.

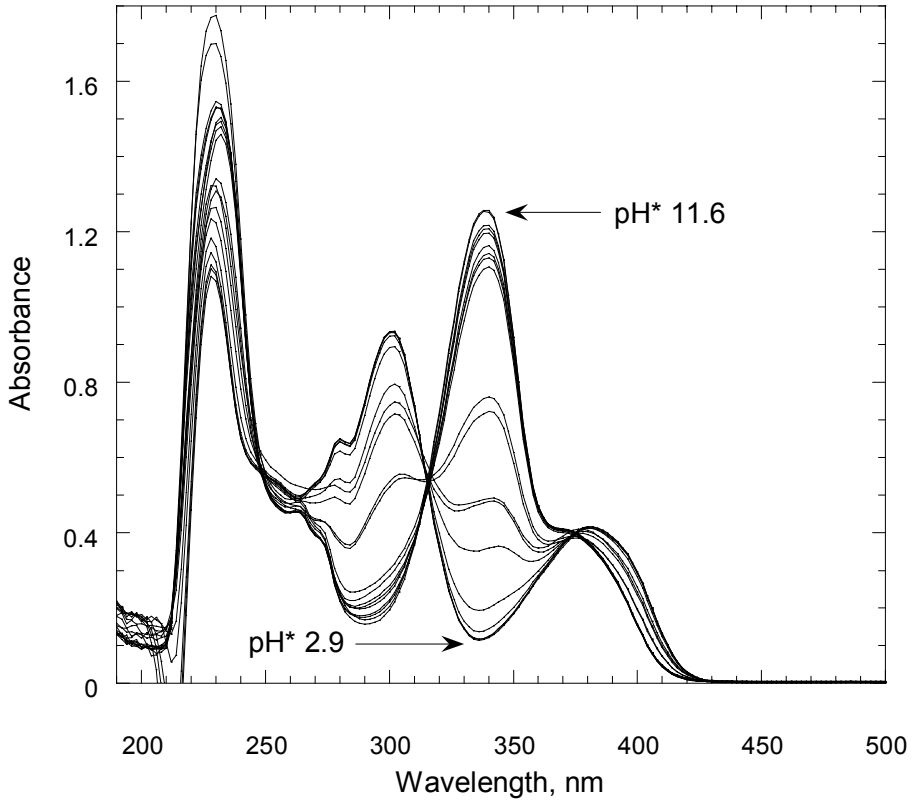

Figure V.43. UV-vis spectra of pH^* titration of 50 μM 23,24-Br_2A23187:Cd^{2+} (1:1)

The plot of absorbance at 342 nm as a function of pH^* (Figure V.44) shows one large change with an inflection point centered approximately at pH^* 5.5, and a smaller change centered at ~ pH^* 11.

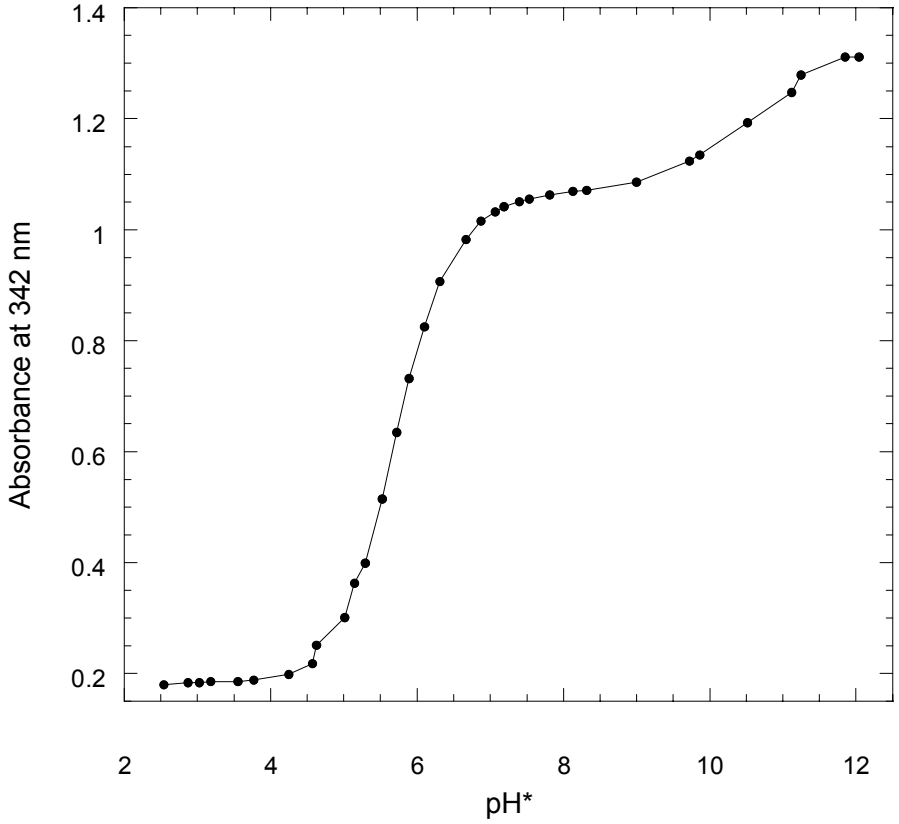

Figure V.44. Absorbance at 342 nm of pH^* titration of 50 μM 23,24-Br_2A23187:Cd^{2+} (1:1)

c. Titrations of 23,24-Br_2A23187:Ca^{2+} as a function of pH^*

The titration of 23,24-Br_2A23187:Ca^{2+} titrated with $(CH_3)_4NOH$ shares all major characteristics of the pH^* titrations of the ligand with Zn^{2+} or Mg^{2+}. The spectra are shown in Figure V.45.

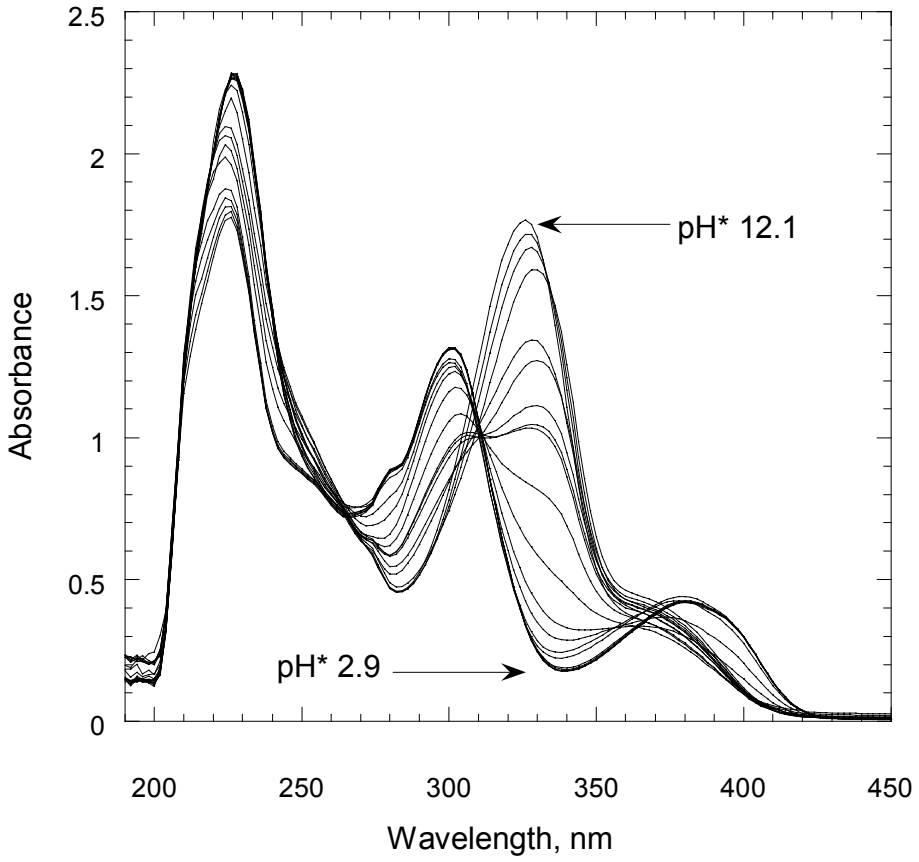

Figure V.45. UV-vis spectra of pH^* titration of 50 μM 23,24-Br_2A23187:Ca^{2+} (1:1)

Figure V. 46 shows the plot of absorbance at 336 nm as a function of pH^* where a single large change, centered at pH^* 9, is observed.

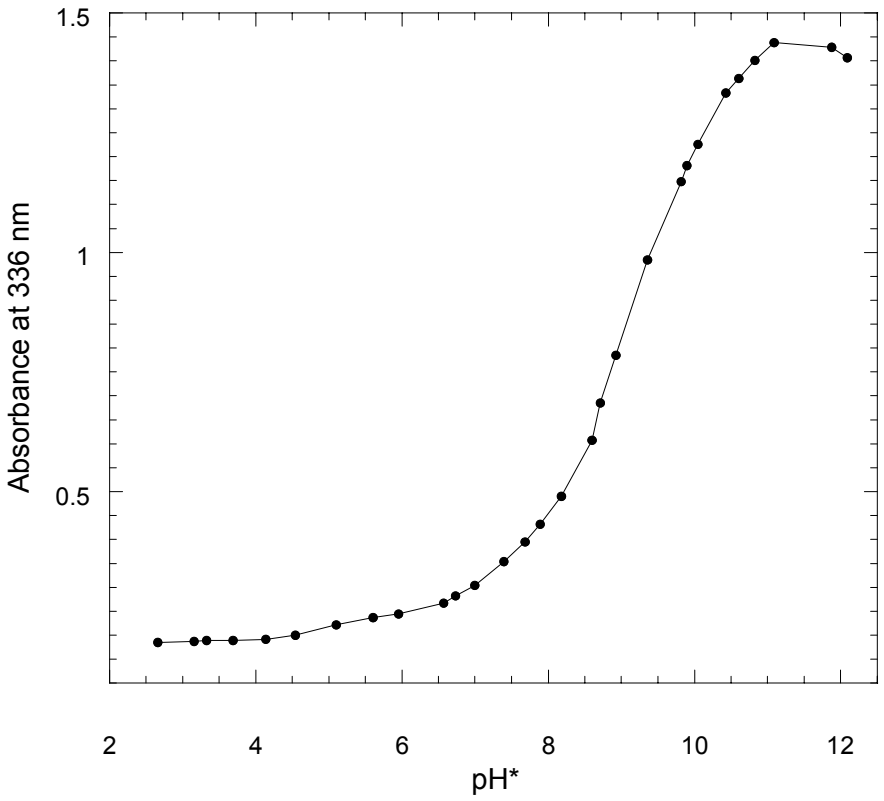

Figure V.46. Absorbance at 336 nm of pH^* titration of 23,24-Br_2A23187:Ca^{2+} (1:1)

d. Titrations of 23,24-Br_2A23187:Mg^{2+} as a function of pH^*

The spectra for the titration of 23,24-Br_2A23187:Mg^{2+} (1:1) with $(CH_3)_4NOH$, shown in Figure V.47, resemble those of analogous pH^* titrations with Zn^{2+}, Cd^{2+}, and Ca^{2+}. The positions of the peaks and isosbestic points, as well as the blue shift at high pH^* are observed.

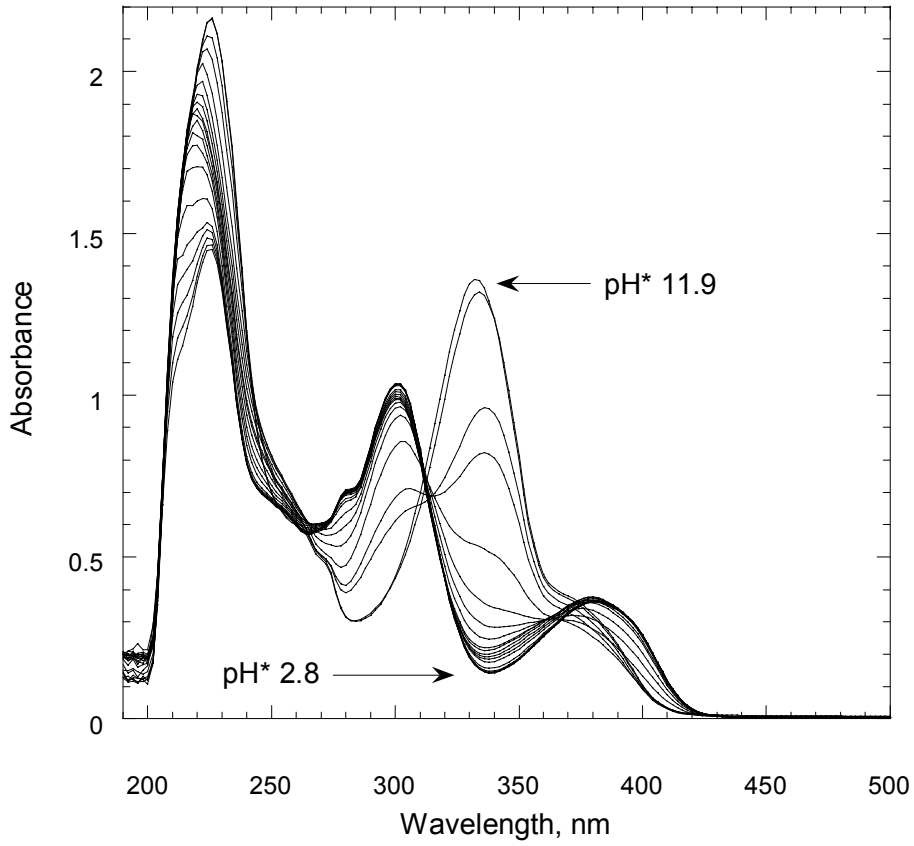

Figure V.47. UV-vis spectra of pH^* titration of 50 μM 23,24-Br_2A23187:Mg^{2+} (1:1)

The plot of absorbance at 340 nm as a function of pH^* (Figure V.48) shows one large absorbance change with an inflection point centered approximately at pH^* 9.

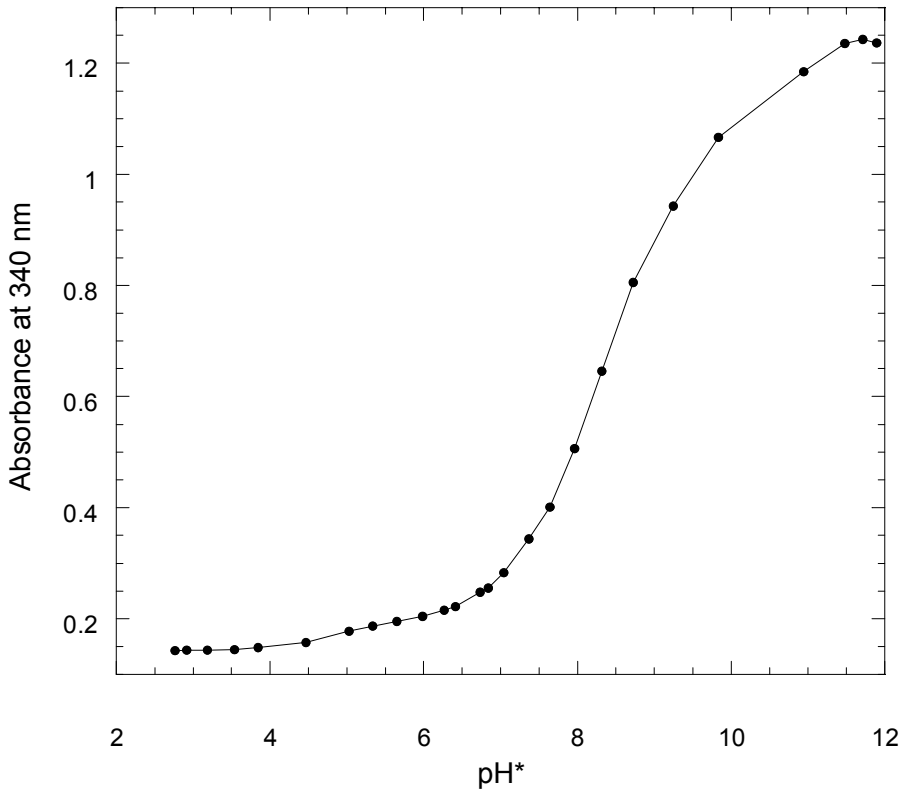

Figure V.48. Absorbance at 340 nm of pH^* titration of 50 μM 23,24-Br_2A23187:Mg^{2+} (1:1)

e. Titrations of 23,24-Br_2A23187:Ni^{2+} as a function of pH^*

The pH^* titration of 23,24-Br_2A23187:Ni^{2+} (1:1) and (2:1) produces spectra very similar to those of pH^* titrations of the ligand with Zn^{2+}, Cd^{2+}, Ca^{2+}, and Mg^{2+}, as shown in Figure V.49. The two large absorbance changes at 300 and 340 nm are present, in addition to the isosbestic point at lower pH^* values between the two peaks. A shift towards lower wavelength is observed in the peak centered at 340 nm at very high pH^* values.

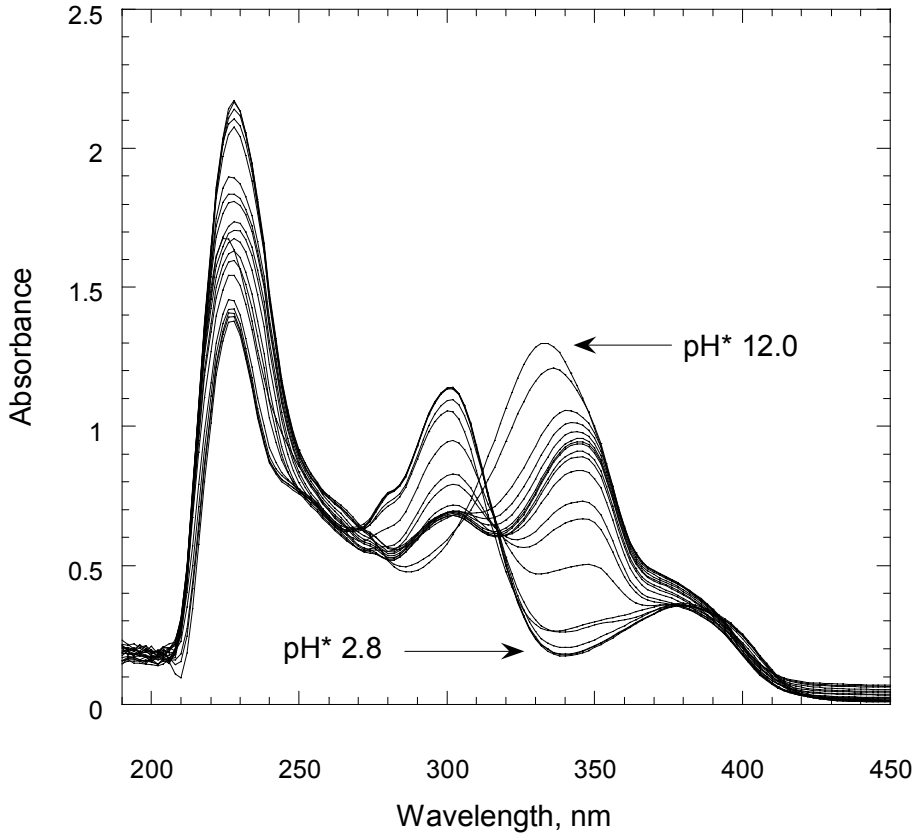

Figure V.49. UV-vis spectra of pH^* titration of 50 μM 23,24-Br_2A23187:Ni^{2+} (1:1)

Figure V.50 shows a plot of absorbance at 336 nm as a function of pH^*, where two inflections are observed- one centered at approximately pH* 5, and the second a $pH^* > 10$.

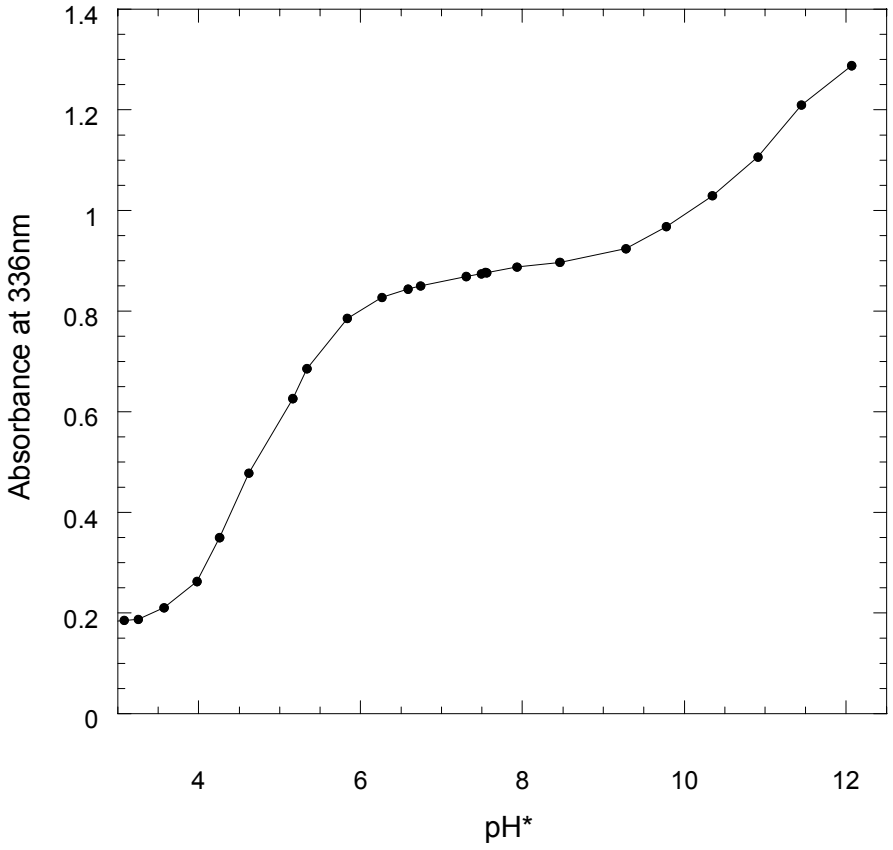

Figure V.50. Absorbance at 336 nm of pH^* titration of 50 μM 23,24-Br_2A23187:Ni^{2+} (1:1)

4. Determination of Protonation and Complexation Constants for 23,24-Br_2A23187

The equilibrium constants for protonation and metal ion complexation with several divalent cations, listed in Table V.3, have been determined by fitting the pH^* titration data with SPECFIT. The protonation constants, determined previously by spectroscopic titration, are held at fixed values. Various models are tried that include every combination of the complexation constants K_{MAH} and K_{MA} as well as the constants for formation of possible complexation species MA_2, MA_2H_2, and MA_2H. The best fit occurred with the model that included the protonation constants and complexation constants for formation of only the species MAH and MA.

An additional check on the quality of the fit produced by SPECFIT is a comparison of the actual absorbance data at a single wavelength and the absorbance predicted by the fit at the same wavelength. The absorbances at several wavelengths were compared in this manner for each data set fit by SPECFIT. Two examples are shown in Figures V.48 and V.49. In Figure V.51 is a plot that compares the actual absorbance at 384 nm of a titration of 23,24-Br_2A23187 with $(CH_3)_4NOH$ to the absorbance values predicted by the fit. In Figure V.52 is a plot that compares the actual absorbance at 386 nm of a titration of 23,24-Br_2A23187:Ca^{2+} (ratio 1:1) titrated as a function of pH^* with the absorbance at each data point calculated by the fit.

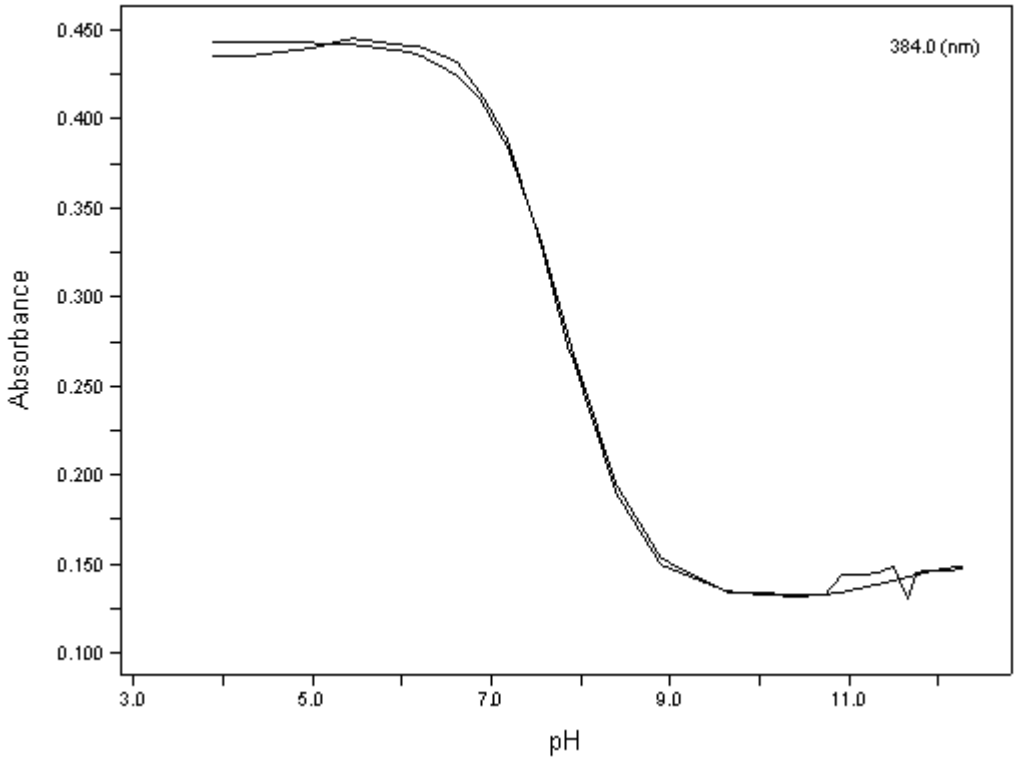

Figure V.51. Comparison of actual and fit absorbances at 384 nm of a titration of ~ 50 μM 23,24-Br_2A23187 with $(CH_3)_4NOH$

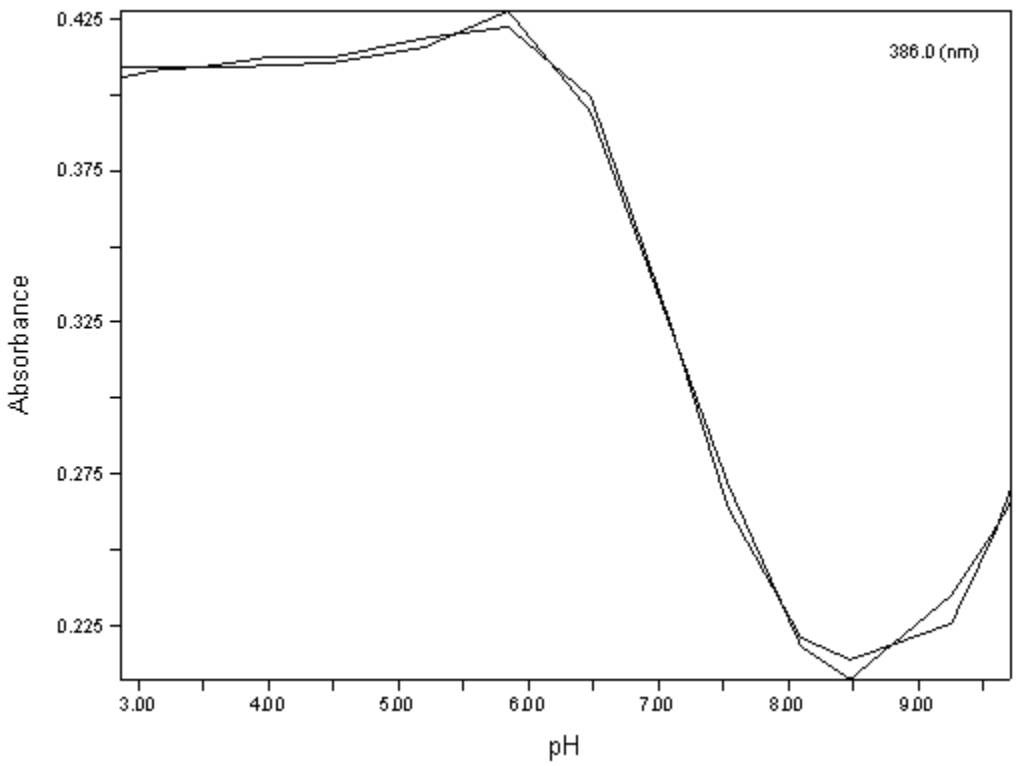

Figure V.52. Comparison of actual and fit absorbance values for a titration of 23,24-Br_2A32187:Ca^{2+} (1:1 ratio) as a function of pH*

Reaction	Equilibrium Constant, K
$H_2A \leftrightarrows H^+ + HA^-$	$K_{a1} = \frac{[H^+][HA^-]}{[H_2A]}$
$HA^- \leftrightarrows H^+ + A^{2-}$	$K_{a2} = \frac{[H^+][A^{2-}]}{[HA^-]}$
$M^{2+} + HA^- \leftrightarrows (M)AH^+$	$K_{HMA} = \frac{[(M)AH^+]}{[M^{2+}][HA^-]}$
$M^{2+} + A^{2-} \leftrightarrows MA$	$K_{MA} = \frac{[MA]}{[M^{2+}][A^{2-}]}$

Table V.3. Protonation and Complexation equilibria for 23,24-Br_2A23187

Metal	A23187: Log K_{HMA}	23,24-Br_2A23187: Log K_{HMA}	23,24-Br_2A23187: Log K_{MA}
Zn^{2+}	6.79	6.6 ± 0.3	12.87 ± 0.07
Cd^{2+}	6.48	5.5 ± 0.2	11.9 ± 0.1
Ca^{2+}	4.5	5.5 ± 0.2	7.8 ± 0.2
Mg^{2+}	4.55	4.5 ± 0.1	7.9 ± 0.2
Ni^{2+}	7.54	7.3 ± 0.05	10.9 ± 0.2

Table V.4. Equilibrium constants for 23,24-Br_2A23187 in 80% CH_3OH/H_2O[4]

The protonation and complexation constant K_{MAH} for A23187 and 23,24-Br_2A23187 with Zn^{2+}, Mg^{2+}, and Ni^{2+} are similar to one another. The complexation constant for Ca^{2+}, however, is almost one order of magnitude greater for 23,24-Br_2A23187 than for the parent compound A23187, and is equivalent to that of Cd^{2+}.

While the complexation constants K_{MA} for A23187 are not known, the trend observed in these constants for 23,24-Br_2A23187 shows that the values for Zn^{2+}, Cd^{2+}, and Ni^{2+} are much greater than those for Mg^{2+} and Ca^{2+} under the conditions of the study. This indicates that they are able to bind to a 23,24-Br_2A23187 ligand species that has a -2 charge and 4 potential coordination sites better than Mg^{2+} and Ca^{2+}. While this may also be true for the parent compound A23187, this trend in binding selectivity is more easily observed in this derivative due to lower pK_a of the pyrrole nitrogen.

C. Transport Kinetics of 23,24-Br_2A23187

The transport of several divalent cations by 23,24-Br2A23187 into POPC vesicles has been studied by collaborators at The Ohio State University. The transport of the metals Zn^{2+}, Cd^{2+}, Mn^{2+}, Co^{2+}, Pb^{2+}, Ni^{2+}, Cu^{2+}, Sr^{2+}, and Ca^{2+} were studied by monitoring changes in the UV-vis absorbance of the chelator Quin-2. The results are illustrated in Figure V.53.

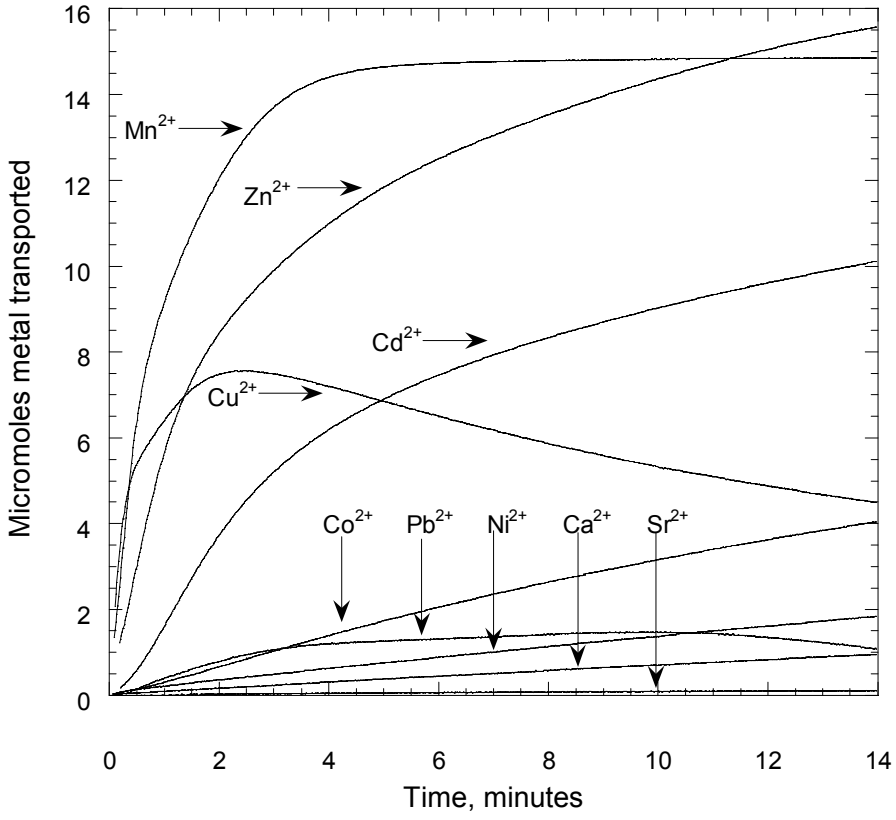

Figure V.53. 23,24-Br_2A23187 transport kinetic data for various divalent cations

These transport data indicate that 23,24-Br_2A23187 transports Mn^{2+} at the highest rate initially, reaching saturation after approximately 4 minutes. Zn^{2+} is transported at a lower rate than Mn^{2+} initially, however, the transport of Zn^{2+} does not level off in the 14 minute time span of the study, and the net micromoles of metal transported at the end of the study is greater for Zn^{2+} than for Mn^{2+}. Cd^{2+} is transported at a significantly lower rate than Zn^{2+}. Because both metals have an outer shell electronic configuration of d10, the difference in transport rates may be attributable to the difference in ionic radii. A single ionophore may encounter greater difficulty in accommodating the larger Cd^{2+}, and thus is less effective is shielding the 2+ ion from the hydrophobic vesicle interior. The acidity of the Cd^{2+} ion is also lower than that of the Zn^{2+} ion, with a pK_a of hydrolysis of 10.1 compared to that of Zn^{2+}, which is 9.0. While this difference does not seem to affect the transport of these metals with either A23187 or 4-ClA23187, a more complicated transport scheme may result in an observable difference in transport selectivity for 23,24-Br_2A23187.

Cu^{2+} is initially transported at a very high rate, but absorbance begins to decrease after approximately 3 minutes. This is due to the same events observed in the 4-ClA23187 transport studies. Cu^{2+} either forms an insoluble complex with Quin-2, or forms an alternate complex (such as two Cu^{2+} ions to one ligand) that possesses different spectral properties than the 2:1 complex that is assumed to form.[5] The same possible events are responsible for the loss of absorbance observed in the Pb^{2+} transport study.

Co^{2+} is transported at a slow, approximately steady rate. Ni^{2+} is transported at a low, approximately steady rate. Ca^{2+} is transported at a very low rate: the only metal included

for study with a lower rate of transport is Sr^{2+}, which is most likely due to steric constraints involved in shielding a large cation from the hydrophobic membrane interior.

D. Summary

The crystal structure of Mg(23,24-Br_2A23187)$_2$ shows that this derivative of A23187 retains the ability to form three bonds per ligand with a central metal ion. The donor atoms (carboxylate oxygen, benzoxazole nitrogen, and carbonyl oxygen) are the same as in the parent compound, and the same interligand hydrogen bonds are formed at each end of the complex between the hydrogen of the pyrrole nitrogen and the metal-unbound carboxylate oxygen of the opposite ligand.

The metal complexation properties of 23,24-Br_2A23187 are studied by potentiometric titrations and UV-vis and CD spectroscopy. Potentiometric and UV-vis titrations indicate that the pK_a's of the ligand are approximately equivalent to those of the parent compound A23187. The first pK_a of 7.8 in 80% CH_3OH/H_2O is due to deprotonation of the carboxylic acid moiety, and is comparable to the pK_a of A23187 in 80% CH_3OH/H_2O of 7.85. The second pK_a of 23,24-Br_2A23187 is 11.4 which comparable to the second pK_a of A23187, as well as 4-ClA23187, in 80% CH_3OH/H_2O of 11.3.

Metal complexation properties of 23,24-Br_2A23187 are similar to those of parent compound A23187 for Zn^{2+}, Cd^{2+}, Mg^{2+}, and Ni^{2+}. The model that best fit the UV-vis titration data for these metals includes the formation of the 1:1 metal:ligand complex

(MAH^+) and, at higher pH^* values, deprotonation of the pyrrole nitrogen to form MA. This deprotonation step results in a complex in which there are 4 potential donor atoms available to bind to the metal, and an overall neutral charge. This complex is potentially favorable for transport through a cell membrane if the ligand is able to shield the metal ion well enough from the hydrophobic environment of the membrane.

REFERENCES:

1. Alleaume, M., and Barrans, Y. *Can. J. Chem.* **1985**, *63*, 3482-3485.

2. Charney, E. *The Molecular Basis of Optical Activity: Optical Rotatory Dispersion and Circular Dichroism*; Wiley: New York **1979**.

3. Martell, A. E. and Motekaitis, R. J. *Determination and Use of Stability Constants*, 2nd Ed., VCH Publishers, Inc.: New York, **1992**.

4. Chapman, C. J., Puri, A. K., Taylor, R. W., and Pfeiffer, D. R. *Arch. Biochem. Biophys*. **1990**, *281*, 44-57.

5. Yuchi, A., Tanaka, A., Hirai, M., Yasui, H., Wada, H., and Nakagawa, G. *Bull. Chem. Soc. Jpn*. **1993**, *66*, 3377-3381.

CHAPTER VI

DISCUSSION

Derivatives of the well-characterized ionophore A23187 have been characterized to investigate the selectivity for the metal ions Zn^{2+} and Mn^{2+} over Ca^{2+}. Such derivatives would aid in studies of these metal ions in biological processes as well as elucidate information about the nature of transport selectivity observed in the parent compound A23187. The interligand hydrogen bond network present in the complexes is thought to play an important role in the formation of membrane permeant MA_2 species. Therefore, the derivatives investigated were designed to disrupt the hydrogen bonding by either steric or electronic means. The benzoxazole and pyrrole moieties were chosen for substitution with large halogen atoms due to their close proximity to the atoms involved in the interligand hydrogen bonding. These disruptions would reduce transport by the 1:2 MA_2 complex in favor of transport by the 1:1 complex. Metal ions best able to transport via this alternate scheme would be preferentially transported.

The structural, protonation, complexation, and transport properties of both derivatives were determined and compared to that of the parent compound. While the binding properties of each derivative provided information about the derivative relative to the parent compound, they did not directly correlate with the transport properties of the ligand. A ligand that binds a metal ion very tightly may not release it readily once the complex travels across the cell membrane, which would result in slower transport.

A. Structural Properties

Methods used to study the structural properties of free acid and complex forms of A23187 and its derivatives include NMR, UV-Vis, and CD spectroscopy for solution states and X-ray crystallography for solid states. Several groups have elucidated the structure of A23187 in free acid form and in calcium-complexed form by ^{1}H and ^{13}C NMR.[1-2] The crystal structures of free acid A23187, $Ca(A23187)_2$, $Fe(A23187)_2$, and $Mg(A23187)_2$ have been solved previously by X-ray crystallography.[3-6] These structures are compared to crystal structures of complexes presented here of A23187 with Zn^{2+}, Cd^{2+}, Mn^{2+}, Cu^{2+}, and Ni^{2+}, as well as the crystal structure of A23187 in free acid form with better resolution than was available at the time of the initial study.

The crystal studies reflect the number of donor atoms bound to the metal ion. For most metal ions included in the study (except for Ca^{2+} and Cu^{2+}), a coordination number of 6 is observed, which is consistent with the preferred coordination numbers for the metal ions. For the calcium complex, a solvent molecule is observed bound to the metal ion, due to the preferred coordination number between 7 and 9 for calcium ions. The copper complex is observed to have a coordination number of 5, with one bidentate and one tridentate ligand. This arrangement results in one interligand hydrogen bond rather than the two interligand hydrogen bonds observed in all other crystal structures of MA_2 complexes.[4-6] This may be the reason for the lack of cooperativity observed for A23187 molecules coordinating with copper ion in 80% CH_3OH.

CD spectra can be used to determine coordination number as a function of solvent. The MgA_2 complex is used as a basis for comparison, for its structure in solid state,

$CHCl_3$, 80% CH_3OH, and in POPC vesicle suspensions has been determined to be the same 6-coordinate complex with two tridentate ligands bound to the magnesium ion in an arrangement with octahedral geometry. Two interligand hydrogen bonds and two intraligand hydrogen bonds are observed in the complex. Because the CD spectra of Zn^{2+}, Mg^{2+}, Co^{2+}, Mn^{2+}, and Ni^{2+} complexes with A23187 appear similar to the CD spectrum of MgA_2 in both 80% CH_3OH and $CHCl_3$, these complexes are thought to be 6-coordinate with two tridentate ligands bound to the metal ion in an arrangement with octahedral geometry. The crystal structures of these metal ions also indicate 6-coordinate, octahedral structures, with two tridentate ligands bound to the metal ion (except NiA_2, which has one tridentate ligand, one bidentate ligand, and one solvent molecule). In the case of NiA_2, the octahedral geometry and both interligand hydrogen bonds are retained despite the presence of a solvent molecule. The difference between the solid and solution states of the complex are thought to be due to packing forces in the solid state structure.

The alternate coordination number of the CaA_2 complex, observed in solid state to be 7, is also reflected in the CD spectra of CaA_2 in 80% CH_3OH. An extra set of peaks at low wavelength (~ 230 nm) is observed in the spectrum of $Ca(A23187)_2$. Other metal ion complexes in 80% CH_3OH that have an extra set of peaks in this wavelength range are metal ions with preferred coordination numbers larger than 6, including the alkaline earth metal ions that are larger than calcium (Sr^{2+} and Ba^{2+}) and metal ions with a 3+ oxidation state (Sc^{3+}, Y^{3+}, La^{3+}, Gd^{3+}, and Lu^{3+}).

In the relatively non-polar, non-coordinating solvent $CHCl_3$, however, the CD spectrum of CaA_2 is observed to be similar to those of MgA_2 and other 6-coordinate complexes. This indicates that in $CHCl_3$, CaA_2 loses the solvent molecule and becomes

6-coordinate with two tridentate ligands bound to the metal ion. If $CHCl_3$ is thought to be representative of the environment of the membrane interior, this observation has implications for Ca^{2+} membrane transport. The difference in coordination number for CaA_2 in 80% CH_3OH and $CHCl_3$ suggests that CaA_2 changes hydration state in going from the membrane surface to the membrane interior.

Stereochemistry is also an observable property of the metal complexes of A23187 by CD. All solution state MA_2 structures except for Cu^{2+} have a negative stereochemistry around the metal center which is confirmed in the crystal structures of the same complexes. In the case of CuA_2, the CD spectrum in 80% methanol indicated positive stereochemistry, which was also found in the solid state.

Since only the magnesium complexes of 4-ClA23187 and 23,24-Br_2A23187 crystallized, the magnesium complex of each ligand is the only one that can be compared directly between the derivatives and parent compound. In each case, the complex has three donor atoms per ligand (a carboxylate oxygen, benzoxazole nitrogen, and ketopyrrole oxygen) to form a 6-coordinate complex with octahedral geometry around the metal center. The stereochemistry around each metal center is negative, like all other A23187-metal ion complex crystal structures except the copper complex. The distance between donor and acceptor atoms thought to be involved in interligand hydrogen bonding for each complex is within the bond distance and bond angle requirements for hydrogen bond formation. However, the interligand hydrogen bond distances observed in the 4-ClA23187 are somewhat longer than those for 23,24-Br_2A23187. This may be due to the decrease in electronegativity of each hydrogen participating in the interligand

hydrogen bond, which is due inductive effects of the bromine atoms on each pyrrole moiety.

From this data it can be concluded that the presence of a halogen at either the 4-position of the benzoxazole ring or the 23 and 24 position of the pyrrole ring does not completely disrupt the ability of the ligand to form intermolecular hydrogen bonds. However, the conditions used to form the complex (ligand dissolved in non-polar solvent extracted with aqueous solution of metal) may force the formation of a complex that would not form under conditions more physiologically relevant. The pH of the solution may also play a factor in the composition of the complex formed.

B. Binding Properties

Comparison of the binding properties of A23187 and derivatives 4-ClA23187 and 23,24-Br_2A23187 illustrate possible reasons for the differences observed in metal transport. Stability constants are compared for two protonation states of each ligand and of various metal complexes.

The pK_as of A23187 and derivatives 4-ClA23187 and 23,24-Br_2A23187 partially illustrate the effects of halogenation on the ligand. The pK_a of the carboxylic acid moiety of the parent compound in 80% methanol is 7.85.[7] Halogenation of the 4 position of the benzoxazole ring lowers the pK_a to 5.9. This effect is likely due to inductive effects of the electronegative chlorine substituent: the chlorine atom shifts electronegativity of the conjugated ring in such a way that the electronegativity of the carbon of the carboxylic acid is increased, which subsequently decreases the electronegativity of the carboxylic

acid oxygen atoms, resulting in a weaker, more easily broken bond between the oxygen and hydrogen of the carboxylic acid moiety. The pK_a of the 23,24-Br_2A23187 is relatively unaffected by substitution on the pyrrole ring: this derivative has a measured pK_a of 7.6 in 80% methanol, which is approximately equal to that of the parent compound.

A second pK_a at approximately 11.4 is detected in both the parent and derivative ligands. The two candidate sites for this equilibrium are the methylamino nitrogen and the pyrrole nitrogen. The pK_a of the methylamino nitrogen was addressed by Pfeiffer et al. in a study of acid-base properties of A23187.[7] Potentiometric studies revealed two pK_as in 65 % methanol-water: 1.28 and 7.19. When the carboxylic acid group is replaced with a methyl ester, a single pK_a at 1.38 is observed, which is justification for assigning the carboxylic acid a pK_a of 7.19 and methylamino nitrogen the lower pK_a. Since the pK_a of 7.85 for A23187 in 80% methanol represents the carboxylic acid deprotonation, the pK_a of 11.4 must represent the protonation of the pyrrole nitrogen. Furthermore, the pK_a of pyrrole is approximately 15. It is conceivable that the keto-substituent serves to lower the pK_a to that observed in pH* titrations of each ligand. The presence of this pK_a is important because it introduces a new binding model into the traditional scheme. It also helps to explain the presence of a third equilibria in the titrations of A23187 with Zn^{2+}, Mn^{2+}, and Ni^{2+} at relatively high pH* values. The initial conclusion from these data is that a third species consisting of one metal, one ligand, and one hydroxide forms at relatively high pH* values.[8] A MA(OH) complex would have a neutral charge and the metal would be surrounded by four donor atoms, theoretically facilitating its passage through a non-polar membrane as a 1:1 complex. Transport selectivity would be observed

based on the likelihood of deprotonation of a water molecule bound to the metal (the pK_a of hydrolysis) and the ability of the metal ion to adopt a coordination number of 4. However, the results from pH* titrations presented here suggest that the deprotonation of the pyrrole nitrogen creates a ligand with four potential donor atoms and a formal charge of -2. These properties would make it possible for a divalent metal to pass through a membrane bound only to this ligand: the overall charge of the complex is neutral, and the coordination requirements of many metals would be satisfied. Transport selectivity would be observed based on the same properties as the MA(OH) complex. This deprotonation is observed for both the parent compound A23187 and the derivatives 4-ClA23187 and 23,24-Br_2A23187.

Metal bound to ligand may affect the pK_a of the pyrrole group. It is feasible for the change in electronegativity of the ketopyrrole donor atom to inductively lower the electronegativity, and thus the pK_a, of the pyrrole nitrogen. Precedence for the phenomenon of a metal affecting the pK_a of a ligand is found in studies of pK_a values of peptides in the presence or absence of coordinating metal ions. For example, glycineamide has pK_a values of 7.07 and 8.33 when coordinated with Cu^{2+}, and pK_a values at least 5 orders of magnitude higher in the absence of Cu^{2+}.[9] These findings support the theory that binding of metal to A23187 or derivative could lower the pK_a of the pyrrole nitrogen enough to create a 4-coordinate 1:1 metal:ligand complex at relevant pH.

The stability constants for A23187 in 80% methanol for Zn^{2+}, Cd^{2+}, Ca^{2+}, Mg^{2+}, and Ni^{2+} are significantly different than those for 4-ClA23187 and the same metals, but very similar to those for 23,24-Br_2A23187. The results are summarized in Table VI.1.

Metal	log K_{HML} A23187	log K_{HML} 4-ClA	log K_{HML} 23,24-Br_2A	log K_{ML} 4-ClA	log K_{ML} 23,24-Br_2A
Zn^{2+}	6.79	3.8	6.6	5.1	12.9
Cd^{2+}	6.48	4.5	5.5	8.0	11.9
Ca^{2+}	4.5	3.7	5.5	6.1	7.8
Mg^{2+}	4.55	4.1	4.5	4.7	7.9
Ni^{2+}	7.54	no data	7.3	no data	10.9

Table VI.1. Comparison of K_{HML} and K_{ML} values for A23187,[8] 4-ClA23187, and 23,24-Br_2A23187 in 80% methanol

The 1:1 (metal:ligand) stability constants for 4-ClA23187 are lower for each metal studied than for the parent compound. While this does not indicate an increase in transport selectivity, it does indicate that the presence of a halogen on the 4 position of the benzoxazole ring affects the ability of the ligand to bind divalent cations. The model that best fit all titration data for this ligand indicates that the ligand first forms a 1 metal, 1 ligand complex in which the pyrrole nitrogen is protonated (MLH), and then loses the hydrogen bound to the pyrrole nitrogen to form a 1 metal, 1 ligand complex (ML). This increases the number of available donor atoms on the ligand to 4, and decreases the charge of the complex to 0. For some metals, this alteration results in a complex that is able to diffuse through a lipid bilayer, while for others, it is insufficient to shield the metal from the non-polar environment.

The 1:1 (metal:ligand) stability constants (K_{MLH}) for 23,24-Br_2A23187 are approximately equal to those of the parent compound, except for Ca^{2+}, which is somewhat higher. This indicates that the presence of halogens at the pyrrole end of the complex do not significantly affect the ability of the ligand to bind metal to form a 1:1 complex. The subsequent formation of a 2:1 complex for any metal ion is not indicated by the model that best fits titration data. The best fit model includes the formation of a 1:1 complex in which the pyrrole nitrogen is deprotonated.

A neutral complex consisting of 1 metal and 1 ligand could possibly diffuse through a lipid bilayer more readily than a 1 metal, 1 ligand, 1 hydroxide complex due to the hydrophilicity of the hydroxide moiety. Transport selectivity would be based on the ability of the complex to deprotonate and form a neutral complex. Possible factors affecting the ability of the complex to deprotonate include the identity of the metal and the ability of the ligand to adopt a conformation that adequately shields the charged metal from the hydrophobic membrane interior. A23187 derivatives with halogen atoms at either end of the molecules could potentially affect either of these properties.

C. Transport Properties

Transport rates of the metals Zn^{2+}, Cd^{2+}, Ca^{2+}, Mg^{2+}, and Ni^{2+} through POPC vesicles by ionophores A23187, 4-ClA23187, or 23,24-Br_2A23187 reflect differences in transport ability between the three ionophores. While the rates can be compared relatively directly between the two derivatives, they can only be compared qualitatively to the parent compound A23187 due to different reaction conditions. In transport studies of the derivatives, metal ion concentrations were 20 μM, while the metal ion concentrations for transport studies with A23187 were 100 μM. Also, 23,24-Br_2A23187 transported metal ions slower overall than either A23187 or 4-ClA23187, so the concentration of 23,24-Br_2A23187 used for transport studies was increased to 0.30 μM (compared to 0.1 μM used for A23187 and 4-ClA23187.)

4-ClA23187 displays transport selectivity into POPC vesicles that is very similar to that of 4-BrA23187.[10] The kinetic data indicates a selectivity order of Zn^{2+}> Cd^{2+}> Mn^{2+}> Co^{2+} > Cu^{2+} > Ni^{2+} > Pb^{2+} > Sr^{2+} ≈ Ca^{2+}. When compared to a more limited study of transport selectivity of 4-BrA23187 and A23187, similarities are apparent between the derivatives. 4-BrA23187 transports metals ions selectively in the following order: Zn^{2+} > Mn^{2+} > Co^{2+} > Ni^{2+} > Ca^{2+} > Sr^{2+}. Compared to the parent compound A23187 (which transports metal ions with the following selectivity order: Zn^{2+} > Mn^{2+} > Ca^{2+} > Co^{2+} > Ni^{2+} > Sr^{2+}), both derivatives retain high transport rates for the metal ions Zn^{2+} and Mn^{2+}, while losing the parent compound's ability to transport Ca^{2+} at significant rates.

23,24-Br_2A23187, however, displays unique transport selectivity. The order of transport selectivity, determined from initial rates, is Cu^{2+} > Mn^{2+} > Zn^{2+} > Cd^{2+} > Pb^{2+} >

$Co^{2+} > Ni^{2+} > Ca^{2+} > Sr^{2+}$. The rank of Cu^{2+} and Pb^{2+} in either order should not be considered significant because of a loss of absorbance observed for both metals during the experiment. These losses are likely due to either an alternate complex formed between the metal ion and the chelate Quin-2 (which would possess alternate spectroscopic properties) or the formation of a metal complex precipitate.[11] The most significant features of the 23,24-Br_2A23187 transport data are the transport rates of Zn^{2+} and Cd^{2+} relative to that of Ca^{2+}. The parent compound A23187, derivative 4-BrA23187, and derivative 4-ClA23187 all have very high rates of transport for the metal ions Zn^{2+}, Mn^{2+}, and Cd^{2+}. While the 23,24-Br_2A23187 derivative retains a high rate of transport for the metal ion Mn^{2+}, it is much slower for transport of Zn^{2+}, and even slower for transport of Cd^{2+}, but transports Ca^{2+} much lower than Zn^{2+} or Cd^{2+}, and therefore has increased transport selectivity for Zn^{2+} and Cd^{2+} over Ca^{2+} relative to the parent compound.

The goal of this research project was to synthesize and characterize derivatives with enhanced selectivity for Zn^{2+}, Mn^{2+}, and Cd^{2+} over Ca^{2+} compared to the parent compound A23187. While both derivatives achieve this goal, they display different complexation properties. 4-ClA23187 has complexation constants for the formation of HML that are lower for all metals studied. The transport kinetics of 4-ClA23187 are similar to those of 4-BrA23187. Increased selectivity is likely due to the increase of 1:1 ligand:metal complex transport over 2:1 ligand:metal transport by destabilization of the hydrogen bonding network observed in the 2:1 complex. Metals such as Zn^{2+}, Mn^{2+}, and Cd^{2+} that can form neutral complexes with one ligand molecule retain transport ability.

The complexation constants of 23,24-Br_2A23187 for formation of HML are similar to those for the parent compound. The transport properties for this derivative are much

different than either the parent compound or 4-ClA23187. While the initial rates of transport are lower for all metal ions compared to 4-ClA23187 or A23187, an increase in transport selectivity is observed for Zn^{2+}, Cd^{2+}, and Mn^{2+} over Ca^{2+}.

Compared to the parent compound, the more electronegative chlorine atom in the 4-position did not result in significantly different stability constants or transport than the derivative with less electronegative bromine in the 4- position. The main difference is that transport of Co^{2+} is enhanced in the 4-Cl derivative relative to the 4-Br derivative. Ca^{2+} transport, while very low in the 4-Br derivative, is slightly lower in the 4-Cl derivative.

The addition of two bromine atoms on the pyrrole end of A23187 significantly affect transport properties, if not binding affinities, relative to the parent compound. It is clear that all metal ion transport studied, except possibly for that of Mn^{2+}, is affected by halogenation. While Zn^{2+} and Cd^{2+} are still transported at a much greater rate than Ca^{2+}, their rates of transport have been reduced and thus the 23,24-Br_2A23187 derivative not as selective as either the 4-ClA23187 derivative or the 4-BrA23187 derivative. The benefit to the 23,24-Br_2A23187 derivative is that its spectrochemical properties make binding much easier to follow than other derivatives discussed.

Another significant finding from the study is the detection of a third protonation state for each ligand. While this state is present for both the derivatives 4-ClA23187 and 23,24-Br_2A23187 and the parent compound A23187, its discovery contributes important information in the development of an accurate transport scheme for this class of ionophore, which may in turn be used to develop an ionophore with enhanced selectivity.

REFERENCES

1. Deber, C. M. and Pfeiffer, D. R. *Biochemistry*, **1976**, **15**, 132-141.

2. Faure, R., Chauvet-Monges, A. M., and Crevat, A. *Spec. Lett*., **1989**, *22*, 945-954.

3. Chaney, M. O., Demarco, P. V., Jones, N. D., and Occolowitz, J. L. *J. Am. Chem. Soc*. **1974**, *96*, 1932-1933.

4. Smith, G. D. and Duax, W. L. *J. Am. Chem. Soc*. **1976**, *98*, 1578-1580.

5. Baker, E., Maslen, E. N., Watson, K. J., and White, A. H. *J. Am. Chem. Soc*. **1984**, *106*, 2860-2864.

6. Alléaume, M. and Barrans, Y. *Can. J. Chem*. **1985**, *63*, 3482-3485.

7. Kaufmann, R. F., Taylor, R. W., and Pfeiffer, D. R. *Biochemistry*, **1982**, *21*, 2426-2435.

8. Chapman, C. J., Puri, A. K., Taylor, R. W., and Pfeiffer, D. R. *Biochemistry*, **1987**, *26*, 5009-5018.

9. Burger, K. *Biocoordination Chemistry: Coordination Equilibria in Biologically Active Systems*; Ellis Horwood: New York **1990**.

10. Erdahl, W., Chapman, C. J., Wang, E., Taylor, R. W., and Pfeiffer, D. R. *Biochemistry*, **1996**, *35*, 13817-13825.

11. Yuchi, A., Tanaka, A., Hirai, M., Yasui, T., Wada, H., and Nakagawa, G. *Bull. Chem. Soc. Jpn*., **1993**, *66*, 3377-3381.